

Phases and phase transitions in living matter

Advisor: Miguel Á. Muñoz

Dept. of Electromagnetism
and Matter Physics



PhD Thesis
February 2018

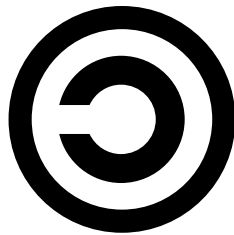


UNIVERSIDAD
DE GRANADA

Pablo Villegas
Góngora

Editor: Universidad de Granada. Tesis Doctorales
Autor: Pablo Villegas G3ngora
ISBN: 978-84-9163-818-6
URI: <http://hdl.handle.net/10481/50139>

(This page is intentionally left blank.)



copyleft



Pablo Villegas, 2018.

©2018 by Pablo Villegas Góngora. This work is licensed under a Creative Commons Attribution-NonCommercial-ShareAlike 4.0 International License. To view a copy of this licence, visit <http://creativecommons.org/licenses/by-nc-sa/4.0/>.

Front cover image by Van Weeden and L. L. Wald, Martinos Center for Biomedical Imaging, Human Connectome Project.



UNIVERSIDAD
DE GRANADA

El doctorando Pablo Villegas Góngora y el director de la tesis Miguel Ángel Muñoz Martínez, catedrático de Universidad,

GARANTIZAMOS, al firmar esta tesis doctoral, *Phases and phase transitions in living matter* (“Fases y transiciones de fase en seres vivos”), que el trabajo ha sido realizado por el doctorando bajo la dirección de los directores de la tesis y, hasta donde nuestro conocimiento alcanza, en la realización del trabajo se han respetado los derechos de otros autores a ser citados cuando se han utilizado sus resultados o publicaciones, así como que el doctorando ha disfrutado de una estancia en el extranjero, durante un período de tres meses, en el *Marine Population Modeling Group, Department of Mathematics and Statistics*, de la Universidad de Strathclyde (Glasgow, Reino Unido).

Granada, a 15 de Enero de 2018

Director de la Tesis:

Fdo: Miguel Ángel Muñoz Martínez

Doctorando:

Fdo: Pablo Villegas Góngora

Agradecimientos

Tras varios meses de parrafadas infinitas, y un largo sufrimiento para conseguir un formato agradable en L^AT_EX, llega un día en que el (agotado) doctorando decide escribir el capítulo final de la tesis: los agradecimientos. Indudablemente, el doctorado ha supuesto una fase que me ha formado científicamente, pero también personalmente. En este capítulo pretendo dar las gracias a todos los que, directa o indirectamente, han puesto su granito de arena en toda esta etapa que termina con la consecución de este libro.

En primer lugar quiero agradecer a mi director de tesis Miguel A. Muñoz, su empeño y dedicación en todos estos años. Desde las primeras clases de Mecánica Estadística, hasta que me apadrinó y sufrió el parto (doloroso) de otra nueva tesis, manteniendo su despacho permanentemente abierto para cualquier idea, discusión o conjetura que se me pudiera ocurrir. También por pensar en un esquema de trabajo sobre “criticalidad” en el que al final ha aparecido algún tipo de orden emergente. Para mí, es un ejemplo de físico estadístico y teórico. Su permanente minuciosidad, cercanía, entusiasmo y forma de trabajar hace que los sinuosos caminos de una tesis doctoral sean un poco más amenos. Gracias también por ayudarme a comprender que, al final, todo puede reducirse a un “contact process”.

Por estricto orden de cercanía, gracias al grupo de Física Estadística por brindarme un estupendo lugar de trabajo donde desarrollar esta tesis. A Pedro Garrido, por recordarnos lo lejos que estamos de la Física Estadística, y estar siempre dispuesto a una conversación, ya sea académica o política. A Joaquín Marro y Antonio Lacomba por sus consejos y su buen humor. A Joaquín Torres por ser una referencia para cualquier duda relacionada con la neurociencia. A Jose por mantener vivo a Proteus (casi siempre) y solucionar con rapidez cualquier problema (informático) que ha aparecido durante la tesis, también por dejarme hacer de ‘beta tester’ y aguantar mis continuas ocurrencias en Proteus. Casi para terminar, a Pablo Hurtado y Paco de los Santos, por haber sido también parte clave de mi formación y conocimiento. Por último, a Dani Manzano por ser una rara avis que nos enseña que hay vida más allá del doctorado.

Esta tesis tampoco podría haber llegado a buen puerto sin la inestimable ayuda de Proteus, pese a sus 'catastrophic shifts' aleatorios y problemas de calentamiento que hacen que la tesis sea más entretenida, especialmente en los veranos granadinos.

Continuando en el ámbito científico a Paolo Moretti, por su entusiasmo y humor, por ser mi primer coautor, un estupendo 'referee', y por enseñarme lo que es la minuciosidad en una investigación, y cómo siempre es posible escalar el tamaño del sistema, al menos, un orden de magnitud más. Al 'host' de la estancia, Juan Antonio Bonachela, que solo se llevó disgustos del caótico doctorando que le llega por sorpresa y casi se lo cargan la primera noche escocesa, pero del que he aprendido (y aprovechado) muchas más cosas de las que yo esperaría en tres meses de verano. De la misma forma, a Carlos, por acogerme en Glasgow y hacer de excelente 'sub-host' y compañero de despacho, haciendo que la estancia en el norte pasara de una forma mucho más agradable, de la misma forma que Kyung y todo el PhD staff de la universidad de Strathclyde.

De igual manera, en el Departamento han sido muchos los que han hecho esta etapa mucho más entretenida y llevadera. Los que están, a Nico por contagiar su entusiasmo, comentar conmigo eternamente la organización de las clases, hacer de secretario/burócrata y haber sido un excelente compañero de mesa, a Ana por su paciencia ante los problemas, su capacidad de aglutinar y terminar proyectos y por arrancarme de la silla para ir a por café, a Serena, una referente en *Mathematica* con la que he compartido una infinidad de horas de trabajo y colaboración científica en estos años, mientras no estaba en selva virgen y a Víctor, reciente fichaje que me recuerda lo fascinante de la Física Estadística en los inicios de la tesis. También a los que se fueron, Jordi por estar siempre dispuesto a aceptar cualquier marrón y ayudar en todo lo posible, a Paula por conseguir que el reloj fuera un poco más despacio y contagiarnos con su alegría y a Vir por las eternas discusiones políticas en las que pretendimos arreglar un poco el mundo en estos años (quizás todavía no está todo perdido).

Tengo que agradecer también especialmente a Javi por los eternos años de carrera, conversaciones y largas prácticas que han desembocado (con los dos) presentando la tesis en paralelo. A Paloma, por intentar nuestro pequeño 'asalto a los cielos' y ser un ejemplo de lucha continua. Igualmente a Jose (principalmente amigo de carrera pero que también fue colaborador científico y al que desde que está exiliado veo menos de lo que me gustaría), a Fer (con el que hablar para llegar a puntos de coherencia comunes, comer carne, o las dos cosas a la vez), Juank, Manu, Ángela, Estefa, Salva, Sebas, Dani, Sam, Patri, Eva, Elia, Miguel, Irene, Juanfran..., todos y todas los que han formado parte de nuestra peña de fútbol, los que ayudaron a lanzar la plataforma de lucha Dignidad Predoctoral y aquellos con los que estos años se han pasado demasiado rápido.

Igualmente a la ciudad de la Alhambra, por suponer una estupenda (y peligrosa) ciudad para tapear y realizar una tesis doctoral. También a todos los veranos cerca del mar que hacen más llevadero el calor del sur y a toda la música, RRV, canción protesta, rock nacional y el exceso de sonidos no relajantes, que han evitado sueños profundos y han hecho menos aburridas las infinitas horas de programación, revisión de códigos y lectura de 'papers'.

Pero, a quien uno debe estar principalmente agradecido es a su familia, y en especial, a mis padres, por enseñarme todo lo que sé y hacer, los dos, de 'captain fantastic' de alguna manera. A mi madre, por su infinita paciencia y a mi padre, por inculcarme la cultura del software libre, y hacerme crecer con un Linux debajo del brazo, desde que (casi) ni existía internet. Por ello, el capítulo sobre Debian es particularmente especial. De un padre matemático y una madre bióloga tenía que emerger un Físico Estadístico. También a mi abuelo y mi abuela, mis tíos y mis primos por su cariño, y a mi hermano Diego por recordarme que siempre puede existir una pequeña aldea que resista todavía y siempre al invasor. También a mi familia política, por haberme acogido como a uno más, y a mi suegra, Maite, por recordarme que, con fuerza de voluntad, todo es posible.

Por último, a Maite, por haber sido mi compañera de viaje y permanecer a mi lado desde hace tanto tiempo, has sido mi brújula y el punto de apoyo por el que todo mereció seguir adelante. Sin toda tu ayuda en estos años, muchas etapas de mi vida nunca hubieran llegado a buen puerto. Simplemente, doy las gracias por tu luz.

A todxs, prometo estar agradecido.

“Dedicated to my parents, for their infinite patience.”

Pablo

Preface

Standing on the shoulders of giants such as Landau, Anderson, Mandelbrot or Bak, emergent phenomena have meant a major step towards the comprehension of macro-structures and patterns in Nature. In particular, the criticality hypothesis, which proposes that –under some circumstances– living systems can lie in the vicinity of a phase transition, i.e. at the borderline between their ordered and disordered phases, has shed much light on the comprehension of several natural phenomena that, until recently, were poorly understood.

This celebrated and provocative idea conjectures that living close to a critical point may confer a large number of benefits such as maximal dynamical range, maximal sensitivity to environmental changes, as well as an excellent trade-off between stability and flexibility.

Based on this assumption, the aim of this thesis is to look into the criticality hypothesis, extending its horizons through the analysis of phases and phase transitions in Nature, developing a better understanding of certain empirical findings and behaviors of biological systems. Thus, the development of models trying to shed light –through numerical simulations and theoretical calculations– on the emergent behavior of particular biological systems constitute the common theme of this thesis.

In **chapter 1** a basic introduction and a schematic review on the criticality hypothesis, as well as some particular examples in living systems such as neuronal dynamics and gene regulation are outlined.

Also, a brief, but necessary introduction to phases and phases transition and the Landau equilibrium theory of critical phenomena is presented. It covers the two principal phase transitions, first order and second order, certain theoretical notions of non-equilibrium systems, together with the introduction of the main self-organizing mechanisms to such phase transitions, as well as a brief summary on the effects of non-homogeneous underlying structures in the dynamical evolution, and phases, of most systems. Above all, one of the principal aims of this chapter is to be intended to allow for a self-contained book.

In **chapter 2** we try to shed light in the origin, nature and functional significance of complex patterns of neural activity in the human cortex, which operates in a state of sempiternal irregular activity, whose meaning and functionality are still not well understood. Such patterns include collective oscillations, emerging out of neural synchronization, as well as highly-heterogeneous outbursts of activity interspersed by periods of quiescence, called “neuronal avalanches”. A fascinating though still controversial hypothesis, to some extent backed by empirical evidence, suggests that the cortex might work at the edge of a phase transition, from which important functional advantages stem. However, the nature of such a phase transition is still not fully understood. Here, we adopt ideas from the physics of phase transitions, to construct a general (Landau-Ginzburg) theory of cortical networks, allowing us to analyze their possible collective phases and phase transitions. We conclude that the empirically reported scale-invariant avalanches can possibly come about if the cortex operated at the edge of a synchronization phase transition, at which neuronal avalanches and incipient oscillations coexist.

Chapter 3 tackles the problem of neuronal synchronization in a more complex and realistic underlying structure (i.e. coupling scheme) given by the actual human-brain connectome network employing a parsimonious (mesoscopic) approach, the Kuramoto model, in order to preserve the essence of a minimal design, with the purpose of studying analytically and computationally the synchronization dynamics and to scrutinize the spontaneous emergence of coherent behavior in neural function.

We elucidate the existence of a so-far-uncovered intermediate phase, placed between the standard synchronous and asynchronous phases, i.e. between order and disorder. This novel phase stems from the hierarchical modular organization of the connectome. Where one would expect a hierarchical synchronization process, we show that the interplay between structural bottlenecks and quenched intrinsic frequency heterogeneities at many different scales, gives rise to frustrated synchronization, metastability, and chimera-like states, resulting in a very rich and complex phenomenology. We uncover the origin of the dynamic freezing behind these features by using spectral graph theory and discuss how the emerging complex synchronization patterns relate to the need for the brain to access –in a robust though flexible way– a large variety of functional attractors and dynamical repertoires without ad hoc fine-tuning to a critical point.

Also, we explore the role of noise, as an effective description of external perturbations, and we discuss how its presence accounts for the ability of the system to escape intermittently from such attractors and explore complex dynamic repertoires of locally coherent states, in analogy with experimentally recorded patterns of cerebral activity.

In **Chapter 4** we revisit the problem of deriving the mean-field values of avalanche exponents in systems with absorbing states. These are well known to coincide with those of an unbiased branching processes, as reported in neural avalanches, for at least, four different universality classes. We report on the emergence of non-universal continuously varying exponent values stemming from the presence of small external driving –that might induce avalanche merging– and that, to the best of our knowledge, has not been noticed in the past.

Such active/quiescent transition is closely related with the “balanced amplification” theoretical approach recently proposed to explain the empirical neural avalanches of activity. Standing on the active phase with an excellent balance between excitation/inhibition, the weak stability of the basin of attraction of the system caused by a reactive dynamics is exploited, i.e. the dynamics is encoded in a “non-normal” matrix. Thus, the system exhibit large fluctuations reminiscent of “up” and “down” states and neural activity. We have progressed in a thorough understanding of such phenomenon as well as it has been extended to a wider scenario: a similar non-critical scale-invariance can be obtained by changing the regulatory mechanism that drives the dynamics, i.e. excluding inhibition and introducing synaptic plasticity.

We believe that a simple and unified perspective as the one presented here can help to clarify the overall picture and underline the super-universality of the behavior giving rise to the unbiased branching processes exponents in active/quiescent phase transitions, as well as review, better understand and clarify certain processes with generic power laws but poised far away from criticality.

Chapter 5 is the first to address other problems beyond neural dynamics such as gene regulation in complex biological systems. To this end, the well-founded Boolean approach to model gene regulatory networks is employed. A much discussed hypothesis proposed that such approach reproduces empirical findings the best if it is tuned to operate at criticality, exploiting its large number of functional advantages. Here, we study the effect of noise within the context of Boolean networks trained to learn complex tasks under supervision. We verify that quasi-critical networks are the ones learning in the fastest possible way –even for asynchronous updating rules– and that the larger the task complexity the smaller the distance to criticality. On the other hand, when additional sources of intrinsic noise in the network states and/or in its wiring pattern are introduced, the optimally performing networks become clearly subcritical. These results suggest that in order to compensate for inherent stochasticity, regulatory and other type of biological networks might become subcritical rather than being critical, all the most if the task to be performed has limited complexity.

In **chapter 6** we analyze the evolving modular structure of the network of dependencies between software packages in the different Debian GNU/Linux distributions released to date. Also, we explore the emergent properties and vulnerability of such networks and their role in the functionality of the system.

In parallel, we show the interesting parallelisms between the architecture and emergent properties of software networks and that of regulatory interactions between genes. Indeed, such analogy allow us for an appealing explanation of recent empirical findings and enigmas of systems biology, the emergent cascading failures of “gene knockout” and possible functionalities of the, sometimes considered futile, non-coding DNA.

Chapter 7 highlights key findings and conclusions derived from this thesis, seen in a global perspective, which allows the reader to appreciate its contribution to the understanding of the emergent (critical) properties and phases of living systems, as well as the open issues and the enormous amount of work that remains to be done.

Although, in order to make this work available to the wider academic community, this thesis is written in English, a brief summary in Spanish (appendix E) is included in order to obtain the degree of Doctor of Philosophy in Physics with European level, fulfilling the requirements of the University of Granada.

Furthermore, some chapters also contain annexes. In particular, chapter 1 (appendix A), chapter 2 (appendix B), chapter 3 (appendix C) and chapter 4 (appendix D), in order to clarify some calculations and remarks that are too specific (or exhaustive) and may be excluded without impairing a proper understanding of each chapter.

Also, a list of publications of the author is reported. Of course, there has been more work beyond that explained here, as part of the learning process that gave birth to this thesis. Some of this additional work has been published and it has also been included in such list of publications.

Granada, February 2018

Contents

Agradecimientos	i
Preface	vii
Table of Contents	xi
List of Figures	xv
List of Tables	xix
1 Introduction to phase transitions and critical phenomena	1
1.1 The criticality hypothesis	3
1.1.1 Criticality beyond physics	6
1.2 Introduction to phase transitions	15
1.2.1 The Landau-Ginzburg theory of phase transitions	15
1.2.2 Dynamical models: non-equilibrium phase transitions	21
1.2.3 Self-organizing mechanisms	25
1.2.4 Griffiths phases: the stretching of criticality	28
References	30
2 Towards a Landau-Ginzburg theory of cortex dynamics: scale free avalanches of synchronization	37
2.1 Introduction	39
2.2 Building a minimal model of neural activity with synaptic plasticity	42
2.2.1 Single-unit model	42
2.2.2 Stochastic network model	46
2.2.3 Phases and phase transitions: Case A	47
2.2.4 Phases and phase transitions: Case B	52
2.3 Synchronization phase transition	53
2.3.1 From activity to phases: oscillators	53
2.3.2 Empirical matches	56

2.4	The case of infinite separation of timescales. Recovering self-organize bistability	62
2.5	Conclusions	67
	References	71
3	Synchronization in the human brain: Stretched criticality and metastability induced by network topology	79
3.1	Introduction	81
3.2	The Kuramoto model	83
3.2.1	Mean-Field approach	84
3.2.2	The Ott-Antonsen ansatz	87
3.2.3	The role of the frequency distribution: $g(\omega)$	88
3.2.4	Chimera states: getting frustration and metastability	91
3.3	Complex networks coupling	93
3.4	The Human Connectome	96
3.4.1	Chimeras	103
3.5	Modeling the HC	105
3.5.1	Communities	105
3.5.2	The two-block model	107
3.5.3	Simple-modular network	110
3.5.4	Hierarchic-modular network	113
3.6	Metastability and noise effects	118
3.7	Conclusions	122
	References	125
4	Reactive and noisy dynamics in simple neural systems: avalanches far away of the critical point	131
4.1	Introduction	133
4.2	Demographic noise and balanced logarithmic potentials	135
4.2.1	A simple calculation for the branching process	136
4.2.2	Random walks in a logarithmic potential	138
4.3	Reactive and noisy dynamics in the Wilson-Cowan model	143
4.3.1	Phenomenology	145
4.3.2	Criticality and balance	145
4.3.3	The roles played by the noise	149
4.4	Reactive dynamics in the Tsodyks-Markram model	154
4.5	Conclusions	157
	References	159
5	Dynamics of sparse gene networks under noisy conditions	165
5.1	Introduction	167
5.2	Boolean network approach	170
5.3	Adaptive evolution of boolean gene-regulatory networks	174

5.4	Emergent properties	183
5.4.1	Convergence times and phases of learning networks	183
5.4.2	Noisy conditions	187
5.4.3	Empirical networks	190
5.5	Conclusions	193
	References	196
6	Emergence of universal topological features: from gene regulatory to Linux modular networks	201
6.1	Introduction	203
6.2	Debian as “mirror” model	206
6.2.1	Evolutionary process of Debian networks	208
6.2.2	Network information and the size of packages.	214
6.3	Conclusions	217
	References	221
7	Conclusions	225
7.1	Concluding remarks	227
7.2	Papers derived from this thesis	233
	References	235
	Annexes	239
A	Introduction to critical phenomena	241
A.1	On the Itô-Stratonovich dilemma	243
	References	244
B	Landau-Ginzburg theory of cortical dynamics	245
B.1	Robustness against dynamical and structural changes	247
B.1.1	Changes in the dynamics	247
B.2	Detrended fluctuation analysis	251
B.3	On the definition of avalanches	253
B.3.1	Oscillations coexisting with scale invariance	253
B.3.2	On avalanches measure	254
	References	257
C	Kuramoto model	259
C.1	Ott-Antonsen ansatz	261
C.1.1	Lorentz distribution of natural frequencies	264
C.2	Complex networks	265
C.2.1	Critical point in homogeneous graphs	265
C.2.2	Equally frequency distributed oscillators $\omega_i = 0$	268

References	271
D Langevin equations in balanced logarithmic potentials	273
D.1 Irrelevance of non-linear terms	275
D.2 First-return time distributions	276
References	277
E Resumen en castellano	279
E.1 Introducción	281
E.1.1 "Criticalidad" más allá de la física	285
E.2 Conclusiones	294

List of Figures

1.1.1 Specific heat of He at the λ -point	4
1.1.2 Liquid-gas coexistence curve for many fluids	6
1.1.3 Logarithmic spiral for different remote systems	7
1.1.4 Scale invariant neuronal avalanches	11
1.1.5 Gene knockout experiments	13
1.2.1 Sketch of a second order phase transition	17
1.2.2 Sketch of a first-order phase transition	21
1.2.3 Sketch of the contact process dynamics	23
1.2.4 Self-organized criticality mechanism	26
1.2.5 Griffiths phases and the stretching of criticality	29
2.2.1 Phase portraits and nullclines for the (deterministic) dynamics of the Landau-Ginzburg model	44
2.2.2 Phase diagram of possible transitions for the Landau-Ginzburg model	45
2.2.3 Illustration of the diverse phases emerging in the model (case A) for a network of $N = 128^2$ units	48
2.2.4 Overall network activity state (case A) as determined by the net- work time-averaged value $\bar{\rho}$	50
2.2.5 Phase transition for the fraction of inactive sites in the system .	51
2.3.1 Synchronization transition elucidated by measuring the Kuramoto parameter	55
2.3.2 Avalanches measured from activity time series	57
2.3.3 Clustered networks of cultured cortical neurons	59
2.3.4 Temporal series for different level of network clustering	61
2.4.1 Phase diagram and phase portraits for the (deterministic) dy- namics. SOB case	63
2.4.2 Avalanche distributions in the SOB limit	65
2.4.3 Independence of the control parameter in the SOB limit	66

3.2.1 Sketch of the Kuramoto model	83
3.2.2 Phase transition in the Lorentz distribution of natural frequencies	89
3.2.3 Phase portrait in the MF Kuramoto model	89
3.2.4 Phase transition in the uniform distribution of natural frequencies	90
3.2.5 Divergence of the critical point in the Kuramoto-Sakaguchi model	92
3.2.6 Chimera in a torus. From: Abrams and Strogatz (2006) [2] . . .	92
3.3.1 Synchronization transition in an Erdős-Rényi network	95
3.4.1 Degree distribution and adjacency matrix of the human connectome network	96
3.4.2 Kuramoto order parameter running on top of the human connectome network.	97
3.4.3 Variability in the emergent broad regime in the human connectome	98
3.4.4 Reordered adjacency matrix of the human connectome network .	100
3.4.5 Local synchronization in the human connectome.	101
3.4.6 Phase portraits of different hierarchical levels of the human connectome	102
3.4.7 Chimera index measurement in different levels of the human connectome network	103
3.5.1 Sketch of the two block model	108
3.5.2 Solution of the two block model	109
3.5.3 4-block modular network	110
3.5.4 Dendrogram of 4-block modular network	110
3.5.5 Kuramoto order parameter running on top of the 4-moduli network	111
3.5.6 Structural analysis of the 4-block modular network	112
3.5.7 Sketch and graph of a Hierarchic-modular Network	114
3.5.8 Kuramoto model on top of a Hierarchic-modular network	115
3.5.9 Global order parameter in a HMN	116
3.5.10 Slow decay of the activity in a Hierarchic-modular network . .	117
3.6.1 Time series displaying metastability of the global synchronization in the Human Connectome and in HMNs.	119
3.6.2 Attractor surfing in a HMN	120
4.2.1 Relation between branching process and Catalan numbers	137
4.2.2 Time evolution of a standard random walk (RW) and a demographic random walk (DRW)	139
4.2.3 Size-avalanche and duration-avalanche distributions for the undriven demographic random walk	140
4.3.1 Sketch of the Wilson-Cowan model	144
4.3.2 Phase portrait of the Wilson-Cowan model	146
4.3.3 Temporal series showing avalanches under a “balance amplification” condition	149

4.3.4 Histogram of the Σ -signal of one Wilson-Cowan column for different values of the noise amplitude	151
4.3.5 Avalanches for the $(1+\epsilon)$ -dimensional model	153
4.4.1 Phase portrait for the “ <i>balanced</i> ” TM model	155
4.4.2 Temporal series for both cases shown in the above figure	156
5.2.1 Examples of real gene-regulatory networks	170
5.2.2 Sketch of a Boolean network	172
5.2.3 Critical point of an Erdős–Rényi Boolean network	173
5.3.1 Network training sketch	175
5.3.2 Computational tasks	177
5.3.3 Boolean functions modification	179
5.3.4 Deviation of the critical point in noisy RBNs	181
5.4.1 RBN without noise	184
5.4.2 Complexity of different computational tasks	186
5.4.3 Dynamical noise in RBN	187
5.4.4 Structural noise in RBN	189
5.4.5 Size versus mean connectivity for empirical biological networks	191
6.2.1 Subgraph showing particular dependences between packages from Buzz distribution	206
6.2.2 Evolution of the total number of Debian packages across distributions	207
6.2.3 Incoming and outgoing distributions for each Debian distribution	208
6.2.4 Evolution of the modularity index for each Debian distribution	210
6.2.5 Evolution of the three main hierarchies identified in the Debian networks	212
6.2.6 Vulnerability index for the different Debian distributions	213
6.2.7 Total number of packages versus total system size for each Debian distribution	214
6.2.8 Genome size as function of the total number of genes (in log-log scale) for many living things	216
B.1.1 Analysis of the non-truncated TM model	248
B.1.2 Analysis of the Wilson-Cowan model	250
B.2.1 Detrended fluctuation analysis of the macroscopic signal for control parameter	252
B.3.1 Analysis of the structure underlying the avalanche-duration distributions	253
B.3.2 Illustration of the first return time statistics of a Random Walk	254
B.3.3 Analysis of first-passage times in a stochastic process	256
C.1.1 Integration contour	264

E.1.1 Calor específico del *He* en el punto λ 283

E.1.2 Curva de coexistencia líquido-gas para muchos fluidos 284

E.1.3 Una espiral logarítmica emerge para diversos sistemas muy lejanos entre sí 286

E.1.4 Avalanchas neuronales con invariancia de escala 290

E.1.5 Experimentos de inactivación genética 292

List of Tables

1.1	Critical exponents in relation to their physical quantities	18
3.1	Structural properties of the Human Connectome and a synthetic network with four modules	110
4.1	Summary of the avalanche exponents for the RW and the DRW .	142

Introduction to phase transitions and critical phenomena

1.1	The criticality hypothesis	3
1.1.1	Criticality beyond physics	6
1.2	Introduction to phase transitions	15
1.2.1	The Landau-Ginzburg theory of phase transitions . .	15
1.2.2	Dynamical models: non-equilibrium phase transitions	21
1.2.3	Self-organizing mechanisms	25
1.2.4	Griffiths phases: the stretching of criticality	28
	References	30

The criticality hypothesis

“The crisis consists precisely in the fact that the old is dying and the new cannot be born; in this interregnum a great variety of incommensurate phenomena appear.”

A. Gramsci

Let us imagine for a moment that all the fundamental laws of Nature could be fully understood, being reduced to their most basic physical microscopic mechanisms (e.g. elementary particles or the fundamental interactions). Would it be possible to solve any physical problem using such knowledge? We can predict in an effective way the motion of a classical particle confined inside a potential, as well as the motion of two interacting particles, but even the case of the three-body problem –being non-integral– presents serious difficulties. To make matters worse, the usual challenges inherent to statistical physics comprise a vast number of interactions (on the order of 10^{24} , the Avogadro’s number), making it impossible to analytically solve the equation of motion of such systems. Instead of this, drawing from statistical physics, we can tackle such (physical) problems of many components from a macroscopic viewpoint, with observables as the mean density of particles, the magnetization or its variance, together with their response to external stimuli.

Hence, through a probabilistic analysis of large interacting microscopic systems (atoms, electrons...) at *thermodynamic equilibrium*¹, statistical physics explains the phenomenological laws and the (emerging) macroscopic physical properties of matter, outlined in *phases* (e.g. solid or gaseous). Such phases bear little resemblance to the nature of their microscopic components, but show emergent collective properties [3]. These also highlight the level of order (or disorder) of the system, determined by the presence (or absence) of certain symmetries or correlations. For instance, both diamond and graphite, composed entirely by carbon atoms, represent different phases due to the microscopical particular structure –i.e. the inherent symmetry– of the crystal. Similarly, snowflakes and water droplets represent different phases stemming from the level of order of

¹Without macroscopic flows of matter or of energy, that is no more than a coarse simplification of the reality. Most systems found in nature are far from equilibrium, i.e. they are non-equilibrium systems permanently exchanging energy and matter, whose study requires more general concepts.

the system. In this way, statistical physics also account for the changes between states of matter and *phase transitions*, in which symmetries can be spontaneously broken –generating ordered phases– at the macroscopic level, but not at the level of individual components.

Phase transitions take place throughout Nature. In our everyday life, H_2O constitutes the most vivid example of changes between different states of matter (e.g. the melting of ice cubes or boiling water) and the water cycle (involving the exchange of energy among the three forms of water) is crucial to make life on Earth possible. The smart use of a phase transition –at the bases of the steam engine– triggered the industrial revolution ushering in our modern society.

All the usual phase transitions (evaporation, melting or sublimation) are *first-order* or discontinuous transitions taking place in a “mixed-phase regime” with phase coexistence, i.e. during the transition there exist some parts of the system in each macroscopic phase (ice does not instantly turn into liquid water). Additionally, the system conserves a memory that depends on its history, the so-called *hysteresis*. One illustrative case that takes place in the vicinity of such phase transition is the supercooled water, where the liquid water, all of a sudden, under some physical stimuli, turns into ice.

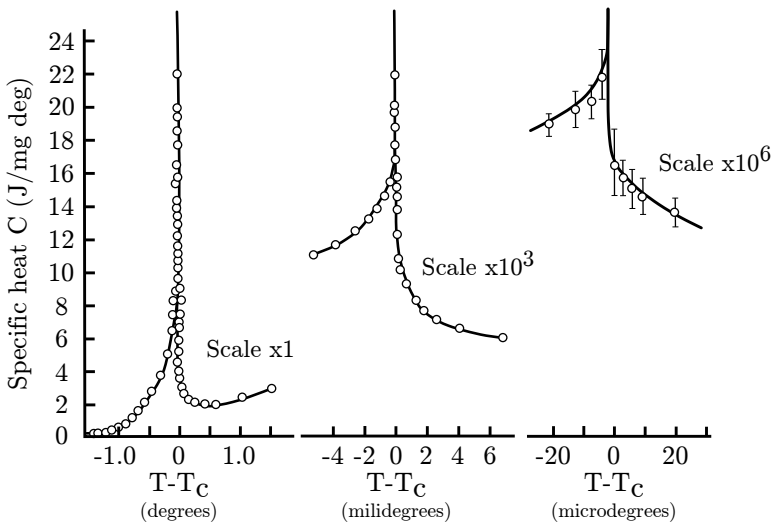


Figure 1.1.1: Energy fluctuations of liquid helium versus the distance to the critical temperature (2.17 K , the so-called Lambda point). At this temperature normal fluid helium becomes in superfluid helium. It should be noted, apart from the divergence, the lack of differences between different scales of temperature, i.e. the scale-invariant behavior around the critical point. Data from [17].

Nevertheless, there are also continuous or *second-order* phase transitions, with no sign of hysteresis (the paradigmatic example is the iron paramagnetic-ferromagnetic transition at the Curie temperature or the superfluid transition of liquid helium, shown in Fig. 1.1.1). They can be distinguished for having long-range correlations (and diverging specific heat), as well as by their distinctive scale-invariant behavior of the relevant observables near the critical point. As example, the dramatic phenomenon of critical opalescence, right at criticality, causes that the normally transparent liquid looks cloudy due to large density fluctuations when the critical temperature is approaching.

✖ **Universality** In continuous phase transitions, the emergent (macroscopic or collective) properties of the system depend on very few parameters (the spatial dimension and the inherent symmetries). If we consider that fluctuations can be neglected (that is conceivably e.g. in high-dimensional scenarios, as will be discussed below), only the symmetries (and their possible changes) play an important role in the macroscopic properties of the system at criticality [11] and, as a corollary to this,

due to the finite nature of the number of relevant parameters, the behavior of many real systems at criticality can be captured from very simple approaches (the Landau theory for systems at equilibrium) and, thus, such systems should share the same *universality class*.

A beautiful, real example of this behavior is shown in Figure 1.1.2, where the liquid-gas coexistence curves of many different fluids –from Ne to CH_4 – collapse in a common curve. It suggests the existence of laws for collective systems beyond micro-details. In this way, the idea of *universality class*, i.e. the fact that many models share the same critical behavior (and thus, emergent properties) independently of their microscopic details, emerges naturally.

The wonder of it all is that, due to their statistical nature, the study and applications of the phenomena associated with phase transitions (or criticality) arising from “pure” physics has permeated many fields far from it: sociology, ecology, neuroscience or earth science. In particular, critical phenomena constitute a starting point to explain or shed light on many poorly understood phenomena –until recently– as the emergence of the Gutenberg–Richter law in earthquakes, neural activity in cortex, solar flares or forest fires, among others [4–6, 12].

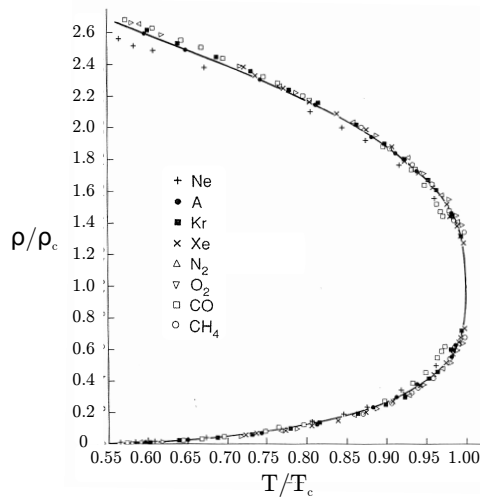


Figure 1.1.2: Liquid-gas coexistence curve for many fluids. The relevant magnitudes, i.e. the order parameter (density) and the control parameter (temperature), have been rescaled by their critical values, collapsing all data into one single universal curve. Observe that the system undergoes a phase transition for some critical temperature (T_c) which clearly depends on the specific compound. Adapted from [11].

1.1.1

Criticality beyond physics

Historically, as discussed for physics, most fields of natural sciences (such as biology, chemistry or earth science, among others) have focused their efforts in a reductionist point of view, assuming that a system is nothing but the sum of its parts, i.e. they have attempted to explain whole systems through the profound behavior of smaller and smaller spatial scales –or organizational units– of individual components and interactions, conforming an orderly framework with the aim of shedding some light on natural phenomena.

However, this point of view poses serious and evident problems to explain and foresee the behavior of systems with a high level of complexity, as living cells, neural networks, ecological trends, snowflakes or to converge with unspoiled fields as social sciences (sociology or economics, for instance). Thus, the important issue of how order can emerge from disorder in living (or natural) systems remained a mystery for a long time (as stated by Schrödinger in “What Is Life? The Physical Aspect of the Living Cell” [58]).

In a seminal work published in 1972 and entitled “More is Different” the Nobel prize Philip Anderson confront by this viewpoint noting that complex systems are irreducible in constituent parts [3].

The ability to reduce everything to simple fundamental laws does not imply the ability to start from those laws and reconstruct the universe. The constructionist hypothesis breaks down when confronted with the twin difficulties of scale and complexity.

This perspective led to look at problems from a global outlook, shifting from the detailed and thorough understanding of the individual components. But the essential question in this case is, how to do so? In particular, in this work Anderson points out that symmetry breaking is a clear example of emergent phenomena. Thus, it is foreseeable that statistical physics –linking microscale and macroscale worlds– and the theory of phase transitions, have a say in all of this.

Examples of collective phenomena (i.e. the emergence of coordinated behavior in large interacting systems) are ubiquitous in nature: swarming is present across a large variety of animal species (flocks of birds, fish stocks, locusts, ant colonies, phytoplankton blooms, krill or myxobacterias). In the same way, different macrostructures emerge for other species (e.g. colonies of ants, mound-building termites, beehives or webs of spiders; see Figure 1.1.3) and massive patterns emerge spontaneously on Earth’s surface (e.g. ripple patterns in sand dunes, the Giant’s causeway or the recently described Namibia’s fairy circles) as long as fractals are ubiquitous our Universe at all scales (from seashells or snowflakes to shorelines or fjords).



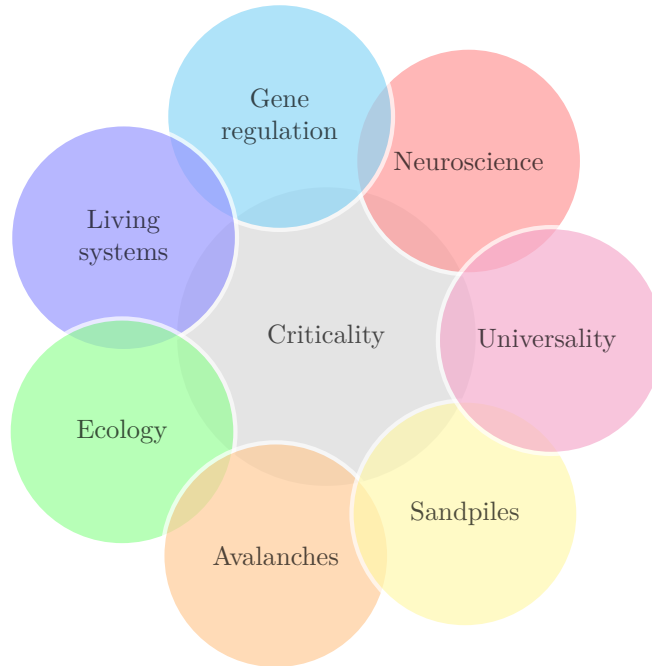
Figure 1.1.3: From left to right: fern frond, Ammonite fossil (*Cleoniceras cleon*), extratropical cyclone near Iceland in 2003 and Whirlpool Galaxy. Even with the myriad of typical scales separating such systems (from *mm* to thousands of light-years) and the inconceivably different physical interactions involved, a massive pattern (a logarithmic spiral) emerges in all of them.

Life is evidently a major source of *complexity* (i.e. emergent phenomena), a common feature that spreads across biology, earth sciences or social sciences; thus, it is to be expected that most systems exhibit (macroscopic) collective behavior with different levels of order (phases) stemming from their (microscopical) components. But, we should emphasize a small –but significant– point, some of them can often show intermediate levels of organization: less structured than a crystal but much more ordered than a random gas, living and natural systems seem to be –under some circumstances– between order and disorder [4, 6, 31, 48], i.e. around a critical point. For instance, biological systems should be resilient against external perturbations (a property of an order phase), but also have enough responsiveness to external stimuli (being disordered, lacking the required robustness and accuracy that biological machinery demands). The *criticality hypothesis* states that the marginal situation between these two impractical tendencies constitutes an optimal compromise and solution, fostering additional benefits, e.g. from long-range correlations.

In this respect, this fine balance between order and disorder has been hypothesized to confer to critical systems a large number of functional advantages such as a large repertoire of dynamical responses, maximal sensitivity to environmental changes, optimal transmission and storage of information as well as to an excellent trade-off between stability and flexibility. This picture that biological systems might extract important functional benefits from operating at criticality, i.e. at the edge of a continuous phase transition, has attracted a lot of recent interest and excitement [1, 4, 46], as well as some skepticism [10, 69].

In the light of the criticality hypothesis, many real examples of inanimate natural phenomena have been understood. For instance, solar flares [12], sand-piles [6], earthquakes [5], rainfall measurements [32], forest fires [40], vortices in superconductors [23] or droplet formation [33], to name but a few, have been reported to exhibit fingerprints of criticality. More recently, with the advent of high-throughput technologies, empirical evidences in living matter have appeared, such as bacterial communities [72], the human hearth [73], networks of living neurons [74], cluster of ants colonies [76], the auditory systems [77] or gene expression [52], along with so many others [48].

It therefore looks as if criticality pervades Nature, spreading its shadow over inanimate matter and living matter. Thus, our main objective here is to look into the criticality hypothesis, extending its horizons through the analysis of (possible) phases and phase transitions in living matter. Our methodology will be based not only on modeling, but also on replicating and contrasting the (sometimes insufficient) empirical findings with the aim of trying to understand more specific quantitative features of living matter.



It should be noted that real biological systems are continuously exchanging energy and matter and thus, it is hard to envision an appropriate description based only on equilibrium tenets (remember that the concepts explored in equilibrium statistical physics are based on thermodynamic equilibrium). Accordingly, the equilibrium tenets have been extended into non-equilibrium descriptions [30, 43] that will be briefly outlined afterward.

However, despite being provocative and charming, such hypotheses appear to be chimerical. Between all possibilities, how can living matter (and natural systems) remain fine-tuned to a particular point? In this context, the theory of self-organized criticality (SOC) provides a framework that explain, without any fine tuning, the prevalence in a critical point. Also, since its very origin, SOC has always been closely linked to the study of the natural phenomena (*“the aim of the science of self-organized criticality is to yield insight into the fundamental question of why nature is complex, not simple, as the laws of physics imply”*, “How Nature Works”, Per Bak [4]), suggesting reasonable explanations to many of the aforementioned examples. We refer to [48, 70] for an extended and recent perspective on further biological systems and a comprehensive summary of the issue.

At this point, we wonder whether the criticality hypothesis can operate in real systems with restless activity. Furthermore, although SOC provides a compelling explanation to the lack of need for fine tuning mechanisms, we ask

ourselves if criticality can be exploited by living matter beyond a single point, in any way. On the other hand, does there exist alternative mechanisms accounting for some empirical findings ascribed to criticality? Is it criticality the optimal evolutionary solution, even in the presence of external perturbations?

Without loss of generality, here we try to shed light on such questions through the study of neural and genetic systems, making use of extensive existing empirical researches, theoretical approaches from complexity sciences, statistical mechanics and stochastic processes as well as extensive computational analysis.

1.1.1.1 Neural dynamics

The mammalian brain consists of myriads of neurons with further connections among them. In particular, an average adult brain comprises $8.6 \cdot 10^{10}$ neurons linked for up to 10^{15} synapses, but also the brain of other animal species like elephants ($\sim 2.57 \cdot 10^{11}$), gray squirrels ($\sim 4.5 \cdot 10^8$) or the naked mole-rat ($\sim 2.7 \cdot 10^7$), possess a formidable number of neurons. Even the human cerebral cortex, that plays a key role in higher order functions as memory, reasoning and abstraction, language or consciousness, has a surprising quantity of neocortical neurons ($\sim 1.6 \cdot 10^{10}$, interestingly enough, a dolphin, the *Globicephala melas* –yielding around $\sim 3.7 \cdot 10^{10}$ – exceeds the case of the human cortex).

However, neuron cells (whose thorough structure are fully understood since the groundbreaking works of Ramón y Cajal, Golgi and others) are capable of generating electrical signals, triggering action potentials, stimulating the outgoing synaptic connections, and propagating the activity to neighboring neurons. It is possible to propose two distinct neural phases: the quiescent one, in which the collective state of neurons are mostly turned off, i.e. activity cannot spread and the active one, in which the collective state of neurons are always turned on, i.e. activity can spread fast. Thus, it would be reasonable to bet that the collective state of neurons cannot be persistently nor quiescent nor active, raising some type of critical phenomena. In fact, it has been noticed that they show irregular outbursts (firing at unison) with certain periods of inactivity, in neuronal cultures *in vitro* and *in vivo*, and deviations in such activity –by excess or by defect– are a signature of diseases as epilepsy, Parkinson’s disease, schizophrenia, or autism [80].

In this respect the important empirical finding of neuronal avalanches by Beggs and Plenz (see Fig. 1.1.4) appears crucial: recorded local field potentials were found to trigger in connection with a large number of neurons, producing collective spikes separated by period of inactivity [9]. Such observation is robust (and universal) across species [54, 61], scales and experimental techniques [9, 44, 67]. The duration and size (total number of spiking neurons) of such

avalanches have been reported to follow a power-law² –suggesting some type of scale-invariant behavior– and obeying finite-size scaling, i.e. its cut-off increase depending on system size. Of course, the paradigm of self-organized criticality –including both conserved and non-conserved variants– has been profusely adopted in neuroscience, and interesting models inspired in SOC have been proposed [15, 38, 45] to account for the empirically observed scale-free avalanches of neuronal activity.

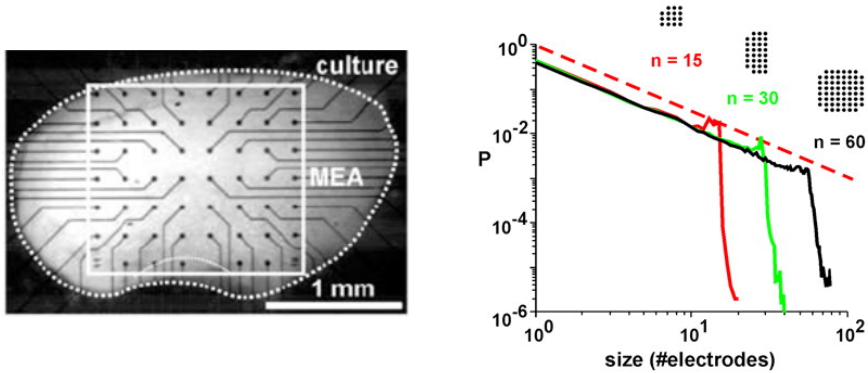


Figure 1.1.4: (left) *In vitro* neuronal culture of rat somatosensory cortex with a microarray monitoring its activity. Black points state electrode positions. (right) Distribution of the total number of network spikes (sizes) separated by periods of inactivity. There is clearly a power law distribution where the cutoff only depends on the total number of electrodes, i.e. the system size, suggesting a scale invariant behavior. Adapted from [9, 53].

From the analysis of brain timeseries, it also has been reported that the cortical activity shows power-laws in the power spectra with the form $1/f$ [39]. This particular decay constitutes an evidence of long-range correlations, and it can be considered as a hallmark of criticality. On the other hand, the dynamic range (related with the susceptibility, i.e. the ability of the system to respond to external stimuli) has been found to be maximal both *in vitro* and *in vivo* in cortical networks with neuronal avalanches [28, 63].

It is important to underline that there is no satisfactory theoretical understanding of why the empirical findings are compatible with branching-process exponents. In particular, it is not clear whether the exponent values appear as a generic consequence of how temporally-defined avalanches are measured (involving thresholding, time binning to discriminate their beginning and end, or

²With the exponents of a mean-field branching process, $\alpha \approx 2$ and $\tau \approx \frac{3}{2}$, for duration and size, respectively.

sub-sampling due to technological and empirical limitations). Therefore alternative explanations have been proposed [69].

Overall, it is usually assumed that the quiescent-to-active phase transition justifies the presence of branching-process exponent values [30, 43]. However, some works have found empirical evidence that scale-free avalanches emerge in concomitance with collective rhythms or neural oscillations [18] in a coherent way, consistent with the edge of a synchronization phase transition [29, 79]. Further explanations relate cortical dynamics to the point of marginal percolation of activity ([67]) or the Ising model ([25]).

Summing up, despite a sufficient number of empirical and theoretical evidences support the critical brain hypothesis, it is still orphan of a compelling theoretical explanation, constituting an open field in which further work is needed.

1.1.1.2 Gene regulatory networks

The last universal common ancestor (LUCA) is the hypothesized living system from which all existing ones descend. Such common venerable ancestor, a single-celled bacteria, of course, that lived from 3.5 to 3.8 billion years ago, is estimated to be composed of 355 inferred genes [75]. Nowadays, the minimal (artificial) bacterial genome (i.e. the set of genes comprising it), a self-replicating bacterium, contains just 437 genes, much smaller, for instance than other bacteria, mammals or plants in nature like *E. Coli* ($\sim 5 \cdot 10^3$ genes), human ($\sim 2.1 \cdot 10^4$ genes) or rice ($\sim 4 - 5 \cdot 10^4$ genes).

Such game board (i.e. the genotype) can show diverse cellular states (phenotypes, resulting from the expression of a fixed genotype). Thus, the simplest bacteria must achieve a complex, intricate dance involving the coordination of thousands of expressing and silencing genes.

Regarding this, Kauffman developed a cutting edge approach considering that cellular states could be identified as attractors of the dynamics of gene networks [36]. In this particular approach, modeling the genes as network nodes linked (in a directed way) by their mutual interactions, it was surmised that poised at the critical point (also called the “edge of chaos”) give the best way to depict real biological networks. In this case, the order phase implies convergence in the dynamics, i.e. the response to external inputs is erased converging on a unique attraction basis (or phenotype) while the disorder phase leads to large divergences and to completely different cellular states. Again, criticality confers an optimal trade-off between being exceedingly ordered/stable and too disordered/noisy [36, 52, 64].

The experimental initiative, however, is rather limited in this issue. Studies based on DNA micro-arrays (measuring and comparing different expression levels in similar cells [22]), as well as gene knock-out experiments (silencing individual genes and following the cascade of differences between two replicas) have

given a few highlights concerning the topic. For example, avalanche size on that gene knock-out experiments [56], as well as the number of affected metabolite ions [26], seems to decay as a power-law with exponent $\tau = 3/2$ (as shown in Figure 1.1.5), compatible with being close to a quiescent/active phase transition. On the other hand, from numerous experiments with micro-arrays there exist different inferred structures, entailing complex networks and showing, in general, an exponential ingoing distribution and a scale-free outgoing distribution ([2]). Through diverse applications of Boolean models on top of such complex structures, across different species of bacteria, it has been found that they might operate very close to criticality [8].

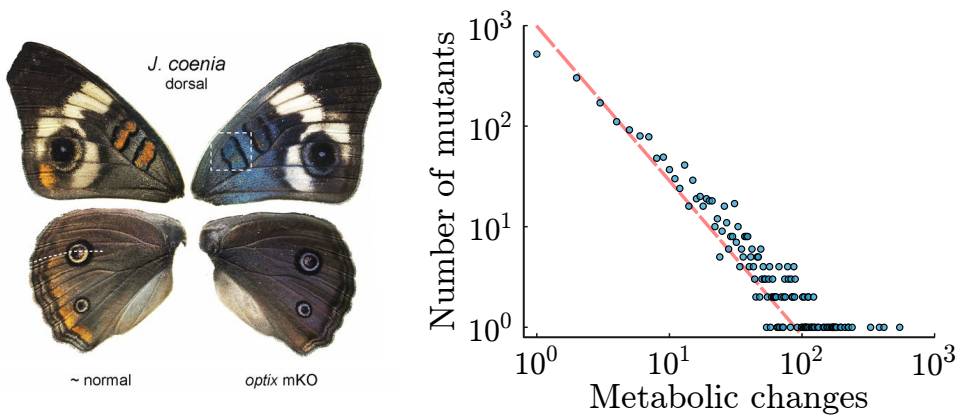


Figure 1.1.5: (left) *optix* gene coordinates (and thus its knock-out drastically changes) the pigment color in the *J. coenia* butterfly. Figure from [82] (right) Total number of metabolite changes for different mutants replica (i.e. with single-gene deletions) of *E. Coli*. It seems to follow a power law distribution with exponent $\tau \approx 3/2$ (the dashed lines are guides to the eye). Data from [26].

Despite being one of the canonical examples of criticality in living systems, as pointed out by Kauffman, there exist important caveats related to the effects (and perils) of thresholding in gene-knockout experiments [48]. Hence, further and better empirical measures and findings in gene knockout experiments are needed, as well as getting larger networks of genes or implementing concrete experiments to measure the dynamic range of genetic systems, all in order to discriminate the possibility that gene-regulatory networks operate indeed in the vicinity of a critical point.

In particular, in this thesis, we try to shed light into some open problems concerning the criticality hypothesis in both fields. Specifically, the development of a minimal model (in the Landau viewpoint) of cortical dynamics able

to combine both avalanches and oscillations in a common perspective and clarify different non-critical methods susceptible to generate power-laws. We also try to understand the effect of real –and modular-complex– cortical networks (the human connectome) in this common perspective (the synchronization paradigm). Finally, we tackle the problem of criticality in Boolean models of gene regulatory networks, in order to understand a little their structural evolutionary process and how external perturbations can affect the machinery of real genetic networks.

As a prelude of all this topics, first it is necessary to expose the Landau theory of critical phenomena, resting in equilibrium tenets, together with a briefly summary of phase transitions, as well as an outline of the non-equilibrium problems studied on subsequent chapters. Thus, familiar readers with these subject areas can skip to the next chapter.

1.2 Introduction to phase transitions

1.2.1

The Landau-Ginzburg theory of phase transitions

The Landau-Ginzburg model is a “meta-model” of phase transitions, i.e. it is a phenomenological theory that unifies many models, ignoring particular microscopic details, and clarify their behavior very close to the critical point. In this spirit, it shows that only very few parameters are needed to characterize the system, namely (i) the dimension of the physical system, d and (ii) the dimension of the order parameter, D [11].

The very heart of this theory is to conceive a quantity describing the energy of the system –at equilibrium– near the critical point, the so-called *Landau free energy*, $\mathcal{F}(\phi)$, where ϕ is the so-called *order parameter* (see the explanatory box). Such free energy, in the absence of external fields, should remain invariant under common relevant symmetries in the Hamiltonian of the system –or in the original microscopic model– at the coarse-grained level³ [51]. So, one of its main points is to forget the microscopic details and to consider just the symmetries.

In particular, as we are interested in the critical point –under the influence of the criticality hypothesis– the order parameter will remains very close to zero and thus, the free energy can be Taylor expanded retaining only the smaller terms. This is no more than the *Landau expansion*,

$$\mathcal{F}(\phi) = \mathcal{F}_0 + h\phi + \frac{a}{2}\phi^2 + \frac{b}{3}\phi^3 + \frac{c}{4}\phi^4 + \dots \quad (1.2.1)$$

where \mathcal{F}_0 is a constant with no influence on the order parameter (and thus, irrelevant). In a particular case⁴ (without loss of generality), it finally reads

$$\mathcal{F}(\phi) = \frac{a}{2}\phi^2 + \frac{b}{3}\phi^3 + \frac{c}{4}\phi^4 + \dots \quad (1.2.2)$$

³For instance, in the case of a system of spins, as the Ising model for ferromagnetism, the magnetization ($m = \langle s_i \rangle$) change it sign, $m \rightarrow -m$ if all the spins are flipped, $s_i \rightarrow -s_i$, i.e. it is invariant under this change. This is a global symmetry that must be present in the free energy, and consequently, being assumed an even function of the magnetization [51].

⁴The absence of external fields imply that $h = 0$, and the fact that the equilibrium state is a minimum of the Landau free energy yields the prescription $(\frac{\partial \mathcal{F}}{\partial \phi})_{\phi=\phi_{eq}} = 0$. Also, the assumption (or definition) of a vanishing order parameter in any of the different phases of the system supports this particular choice.

ORDER PARAMETER

With the aim of developing a quantitative study of phase transitions, it is necessary to identify a measure of the degree of order of the system, the *order parameter*, $\phi(\mathbf{x}, t)$. Normally, it vanishes in one phase (above the critical point) and it is not equal to zero in the other. Examples are the magnetization (local orientation of spins) in a ferromagnetic system or the difference between densities in the liquid-gas transition (many more examples are presented in [11]). Although $\phi(\mathbf{x}, t)$ can fluctuate in space and time in the whole system, sometimes it is only necessary the stationary state of ϕ , i.e. a long-time average at equilibrium. However, we should, obviously, not rule out the fluctuations of ϕ , because they are of vital importance, as will be outlined below.

From a theoretical viewpoint, order parameters stem from symmetry breaking. For instance, in the ferromagnetic-paramagnetic phase transition, below the Curie temperature (acting as the dubbed *control parameter*) the spins align parallel to each other, and above it, the spins are randomly aligned, i.e. they have up-down symmetry due to thermal noise. Another example is the freezing of a fluid, breaking the continuous translational symmetry. Thus, typically, the high-temperature phase has more symmetries than the low-temperature phase or, in other words, the system 'lose' symmetries and is *more ordered*.

Before we go any further, let us make the following considerations,

- The phases of the (equilibrium) system correspond to the different minima of the Landau free energy.
- The symmetries of the order parameter totally jeopardize the presence of the cubic term. For example, if the system has orientational symmetry, only even functions should be considered. Thus, in particular, for the Ising-like models it takes the particular form $\mathcal{F}(\phi) = \frac{a}{2}\phi^2 + \frac{c}{4}\phi^4$.
- To ensure thermodynamic stability, the positivity of the highest term must be imposed. Besides, the free energy could be conditioned if the series expansion is cut down in an odd term—requiring additional considerations—because it would be unbounded from below.
- How many terms should be considered in the series expansion? Fluctuations, directly related with the dimension of the system, set the upper limit [11]. Usually, beyond four dimensions is enough with the ϕ^4 term to maintain the emergent properties unaltered, but careful, all ϕ^n terms are relevant in two dimensions. In conclusion, depending upon the dimension of the system, the Landau theory may lack such irrelevant terms and thus, as soon as the physics is captured, the series can be truncated.

- There exists an upper critical dimension in which the Landau (or the mean-field) theory gives exact predictions, according to the critical properties observed in numerical (or empirical) studies.⁵ For example, this applies for the Ising model (with $d_c = 4$), or a field-theoretical formulation with a term ϕ^3 , related with percolation (with $d_c = 6$) [60].

1.2.1.1 Second-order phase transitions

Let us start discussing the paradigmatic example of a Landau free energy including only the first two even terms (due to symmetries in the coarse-grained level of the system to be studied) that takes the form (see inset of Figure 1.2.1)

$$\mathcal{F}(\phi) = \frac{a}{2}\phi^2 + \frac{c}{4}\phi^4 \quad (1.2.3)$$

By simple differentiation of the free energy, it can be seen that the order parameter (ϕ) that minimizes $\mathcal{F}(\phi)$ satisfies

$$a\phi + b\phi^3 = 0 \Rightarrow \begin{cases} \phi = 0 & \text{if } a \geq 0 \\ \phi^2 = -\frac{a}{b} & \text{if } a < 0 \end{cases} \quad (1.2.4)$$

meaning that, for $a_c = 0$, the system undergoes, in a continuous way, a phase transition and, just below the critical point⁶ $\phi \propto a^{1/2}$ (outlined in Figure 1.2.1). Thus, $\beta = 1/2$ is a *critical exponent* characterizing the growth of the order parameter near the critical point.

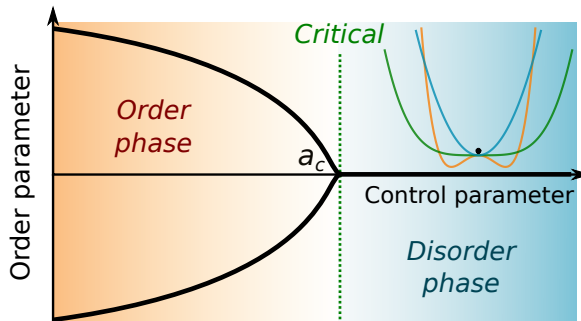


Figure 1.2.1: Sketch of a second order phase transition. The order parameter begins to grow continuously just below the critical point (or in further cases, just above) Inset: Representation of the Landau free energy in the disorder phase (blue), the critical point (green) and the order phase (orange).

⁵If the lowest power of ϕ –after the ϕ^2 term– is of order ϕ^r , it is given by $d_c = \frac{2r}{r-2}$ [11].

⁶Or, more generally, shifting a from the origin, and regarding it as an effective temperature, $\phi \propto (T_c - T)^{1/2}$ just below the critical point.

A wide set of critical exponents describes the physical behavior near a (continuous) second-order phase transition. The possible cases, related with their corresponding physical quantity, are summarized in Table 1.1. In particular, some relevant quantities are the specific heat (c_v , related with the variance of the energy fluctuations) and the susceptibility (the response against external perturbations, χ , related to thermal fluctuations in the order parameter through the fluctuation-dissipation theorem), both showing -almost always- a divergence just at the critical point (and, in the case of the susceptibility, necessarily implies the divergence of the correlation length and thus, the presence of long-range correlations).

Exponent	Definition
α	$c_v \sim T - T_c ^{-\alpha}$
β	$\phi \sim (T_c - T)^\beta$
γ	$\chi \sim T - T_c ^{-\gamma}$
δ	$\phi \sim h^{\frac{1}{\delta}}, h \rightarrow 0$
η	$G(r) \sim 1/r^{d-2+\eta}$
ν	$\xi \sim T - T_c ^{-\nu}$

Table 1.1: Critical exponents in relation to their physical quantities. Together with the growth of the order parameter (ϕ), some quantities such as the specific heat (c_v), the compressibility and the susceptibility (κ , χ), the dependence of the order parameter on the external field (ϕ), the two-point correlation function ($G(r)$) and the correlation length (ξ) has exponents α , β , γ , δ , η and ν , respectively.

A fixed set of critical exponents, universally shared by diverse systems, shape the so-called *universality classes*, in which the same fundamental dynamics emerge. In the particular case of the Eq. (1.2.3), denominated the *mean-field universality class*, the critical exponents are $\beta = 1/2$, $\alpha = 0$, $\gamma = 1$, $\delta = 3$, $\nu = \frac{1}{2}$ and $\eta = 0$, with critical upper dimension $d_c = 4$ (for a proper deduction of the critical exponents we refer to [11]).

A direct consequence of the particular form of the physical quantities around the critical point is the emergence -in the relevant observables- of power law distributions of the form $P(x) \sim x^{-\alpha}$, where α is a positive real number referred to the critical exponents of the system. In this sense, their omnipresence in nature [59] (in particular, remember Figures 1.1.4 and 1.1.5), strongly encouraged to delve into this approach. However, this leads to a necessary but not sufficient condition to ensure that a system is poised at criticality or, in other words, generic power laws are an effect but not a cause of criticality.

Example 1.1 PERCOLATION UNIVERSALITY CLASS

A very special case is one that considers the Landau expansion until the term ϕ^3 , (taking $b > 0$ and $\phi \in (0, +\infty)$ to avoid physical difficulties) giving rise to

$$\mathcal{F}(\phi) = \frac{a}{2}\phi^2 + \frac{b}{3}\phi^3$$

In a straightforward and easy way, one can infer that: (i) it is a second-order phase transition and, (ii) the critical exponents are $\beta = 1$, $\gamma = 1$, $\delta = 2$ and $\alpha = -1$, together with an upper critical dimension $d_c = 6$. Such exponents belong to the so-called *ordinary percolation universality class*. This is because a delicate and cumbersome relation maps the percolation problem, i.e. filtering of fluids through porous materials, onto a $q \rightarrow 1$ Potts model^a [24, 66, 78]. The free energy of its field-theoretical approximation contains a term ϕ^3 leading to those particular values of the critical exponents.

^aIn fact, the Potts model is a generalization of the Ising model with q possible states (and therefore recovering it in the case of $q = 2$). In such case, the free energy [78], for small ϕ , is $\mathcal{F} = \frac{q-1}{2q}(q - \gamma K)\phi^2 - \frac{1}{6}(q-1)(q-2)\phi^3 + \dots$, accounting for the ϕ^3 term. Pay close attention to the vanishing of the ϕ^3 in the $q = 2$ particular case in accordance to the present symmetries in the Ising model.

✖ **Scale invariance** Also a necessary but not sufficient feature to know that a system is in the vicinity of a critical point of a second-order phase transition is the *scale invariance*, i.e. the systems remains –apparently– unchanged if the relevant properties (length, energy, etc.) are rescaled by a common factor, involving a fractal nature [41, 65], and lacking a characteristic scale.

Example 1.2 WHY ARE POWER LAWS SCALE-FREE?

The condition for a general function (or in particular, a probability distribution) to be scale invariant is to fulfill,

$$f(\lambda x) = \lambda^n f(x)$$

or, in other words, to be an homogeneous function. A simple monomial and, by extension, any power law distribution, $P(x) \propto x^{-\alpha}$ with $\alpha > 0$, satisfy such requirement. Likewise, the logarithmic spiral intersects any radii from the origin at distances which are in geometric progression, and thus, increase its size geometrically, being scale invariant.

In conclusion, second-order phase transitions have some very interesting features which we proceed to list. Just in the critical point, the system experiences a symmetry breaking, where the ergodicity is broken (i.e. it is confined in a subregion of the phase space), the susceptibility diverges producing long-range correlations and their relevant properties are scale-invariant or fractal, which is reflected in power law distributions.

1.2.1.2 First-order phase transitions

Let us now come back and take the whole Landau free energy until the ϕ^4 term,

$$\frac{\mathcal{F}(\phi)}{\beta} = \frac{a}{2}\phi^2 + \frac{b}{3}\phi^3 + \frac{c}{4}\phi^4 \quad (1.2.5)$$

with, for simplicity, the particular choice of $c = 1$ (fulfilling $c > 0$ as previously discussed). Now, the order parameter increases as,

$$\begin{cases} \phi = 0 & a > 0 \\ \phi = \frac{-b \pm \sqrt{b^2 - 4a}}{2} & a \leq 0 \end{cases} \quad (1.2.6)$$

clearly distinguishing two possible cases for $b > 0$ and $b < 0$. In the first one, the order parameter grows continuously just after the critical point, leading to a *second-order* phase transition. Conversely, if $b > 0$ there exists a discontinuous jump between the state with $\phi = 0$ and its value in the emergent new phase (see Figure 1.2.2) leading to a discontinuous or *first-order* phase transition. In short, the nature of the phase transition only depends on the sign before the ϕ^3 term. In the second scenario, always exists a local minimum of $\mathcal{F}(\phi)$ in the order phase leading to a bistable behavior, i.e. two local minima coexist (as stated in the inset of Figure 1.2.2) and the system can remain trapped in both, leading to the so-called hysteresis effects, and running away by the influence of thermal fluctuations. The special point at which two local minima coexist and have the same value (or depth of \mathcal{F}) is usually called the *Maxwell point*.

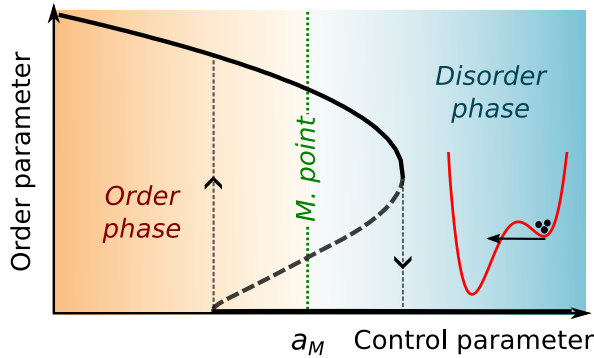


Figure 1.2.2: Sketch of a first-order phase transition. The order parameter grows discontinuously just below the Maxwell point (or in further cases, just above) Inset: Representation of the Landau free energy after the Maxwell point with a deeper second state with non-zero value of the order parameter (red).

1.2.2

Dynamical models: non-equilibrium phase transitions

As stated in the latter free energy (see inset of Figure 1.2.2), it can happen that the deterministic evolution of the system does not sample the whole ensemble of available states. To cope with the problem, it can be introduced some source of randomness, mimicking thermal fluctuations, which are a sign of the temperature allowing the system to wander around all the possible states, in the same way as in the Boltzmann distribution.

Thus, a *Langevin equation* for the dynamical evolution of the order parameter, $\phi(\mathbf{x}, t)$, could be considered⁷, constituting the first example of a stochastic differential equation (SDE) with additive noise [11, 16],

$$\frac{\partial \phi}{\partial t} = - \underbrace{\frac{\delta \mathcal{F}(\phi)}{\delta \phi}}_{A(\phi)} + C \xi(\mathbf{x}, t) \quad (1.2.7)$$

where $\mathcal{F}(\phi)$ is the Landau free energy, and $\xi(\mathbf{x}, t)$ is a zero-mean delta-correlated Gaussian noise with $\langle \xi(t) \rangle = 0$ and $\langle \xi(t) \xi(t') \rangle = \frac{\sigma^2}{2} \delta(t - t')$.

⁷Also, in order to account for spatial effects, the coupling between j neighbors is described by the leading-order term containing derivatives (i.e. finite differences) of the activity between any pair of coupled nodes, i.e. by adding a diffusion term $D \nabla^2 \phi_i \equiv D \sum_j (\phi_j - \phi_i)$ and thus, leading to $\frac{\partial \phi}{\partial t} = \nabla^2 \phi - \frac{\partial V(\phi)}{\partial \phi} + \xi(\mathbf{x}, t)$.

It is equivalent⁸ to the so-called *Fokker-Planck equation* [27, 68, 71], i.e. a dynamical equation for the probability of being in a specific location of the phase space, that takes the form

$$\dot{P}(\phi, t) = -\frac{\partial}{\partial \phi} A(\phi) P(\phi, t) + \frac{1}{2} \frac{\partial^2}{\partial \phi^2} C^2 P(\phi, t) \quad (1.2.8)$$

An essential property, however, that need to be met in order to ensure that a system are at equilibrium, is the detailed balance condition: *each elementary process –at equilibrium– should be equilibrated by its reverse process*. That is to say, if the transitions $\alpha \rightarrow \alpha'$ between different states are to be considered, through the transition probability per time (i.e. the transition rates $W(\alpha \rightarrow \alpha')$), the following condition must be fulfilled

$$\frac{W(\alpha \rightarrow \alpha')}{W(\alpha' \rightarrow \alpha)} = \frac{p_\alpha}{p_{\alpha'}} \quad (1.2.9)$$

where p_α ($p_{\alpha'}$) is the probability density⁹ –at equilibrium– for the occurrence of state α (α').

In this respect, in non-equilibrium problems, such condition is broken and (mostly) the Landau free energy will not exist [30, 43]. But, it is yet possible (and necessary) to employ stochastic process techniques such as the Master equation, the Fokker-Planck or the Langevin equation (for a detailed discussion on the matter we refer to [27, 71]). In any case, they exhibit similar features –with extra degrees of freedom– to the equilibrium phase transitions (like an existence of shared and enhanced universality classes), although their in-depth analysis requires of further analytical techniques.

Coming back to the ϕ^4 -Landau theory, we can raise the Langevin equation,

$$\dot{\phi} = -a\phi - b\phi^2 - c\phi^3 + \xi(x, t) \quad (1.2.10)$$

In a nutshell, two archetypical dynamical equations –depending on the sign of b – have resulted for both, first and second-order phase transitions, fostering their dynamical study and opening a wide and fascinating new field.

⁸In the Itô sense, equivalent to a Stratonovich one for additive noise but not for multiplicative noise [27, 71]. Although there exists an equivalence between both treatments, the modeling of phenomena, in the Itô or Stratonovich sense, yields different solutions, giving rise to the Itô-Stratonovich dilemma (a discussion on this issue is addressed in the appendix A.1).

⁹Usually, the Gibbs probability distribution $p_\alpha \sim e^{-\frac{E_\alpha}{k_B T}}$, where E_α is the state energy.

✳ **On the origin of inherent noise** A prime example of a non-equilibrium problem arise from the microscopical reactions for the *contact process* describing the propagation of activity (which is in substance similar to a *birth-death process* [27]). For that purpose, on the basis of the *Master equation* for a Markov process [27, 71], and given the microscopic probabilistic rules for the transitions in the system, it is possible to set up a probabilistic description of it.

Let us consider the following microscopical rules (summarized in Figure 1.2.3):

- i) A site of our network/lattice, of size N , can be active (A) or inactive (I)
- ii) If the site is in the active state, it can be inactivated or activate a random neighbor (provided it is inactive), with rates μ and λ , respectively.

$$\begin{cases} A \xrightarrow{\lambda} A + 1 \\ A \xrightarrow{\mu} A - 1 \end{cases}$$

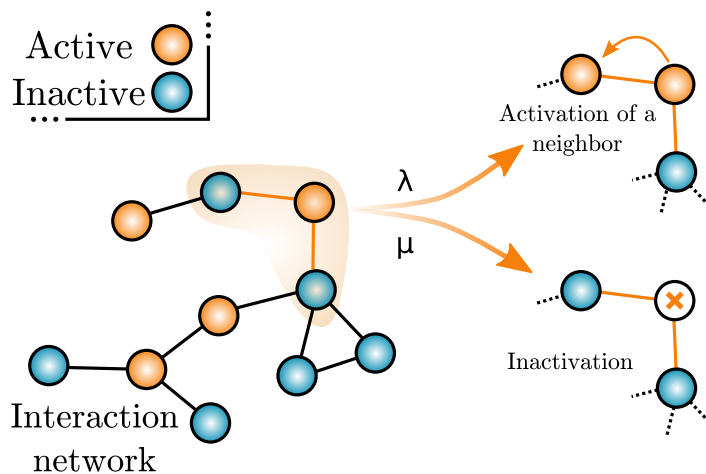
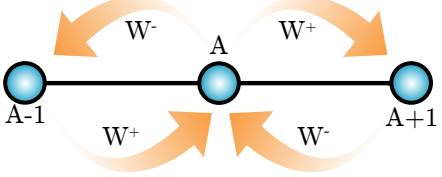


Figure 1.2.3: Sketch of the contact process dynamics. Each node is in an active or an inactive state and active nodes can be inactivated (at rate μ) or propagate their activity to a non-active neighbor (at rate λ). Observe that the underlying structure, a complex network, is heterogeneous rather than a regular lattice.

From both simple microscopical rules it is possible –resting upon probability conservation– to employ the master equation to propose a dynamical equation for the probability of having A active sites at time t ,

$$\frac{dP_A(t)}{dt} = W_{A-1}^+ P_{A-1}(t) + W_{A+1}^- P_{A+1}(t) - W_A^+ P_A(t) - W_A^- P_A(t)$$


where W_A^+ , W_A^- are the transition rates, i.e. the transition probabilities per unit time from a state with A active nodes to other with $A + 1$ (or $A - 1$), which in the present case, the contact process¹⁰, are $W_A^+ = \lambda A \left(1 - \frac{A}{N}\right)$ and $W_A^- = \mu A$.

This equation can be rewritten in terms of the macroscopical density of active states, $\rho(t) = \frac{A(t)}{N}$, at time t

$$\frac{1}{N} \frac{\partial P(\rho, t)}{\partial \rho} = w^+ \left(\rho - \frac{1}{N}\right) P\left(\rho - \frac{1}{N}, t\right) + w^- \left(\rho + \frac{1}{N}\right) P\left(\rho + \frac{1}{N}, t\right) - w^+(\rho) P(\rho, t) - w^-(\rho) P(\rho, t)$$

where $w^+(\rho) = \frac{W_A^+}{N} = \lambda \rho (1 - \rho)$ and $w^-(\rho) = \frac{W_A^-}{N} = \mu \rho$ are the rescaled transition rates as function of the population density of active nodes rather than the total number of active nodes.

Solve the problem analytically may be a long and hard path. Thus, instead of find and analytical solution, it could be easily scrutinized through the Fokker-Planck approximation employing the Van Kampen's expansion [71] (also known as the Ω -expansion, the limit of small jumps, i.e. the Taylor expansion¹¹ in a –large– system of size Ω),

$$\begin{aligned} \frac{\partial P(\rho, t)}{\partial t} = & -\frac{\partial}{\partial \rho} \left\{ [w^+(\rho) - w^-(\rho)] P(\rho, t) \right\} \\ & + \frac{1}{2N} \frac{\partial^2}{\partial \rho^2} \left\{ [w^+(\rho) + w^-(\rho)] P(\rho, t) \right\} + \mathcal{O}\left(\frac{1}{N^2}\right) \end{aligned}$$

¹⁰It is possible to activate λI nodes, as long as such node is a neighbor of an active node in the lattice, $\frac{A}{N}$. Thus, $W_A^+ = \lambda \frac{A}{N} I = \lambda A \left(1 - \frac{A}{N}\right)$.

¹¹Up to second order, $P\left(\rho \pm \frac{1}{N}, t\right) = P(\rho, t) \pm \frac{1}{N} \partial_\rho P(\rho, t) + \frac{1}{2N^2} \partial_\rho^2 P(\rho, t)$.

which mapped in a Langevin equation –grouping terms for small ρ – becomes,

$$\dot{\rho} = -\mu\rho + \lambda\rho(1 - \rho) + \sqrt{\rho}\xi(t) \quad (1.2.11)$$

including a *multiplicative noise* term ($\sqrt{\rho}$) depending on the state of the system, being $\xi(\mathbf{x}, t)$ a zero-mean delta-correlated Gaussian noise. In this case, a second-order phase transition¹² emerges for the marginal situation with $\lambda = \mu$.

The multiplicative noise term vanishes if $\rho = 0$ and, as a result, the system can get trapped¹³ into the so-called *absorbing state* for any finite value of N . Thus, the system presents an analogous phase diagram to the one shown in Figure 1.2.1, but with *absorbing* and *active* phases, and it explains, for example, the spreading of infectious diseases. In order to avoid such a situation, a spontaneous creation of particles can be introduced, disturbing as little as possible the original system, to extricate itself of the absorbing state. Observe, also, that in the case with additive white noise, although a vanishing order parameter exists in the deterministic case, the description of *absorbing phase* is not accurate since the system is able to fluctuate and reach values of $\rho \neq 0$.

1.2.3

Self-organizing mechanisms

✖ **Self-organized criticality (SOC)** Many biological and natural systems, as earthquakes, solar flares, vortices in superconductors, forest fires, epidemics or neuronal avalanches of activity, among others [6, 12, 23, 38, 40], show features of criticality, as if they had been carefully tuned to dwell in the vicinity of a phase transition. The theory of self-organized criticality (SOC) –started to be developed 30 years ago– explains how systems can become self-organized to the edge of a continuous phase transition, i.e. to the vicinity of a critical point characterized by scale-free avalanches of activity, without the apparent need of parameter fine tuning [4, 6, 20, 55]. This theory (or mechanism) is often invoked to explain the emergence of scale-free distributed bursts of activity interspersed by periods of quiescence in very diverse settings, covering both inanimate and living systems.

The mechanism for self-organization (as exemplified by its most paradigmatic examples, i.e. the sandpile models [6, 19, 42]) relies on a couple of essential features. The first one is the presence of two infinitely separated timescales: one characterizes the fast dynamics of the system activity (ρ), while the slow one controls the dynamics of the background field (E , which, acting as an effective

¹²Due to the minus sign in front of λ , coming along with ρ^2 . It is easy to see that, if we wish to obtain a first-order phase transition, such a term should be positive and another additional term proportional to $+\rho^3$ must appear, leading to $\dot{\rho} = a\rho + b\rho^2 - c\rho^3 + \sqrt{\rho}\xi(t)$.

¹³Constituting essentially a non-equilibrium problem [21, 30, 43], because the “detailed balance” condition is blatantly violated.

order parameter, creates a feedback loop which is ultimately responsible for the self-organization to the edge of a phase transition [20]). This energy variable¹⁴ fosters the creation of activity through different possibilities, e.g. by taking into account an equation $\dot{E} = h - \epsilon\rho$, in the limit $h, \epsilon \rightarrow 0$ with $\frac{h}{\epsilon} \rightarrow 0$, or increasing E and ρ at some point with a fixed amount (when the system has fallen into the absorbing state), until an avalanche is triggered. A second important feature is that the dynamics is conserved (i.e. dissipation can only occur at the system boundaries), even if SOC models lacking conservation –as exemplified by fire forest models, earthquake models, etc.– have also a long tradition in the field. The main difference is that while conserved mechanisms drive the dynamics exactly to the critical point, non-conserved ones generate an effective dynamics which wanders around the critical point, with excursions to both sides of the transition point but not sitting exactly on it (see [14] and references therein).

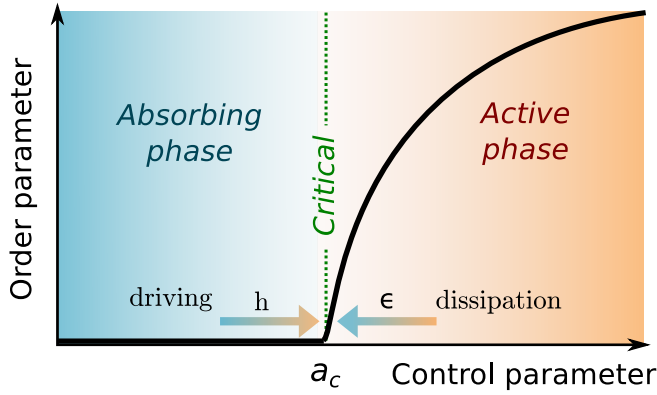


Figure 1.2.4: Self organization to the critical point leading to the emergence of criticality in a natural way in conserved systems. Two forces acts over the system, namely the driving (h), predominating in the absorbing phase, and the dissipation (ϵ), of growing relevance when the activity is triggered and an avalanche invades and propagates across the system.

In SOC systems, the phase transition is described employing the next set of Langevin equations with spatial coupling and noise,

$$\begin{cases} \dot{\rho}_i(t) = [-a + E(t)]\rho_i(t) - b\rho_i^2(t) + D\nabla^2\rho_i(t) + \sigma^2\eta_i(t) \\ \dot{E}_i(t) = D\nabla^2\rho_i(t) \end{cases}$$

where $\eta_i(t)$ is a Gaussian white noise term, with $\langle \eta_i(t)\eta_j(t') \rangle = \rho_i(t)\delta(t-t')\delta_{ij}$, ρ and E are fields, a and b are positive constant parameters, D and σ^2 are diffusion and noise constants, and $\nabla^2\rho_i \equiv \sum_j(\rho_j - \rho_i)$ stands for the diffusive coupling between each unit i and its neighbors j .

¹⁴In particular, for sandpiles, is the total number of sand grains.

✖ **Self-organized bistability (SOB)** A mechanism similar in spirit to SOC has been discovered to be able to self-organize systems exhibiting a discontinuous phase transition to its very edge, i.e. to the (Maxwell) point of bistability of two alternative phases. Indeed, self-organized bistability (SOB) has been proposed as a new and very general paradigm for the organization to points of bistability. In this case, avalanches turn out to be bimodal, i.e. their sizes and times distributions consist of a power-law complemented with a bump, corresponding to frequent anomalously large events [57]. Such a theory –relying also on conservation and on infinitely separated timescales, with the same dynamics for the energy field (E)– offers a simple explanation for why some real sandpiles (the archetype of SOC) are empirically observed to exhibit deviations from perfect scaling behavior, showing huge avalanches in a quasi-periodic fashion together with smaller scale-free ones [57, 81].

In SOB systems, the phase transition is described employing the next set of Langevin equations with spatial coupling and noise¹⁵,

$$\begin{cases} \dot{\rho}_i(t) = [-a + E(t)]\rho_i(t) + b\rho_i^2(t) - c\rho_i^3(t) + D\nabla^2\rho_i(t) + \sigma^2\eta_i(t) \\ \dot{E}_i(t) = D\nabla^2\rho_i(t) \end{cases}$$

where $\eta_i(t)$ is a Gaussian white noise term, with $\langle\eta_i(t)\eta_j(t')\rangle = \rho_i(t)\delta(t-t')\delta_{ij}$, ρ and E are fields, a , b , c are positive constant parameters, D and σ^2 are diffusion and noise constants, and $\nabla^2\rho_i \equiv \sum_j(\rho_j - \rho_i)$ stands for the diffusive coupling between each unit i and its neighbors j .

1.2.3.1 Avalanches

All systems with absorbing states share the common feature of exhibiting avalanche-like behavior, meaning that if the absorbing state is perturbed by a localized seed of activity, this can trigger a cascade of events before falling back again into the absorbing state¹⁶. It is common knowledge that avalanches turn out to be scale invariant at critical points; in particular, the avalanche-size (S) and avalanche-duration (T) probability distribution functions can be written at criticality as

$$\begin{aligned} P(S) &\sim S^{-\tau}\mathcal{G}_S(S/S_C) \\ P(T) &\sim T^{-\alpha}\mathcal{G}_T(T/T_C), \end{aligned} \quad (1.2.12)$$

where $\mathcal{G}_S(S/S_C)$ and $\mathcal{G}_T(T/T_C)$ are cut-off functions, and the cut-off scales, S_C and T_C , depend only on system size right at the critical point, and on the distance to criticality away from it [35].

¹⁵An additional cubic term (whose need has been widely discussed in the Landau theory of phase transitions) is included to avoid divergences, i.e. the case $\rho \rightarrow \infty$.

¹⁶An extended discussion on how avalanches should be measured is discussed in later chapters and, specifically, in appendix B.3.2.

Similarly, the averaged avalanche size scales with the duration as $\langle S \rangle \sim T^\gamma$, where the exponent γ needs to obey the scaling relation [7, 62],

$$\gamma = \frac{\alpha - 1}{\tau - 1}. \quad (1.2.13)$$

For the particular cases concerned here, SOC and SOB, for avalanches propagating in high dimensional systems (or in densely connected networks) mean-field exponent values take the value $\tau \approx 1.26$, $\alpha \approx 1.48$, $\gamma \approx 1.84$ and $\tau = 3/2$, $\alpha = 2$, $\gamma = 2$, respectively. A compilation of avalanche exponents for different dimensions and universality classes, as well as scaling relationships, can be found in [13, 34, 37, 49].

1.2.4

Griffiths phases: the stretching of criticality

The two possible transitions that has just been explained lie in homogeneous or mean-field systems. However, it is not surprising to sight in nature heterogeneous systems, in contrast with homogeneous regular lattices. In particular, one can imagine the so-called *quenched disorder* that stems from inhomogeneities in the system and microscopical effects (that are considered frozen in time) as, e.g. infection rates, activity propagation, population density in neuronal cultures, etc. Another possibility is the *topological disorder* that generates isolated, highly connected or modular structures (see lower panel of Figure 1.2.5, it is worth noting the real case of the human brain connectome network). In both cases –*quenched disorder* and *topological disorder*– the usual critical point separating the absorbing and the active phase can be altered and stretched generating *rare active regions* [47, 50], even if the system is globally in the absorbing phase (see upper panel of Figure 1.2.5). This critical-like phase is called a *Griffiths phase* and can be very relevant in inhomogeneous biological systems [47, 48, 50].

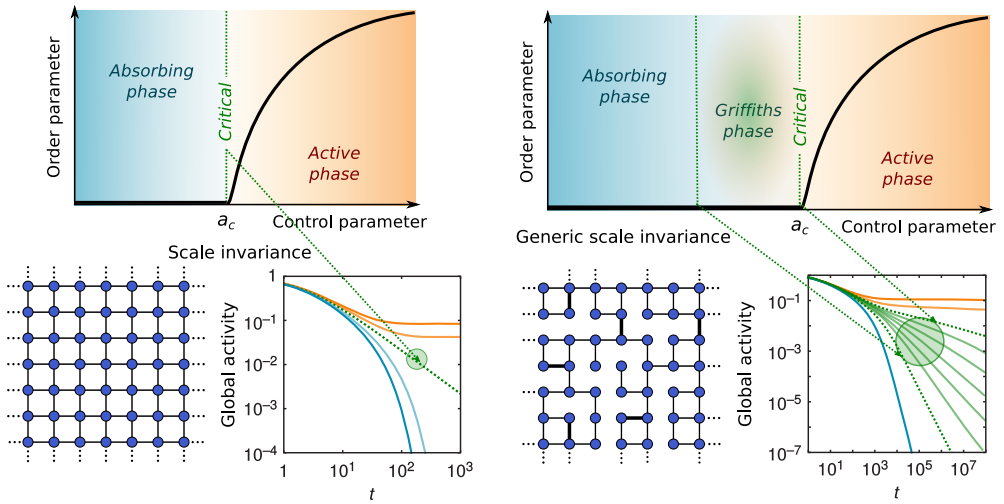


Figure 1.2.5: Phase transition in homogeneous (left) and heterogeneous (right) systems separating the absorbing phase and the active one. Observe the inhomogeneities present in the lattice, although a large amount of local properties and possible networks can be considered. A Griffiths phase can emerge in the neighborhood of the phase transition of such systems. In the Griffiths phase, some critical-like features emerge, as a power-law decay to the stationary state of the global activity[47].

References

- [1] ADAMI, C. «Self-organized criticality in living systems». *Phys. Lett. A* **203**, 29–32 (1995).
- [2] ALDANA, M. «Boolean dynamics of networks with scale-free topology». *Physica D* **185**, 45–66 (2003).
- [3] ANDERSON, P. W. *et al.* «More is different». *Science* **177**, 393–396 (1972).
- [4] BAK, P. *How nature works: the science of self-organized criticality* (Copernicus, New York, 1996).
- [5] BAK, P. & TANG, C. «Earthquakes as a self-organized critical phenomenon». *J. Geophys. Res.* **94**, 15635 (1989).
- [6] BAK, P., TANG, C. & WIESENFELD, K. «Self-organized criticality: An explanation of the $1/f$ noise». *Phys. Rev. Lett.* **59**, 381 (1987).
- [7] BALDASSARRI, A., COLAIORI, F. & CASTELLANO, C. «Average shape of a fluctuation: Universality in excursions of stochastic processes». *Phys. Rev. Lett.* **90**, 060601 (2003).
- [8] BALLEZA, E. *et al.* «Critical dynamics in genetic regulatory networks: examples from four kingdoms». *PLoS One* **3**, e2456 (2008).
- [9] BEGGS, J. M. & PLENZ, D. «Neuronal avalanches in neocortical circuits». *J. Neurosci.* **23**, 11167–11177 (2003).
- [10] BEGGS, J. M. & TIMME, N. «Being critical of criticality in the brain». *Front. Physiol.* **3** (2012).
- [11] BINNEY, J. J., DOWRICK, N. J., FISHER, A. J. & NEWMAN, M. *The theory of critical phenomena: an introduction to the renormalization group* (Oxford University Press, Oxford, 1992).
- [12] BOFFETTA, G., CARBONE, V., GIULIANI, P., VELTRI, P. & VULPIANI, A. «Power laws in solar flares: self-organized criticality or turbulence?». *Phys. Rev. Lett.* **83**, 4662 (1999).
- [13] BONACHELA, J. *Universality in self-organized criticality*. Ph.D. thesis, Ph. D. Thesis, University of Granada, Granada, Spain (2008).
- [14] BONACHELA, J. A. & MUÑOZ, M. A. «Self-organization without conservation: true or just apparent scale-invariance?». *J. Stat. Mech.* P09009 (2009).

-
- [15] BONACHELA, J., DE FRANCISCIS, S., TORRES, J. & MUÑOZ, M. A. «Self-organization without conservation: are neuronal avalanches generically critical?». *J. Stat. Mech. Theory Exp.* **2010**, P02015 (2010).
- [16] BRAY, A. J. «Theory of phase-ordering kinetics». *Adv. Phys.* **51**, 481–587 (2002).
- [17] BUCKINGHAM, M. & FAIRBANK, W. «Chapter III: The Nature of the λ -Transition in Liquid Helium». *Progress in Low Temperature Physics* **3**, 80–112 (1961).
- [18] BUZSAKI, G. *Rhythms of the Brain* (Oxford University Press, Oxford, 2006).
- [19] CHRISTENSEN, K., CORRAL, A., FRETTE, V., FEDER, J. & JØSSANG, T. «Tracer Dispersion in a Self-Organized Critical System». *Phys. Rev. Lett.* **77**, 107–110 (1996).
- [20] DICKMAN, R., MUÑOZ, M. A., VESPIGNANI, A. & ZAPPERI, S. «Paths to self-organized criticality». *Braz. J. Phys.* **30**, 27–41 (2000).
- [21] DORNIC, I., CHATÉ, H. & MUÑOZ, M. A. «Integration of Langevin equations with multiplicative noise and the viability of field theories for absorbing phase transitions». *Phys. Rev. Lett.* **94**, 100601 (2005).
- [22] EISEN, M. B., SPELLMAN, P. T., BROWN, P. O. & BOTSTEIN, D. «Cluster analysis and display of genome-wide expression patterns». *Proc. Natl. Acad. Sci. USA* **95**, 14863–14868 (1998).
- [23] FIELD, S., WITT, J., NORI, F. & LING, X. «Superconducting vortex avalanches». *Phys. Rev. Lett.* **74**, 1206 (1995).
- [24] FORTUIN, C. M. & KASTELEYN, P. W. «On the random-cluster model: I. Introduction and relation to other models». *Physica* **57**, 536–564 (1972).
- [25] FRAIMAN, D., BALENZUELA, P., FOSS, J. & CHIALVO, D. R. «Ising-like dynamics in large-scale functional brain networks». *Phys. Rev. E* **79**, 061922 (2009).
- [26] FUHRER, T., ZAMPIERI, M., SÉVIN, D. C., SAUER, U. & ZAMBONI, N. «Genomewide landscape of gene–metabolome associations in *Escherichia coli*». *Mol. Sys. Biol.* **13**, 907 (2017).
- [27] GARDINER, C. W. *Handbook of stochastic methods: for physics, chemistry and the natural sciences; 3rd ed.* Springer Series in Synergetics (Springer, Berlin, 2004).

- [28] GAUTAM, S. H., HOANG, T. T., MCCLANAHAN, K., GRADY, S. K. & SHEW, W. L. «Maximizing sensory dynamic range by tuning the cortical state to criticality». *PLoS Comp. Biol.* **11**, e1004576 (2015).
- [29] GIREESH, E. D. & PLENZ, D. «Neuronal avalanches organize as nested theta- and beta/gamma-oscillations during development of cortical layer 2/3». *Proc. Natl. Acad. Sci. USA* **105**, 7576–7581 (2008).
- [30] HENKEL, M., HINRICHSSEN, H. & LÜBECK, S. *Non-equilibrium phase transitions. Volume 1: Absorbing Phase Transitions* (Springer, Dordrecht, 2008).
- [31] HIDALGO, J. *et al.* «Information-based fitness and the emergence of criticality in living systems». *Proc. Natl. Acad. Sci. USA* **111**, 10095–10100 (2014).
- [32] PETERS, O., HERTLEIN, C. & CHRISTENSEN, K. «A complexity view of rainfall». *Phys. Rev. Lett.* **88**, 018701 (2001).
- [33] PLOURDE, B., NORI, F. & BRETZ, M. «Water droplet avalanches». *Phys. Rev. Lett.* **71**, 2749 (1993).
- [34] HUYNH, H. N. & PRUESSNER, G. «Abelian Manna model in three dimensions and below». *Phys. Rev. E* **85**, 061133 (2012).
- [35] KADANOFF, L. P., NAGEL, S. R., WU, L. & ZHOU, S.-M. «Scaling and universality in avalanches». *Phys. Rev. A* **39**, 6524 (1989).
- [36] KAUFFMAN, S. A. «The origins of order: Self-organization and selection in evolution». In *Spin Glasses and Biology*, 61–100 (World Scientific, 1993).
- [37] LÜBECK, S. «Universal scaling behavior of non-equilibrium phase transitions». *Int. J. Mod. Phys. B* **18**, 3977–4118 (2004).
- [38] LEVINA, A., HERRMANN, J. M. & GEISEL, T. «Dynamical synapses causing self-organized criticality in neural networks». *Nat. Phys.* **3**, 857–860 (2007).
- [39] LINKENKAER-HANSEN, K., NIKOULINE, V. V., PALVA, J. M. & ILMONIEMI, R. J. «Long-range temporal correlations and scaling behavior in human brain oscillations». *J. Neurosci.* **21**, 1370–1377 (2001).
- [40] MALAMUD, B. D., MOREIN, G. & TURCOTTE, D. L. «Forest fires: an example of self-organized critical behavior». *Science* **281**, 1840–1842 (1998).

-
- [41] MANDELBROT, B. B. & PIGNONI, R. *The fractal geometry of nature* (WH Freeman, San Francisco, 1983).
- [42] MANNA, S. S. «Two-state model of self-organized criticality». *J. Phys. A: Math. Gen.* **24**, L363–L369 (1991).
- [43] MARRO, J. & DICKMAN, R. *Nonequilibrium phase transitions in lattice models* (Cambridge University Press, Cambridge, 2005).
- [44] MEISEL, C., OLBRICH, E., SHRIKI, O. & ACHERMANN, P. «Fading signatures of critical brain dynamics during sustained wakefulness in humans». *J. Neurosci.* **33**, 17363–17372 (2013).
- [45] MILLMAN, D., MIHALAS, S., KIRKWOOD, A. & NIEBUR, E. «Self-organized criticality occurs in non-conservative neuronal networks during ‘up’ states». *Nat. Phys.* **6**, 801–805 (2010).
- [46] MORA, T. & BIALEK, W. «Are biological systems poised at criticality?». *J. Stat. Phys.* **144**, 268–302 (2011).
- [47] MORETTI, P. & MUÑOZ, M. A. «Griffiths phases and the stretching of criticality in brain networks». *Nat. Comm.* **4** (2013).
- [48] MUÑOZ, M. A. «Colloquium: Criticality and dynamical scaling in living systems». *arXiv preprint arXiv:1712.04499* (2017).
- [49] MUÑOZ, M. A., DICKMAN, R., VESPIGNANI, A. & ZAPPERI, S. «Avalanche and spreading exponents in systems with absorbing states». *Phys. Rev. E* **59**, 6175 (1999).
- [50] MUÑOZ, M. A., JUHÁSZ, R., CASTELLANO, C. & ÓDOR, G. «Griffiths phases on complex networks». *Phys. Rev. Lett.* **105**, 128701 (2010).
- [51] NISHIMORI, H. & ORTIZ, G. *Elements of phase transitions and critical phenomena* (Oxford University Press, Oxford, 2010).
- [52] NYKTER, M. *et al.* «Gene expression dynamics in the macrophage exhibit criticality». *Proc. Natl. Acad. Sci. USA* **105**, 1897–1900 (2008).
- [53] PAJEVIC, S. & PLENZ, D. «Efficient network reconstruction from dynamical cascades identifies small-world topology of neuronal avalanches». *PLoS Comp. Biol.* **5**, e1000271 (2009).
- [54] PETERMANN, T. *et al.* «Spontaneous cortical activity in awake monkeys composed of neuronal avalanches». *Proc. Natl. Acad. Sci. USA* **106**, 15921–15926 (2009).

- [55] PRUESSNER, G. *Self-organized criticality* (Cambridge Univ. Press, Cambridge, 2012).
- [56] RÄMÖ, P., KESSELI, J. & YLI-HARJA, O. «Perturbation avalanches and criticality in gene regulatory networks». *J. Theor. Biol.* **242**, 164–170 (2006).
- [57] DI SANTO, S., BURIONI, R., VEZZANI, A. & MUÑOZ, M. A. «Self-Organized Bistability Associated with First-Order Phase Transitions». *Phys. Rev. Lett.* **116**, 240601 (2016).
- [58] SCHRÖDINGER, E. *What Is Life? The Physical Aspects of the Living Cell* (Cambridge University Press, Cambridge, 1944).
- [59] SCHROEDER, M. *Fractals, chaos, power laws: Minutes from an infinite paradise* (Courier Corporation, New York, 2009).
- [60] SCHWABL, F. *Statistical Mechanics* (Springer, New York, 2003).
- [61] SCOTT, G. *et al.* «Voltage imaging of waking mouse cortex reveals emergence of critical neuronal dynamics». *J. Neurosci.* **34**, 16611–16620 (2014).
- [62] SETHNA, J. P., DAHMEN, K. A. & MYERS, C. R. «Crackling noise». *Nature* **410**, 242–250 (2001).
- [63] SHEW, W. L., YANG, H., PETERMANN, T., ROY, R. & PLENZ, D. «Neuronal avalanches imply maximum dynamic range in cortical networks at criticality». *J. Neurosci.* **29**, 15595–15600 (2009).
- [64] SHMULEVICH, I., KAUFFMAN, S. A. & ALDANA, M. «Eukaryotic cells are dynamically ordered or critical but not chaotic». *Proc. Natl. Acad. Sci. USA* **102**, 13439–13444 (2005).
- [65] SORNETTE, D. *Critical phenomena in natural sciences: chaos, fractals, selforganization and disorder: concepts and tools* (Springer, Berlin, 2006).
- [66] STEPHEN, M. J. «Site-cluster distributions and equation of state for the bond percolation model». *Phys. Rev. B* **15**, 5674 (1977).
- [67] TAGLIAZUCCHI, E., BALENZUELA, P., FRAIMAN, D. & CHIALVO, D. R. «Criticality in large-scale brain fMRI dynamics unveiled by a novel point process analysis». *Front. Physiol.* **3** (2012).
- [68] TORAL, R. & COLET, P. *Stochastic numerical methods: an introduction for students and scientists* (John Wiley & Sons, Weinheim, 2014).
- [69] TOUBOUL, J. & DESTEXHE, A. «Power-law statistics and universal scaling in the absence of criticality». *Phys. Rev. E* **95**, 012413 (2017).

- [70] VALVERDE, S., OHSE, S., TURALSKA, M., WEST, B. J. & GARCIA-OJALVO, J. «Structural determinants of criticality in biological networks». *Front. Physiol.* **6** (2015).
- [71] VAN KAMPEN, N. G. *Stochastic processes in physics and chemistry* (Elsevier, North-Holland, 1992).
- [72] GARCIA-OJALVO, J., ELowitz, M. B. & STROGATZ, S. H. «Modeling a synthetic multicellular clock: repressilators coupled by quorum sensing». *Proc. Nat. Acad. Sci. USA* **101**, 10955–10960 (2004).
- [73] KIYONO, K., STRUZIĆ, Z. R., AOYAGI, N., TOGO, F. & YAMAMOTO, Y. «Phase transition in a healthy human heart rate». *Phys. Rev. Lett.* **95**, 058101 (2005).
- [74] HAIMOVICI, A., TAGLIAZUCCHI, E., BALENZUELA, P. & CHIALVO, D. R. «Brain organization into resting state networks emerges at criticality on a model of the human connectome». *Phys. Rev. Lett.* **110**, 178101 (2013).
- [75] WEISS, M. C. *et al.* «The physiology and habitat of the last universal common ancestor». *Nat. Microbiol.* **1**, 16116 (2016).
- [76] VANDERMEER, J., PERFECTO, I. & PHILPOTT, S. M. «Clusters of ant colonies and robust criticality in a tropical agroecosystem». *Nature* **451**, 457–459 (2008).
- [77] CAMALET, S., DUKE, T., JÜLICHER, F. & PROST, J. «Auditory sensitivity provided by self-tuned critical oscillations of hair cells». *Proc. Natl. Acad. Sci. USA* **97**, 3183–3188 (2000).
- [78] WU, F.-Y. «The potts model». *Rev. Mod. Phys.* **54**, 235 (1982).
- [79] YANG, H., SHEW, W. L., ROY, R. & PLENZ, D. «Maximal variability of phase synchrony in cortical networks with neuronal avalanches». *J. Neurosci.* **32**, 1061–1072 (2012).
- [80] YANG, H., SHEW, W. L., ROY, R. & PLENZ, D. «Maximal variability of phase synchrony in cortical networks with neuronal avalanches». *J. Neurosci.* **32**, 1061–1072 (2012).
- [81] YOSHIOKA, N. «A sandpile experiment and its implications for self-organized criticality and characteristic earthquake». *Earth, Planets Space* **55**, 283–289 (2003).
- [82] ZHANG, L., MAZO-VARGAS, A. & REED, R. D. «Single master regulatory gene coordinates the evolution and development of butterfly color and iridescence». *Proc. Natl. Acad. Sci. USA* **114**, 10707–10712 (2017).

Towards a Landau-Ginzburg theory of cortex dynamics: scale free avalanches of synchronization

2.1	Introduction	39
2.2	Building a minimal model of neural activity with synaptic plasticity	42
2.2.1	Single-unit model	42
2.2.2	Stochastic network model	46
2.2.3	Phases and phase transitions: Case A	47
2.2.4	Phases and phase transitions: Case B	52
2.3	Synchronization phase transition	53
2.3.1	From activity to phases: oscillators	53
2.3.2	Empirical matches	56
2.4	The case of infinite separation of timescales. Recovering self-organize bistability	62
2.5	Conclusions	67
	References	71

2.1 Introduction

“Everything should be made as simpler as possible, but not simpler”

A. Einstein

Landau was pioneer to propose a revolutionary approach to the analysis of phases of matter and the phase transitions they experience. It consists in a parsimonious, coarse-grained, and deterministic description of states of matter in which –relying in the idea of universality– only relevant ingredients (such as symmetries and conservation laws) need to be taken into account and in which most microscopic details are safely neglected [8, 77]. Ginzburg went a step further by realizing that fluctuations are an essential ingredient to be included in any sound theory of phase transitions, especially in low-dimensional systems. The resulting Landau-Ginzburg theory, including fluctuations and spatial dependence, constitutes a firm ground on top of which the standard theory of phases of matter rests, and can be seen as a meta-model of phase transitions [8].

Similar coarse-grained theories are nowadays used in interdisciplinary contexts where diverse collective phases stem out of the interactions among many elementary constituents; e.g. in population dynamics [69, 85] and in neuroscience [12, 13, 16]. Our goal here is to analyze a Landau-Ginzburg theory for cortical neural networks with the hope of shedding light –from a very general perspective– on the collective phases and phase transitions that dynamical cortical networks can harbor and, more specifically, on the intriguing experimental finding of *neuronal avalanches*, as described in what follows.

The cerebral cortex exhibits spontaneous activity even in the absence of any apparent task or external stimuli [4, 28, 68]. A salient aspect of this, so-called, *resting-state* dynamics, as revealed by *in vivo* and *in vitro* measurements, is that it exhibits outbursts of electrochemical activity, characterized by brief episodes of coherence –during which many neurons fire within a narrow time window– inter-spaced by periods of relative quiescence, giving rise to collective oscillatory rhythms [63, 72]. Shedding light on the origin, nature, and functional meaning of such an intricate synchronization dynamics is a fundamental challenge in Neuroscience [17].

Upon experimentally enhancing the spatio-temporal resolution of activity recordings, Beggs and Plenz made the remarkable finding that, actually, synchronized outbursts of neural activity could be decomposed into complex spatio-

temporal patterns, thereon named “neuronal avalanches” [6]. The sizes and durations of such avalanches were reported to be distributed as power-laws, i.e. to be organized in a scale-free way, they obey finite-size scaling [64], a trademark of scale invariance [8], and the corresponding exponents are compatible with those of an unbiased branching process.

Scale-free avalanches of neuronal activity have been consistently reported to occur across neural tissues, preparation types, experimental techniques, scales, and species [7, 34, 35, 54, 62, 67, 74, 80]. This has been taken as empirical evidence backing the criticality hypothesis, i.e. the conjecture that the awake brain might extract essential functional advantages –including maximal sensitivity to stimuli, large dynamical repertoires, optimal computational capabilities, etc.– from operating close to a critical point, separating two different phases [19, 20, 58, 71].

In order to make further progress, it is of crucial importance to clarify the nature of the phase transition marked by such an alleged critical point. It is usually assumed that it corresponds to the threshold at which neural activity propagates marginally in the network, i.e. to the critical point of a quiescent-to-active phase transition [6], justifying the emergence of branching-process exponents [39, 51]. However, several experimental investigations found evidence that scale-free avalanches emerge in concomitance with collective oscillations, suggesting the presence of a synchronization phase transition [33, 89].

From the theoretical side, on the one hand, very interesting models accounting for the self-organization of neural networks to the neighborhood of the critical point of a quiescent-to-active phase transition have been proposed [2, 3, 7, 47, 56]. These approaches rely on diverse regulatory mechanisms [37], such as synaptic plasticity [50], spike-time-dependent plasticity [73], excitability adaptation, etc. to achieve network self-organization to the vicinity of a critical point. These models have in common that they rely on extremely large separation of dynamical timescales (as in models of self-organized criticality (SOC) [5, 43]) which might not be a realistic assumption [2, 10, 47]. Some other models are more realistic from a neurophysiological viewpoint [7, 56], but they give rise to scale-free avalanches if and only if causal information, which is available in computational models but not accessible in experiments [52]. Thus, in our opinion, a sound model justifying the empirical observation of apparent criticality is still missing.

On the other hand, well-known simple models of networks of excitatory and inhibitory spiking neurons exhibit differentiated synchronous and asynchronous phases with a synchronization phase transition in between [1, 14, 15, 84]. However, avalanches do not usually appear (or are not looked for) in such modeling approaches, with a few recent exceptions [31, 67, 82].

Concurrently, during deep sleep and also under anesthesia the cortical state has long been known to exhibit, so-called, “up and down” transitions between states of high and low neural activity, respectively, giving rise to slow (δ) oscillations [25, 78], which clearly deviate from the apparent criticality of the awake brain, and which have also been modeled on their own [41, 55, 56]. Thus, it would be highly desirable to design theoretical models describing within a common framework the possibility of criticality, oscillations, and up-down transitions.

Our aim here, as advanced above, is to clarify the nature of the phases and phase transitions of dynamical network models of the cortex by constructing a general unifying theory ‘*a la Landau-Ginzburg*’ based on minimal assumptions, allowing us, in particular, to elucidate what the nature of the alleged criticality is. The model can be seen as a variant of the well-known Wilson-Cowan model including, crucially, stochasticity and a spatial dependence. Employing analytical and computational techniques, we show that our theory explains the emergence of scale-free avalanches, as episodes of marginal and transient synchronization in the presence of a background of ongoing irregular activity, reconciling the oscillatory behavior of cortical networks with the presence of scale-free avalanches. Last but not least, our approach also allows for a unification of existing models describing diverse specific aspects of the cortical dynamics, such as up and down states and up-and-down transitions, within a common mathematical framework.

2.2

Building a minimal model of neural activity with synaptic plasticity

We construct a mesoscopic Landau-Ginzburg description of neuronal activity, where the building blocks are not single neurons but local neural populations. These can be thought as small sections of neural tissue [22, 44] consisting of a few thousand cells (i.e. still far away from the large-network limit), and susceptible to be described by a few mesoscopic variables. Even though this effective description is constructed here on phenomenological bases, more formal derivations of similar equations from microscopic models exist in the literature (see e.g. [7]). In what follows, first (i) we model the mesoscopic neural activity at a single “unit”, then (ii) we analyze its deterministic behavior as a function of parameter values, and later on (iii) we study the dynamics of a network of coupled units, defining a stochastic cortical network.

2.2.1

Single-unit model

In the Wilson-Cowan (WC) model the dynamics of the average firing rate or global activity, ρ , is governed by the equation

$$\dot{\rho}(t) = -a\rho(t) + (1 - \rho(t))S(W\rho(t) - \Theta) \quad (2.2.1)$$

where a controls the spontaneous decay of activity, W is the synaptic strength, Θ is a threshold value, and $S(x)$ is a sigmoid (transduction) function, e.g. $S(x) = \tanh(x)$ [7, 88]. We adopt this well-established model and, at each single unit we consider a dynamical model in which the excitatory activity, ρ , for simplicity, keep only the leading terms (following the Landau approach) in a power-series expansion, yielding the deterministic part¹:

$$\dot{\rho}(t) = [-a + R(t)]\rho(t) + b\rho^2(t) - \rho^3(t) + h \quad (2.2.2)$$

where h is an external driving field, $a > 0$ controls the spontaneous decay of activity, which is partially compensated by the generation of additional activity

¹We keep up to third order to include the effect of the sigmoid response function; a variant of the model considering the non-truncated Wilson-Cowan equation leads to almost identical results; see appendix B.1

at a rate proportional to the amount of available *synaptic resources* at a given time, $R(t)$; the quadratic term, with a parameter $b > 0$ controls non-linear integration effects², and the cubic term imposes a saturation level for the activity, to avoid unbounded growth.

A second equation describes the dynamics of the available resources, $R(t)$, through the combined effect of synaptic depression and synaptic recovery, as encoded in the celebrated model of Tsodyks and Markram (TM) [50, 83]:

$$\dot{R}(t) = \frac{1}{\tau_R}(\xi - R(t)) - \frac{1}{\tau_D}R(t)\rho(t), \quad (2.2.3)$$

where τ_R (resp. τ_D) is the characteristic recovery (depletion) time, and ξ is the baseline level of non-depleted synaptic resources.

2.2.1.1 Mean-field analysis

We analyze, both analytically and computationally, the dynamics of the single unit, as given by Eqs. (2.2.2) and (2.2.3). We obtain the fixed points (ρ^* , R^*) of the dynamics –i.e. the possible steady-states at which the system can settle– as a function of the baseline-level of synaptic resources, ξ , which plays the role of a control parameter (all other parameters are kept fixed to reasonable values, as summarized in the caption of Fig. 2.2.1). For small values of ξ , the system falls into a quiescent or *down* state with $\rho^* \approx 0$ and $R^* \approx \xi$ ³. Instead, for large values of ξ there is an active or *up* state with self-sustained spontaneous activity $\rho^* > 0$ and depleted resources $R^* < \xi$. In between these two limiting phases, two alternative scenarios can appear, depending on the time scales τ_D and τ_R .

- (A) A stable limit cycle (corresponding to an unstable fixed point, with complex eigenvalues) emerges for intermediate values of ξ (in between two Hopf bifurcations) as illustrated in Fig.2.2.1A. This Hopf-bifurcation scenario has been extensively discussed in the literature (see e.g. [53]) and it is at the basis of the emergence of oscillations in neural circuits.
- (B) An intermediate regime of bistability including three fixed points is found for intermediate values of ξ (in between two saddle-node bifurcations): the up and the down ones, as well as an unstable fixed point in between (as illustrated in Fig.2.2.1B). This saddle-node scenario is the relevant one in models [41, 46, 56] describing transitions between up (active) and down (quiescent) states as they occur in the brain during sleep or under anesthesia [25, 78]

²Single neurons integrate many presynaptic spikes to go beyond threshold, and thus their response is non-linear: the more activity the more likely it is self-sustained [44]. In fact, the WC model includes a sigmoid response function with a threshold, implying that activity has to be above some minimum value to be self-sustained, and entailing $b > 0$ in the series expansion.

³Deviations from $\rho^* = 0$ stem from the small but non-vanishing external driving $h \neq 0$.

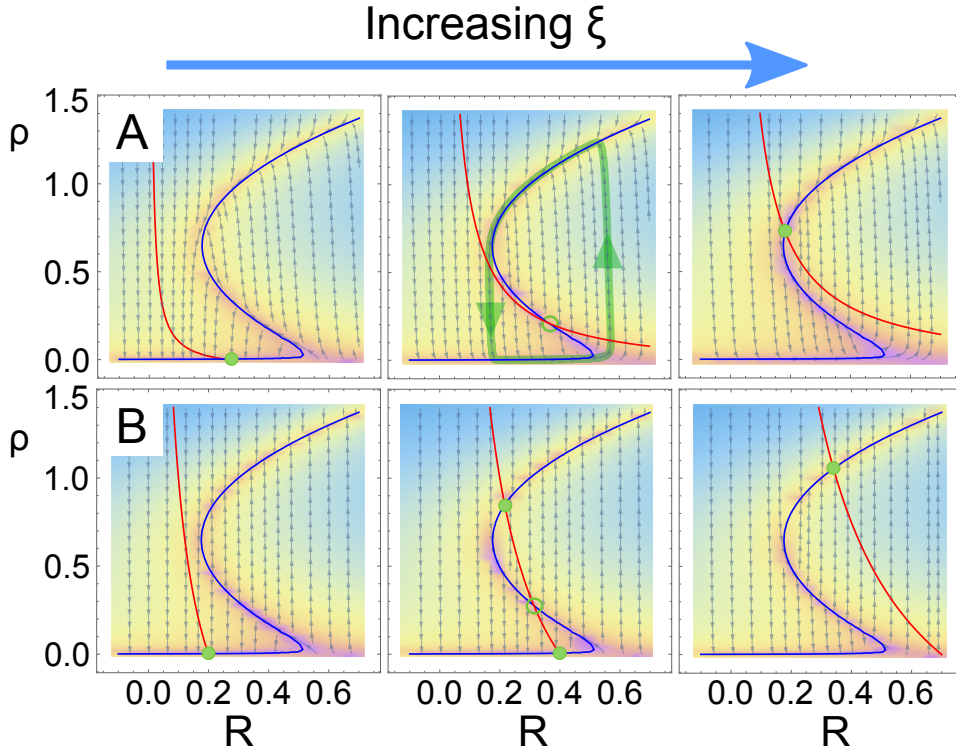


Figure 2.2.1: Phase portraits and nullclines for the (deterministic) dynamics, Eqs. (2.2.2) and (2.2.3). Nullclines are colored in blue ($\dot{\rho} = 0$) and red ($\dot{R} = 0$), respectively; fixed points (ρ^*, R^*) –at which nullclines intersect– are highlighted by green full (empty) circles for stable (unstable) fixed points. Background color code (shifting from blue to purple) represents the intensity of the vector field $(\dot{\rho}, \dot{R})$, whose direction is represented by small grey arrows. A trajectory illustrating a limit cycle is showed in green in (A). The system exhibits either (A) an oscillatory regime or (B) a region of bistability, in between a down (left) and an up (right) state. To shift from case (A) to case (B) the timescale of resources depletion, τ_D^{-1} , is 0.016 and 0.001, respectively. Other parameter values: $h = 10^{-3}$, $a = 0.6$, $b = -1.3$, $\tau_R = 10^3$; control parameter, from left to right, $\xi = 0.3, 1.6, 2.3$ in the upper panel and $\xi = 0.2, 0.4, 0.7$ in the lower one.

Two remarks are in order. The first is that one can shift from one scenario to the other just by changing one parameter, e.g. the synaptic depletion timescale τ_D ⁴; thus, as shown in Fig. 2.2.2, when the recovery time (τ_R) is much bigger than the depletion time (τ_D) the system is in the case A, while for bigger values of the depletion time (τ_D) it falls into the case B with a transition between up (active) and down (quiescent) states. The second and important one is that none of the two scenarios exhibits a continuous transition (transcritical bifurcation) separating the up from the down regimes; thus, at this deterministic level there is no precursor of a critical point for marginal propagation of activity.

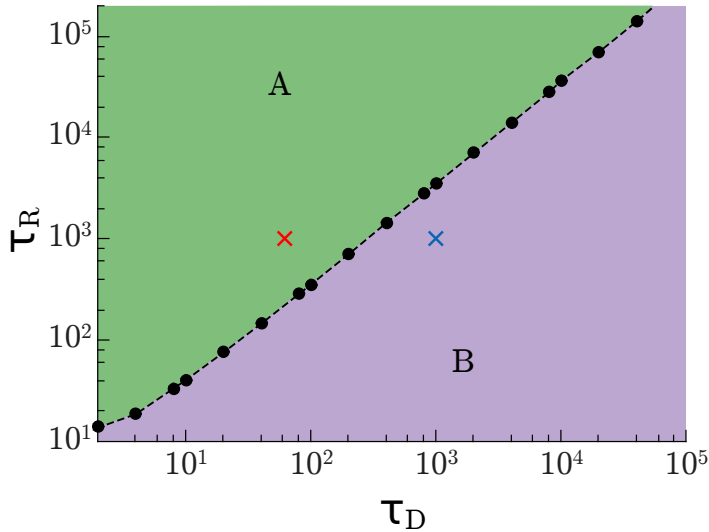


Figure 2.2.2: Phase diagram. It is possible to shift from case (A) to case (B) and viceversa by changing just one parameter; e.g. the timescale of resources depletion, τ_D^{-1} . Red (blue) cross show the particular case chosen in the Fig. 2.2.1 for the case A (B). Other parameter values: $h = 10^{-3}$, $a = 0.6$, $b = -1.3$, $\tau_R = 10^3$.

⁴Note that the slope of the the nullcline deriving from Eq.(2.2.3) (red in Fig.2.2.1) is proportional to τ_D : if it is small enough, there exists only one unstable fixed point, giving rise to a Hopf bifurcation; otherwise the nullclines intersect at three points, generating the bistable regime.

2.2.2

Stochastic network model

We now introduce stochastic and spatial effects in a simple way. For this we consider a network of N nodes coupled following a given connection pattern. Each network node represents a mesoscopic region of neural tissue or “unit” as described above. On top of this deterministic dynamics, we consider that each unit (being finite) is affected by intrinsic fluctuations [7, 13, 23]. More specifically, Eq.(2.2.2) is complemented with an additional term $+A(\rho)\eta(t)$ which includes a (zero-mean, unit-variance) Gaussian noise and a density-dependent amplitude $A(\rho)$ ⁵. In the limit of slow external driving and up to leading order this can be written as $A(\rho) = \sqrt{\rho(t)}$; this stems from the fact that the spiking of each single neuron is a stochastic process, and the overall fluctuation of the density of a collection of them scales with its square-root, as dictated by the central limit theorem [30] (see also chapter 1 or [7] for a detailed derivation).

At large macroscopic scales, the cortex can be treated as a two-dimensional sheet consisting mostly of short-range connections [11]⁶. Although long-range connections are also known to exist, and small-world effects have been identified in local cortical regions [76], here we consider a two-dimensional square lattice (size $N = L^2$) of mesoscopic units as the simplest way to embed our model into space. Afterward, we shall show that our main results are robust to the introduction of more realistic network architectures including additional layers of complexity such as long-range connections and spatial heterogeneity.

Following the minimal Landau-Ginzburg approach we adopted, coupling between units is described by the leading-order term containing derivatives (i.e. finite differences) of the activity between any pair of coupled nodes, i.e. a diffusion term. This type of diffusive coupling between neighboring mesoscopic units stems from electrical synapses [44, 81] and has been analytically derived starting from models of spiking neurons [16]⁷. Thus, the set of stochastic equations is:

$$\begin{cases} \dot{\rho}_i(t) = (-a + R_i + b\rho_i)\rho_i - \rho_i^3 + h + \nabla^2\rho_i + \sqrt{\rho_i}\eta_i \\ \dot{R}_i(t) = \frac{1}{\tau_R}(\xi - R_i) - \frac{1}{\tau_D}R_i\rho_i \end{cases} \quad (2.2.4)$$

where ρ_i and R_i are the activity and resources at a given node i with $i = 1, 2, \dots, N$, $\nabla^2\rho_i \equiv \sum_j(\rho_j - \rho_i)$ describes the diffusive coupling of unit i with its neighbors j , and $\eta_i(t)$ is a Gaussian white noise term, with $\langle \eta_i(t)\eta_j(t') \rangle = \delta(t - t')\delta_{ij}$. For the forthcoming analyses we resort to numerical integration

⁵A noise term could be also added to the equation for synaptic resources [55], but it does not significantly affect the results.

⁶At the basis of, so-called, neural-field models, with a long tradition in neuroscience [24].

⁷More elaborated approaches including coupling kernels between different regions, as well as asymmetric ones, are also often considered in the literature (e.g. [12]), but here we stick to the simplest possible coupling.

of the stochastic equations –which is feasible thanks to the exact and efficient scheme developed by Dornic *et al.* [26] to integrate eqs. such as Eq.(2.2.4) with multiplicative noise– keeping, as above, all parameters⁸, except for ξ , fixed, and employing $\delta t = 0.01$ as integration timestep.

Importantly, we have considered variants of this model, avoiding the truncation of the power-series expansion, and also including an inhibitory population as the chief regulatory mechanism: either of these leads to essentially the same phenomenology and phases as described in what follows, backing the robustness of our conclusions (see appendix B.1).

2.2.3

Phases and phase transitions: Case A

We start analyzing sets of parameters lying within the deterministic case A above, i.e. with a limit cycle. We study the possible phases that emerge as the baseline level of synaptic resources, ξ is varied. These are illustrated in Fig.2.2.3 where characteristic snapshots, overall-activity time series and probability distributions, as well as raster plots are plotted.

✖ **Down-state phase (A1)** If ξ is sufficiently small (i.e. $\xi \lesssim 0.75$), resources R are always scarce and the system is unable to produce self-sustained activity (i.e. it is hardly excitable) giving rise to a down-state phase, characterized by very small stationary values of the network time-averaged activity $\bar{\rho} \equiv \frac{1}{T} \int_0^T dt \frac{1}{N} \sum_{i=1}^N \rho_i(t)$ for large times T (see Fig.2.2.3a). The quiescent state is disrupted only locally by the effect of the driving field h , which creates local activity, hardly propagating to neighboring units.

✖ **Synchronous irregular (SI) phase (A2)** Above a certain value of resource baseline ($\xi \gtrsim 0.75$) there exists a wide region in parameter space in which activity generated at a seed point is able to propagate to neighboring units, triggering a wave of activity which transiently propagates through the whole network until resources are exhausted, activity ceases, and the recovery process restarts (see Fig.2.2.3b). Such waves or “network-spikes” appear in an oscillatory, though not perfectly periodic, fashion, with an average separation time that decreases with ξ . In the terminology of Brunel [14], this corresponds to a *synchronous irregular* (SI) state/phase, since the collective activity is time-dependent and individual spiking is irregular (as discussed below). This wax-and-wane state resembles the huge bursts of anomalous synchronous activity as they appear in e.g. epileptic tissues [40].

⁸For simplicity, some time dependences have been omitted and some coefficients have been fixed to unity; periodic boundary conditions are considered.

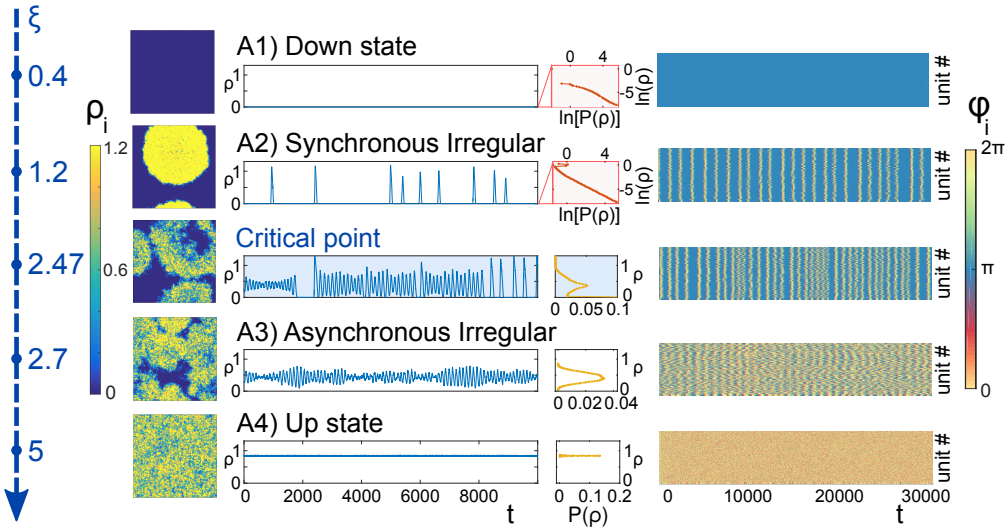


Figure 2.2.3: Illustration of the diverse phases emerging in the model (case A) for a network of $N = 128^2$ units. The baseline of synaptic resources, ξ , increases from top to bottom (see left blue arrow). *First column:* Snapshots of typical configurations; the color code represents the level of activity at each unit. The synchronous irregular case is characterized by waves of activity growing and transiently invading the whole system, before extinguishing the resources and coming to an end; while in the nested-oscillation or asynchronous irregular regime multiple traveling waves coexist, interfering with each other. *Second column:* Time series of the overall activity averaged over the whole network. In the down state activity vanishes, appearing synchronous bursts, interspersed by almost silent intervals in the synchronous phase. At the critical point network spikes begin to superimpose, giving rise to complex oscillatory patterns (nested oscillations) and marginally self-sustained global activity all across the asynchronous regime; finally, in the up state the global activity converges to steady-state with small fluctuations. *Third column:* Steady state probability distribution $P(\rho)$ for the global activity: in the A1 and A2 regimes the distributions are shown in a double-logarithmic scale; observe the approximate power-law for very small values of ρ stemming from the presence of multiplicative noise. *Fourth column:* Different levels of synchronization across phases: a sample of 200 randomly chosen units are mapped into oscillators (see below); the plot shows the time evolution of their corresponding phases ϕ_k^A .

✖ **Asynchronous irregular (AI) phase (A3)** For even larger values of resource baseline ($\xi \gtrsim 2.15$), the level of synaptic recovery is sufficiently high as to allow for resource-depleted regions to recover before the previous wave has come to an end. Thereby, diverse spatially extended waves coexist in the network, giving rise to a collective complex oscillatory pattern (see Fig.2.2.3d; which is strikingly similar to, e.g. EEG data of α -rhythms [75]). The amplitude of these oscillations, however, decreases upon increasing network size (as many different local waves are averaged and deviations from the mean tend to be washed away). This regime can be assimilated to an *asynchronous irregular* (AI) phase of Brunel [14].

For all the considered network sizes the time-averaged overall activity, $\bar{\rho}$, starts taking a distinctively non-zero value above $\xi \approx 0.75$ (see Fig.2.2.4), reflecting the upper bound of the down or quiescent state (transition between (A1) and (A2)). This phase transition is rather trivial and corresponds to the onset on network spikes. More interestingly, it exhibits an abrupt increase at values of ξ between 2 and 3, signaling the transition from (A2) to (A3). However, the jump amplitude decreases as N increases, suggesting a smoother transition in the large- N limit. Thus it is not clear *a priori* –using $\bar{\rho}$ as an indicator, whether there is a true sharp phase transition or there is just a crossover between the synchronous and the asynchronous regime. To elucidate the existence of a true critical point, we measured the standard deviation of the network-averaged global activity $\bar{\rho}$, σ_{ρ} . Direct application of the central limit theorem [30] would imply that such a quantity should decrease as $1/\sqrt{N}$ for large N and thus $\chi \equiv \sqrt{N}\sigma_{\rho}$ should converge to a constant. However, Fig.2.2.4B shows that χ exhibits a very pronounced peak located at the (size-dependent) transition between the SI and the AI phases that grows with N –i.e. diverges in the thermodynamic limit–, revealing anomalous scaling, as occurs in critical points. Also, a finite-size scaling analysis of the value of ξ at the peak (for each N), i.e. $\xi_c(N)$, reveals the existence of a *bona fide* continuous synchronous-asynchronous phase transition at $\xi_c^{\infty} \simeq 2.15(5)$ in the infinite-size network limit (see Fig.2.2.4C). Moreover, a (detrended fluctuation) analysis of timeseries reveals the emergence of long-range temporal correlations right at ξ_c (see appendix B.2).

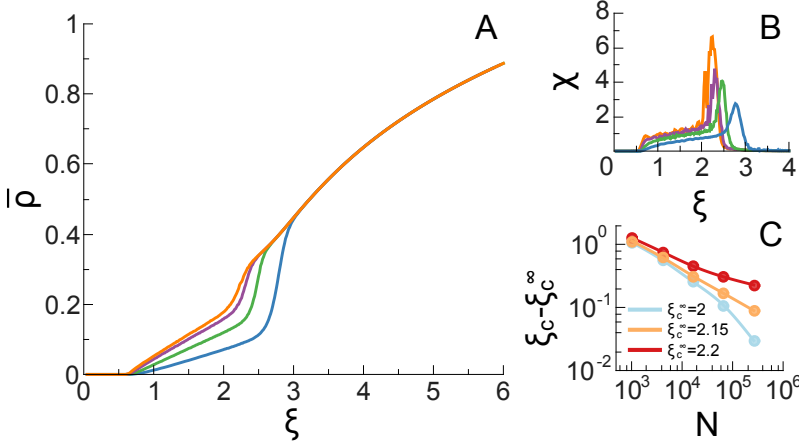


Figure 2.2.4: Overall network activity state (case A) as determined by the network time-averaged value $\bar{\rho}$ ($h = 10^{-7}$). (A) Order parameter $\bar{\rho}$ as a function of the control parameter ξ for various system sizes $N = 2^{12}, 2^{14}, 2^{16}, 2^{18}$ (from bottom to top); observe that $\bar{\rho}$ grows monotonically with ξ and that an intermediate regime, in which $\bar{\rho}$ grows with system size, emerges between the up and the down states. (B) Inset: Standard deviation of the averaged overall activity in the system multiplied by \sqrt{N} ; $\chi = \sigma_{\rho} \sqrt{N}$ (see main text); The point of maximal variability coincides with the point of maximal slope in (A) for all network sizes N . (C) Finite-size scaling analysis of the peaks in (B). The distance of the size-dependent peak locations $\xi_c(N)$ from their asymptotic value for $N \rightarrow \infty$, ξ_c^{∞} , scales as a power law of the system size, taking $\xi_c^{\infty} \approx 2.15$, revealing the existence of true scaling as corresponds to criticality.

About the nature of nested oscillations. In order to unveil the nature of the nested oscillation (AI) phase and to explicit whether it is a finite size effect or it survives in the thermodynamic limit, the existence of a second (hidden) phase transition between the up state and the nested oscillation phase is questioned. In fact, in principle, those two regimes show a qualitative difference: in the AI phase each single unit keeps switching between the *on* and *off* states and there exists a macroscopic fraction of *off* sites, whereas in the active phase units are permanently in the *on* state and, even if fluctuations might lead some unit to the *off* state, the macroscopic fraction of them is null. The fraction of inactive units, ρ_0 , can thus be chosen as an order parameter for this putative phase transition. In Figure 2.2.5 we plot the average over time of ρ_0 in function of ξ and we verify that this "complementary" order parameter detects the same phase transition already characterized in the main text, thus unveiling that, in the thermodynamic limit, there exists no difference between the nested

oscillation regime and the up state. Therefore, the nested oscillations can be understood as the partial synchronization of a small number of units, which produces effects at the network level only if the system is finite. Conversely in the infinite size limit the total activity of the system is constant, since many small incoherent clusters of synchronized activity coexist and superimpose, producing a null net effect.

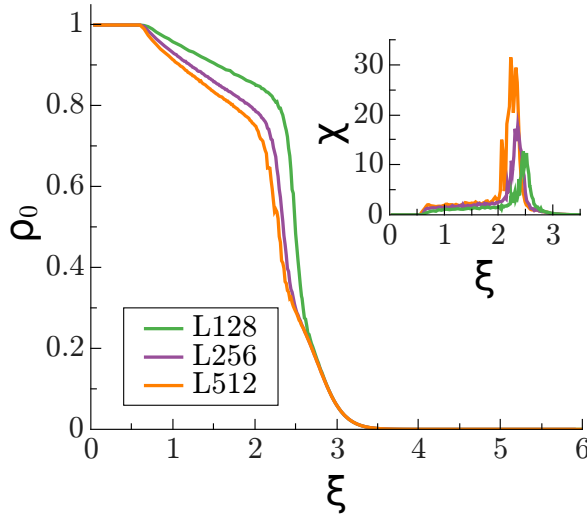


Figure 2.2.5: Phase transition for the fraction of inactive sites in the system. Inset: Variance over runs of fixed length of the average value of the control parameter multiplied by \sqrt{N} in order to highlight the deflections with respect to central limit theorem ($\chi = \sqrt{N}\sigma_{\rho_0}$). Note that for all the system sizes the peaks are located approximately in the same spots as in Fig. 2.2.4.

✳ **Up-state phase (A4)** For even larger values of ξ , plenty of synaptic resources are available at all times, giving rise to a state of perpetual activity with small fluctuations around the mean value (Fig.2.2.3e), i.e. an up state. Let us finally remark, that as just explicitly shown, the AI phase and the Up-state cannot be distinguished in the infinite network-size limit, in which there are so many waves to be averaged that a homogeneous steady state emerges on average in both cases.

2.2.4**Phases and phase transitions: Case B**

We discuss the much simpler scenario for which the deterministic/mean-field dynamics predicts bistability, i.e. case B above, which is obtained e.g. considering a slower dynamic for synaptic-resource depletion. In this case, the introduction of noise and space, does not alter the deterministic picture. Indeed, computational analyses reveal that there are only two phases: a down state and an up one for small and large values of ξ , respectively. These two phases have the very same features as their corresponding counterparts in case A. The phase transition between them is discontinuous (much as in Fig. 2.2.1B) and thus, for finite networks, fluctuations induce spontaneous transitions between the up and the down state when ξ takes intermediate values, in the regime of phase coexistence. Thus, in case B, our theory constitutes a sound Landau-Ginzburg description of existing models, such as those in [41, 55, 56], describing up and down state transitions.

Synchronization phase transition

The Landau-Ginzburg model has shown us thus far, that, at least, there exists a non-trivial phase transition (in the sense that stays outside a continuous quiescent/active phase transition) between the synchronous irregular phase and the asynchronous irregular one, characterized by the emergence of oscillations and waves of activity propagating and invading the whole system. It is however not unreasonable to assume that this type of transition belongs to a synchronization/desynchronization one but, to test this assumption, the units of the system must be considered as oscillators. So, the main question now is: how to deal with the conversion from 'activity units' to oscillators in a network? In this section, we tackle this problem, and we also deep in some possible empirical findings that can be reproduced in our theory.

2.3.1

From activity to phases: oscillators

Our first objective must be to assign an effective phase $\phi_k(t)$ to the time-series at unit k , $\rho_k(t)$. In principle, there are two possible solutions to this problem. The first one involves the computing of its *analytic signal representation*, which directly maps any given real-valued timeseries into an oscillator with time-dependent phase and amplitude, and the second one, in concomitance with the empirical treatment of the real time-series, consists in its conversion to spiking pattern of activity.

✳ **Analytic signal representation** The Hilbert transform $\mathcal{H}(\cdot)$ is a bounded linear operator largely used in signal analysis as it provides a tool to transform a given real-valued function $u(t)$ into a complex analytic function, called the *analytic signal representation*. This is defined as $\mathcal{A}_u(t) = u(t) + i\mathcal{H}[u(t)]$ where the Hilbert transform of $u(t)$ is given by: $\mathcal{H}[u(t)] = h * u = \frac{1}{\pi} \lim_{\epsilon \rightarrow 0} \int_{\epsilon}^{\infty} \frac{u(t+\tau) - u(t-\tau)}{\tau} d\tau$. Expressing the analytic signal in terms of its time-dependent amplitude and phase (polar coordinates) makes it possible to represent any signal as an oscillator. In particular, the associated phase is defined by $\phi_k^A = \arctan \text{Im}(\mathcal{A}_k) / \text{Re}(\mathcal{A}_k)$.

✖ **Phases from spiking patterns** Another possibility is to consider that local timeseries at each single unit, $\rho_k(t)$, can be mapped into time sequences of point-like (“unit spiking”) events. For this, a local threshold $\theta \ll 1$ is defined, allowing to assign a state on/off to each single unit/node (depending on whether it is above/below such a threshold) at any given time. If the threshold is low enough, the procedure is independent of its specific choice. A single (discrete) “event” can be assigned to each node i , e.g. at the time of the maximal ρ_i within the on-state⁹. Once the continuous timeseries has been mapped into a spiking series, the phase at each unit can be constructed as $\phi_k^{(\mathcal{B})}(t) = 2\pi(t - t_n^k)/(t_{n+1}^k - t_n^k)$ where $t \in [t_n^k, t_{n+1}^k)$ and t_n^k is the time of the n^{th} spike of node/unit k .

That said, to shed further light on the nature of such a transition, it is also convenient to employ a more adequate (synchronization) order-parameter, e.g. the Kuramoto index K [45, 65] that vanishes in the asynchronous phase and takes non-zero values in the synchronous one. In particular, K is defined by $K \equiv \frac{1}{N} \left\langle \left| \sum_{k=1}^N e^{i\phi_k(t)} \right| \right\rangle$ –where i is the imaginary unit, $|\cdot|$ is the modulus of a complex number, $\langle \cdot \rangle$ here indicates averages over time and independent realizations, and k runs over units, each of which is characterized by a phase $\phi_k(t) \in [0, 2\pi]$, which can be defined in various ways.

Using the resulting phases, $\phi_k^{\mathcal{A}}(t)$ (or $\phi_k^{\mathcal{B}}(t)$), the Kuramoto index $K_{\mathcal{A}}$ (or $K_{\mathcal{B}}$) can be calculated. As illustrated in Fig. 2.3.1A, this reveals the presence of a synchronization transition: the value of $K_{\mathcal{A}}$ clearly drops, at the previously determined critical point $\xi_c(N)$. The spiking method to define a time-dependent phase for each unit reveals even more vividly the existence of a synchronization transition at $\xi_c(N)$ as shown in Fig. 2.3.1B. Finally, we have also estimated the coefficient of variation¹⁰ (CV) of the distance between the times at which each of these effective phases crosses the value 2π ; it reveals the presence of a sharp peak of variability, converging for large network sizes to the critical point $\xi_c^\infty \approx 2.15$ (see inset of Fig. 2.3.1B).

⁹Other conventions to define an event are possible, but results are quite robust to the specific way in which this procedure is implemented.

¹⁰Given a set of spikes, it is defined as the standard deviation divided by the mean inter-spike interval.

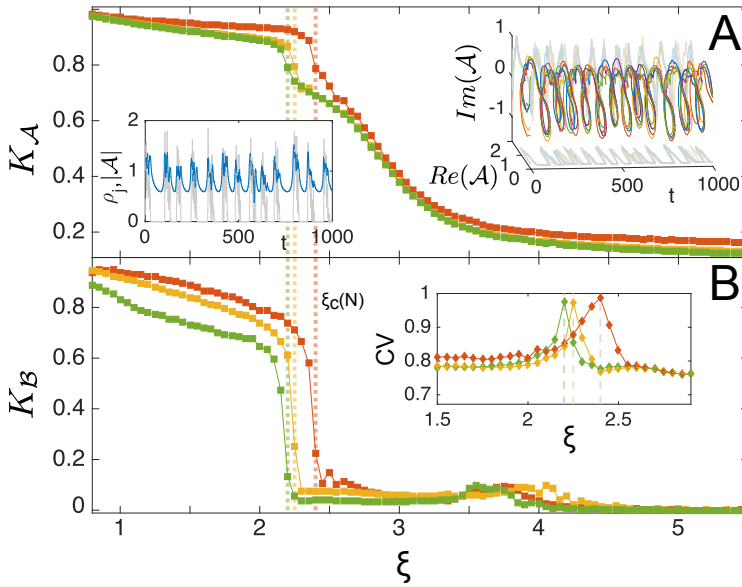


Figure 2.3.1: Synchronization transition elucidated by measuring the Kuramoto parameter as estimated using (A) the analytic signal representation $\mathcal{A}_k(t)$ of activity time series $\rho_k^A(t)$ at different units k and for various system sizes ($N = 128^2$ (red), 256^2 (orange), 512^2 (green)). For illustrative purposes, the top right inset of (A) shows the analytical representation (including both a real and an imaginary part) of 5 sample units as a function of time; the left inset shows the time evolution of one node (gray) together with the amplitude of its analytic representation (blue). Both insets, vividly illustrate the oscillatory nature of the unit dynamics. (B) Similar result to (A), but employing a different method to compute time-dependent phases of effective oscillators $\rho_k^B(t)$. This alternative method captures more clearly the abruptness of the transition; the point of maximum slope of the curves corresponds to the value of the transition points $\xi_c(N)$ in (A). The inset in (B) shows the coefficient of variation CV of the times between two consecutive crossing of the value 2π ; it exhibits a peak of variability at the critical point $\xi_c(N)$.

Thus, recapitulating, different measurements reveal the existence of a bona fide synchronization phase transition in our model. On the other hand, the phase transitions separating the down state, from the synchronous irregular regime (A1-A2 transition) is rather trivial, as it just corresponds to the onset of network spikes, with no sign of interesting critical features, while in between the asynchronous and the up state (A3-A4) there is no true phase transition, as both phases are indistinguishable in the infinitely-large-size limit. On the other

hand, different measurements clearly reveal the existence of a bona fide synchronization phase transition (A2-A3) at which non-trivial features characteristic of criticality emerge.

2.3.2

Empirical matches

2.3.2.1 Avalanches

For ease of comparison with empirical results, we define a protocol to analyze avalanches, that closely resembles the experimental one as introduced by Beggs and Plenz [6]. As before, individual-unit activity timeseries can be mapped into a discrete-time “spiking” pattern (see Fig.2.3.2A). Remember that a unit “spike” corresponds to a period in which the activity at a given unit is above a given small threshold in between two windows of quiescence (activity below threshold) for such a unit. The only difference is that now a weight proportional to the integral of the activity time series spanned between two consecutive threshold crossings is assigned to each single event (see Fig.2.3.2A). Hence, as illustrated in Fig.2.3.2B, the network activity can be represented by a raster plot of weighted spiking units.

Following the standard experimental protocol, we estimate the *inter-spike interval (ISI)*, which are no more than the mean time distance between two consecutive events. Thus, once a discrete time binning Δt is chosen and each individual spike is assigned to one such bin. An avalanche is defined as a consecutive sequence of temporally-contiguous occupied bins preceded and ended by empty bins (see Fig.2.3.2 B and C).

As shown in Figure 2.3.2D, for the avalanche-size distribution, near criticality, a power law with an exponent similar to the experimentally measured one ($3/2$) is recovered. Away from the critical point, either in the synchronous phase (blueish colors) and the asynchronous one (orangish) clear deviations from power-law behavior are observed. Observe the presence of “heaps” in the tails of the distributions, especially in the synchronous regime; these correspond to periodic waves of synchronized activity; they also appear at criticality, but at progressively larger values for larger system sizes. In the same way (see 2.3.2D), for the avalanche-duration distribution, the experimentally measured exponent 2 is reproduced using $\Delta t = ISI$, whereas deviations from such a value are measured for smaller (larger) time bins, in agreement with experimentally reported results. After reshuffling times, the distributions become an exponential, with characteristic timescales depending on Δt (dashed lines).

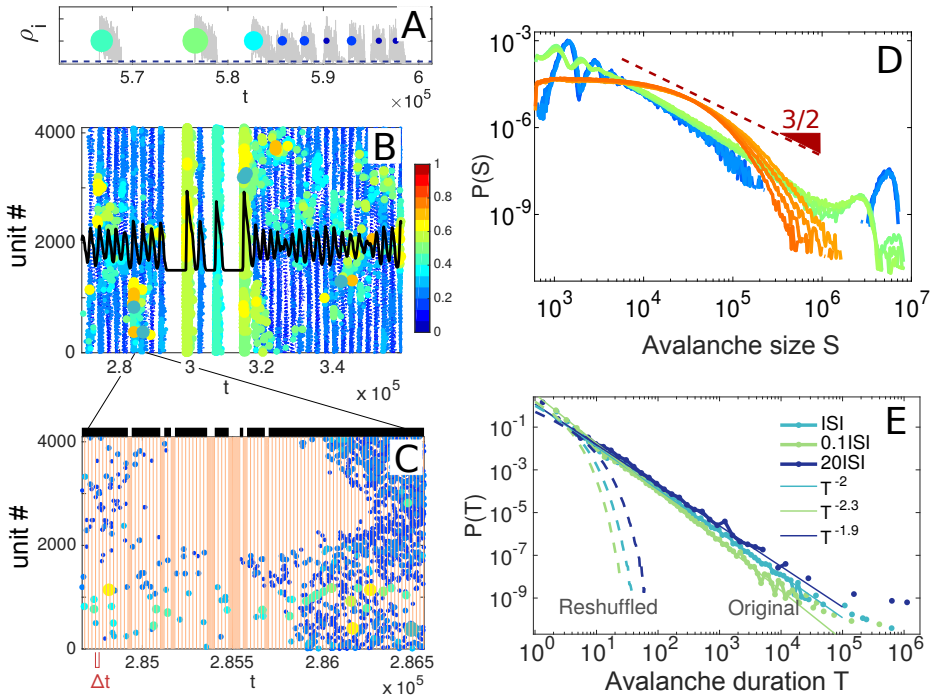


Figure 2.3.2: Avalanches measured from activity time series. (A) Illustration of the activity timeseries $\rho_i(t)$ at a given unit i . A single “unit spike” is defined at the time of the maximal activity in between two threshold crossings (θ , dashed blue line); a weight equal to the area covered in between is assigned to each event (note the color code). (B) Raster plot obtained using the procedure above for each unit ($N = 64^2$). Observe that large events coexist with smaller ones, and that these last ones, occur in a rather synchronous fashion. The overall time-dependent activity is marked with a black line. (C) Zoom of (B) illustrating the time resolved structure and using a time binning Δt equal to the network-averaged ISI . Shaded columns correspond to empty time bins, i.e. with no spike. Avalanches are defined as sequences of events occurring in between two consecutive empty time bins and are represented by the black bars above the plot. (D) Avalanche-size distribution (sum of the weighted spikes it comprises) for diverse values of ξ (from 1.85 to 2.05, in blueish colors, from 2.7 to 2.9 in greenish colors, and from 3.3 to 3.45 in orangish colors) measured from the raster plot. The slope $3/2$ is plotted as a reference. (E) Avalanche-duration distribution, for different choices of the time bin. The experimentally measured exponent 2 is reproduced using $\Delta t = ISI$. After reshuffling times, the distributions become an exponential (dashed lines).

Using this, quite remarkably, several well-known experimental key features are reproduced if ξ is tuned to a value close to the synchronization transition, namely:

- i) Avalanches of activity are broadly (power-law) distributed in size at the critical point, with scale invariance coexisting with oscillatory behavior (as revealed by the “heaps” in the tails of the curves of in Fig.2.3.2D, that correspond to anomalously large events or “waves” of synchronization, which have a periodic nature as elucidated in appendix B.3.1). Similarly, power-law distributed avalanche durations (or times) are observed at the critical point (see Fig.2.3.2E).
- ii) Away from the critical point, both in the sub-critical and in the supercritical regime, deviations from this behavior are observed; in particular, in the subcritical or synchronous regime, the peak of periodic large avalanches becomes much more pronounced, while in the asynchronous phase, such a peak is lost (see Fig.2.3.2D);
- iii) When Δt is chosen to be equal to the *ISI* (inter-spike interval, i.e. the time interval between any two consecutive spiking events) in the network, avalanche sizes and durations obey –at criticality– finite-size scaling with exponent values compatible with the standard ones, i.e. those of an unbiased branching process (see Fig.2.3.2B and C);
- iv) Changing Δt , power-law distributions with varying exponents are obtained at criticality (the larger the time bin, the smaller the exponent) as originally observed experimentally by Beggs and Plenz (Fig.2.3.2E).
- v) Reshuffling the times of occurrence of unit’s spikes, the statistics of avalanches is dramatically changed, giving rise to exponential distributions (as expected for an uncorrelated Poisson point process) thus revealing the existence of a non-trivial temporal organization in the dynamics (Fig.2.3.2E).

Summing up, our model tuned to the edge of a synchronization/desynchronization phase transition reproduces all chief empirical findings for neural avalanches. These findings strongly suggest that the critical point alluded by the criticality hypothesis of cortical dynamics does not correspond to a quiescent/active phase transition --as modeling approaches usually assume-- but to a synchronization phase transition, at the edge of which oscillations and avalanches coexist.

It is important to underline that our results, in what respect avalanches, are purely computational. To date, we do not have a theoretical understanding of why results are compatible with branching-process exponents.

2.3.2.2 Heterogeneity effects

It is of particular interest the study of Okujeni et al. [61], in which the authors were able to experimentally tune the network architecture in neuronal cultures, and make it either poorly or highly clustered, as illustrated in Figure 2.3.3A, simply by changing the level of protein kinase C (an enzyme regulating neurite growth and its level of aggregation or clustering). In the case in which clusters emerge (rightmost picture) the network is strongly heterogeneous at a mesoscopic level, with some mesoscopic regions having a high neuronal density and some others being almost empty. On the other hand, un-clustered networks are much more homogeneous at a mesoscopic scale. Detailed experimental analyses of the neural activity on these cultures revealed that, as illustrated in Figure 2.3.4A, the activity time series look quite different in the different cases: peaks of activity (synchronization events or “network spikes”) occur more rarely for poorly clustered networks, while increasing the degree of clustering –keeping other experimental conditions fixed– the level of activity increases, i.e. clustering promotes the generation of spontaneous network activity.

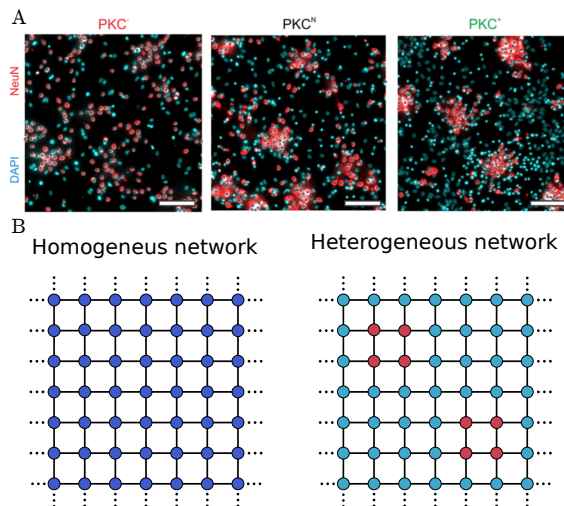


Figure 2.3.3: (A) Spatial distribution of neurons (white circles) for rising values of protein kinase C (from Okujeni et al. [61]). The higher the value of PKC the more aggregated (or clustered) the network of cultured cortical neurons. (B) Sketch of the considered networks: homogeneous to the left and heterogeneous/clustered to the right. In both cases the network-average value of the activity-decay parameter a is taken to be equal. However, while in the homogeneous case the value of a is constant across the network, in the heterogeneous one there are some areas (marked with red nodes) with a lower value of a .

To verify if this finding can be explained within the context of our general theoretical framework, we considered a variant of the homogeneous square lattice (see the sketch in Figure 2.3.3B) in which we include some degree of mesoscopic heterogeneity mimicking that of empirical networks. In particular, clusters describe regions more densely populated by neurons. Given that each of the nodes in the lattice represents a mesoscopic region, spatial heterogeneity in parameter values (e.g on “a”, “b”) accounts for spatially heterogeneity in its internal propensity to sustain activity; in particular regions with more neuronal density have a smaller value of a , i.e. are more likely to sustain activity.

In order to model these experimental results, we developed a heterogeneous network in which we keep fixed the mean value of the parameter a (that controls the decay of the activity at each single unit), but inducing some areas with low local values of a_1 , i.e. with a smaller propensity for activity to decay (red nodes in Fig. 2.3.3B), while in the rest of the network larger values of a , a_2 , are considered (keeping the network-average value of a constant). As shown in Fig. 2.3.4B, the lower the local value of a_1 , the more facilitated the emergence of spontaneous activity, leading the system closer and closer to the critical point or the asynchronous irregular phase, and reproducing quite remarkably the chief experimental observations of Okujeni *et al.* The similarity, as shown in Fig. 2.3.4A, is remarkable: more homogeneous lattices show network spikes more separated in time, while more heterogeneous ones exhibits clustered spikes, with persistent activity in some units, in a way that closely resembles that of experiments. This computational experiments clearly reveal that refined variants of our general model are able to closely reproduce experimental observations.

Apart from this, long-range connections among local regions also exist in the cortex, and mesoscopic units are not necessarily homogeneous across space. Even if most of the neuronal connections occur within the local neighborhood, long-range white-matter connectivity allows for information to be distributed and processed across the whole cortex. Such long-range connections comprise only about 10% of the total connections in the brain, but their role is crucial for brain functionality [42, 76]. The simplest possible approximation beyond a lattice is a small-world network (as done in the Watts-Strogatz model [87]). In fact, our main results (i.e. the existing phases and phase transitions) are insensitive to the introduction of a small percentage of long-range connections.

However, there exists empirically-obtained large-scale networks of the human brain, and their heterogeneous and hierarchical-modular architecture is known to influence dynamical process operating on them [59, 76] and optimize the transmission of information. But nevertheless, our approach refers to the cortex in the context of the neural field models –that can be treated as a continuous sheet– and not to a network of neural masses [11]. So, to consider real neuroanatomical connections –encoded in the *human connectome network*– the diffusive coupling (or the model) should be re-examined.

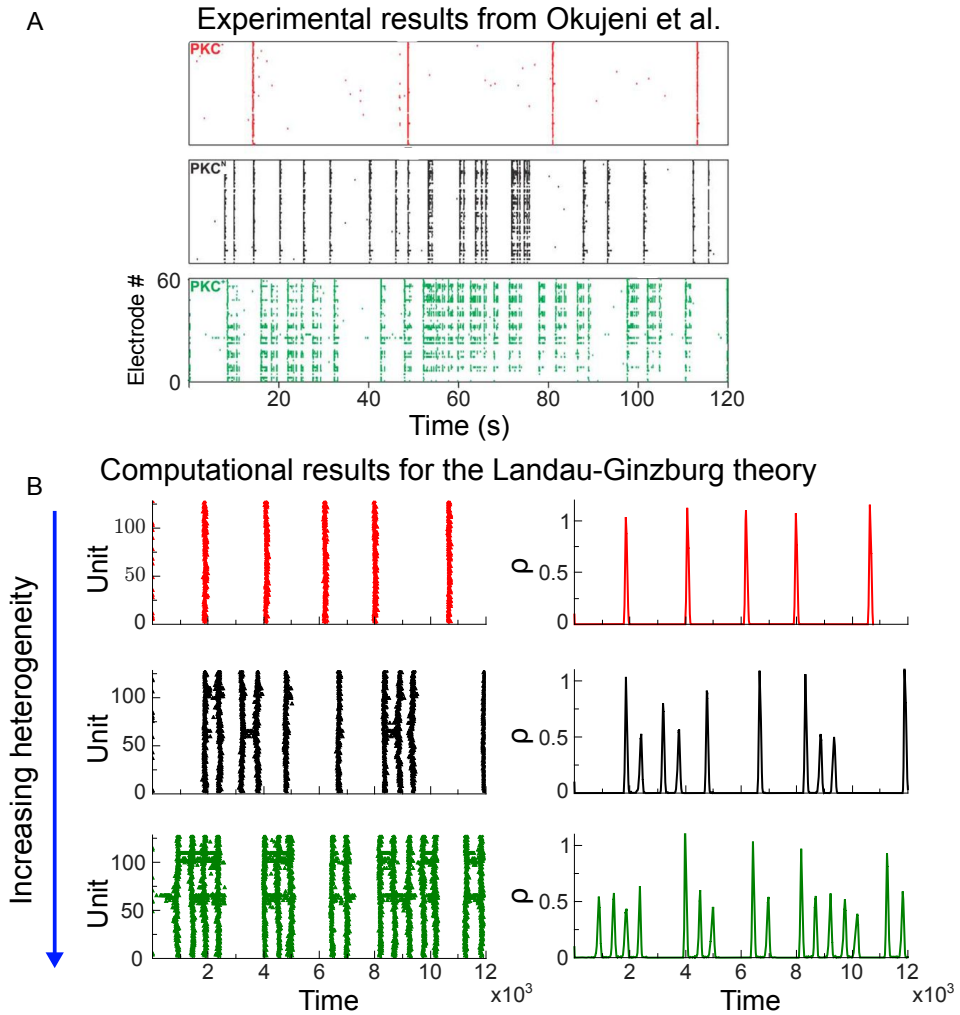


Figure 2.3.4: Temporal series for different level of network clustering. Panel A shows the experimental results of Okujeni [61] (adapted figure from the original paper) for increasing levels of aggregation in a neural network. Panel B shows three temporal series for different levels of network clustering and a fixed value of $\xi = 1.2$. In the first one (red) the network is homogeneous with $a_1 = a_2 = 1$. Observe that smaller values of a_1 produce a more active network, in particular for $a_1 = -0.7$ (black) and $a_1 = -0.928$ (green). In both cases, the clustering facilitate the spontaneous activity. Other parameter values: $b = 1.5, \tau_D = 10^2, \tau_R = 10^3, h = 10^{-7}$.

2.4

The case of infinite separation of timescales. Recovering self-organized bistability

It has been speculated that self-organized bistability (SOB) might be relevant in e.g. the neuronal dynamics of the brain, which –during deep sleep or under anesthesia– exhibits bistability, with an alternation between high and low levels of neural activity, called up and down states, respectively [7, 41, 57]. This underlying bistability, together with the empirical observation of scale-free avalanches –appearing sometimes in concomitance with anomalously large outbursts– in the awake resting brain, suggests indeed that the neuronal avalanches in the awake state could stem from the self-organization to the edge of bistability, rather than the usually postulated self-organization to criticality.

Remarkably, our physiologically-inspired model –the set of equations (2.2.2) and (2.2.3)– proposed to shed light on the large-scale features of brain activity, and relying on synaptic plasticity as a chief regulatory mechanism, exhibits profound analogies with the theory of SOB [70]. As a matter of fact, the first equation is identical with the equation for activity in SOB, which describes in the simplest possible way a first order phase transition. Thus, it is natural to scrutinize whether self-organized bistability plays any relevant role in neuroscience.

On the other hand, formal differences appear in the second one, for the so-called “background (energy) field” (which here is interpreted as a synaptic-resource field). An important one is that in SOB the background field is conserved in the bulk; only driving events and boundary dissipation make the total integral value fluctuate in time, providing a mechanism, out of which –in the limit of small driving and dissipation– the system self-organizes to the very edge of the first-order phase transition, as described in [70].

However, the above equation for $\dot{R}(t)$ is not conserved in general. It includes a (positive) term for the charging/recovery of resources which is tantamount to driving in SOB as well as a (negative) term for the activity-dependent consumption of resources. For neuro-physiologically plausible values of the characteristic times of these two processes, a rich phenomenology emerges, as extensively discussed until now.

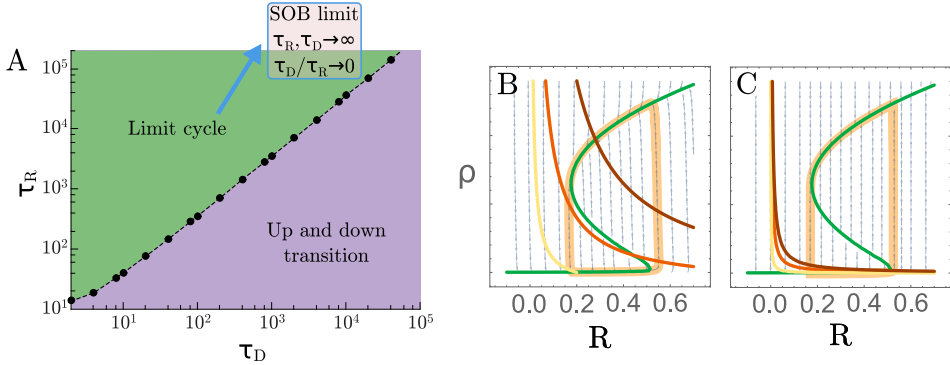


Figure 2.4.1: Phase diagram and phase portraits for the (deterministic) dynamics of Eqs. (2.2.2) and (2.2.3). (A) It is possible to recover the SOB limit by taking some conditions in the aforementioned case A (limit cycle). (B) Nullclines for $\dot{\rho} = 0$ is colored in green, and three nullclines for $\dot{R} = 0$ for three different values of ξ are plotted in yellow, orange and brown; small grey arrows represent the vector field for $(\dot{\rho}, \dot{R})$ and light orange curve represent a trajectory for the intermediate value of ξ (orange curve). The system falls in the –widely discussed above– case A, showing a limit cycle between the down and the up state ($\tau_D/\tau_R = 10^{-1}$, $\tau_R = 10^3$ and $\xi = 0.2, 1.5, 3.5$ for yellow, orange and brown curves respectively) (C) The system approaches to the SOB limit behavior and the dependence on the control parameter vanishes ($\tau_D/\tau_R = 10^{-3}$, $\tau_R = 10^7$ and $\xi = 1, 5, 10$). Other parameters are $h = 10^{-3}$, $a = 0.6$, $b = 1.3$, $c = 1$, in both cases.

In this particular case, as discussed above, there are two possible scenarios –for a plausible separation of the characteristic scales of synaptic resources, τ_R and τ_D – according to the relation between the timescales for the recovery and depletion (τ_R and τ_D , respectively). Remember that, between the quiescent or ‘down’ state with $\rho^* \approx 0$ and the active or ‘up’ state with self sustained activity there exists a stable limit cycle (case A) or a regime of bistability (case B). The phase diagram of Figure 2.4.1A show the different possible cases that emerge when the control parameter ξ is varied (cases A and B).

But, nevertheless, by the mere fact of enhance the difference between the charging/consumption ratio of resources –as shown in Fig. 2.4.1C in the same non-conserved framework– the limit of *SOB* can be recovered for infinitely slow synaptic dynamics. Thus, keeping in mind that the mechanism of the recovery of synaptic resources (happening at a timescale τ_R) plays the role of driving, while the depletion of resources (at the characteristic scale τ_D) in presence of neural activity plays the role of dissipation, the limit of infinite separation of timescales can be recovered considering the case with $1/\tau_R \rightarrow 0$ and $1/\tau_D \rightarrow 0$, while

$\tau_D/\tau_R \rightarrow 0$ (see phase diagram of Figure 2.4.1A). And now, in fact, the larger the synaptic timescales, the weaker the dependence on the control parameter ξ (see Fig. 2.4.1C). This allows to reproduce one of the main features of the self-organization mechanism: the independence on any tuning parameter. Moreover, the relation between the two timescales is such that the slope of the nullcline $\dot{R} = 0$ goes to zero in the thermodynamic limit, making sure that (for any –reasonable– value of the parameter ξ) only one unstable fixed point exists¹¹, giving rise to a limit cycle, much as in the mean field SOB case [70].

We have hypothesized that the emergent collective behavior of a network of mesoscopic regions of neural tissue is poised at a synchronization phase transition, in the aforementioned case A, that is able to reproduce multiple empirical findings. But, as in real mesoscopic populations [6], which displays local field potentials exhibiting sharp negative peaks indicative of population spikes, this particular signal processing should be kept. Otherwise, a measure of global activity over threshold (probably meaningless in such a case), as it is usually done in absorbing/active phase transitions, poses some problems to the detection of spatially extended scale-invariant activity with the branching process exponents (see appendix B.3.2 for an extended discussion on the proper measure of avalanches over a threshold). Such ideal definition of avalanches is based on the fact that, under a slow charging, i.e. a slow adding of activity, the (quiescent) system end up triggering a concatenation of events until fell again in the absorbing/quiescent state. As far as we know, both formalisms –in the vicinity of a critical point– can lead to avalanches following a scale-invariant law for the the avalanche-size (S) and avalanche-duration (T) as $P(S) \sim S^{-\tau}$ and $P(T) \sim T^{-\alpha}$, respectively. Likewise, the averaged avalanche size scale as $\langle S \rangle \sim T^\gamma$ ¹².

On the other hand, in the original case of SOB, the ideal definition of avalanches leads to spatially extended cascades of activity showing scale-invariant behavior, complemented with anomalous events of activity spanning the whole system size, and following the mean-field exponents of the (Galton-Watson) unbiased branching process [38, 48, 70, 86]. Also, at the steady state, and in the limit of infinite size, the system self-organizes to the Maxwell point of a first order phase transition, where active and absorbing phases coexist, being equally stable and continuously trying to invade each other.

In fact, in the case of very large synaptic timescales –bringing us closer to the case of SOB– we can appreciate this proper measure of avalanches (see Fig.2.4.2), intended as activity over threshold. The behavior reports scale-invariant episodes of activity, which fits very well with the exponents of the branching process universality class, together with anomalous "king" avalanches, whose sizes scale with the system size, much as in the conserved SOB system.

¹¹As long as the Maxwell point is not in the vicinity of $R = 0$

¹²And it obey the scaling relation $\gamma = \frac{\alpha-1}{\tau-1}$

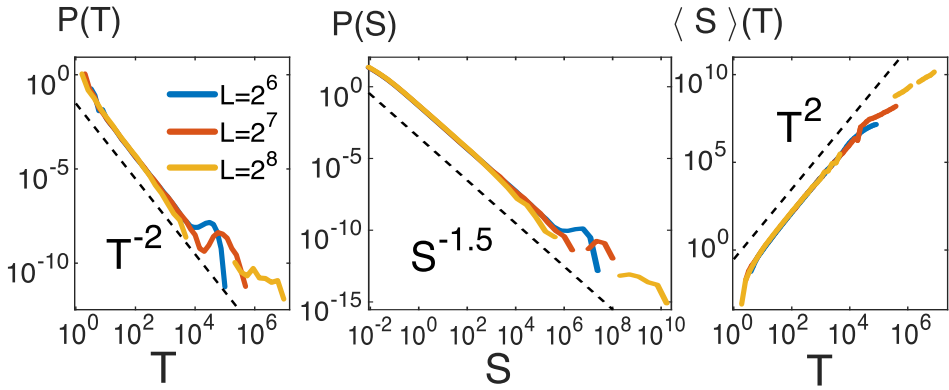


Figure 2.4.2: Avalanche distributions in the limit of extremely slow synaptic-resources dynamics, for the spatially extended noisy system. Probability distribution for avalanche durations T (left), avalanche sizes S (center) and average avalanche size as a function of duration (right) in log-log scale, for square-lattice systems of sizes $N = 64^2$, 128^2 and 256^2 . The dashed lines are plotted as a guide to the eye, and have the slopes corresponding to the expectations for an unbiased branching process ($\alpha = -2$, $\tau = -3/2$ and $\gamma = 2$, respectively) as experimentally observed. The “bumps” in the blue curves, correspond to anomalously large events, i.e. synchronized spiking events, obeying finite-size scaling. Parameters: $b = 0.5$, $a = 1$, $h = 10^{-7}$, $\tau_D = 10^4$, $\tau_R = 10^6$, $\sigma = D = 1$.

On the other hand, in Fig. 2.4.3 we plot a measure of avalanche statistics, showing the weak dependence on the control parameter ξ , if SOB conditions are fulfilled, whereas in the limit of infinitely slow dynamics the dependence on the control parameter vanishes completely, as expected for a well-behaved self-organizing mechanism.

At first, we have accomplished the theoretical abstraction of recovery SOB dynamics from the Landau-Ginzburg theory of cortex. However, it makes apology of the (sometimes) stormy relation between physics and biology, in the sense that “well-behaved” physical theories are not mere copies of the intricate Nature. They involve some idealization and, in particular, SOB depicts a highly idealized reality, going much further than the Landau-Ginzburg model. For instance if we take as a reference the neural activity timescale¹³, as reported by neurophysiological measurements, such scales are comprised between few tens and few hundreds of milliseconds [17, 53]. Such timescales are outside the scope of the proposed SOB limit, which requires much slower dynamics for its

¹³The unit of time, in the Landau-Ginzburg model, should be understood in terms of the spontaneous decay of activity.

idealistic outlook. On the other side, the Landau-Ginzburg model –leading to verifiable predictions– is able to undertake such timescales as a starting point.

Summing up, SOB limit could be seen as a limiting unrealistic case of the Landau-Ginzburg model that, however, is able to provide certain theoretical context to the exponents reported both in the Landau-Ginzburg model and in neural avalanches. Also, further work is needed to merge both definitions of avalanches, as well as in a thorough theoretical understanding of why results are compatible with branching-process exponents.

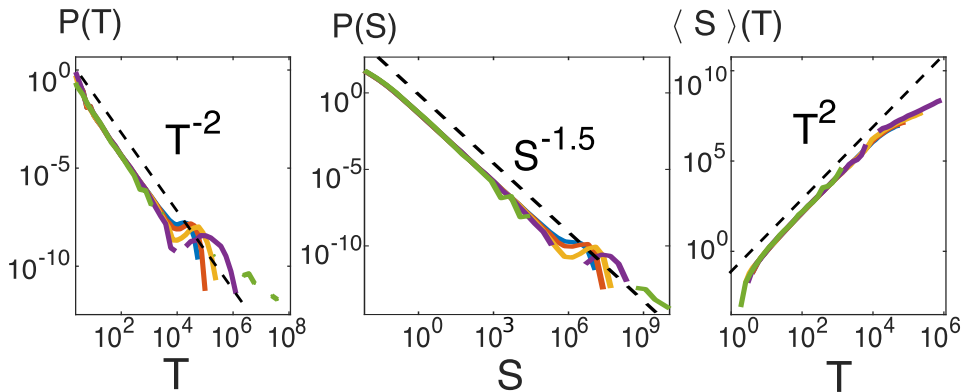


Figure 2.4.3: The control parameter has no influence in the limit of extremely slow synaptic-resources dynamics, for the spatially extended noisy system ($N = 128^2$) in double logarithmic scale. Different colors depicts different values of ξ ($\xi = 1, 3, 5, 7, 10$). There is no change in the probability distributions for avalanche durations T (left), avalanche sizes S (center) and average avalanche size as a function of duration (right). The dashed lines are plotted as a guide to the eye and their slopes correspond to unbiased branching process exponents. Other parameters are exactly the same as in Fig. 2.4.2.

Conclusions

The brain of mammals is in a state of sempiternal irregular activity. Understanding the origin, meaning, and functional significance of such an energetically costly dynamical state are fundamental problems, whose importance cannot be overemphasized. The –so called– criticality hypothesis conjectures that the underlying dynamics of cortical networks is such that it is posed at the edge of a continuous phase transition, separating qualitatively different phases or regimes, with different degrees of order. Experience from statistical physics and the theory of phase transitions teaches that critical points are rather singular locations in phase diagrams, with very remarkable and peculiar features, such as scale invariance, i.e. the fact that fluctuations of wildly diverse spatio-temporal scales can emerge spontaneously, allowing the system dynamics to generate complex patterns of activity in a simple and natural way. A number of other features of criticality, including scale invariance, have been conjectured to be functionally convenient and susceptible to be exploited by biological (as well as artificial) computing devices. Thus, the hypothesis that the brain actually works at the borderline of a phase transition has gained momentum in recent years, even if some skepticism remains [82]. However, what these phases are, and what the nature of the putative critical point is, are questions that still remain to be fully settled.

Aimed at shedding light on these issues, here we followed a classical statistical-physics approach. Following the parsimony principle of Landau and Ginzburg in the study of phases of the matter and the phase transitions they experience, we proposed a simple stochastic mesoscopic theory of cortical dynamics that allowed us to classify the possible emerging phases of cortical networks under very general conditions. For the sake of specificity and concreteness we focused on a regulatory dynamics –preventing the level of activity to explode– controlled by synaptic plasticity (depletion and recovery of synaptic resources), but analogous results can be obtained considering e.g. inhibition as the chief regulatory mechanism. As a matter of fact, our conclusions are quite robust and general and do not essentially depend on specific details of the implementation, the nature of the regulatory mechanism, or the network architecture.

The mesoscopic approach upon which our theory rests is certainly not radically novel; quite a few related models exist in the literature. For instance, neural-mass or neural-field models [12, 21, 27, 29, 36], rate or population activity equations [22, 32], are similar in spirit, and have been successfully employed

to analyze activity of populations of neurons and synapses, and their emerging collective regimes, at a mesoscopic scale.

However, importantly, taking advantage of experience from the theory of phase transitions, we introduce two additional key ingredients: intrinsic stochasticity stemming from the non-infinite size of mesoscopic regions, and spatial dependence. In this way, our theory consists of a set of stochastic Wilson-Cowan equations and can be formulated as a field theory, employing standard techniques [79]. Let us mention that Buice and Cowan developed a very similar (field theoretic) approach in which fluctuation effects in neural networks were analyzed [16]. Their theory turns out to include a continuous phase transition from a quiescent to an active phase, with a critical point in between. This is in blatant contrast with our findings here. Note, however, that their picture can be easily recovered in our framework, just by changing the sign of a parameter: i.e. making b in Eq.(2.2.2) negative. The meaning of this is that neural integration effects are neglected (as discussed below). This change of sign leads to an underlying *continuous* phase transition between a quiescent and an active phase; and in such a case (i.e. with $b < 0$) our theory constitutes a sound Landau-Ginzburg description of microscopic models of neural dynamics exhibiting criticality and a continuous phase transition (see [10, 47]). We believe, however, that this scenario does not properly capture the essence of cortical dynamics as, in actual networks of spiking neurons, there are spike-integration mechanisms, meaning that many inputs are required to trigger further activity. This is, indeed, captured in the Wilson-Cowan model –at the basis of our approach– which includes a sigmoid response function, implying that activity has to be above some threshold to be self-sustained, and implying, after expanding in power-series that the parameter b has to be positive, precluding the existence of a continuous quiescent/active phase transition.

Using our Landau-Ginzburg approach, we have shown that the stochastic and spatially extended neural networks can harbor two different scenarios depending on parameter values: case (A) including a limit cycle at the deterministic level and the possibility of oscillations and case (B) leading to bistability (see Fig. 2.2.1).

In the simpler case (B) our complete theory generates a down and a homogeneous up-state phase, with a discontinuous transition separating them, and the possibility of up-down transitions when the system operates in the bistability region. In this case, our theory constitutes a sound mesoscopic description of existing microscopic models for up-and-down transitions [41, 46, 56, 66] as observed in the cortex during deep sleep or under anesthesia [25, 78].

On the other hand, in case (A), we find diverse phases including oscillatory and bursting phenomena: down states, synchronous irregular, asynchronous irregular, and active states. As a side remark, note that, in the search of a mesoscopic description of cortical networks of spiking neurons, we constructed

a coarse-grained model for the network activity. However, our analyses readily revealed the “spiking” nature of the activity dynamics, underlying the fundamental role of oscillations and partial synchronization in neural dynamics across scales. Hence, our results justify the use of models of effective coupled oscillators to scrutinize the large-scale dynamics of brain networks [18] (as explained below in the chapter 3). As a matter of fact, these models seem to achieve the best performance –in reproducing empirically observed resting-state networks [76]– when operating close to the synchronization phase transition point.

Within our framework, it is possible to define a protocol to analyze avalanches, resembling very closely the experimental one [6, 7, 54, 64, 74]. Thus, in contrast with other computational models, causal information is not explicitly needed/employed here to determine avalanches –they are determined from raw data– and results can be straightforwardly compared to experimental ones for neuronal avalanches, without conceptual gaps [52].

The model reproduces all the main features observed experimentally: (i) Avalanche sizes and durations distributed in a scale-free way emerge at the critical point of the synchronization transition. (ii) The corresponding exponent values depend on the time bin Δt , required to define avalanches, but (iii) fixing the time bin Δt to coincide with the inter-spike interval, *ISI*, the same statistics as in empirical networks, i.e. the critical exponents compatible with those of an unbiased branching process (which is subsequently addressed) are obtained; and finally (iv) scale-free distributions disappear if events are reshuffled in time, revealing a non-trivial temporal organization.

Thus, the main outcome of our analyses is that the underlying phase transition at which scale-free avalanches emerge does not separate a quiescent state from a fully active one but a synchronization transition, separating regimes in which mesoscopic units tend to become active synchronously or asynchronously, respectively. This is a crucial observation, as most of the existing modeling approaches for critical avalanches in neural dynamics to date rely on a continuous quiescent/active phase transition, and this is not a pertinent choice as we have argued above.

Let us also remark that –consistently with our findings– the amazingly detailed model put together by the Human Brain Project consortium seems to suggest that the model best reproduces experimental features when tuned near to its synchronization critical point [49]. In such a study, the concentration of Calcium ions, Ca^{2+} needs to be carefully tuned to its actual nominal value to set the network state. Similarly, in our approach, the role of the calcium concentration is played by the parameter ξ , regulating the maximum level reachable by synaptic resources. Interestingly, the calcium concentration is well-known to modulate the level of available synaptic resources (i.e. neurotransmitter release from neurons; see e.g. [22, 50, 83]), hence, both quantities play a similar role.

Let us emphasize that here we have not made any attempt whatsoever to explore how could potentially the network self-organize to operate in the vicinity of the synchronization critical point. Adaptive, homeostatic and self-regulatory mechanisms accounting for this will be analyzed in a future work. Also, here we have not looked for the recently uncovered *neutral neural avalanches* [52], as these require causality information to be considered, and such detailed causal relationships are blurred away in mesoscopic coarse grained descriptions.

Summing up, our Landau-Ginzburg theory with parameters lying in case (B) constitutes a sound description of the cortex during deep sleep or during anesthesia, when up and down transitions are observed. On the other hand, case (A) when tuned close to the synchronization phase transition can be a sound theory for the awake cortex, in a state of alertness. A detailed analysis of how the transition between deep-sleep (described by case (B)) and awake (or REM sleep, described by case (A)) may actually occur in these general terms is beyond our scope here, but let us remark that, just by modifying the speed at which synaptic resources recover it is possible to shift between the two cases, making it possible to speculate on how such transitions could be easily induced.

A simple extension of our theory, including spatial heterogeneity has been shown to be able to reproduce remarkably well experimental measurements of activity in neural cultures with structural heterogeneity, opening the way to more stringent empirical validations of the general theory proposed here.

Even if further experimental, computational and analytical studies are certainly required to definitely settle the controversy about the possible existence, origin, and functional meaning of the possible phases and phase transitions in cortical networks, we hope that the general framework introduced here –based on very general and robust principles– helps in clarifying the picture and in paving the way to future developments in this fascinating field.

References

- [1] AMIT, D. J. & BRUNEL, N. «Model of global spontaneous activity and local structured activity during delay periods in the cerebral cortex». *Cereb. Cortex* **7**, 237–252 (1997).
- [2] DE ARCANGELIS, L. «Are dragon-king neuronal avalanches dungeons for self-organized brain activity?». *Eur. Phys. J. Spec.Top.* **205**, 243–257 (2012).
- [3] DE ARCANGELIS, L., PERRONE-CAPANO, C. & HERRMANN, H. J. «Self-Organized Criticality Model for Brain Plasticity». *Phys. Rev. Lett.* **96**, 028107 (2006).
- [4] ARIELI, A., STERKIN, A., GRINVALD, A. & AERTSEN, A. «Dynamics of ongoing activity: explanation of the large variability in evoked cortical responses». *Science* **273**, 1868 (1996).
- [5] BAK, P. *How nature works: the science of self-organized criticality* (Copernicus, New York, 1996).
- [6] BEGGS, J. M. & PLENZ, D. «Neuronal avalanches in neocortical circuits». *J. Neurosci.* **23**, 11167–11177 (2003).
- [7] BELLAY, T., KLAUS, A., SESHADRI, S. & PLENZ, D. «Irregular spiking of pyramidal neurons organizes as scale-invariant neuronal avalanches in the awake state». *Elife* **4**, e07224 (2015).
- [8] BENAYOUN, M., COWAN, J. D., VAN DRONGELEN, W. & WALLACE, E. «Avalanches in a stochastic model of spiking neurons». *PLoS Comp. Biol.* **6**, e1000846 (2010).
- [9] BINNEY, J. J., DOWRICK, N. J., FISHER, A. J. & NEWMAN, M. *The theory of critical phenomena: an introduction to the renormalization group* (Oxford University Press, Oxford, 1992).
- [10] BONACHELA, J., DE FRANCISCIS, S., TORRES, J. & MUÑOZ, M. A. «Self-organization without conservation: are neuronal avalanches generically critical?». *J. Stat. Mech. Theory Exp.* **2010**, P02015 (2010).
- [11] BREAKSPEAR, M. «Dynamic models of large-scale brain activity». *Nat. Neurosci.* **20**, 340–352 (2017).
- [12] BRESSLOFF, P. C. «Spatiotemporal dynamics of continuum neural fields». *J. Phys. A Math. Theor.* **45**, 033001 (2012).

-
- [13] BRESSLOFF, P. C. «Metastable states and quasicycles in a stochastic Wilson-Cowan model of neuronal population dynamics». *Phys. Rev. E* **82**, 051903 (2010).
- [14] BRUNEL, N. «Dynamics of sparsely connected networks of excitatory and inhibitory spiking neurons». *J. Comput. Neurosci.* **8**, 183–208 (2000).
- [15] BRUNEL, N. & HAKIM, V. «Sparsely synchronized neuronal oscillations». *Chaos* **18**, 015113 (2008).
- [16] BUICE, M. A. & COWAN, J. D. «Field-theoretic approach to fluctuation effects in neural networks». *Phys. Rev. E* **75**, 051919 (2007).
- [17] BUZSAKI, G. *Rhythms of the Brain* (Oxford University Press, Oxford, 2006).
- [18] CABRAL, J., HUGUES, E., SPORNS, O. & DECO, G. «Role of local network oscillations in resting-state functional connectivity». *Neuroimage* **57**, 130–139 (2011).
- [19] CHIALVO, D. R. «Emergent complex neural dynamics». *Nat. Phys.* **6**, 744–750 (2010).
- [20] CHIALVO, D. R. «Critical brain networks». *Phys. A* **340**, 756–765 (2004).
- [21] DAVID, O. & FRISTON, K. J. «A neural mass model for MEG/EEG:: coupling and neuronal dynamics». *NeuroImage* **20**, 1743–1755 (2003).
- [22] DAYAN, P. & ABBOTT, L. «Theoretical neuroscience: computational and mathematical modeling of neural systems». *J. Cogn. Neurosci.* **15**, 154–155 (2003).
- [23] DECO, G. & JIRSA, V. K. «Ongoing cortical activity at rest: criticality, multistability, and ghost attractors». *J. Neurosci.* **32**, 3366–3375 (2012).
- [24] DECO, G., JIRSA, V. K., ROBINSON, P. A., BREAKSPEAR, M. & FRISTON, K. «The dynamic brain: from spiking neurons to neural masses and cortical fields». *PLoS Comp. Biol.* **4**, e1000092 (2008).
- [25] DESTEXHE, A. «Self-sustained asynchronous irregular states and Up Down states in thalamic, cortical and thalamocortical networks of nonlinear integrate-and-fire neurons». *J. Comput. Neurosci.* **27**, 493–506 (2009).
- [26] DORNIC, I., CHATÉ, H. & MUÑOZ, M. A. «Integration of Langevin equations with multiplicative noise and the viability of field theories for absorbing phase transitions». *Phys. Rev. Lett.* **94**, 100601 (2005).

- [27] EL BOUSTANI, S. & DESTEXHE, A. «A master equation formalism for macroscopic modeling of asynchronous irregular activity states». *Neural Comput.* **21**, 46–100 (2009).
- [28] FOX, M. D. & RAICHLE, M. E. «Spontaneous fluctuations in brain activity observed with functional magnetic resonance imaging». *Nat. Rev. Neurosci.* **8**, 700–711 (2007).
- [29] FREEMAN, W. J. *Mass action in the nervous system* (Elsevier Science & Technology, New York, 1975).
- [30] GARDINER, C. W. *Handbook of stochastic methods: for physics, chemistry and the natural sciences; 3rd ed.* Springer Series in Synergetics (Springer, Berlin, 2004).
- [31] GAUTAM, S. H., HOANG, T. T., MCCLANAHAN, K., GRADY, S. K. & SHEW, W. L. «Maximizing sensory dynamic range by tuning the cortical state to criticality». *PLoS Comp. Biol.* **11**, e1004576 (2015).
- [32] GERSTNER, W., KISTLER, W. M., NAUD, R. & PANINSKI, L. *Neuronal dynamics: From single neurons to networks and models of cognition* (Cambridge University Press, Cambridge, 2014).
- [33] GIREESH, E. D. & PLENZ, D. «Neuronal avalanches organize as nested theta- and beta/gamma-oscillations during development of cortical layer 2/3». *Proc. Natl. Acad. Sci. USA* **105**, 7576–7581 (2008).
- [34] HAHN, G. *et al.* «Neuronal avalanches in spontaneous activity in vivo». *J. Neurophysiol.* **104**, 3312–3322 (2010).
- [35] HAIMOVICI, A., TAGLIAZUCCHI, E., BALENZUELA, P. & CHIALVO, D. R. «Brain organization into resting state networks emerges at criticality on a model of the human connectome». *Phys. Rev. Lett.* **110**, 178101 (2013).
- [36] HAKEN, H. *Principles of brain functioning: a synergetic approach to brain activity, behavior and cognition*, vol. 67 (Springer Science & Business Media, 2013).
- [37] HARNACK, D., PELKO, M., CHAILLET, A., CHITOUR, Y. & VAN ROSSUM, M. C. «Stability of neuronal networks with homeostatic regulation». *PLoS Comp. Biol.* **11**, e1004357 (2015).
- [38] HARRIS, T. E. *The theory of branching processes* (Courier Corporation, 2002).

- [39] HENKEL, M., HINRICHSEN, H. & LÜBECK, S. *Non-equilibrium Phase Transitions: Absorbing phase transitions*. Theoretical and mathematical physics (Springer, Berlin, 2008).
- [40] HOBBS, J. P., SMITH, J. L. & BEGGS, J. M. «Aberrant neuronal avalanches in cortical tissue removed from juvenile epilepsy patients». *J. Clin. Neurophysiol.* **27**, 380–386 (2010).
- [41] HOLCMAN, D. & TSODYKS, M. «The emergence of up and down states in cortical networks». *PLoS Comp. Biol.* **2**, e23 (2006).
- [42] JBABDI, S., SOTIROPOULOS, S. N., HABER, S. N., VAN ESSEN, D. C. & BEHRENS, T. E. «Measuring macroscopic brain connections in vivo». *Nat. Neurosci.* **18**, 1546–1555 (2015).
- [43] JENSEN, H. J. *Self-organized criticality: emergent complex behavior in physical and biological systems* (Cambridge university press, Cambridge, 1998).
- [44] KANDEL, E. R., SCHWARTZ, J. H., JESSELL, T. M., SIEGELBAUM, S. A. & HUDSPETH, A. J. *Principles of neural science* (McGraw-hill, New York, 2000).
- [45] KURAMOTO, Y. «Self-entrainment of a population of coupled nonlinear oscillators». *Lect. Notes Phys.* **39**, 420–422 (1975).
- [46] LEVINA, A., HERRMANN, J. M. & GEISEL, T. «Phase Transitions towards Criticality in a Neural System with Adaptive Interactions». *Phys. Rev. Lett.* **102**, 118110 (2009).
- [47] LEVINA, A., HERRMANN, J. M. & GEISEL, T. «Dynamical synapses causing self-organized criticality in neural networks». *Nat. Phys.* **3**, 857–860 (2007).
- [48] LIGGETT, T. *Interacting Particle Systems*. Classics in Mathematics (Springer, Berlin, 2004).
- [49] MARKRAM, H. *et al.* «Reconstruction and simulation of neocortical microcircuitry». *Cell* **163**, 456–492 (2015).
- [50] MARKRAM, H. & TSODYKS, M. «Redistribution of synaptic efficacy between pyramidal neurons». *Nature* **382**, 807–810 (1996).
- [51] MARRO, J. & DICKMAN, R. *Nonequilibrium phase transitions in lattice models* (Cambridge University Press, Cambridge, 2005).

- [52] MARTINELLO, M. *et al.* «Neutral theory and scale-free neural dynamics». *Phys. Rev. X* **7**, 041071 (2017).
- [53] MATTIA, M. & SANCHEZ-VIVES, M. V. «Exploring the spectrum of dynamical regimes and timescales in spontaneous cortical activity». *Cogn. Neurodyn.* **6**, 239–250 (2012).
- [54] MAZZONI, A. *et al.* «On the dynamics of the spontaneous activity in neuronal networks». *PLoS One* **2**, e439 (2007).
- [55] MEJIAS, J. F., KAPPEN, H. J. & TORRES, J. J. «Irregular dynamics in up and down cortical states». *PLoS One* **5**, e13651 (2010).
- [56] MILLMAN, D., MIHALAS, S., KIRKWOOD, A. & NIEBUR, E. «Self-organized criticality occurs in non-conservative neuronal networks during 'up' states». *Nat. Phys.* **6**, 801–805 (2010).
- [57] MONGILLO, G., HANSEL, D. & VAN VREESWIJK, C. «Bistability and spatiotemporal irregularity in neuronal networks with nonlinear synaptic transmission». *Phys. Rev. Lett.* **108**, 158101 (2012).
- [58] MORA, T. & BIALEK, W. «Are biological systems poised at criticality?». *J. Stat. Phys.* **144**, 268–302 (2011).
- [59] MORETTI, P. & MUÑOZ, M. A. «Griffiths phases and the stretching of criticality in brain networks». *Nat. Comm.* **4** (2013).
- [60] MORETTI, P. & MUÑOZ, M. A. «Griffiths phases and the stretching of criticality in brain networks». *Nat. Comm.* **4**, – (2013).
- [61] OKUJENI, S., KANDLER, S. & EGERT, U. «Mesoscale architecture shapes initiation and richness of spontaneous network activity». *J. Neurosci.* **37**, 3972–3987 (2017).
- [62] PASQUALE, V., MASSOBRIO, P., BOLOGNA, L., CHIAPPALONE, M. & MARTINOIA, S. «Self-organization and neuronal avalanches in networks of dissociated cortical neurons». *Neuroscience* **153**, 1354–1369 (2008).
- [63] PERSI, E., HORN, D., VOLMAN, V., SEGEV, R. & BEN-JACOB, E. «Modeling of synchronized bursting events: the importance of inhomogeneity». *Neural Comput.* **16**, 2577–2595 (2004).
- [64] PETERMANN, T. *et al.* «Spontaneous cortical activity in awake monkeys composed of neuronal avalanches». *Proc. Natl. Acad. Sci. USA* **106**, 15921–15926 (2009).

- [65] PIKOVSKY, A., ROSENBLUM, M. & KURTHS, J. *Synchronization: a universal concept in nonlinear sciences*, vol. 12 (Cambridge university press, Cambridge, 2003).
- [66] PITTORINO, F., IBÁÑEZ-BERGANZA, M., DI VOLO, M., VEZZANI, A. & BURIONI, R. «Chaos and Correlated Avalanches in Excitatory Neural Networks with Synaptic Plasticity». *Phys. Rev. Lett.* **118**, 098102 (2017).
- [67] POIL, S.-S., HARDSTONE, R., MANSVELDER, H. D. & LINKENKAER-HANSEN, K. «Critical-state dynamics of avalanches and oscillations jointly emerge from balanced excitation/inhibition in neuronal networks». *J. Neurosci.* **32**, 9817–9823 (2012).
- [68] RAICHLE, M. E. «The restless brain». *Brain. Connect.* **1**, 3–12 (2011).
- [69] REICHENBACH, T., MOBILIA, M. & FREY, E. «Self-organization of mobile populations in cyclic competition». *J. Theor. Biol.* **254**, 368–383 (2008).
- [70] DI SANTO, S., BURIONI, R., VEZZANI, A. & MUÑOZ, M. A. «Self-Organized Bistability Associated with First-Order Phase Transitions». *Phys. Rev. Lett.* **116**, 240601 (2016).
- [71] SCHUSTER, H. G., PLENZ, D. & NIEBUR, E. *Criticality in neural systems* (John Wiley & Sons, Weinheim, 2014).
- [72] SEGEV, R., SHAPIRA, Y., BENVENISTE, M. & BEN-JACOB, E. «Observations and modeling of synchronized bursting in two-dimensional neural networks». *Phys. Rev. E* **64**, 011920 (2001).
- [73] SHIN, C.-W. & KIM, S. «Self-organized criticality and scale-free properties in emergent functional neural networks». *Phys. Rev. E* **74**, 045101 (2006).
- [74] SHRIKI, O. *et al.* «Neuronal avalanches in the resting MEG of the human brain». *J. Neurosci.* **33**, 7079–7090 (2013).
- [75] DA SILVA, F. L. «Neural mechanisms underlying brain waves: from neural membranes to networks». *Electroencephalogr. Clin. Neurophysiol.* **79**, 81–93 (1991).
- [76] SPORNS, O. *Networks of the Brain* (MIT Press, USA, 2010).
- [77] STANLEY, H. E. *Introduction to phase transitions and critical phenomena* (Oxford University Press, Oxford, 1987).

- [78] STERIADE, M., NUNEZ, A. & AMZICA, F. «A novel slow (< 1 Hz) oscillation of neocortical neurons in vivo: depolarizing and hyperpolarizing components». *J. Neurosci.* **13**, 3252–3265 (1993).
- [79] TÄUBER, U. C. *Critical dynamics: a field theory approach to equilibrium and non-equilibrium scaling behavior* (Cambridge University Press, Cambridge, 2014).
- [80] TAGLIAZUCCHI, E., BALENZUELA, P., FRAIMAN, D. & CHIALVO, D. R. «Criticality in large-scale brain fMRI dynamics unveiled by a novel point process analysis.». *Front. Physiol.* **3** (2012).
- [81] TORRES, J. J. & VARONA, P. «Modeling biological neural networks». In *Handbook of Natural Computing*, 533–564 (Springer, 2012).
- [82] TOUBOUL, J. & DESTEXHE, A. «Power-law statistics and universal scaling in the absence of criticality». *Phys. Rev. E* **95**, 012413 (2017).
- [83] TSODYKS, M. & MARKRAM, H. «The neural code between neocortical pyramidal neurons depends on neurotransmitter release probability». *Proc. Natl. Acad. Sci. USA* **94**, 719–723 (1997).
- [84] VAN VREESWIJK, C. «Partially synchronized states in networks of pulse-coupled neurons». *Phys. Rev. E* **54**, 5522–5537 (1996).
- [85] VILLA MARTÍN, P., BONACHELA, J. A., LEVIN, S. A. & MUÑOZ, M. A. «Eluding catastrophic shifts». *Proc. Natl. Acad. Sci. USA* **112**, E1828–E1836 (2015).
- [86] WATSON, H. W. & GALTON, F. «On the probability of the extinction of families». *J. Royal Anthropol. Inst.* **4**, 138–144 (1875).
- [87] WATTS, D. J. & STROGATZ, S. H. «Collective dynamics of 'small-world' networks». *Nature* **393**, 440–442 (1998).
- [88] WILSON, H. R. & COWAN, J. D. «Excitatory and inhibitory interactions in localized populations of model neurons». *Biophys. J.* **12**, 1–24 (1972).
- [89] YANG, H., SHEW, W. L., ROY, R. & PLENZ, D. «Maximal variability of phase synchrony in cortical networks with neuronal avalanches». *J. Neurosci.* **32**, 1061–1072 (2012).

Synchronization in the human brain: Stretched criticality and metastability induced by network topology

3.1	Introduction	81
3.2	The Kuramoto model	83
3.2.1	Mean-Field approach	84
3.2.2	The Ott-Antonsen ansatz	87
3.2.3	The role of the frequency distribution: $g(\omega)$	88
3.2.4	Chimera states: getting frustration and metastability	91
3.3	Complex networks coupling	93
3.4	The Human Connectome	96
3.4.1	Chimeras	103
3.5	Modeling the HC	105
3.5.1	Communities	105
3.5.2	The two-block model	107
3.5.3	Simple-modular network	110
3.5.4	Hierarchic-modular network	113
3.6	Metastability and noise effects	118
3.7	Conclusions	122
	References	125

3.1

Introduction

“Oscillators of all brain, unite!”

Misattributed to K. Marx

Neuro-imaging techniques have allowed the identification of structural connections –at an individual-based level– making possible the reconstruction of structural human brain networks, composed of hundreds of neural regions and thousands of white-matter fiber interconnections. All this enables the possibility of a ‘road map’ of the brain: the well known “human connectome” (HC) [33, 36], which, moreover is arranged in a set of moduli –with a much larger intra than inter connectivity– structured in a hierarchical fractal-like fashion across multiple scales [17, 37, 38, 47, 64, 76].

On the other hand, the inference of correlations in neural activity between different brain regions, as detected in EEG or fMRI time series, and enables the reconstruction of “functional” connections, and thereby functional networks. Disclosing the structural and functional networks relationship is a key issue in modern neuroscience. Notable in this regard are the pioneering works that remark the profound implications for neural dynamics behind the hierarchical-modular organization of structural brain networks [39, 44, 76, 77]. In an entirely different way to the usual simpler network structures, –as the archetypal Erdős-Rényi networks– neural activity propagates in hierarchical networks in a rather distinctive way [48]; beside the usual two phases –percolating and non-percolating– commonly exhibited by models of activity propagation, an intermediate “Griffiths phase” [70] emerges on the HC network [48, 49]. The great variety of relatively-isolated moduli or “rare regions” promote the emergence of this novel phase, where dynamical activity remains mostly localized for long time periods, generating slow dynamics and very large responses [48, 49, 70].

Brain function requires coordinated or coherent neural activity at a wide range of scales and thus, synchronization is a keystone in modern computational neuroscience [16, 18, 26]. Besides, along with all these, synchronization plays a key role in vision, memory and other cognitive functions [65], such as the circadian rhythms in mammals [41], as well as in pathologies such as epilepsy [40].

Then, as a logical further development, one possibility is –in the spirit of contemplate realistic neural connections such as electrical, chemical, excitatory and inhibitory or dynamical synapses– to embedding the Tsodyks-Markram equations for synaptic plasticity of the above chapter in the human brain networks, implementing a more realistic coupling scheme than simple diffusion, in the same line as neural mass models [23, 30], or some type of direct interactions [24, 25, 45]. However, in order to preserve the essence of a minimal design, the prototypical Kuramoto model –widely used in neuroscience– allow us to analyze synchronization effects considering only couplings between mesoscopic units acting as oscillators [15, 22, 35].

Here we scrutinize the special features of synchronization [56] –as exemplified by the canonical Kuramoto model [4, 42, 66]– in a context of topological increasing complexity, i.e. from “all to all” coupling and mean-field analysis, to random network couplings and, finally, operating on top of the actual HC network [33, 36]. This interesting and particular case comprise a set of 998 nodes, each of them representing a mesoscopic population of neurons producing self-sustained oscillations [19], whose mutual connections are encoded by a symmetric –binary or weighted– connectivity matrix \mathbf{W} [33, 36]. We uncover the existence of a novel intermediate phase for synchronization dynamics stemming from the hierarchical organization of the HC, constituting the optimal regime for the brain to harbor complex behavior and large dynamical repertoires, presenting a plethora of complex and interesting dynamical features.

After dissect the special features of synchronization dynamics, the last step is to describe in more detail the complex behavior within such an intermediate regime, both in individual moduli and at a global brain level. We measure the fluctuations of the global order parameter as a function of the overall coupling strength, and we show that there is a broad region (rather than a unique “critical” point) with huge variability and response.

As we shall see in detail, this behavioral richness comes, at a first glance, from the modular structure of the human brain, and the story becomes interesting when a great variety of sizes and modules are blended in a fractal-like way. Thus, it is not enough with a simple modular network, and we should assemble a hierarchic-modular network to replicate the observed phenomena.

Finally, we assess the role of noise and perturbations in the robustness of the metastable stated arising in the intermediate regime, and we show that adding intrinsic fluctuations to the picture of synchronization dynamics in hierarchical modular networks accounts for the ability of the brain to explore different attractors, giving access to the varied functional configurations recorded in experiments [20, 24, 34].

3.2

The Kuramoto model

The paradigmatic Kuramoto model [42] was introduced by Yoshiki Kuramoto in 1975 with the goal of understanding the behavior of chemical and biological oscillators. However, over the time, the scope of the model exceed its germ, pervading fields that Kuramoto could never had imagined [15, 22, 62, 72]. In its usual formulation, it consists in a set of N coupled oscillators (see sketch in Fig. 3.2.1) governed by the next set of differential equations,

$$\dot{\theta}_j = \omega_j + k \sum_{l=1}^N W_{jl} \sin(\theta_l - \theta_j) \quad (3.2.1)$$

where θ_j is the phase of node j at time t , ω_j is the natural frequency of each oscillator, that should be extracted from some predefined probability distribution ($g(\omega)$), W_{jl} are the couplings between the different oscillators, and k is the coupling strength.

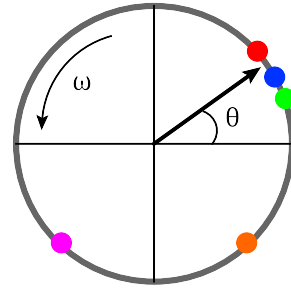


Figure 3.2.1: Phase (θ_j) and frequency (ω_j) in a set of oscillators.

In order to measure and quantify the level of synchronization in the whole system, i.e. to determine the difference between phases over time, the Kuramoto order parameter is the polar form of the complex sum of all phases,

$$Z(t) = R(t)e^{i\psi(t)} = \frac{1}{N} \sum_{j=1}^N e^{i\theta_j(t)} \quad (3.2.2)$$

where $0 \leq R \leq 1$ gauges the overall coherence and $\psi(t)$ is the average phase.

For an (infinitely) large population of oscillators interacting –in a fully connected network, as will be shown immediately– the model exhibits a phase transition at some value of k , separating a coherent steady state ($R > 0$) from an incoherent one ($R = 0$, plus $1/\sqrt{N}$ finite-size corrections) [4, 6, 42, 66]. On the other hand, in the absence of frequency heterogeneity perfect coherence always emerges reaching a coherent state [65]. Thus, frequency heterogeneity –or noise– leads to a phase transition at some critical value of the coupling strength, k_c , being able to frustrate synchronization if the coupling strength is weak.

3.2.1

Mean-Field approach

The first step to be taken is to understand the Kuramoto model in its simplest form. For that purpose, an all-to-all coupling scheme –or mean-field (MF) approach– bring us an useful way to study it theoretically in depth [4, 56], meaning that W_{jl} is a matrix with zero diagonal values and ones in the rest of the matrix. To achieve this end, using the order parameter from Eq. (3.2.2), multiplying by $e^{-i\theta_j}$ and regarding the imaginary part, it is easy to see that Eq. (3.2.1) now is,

$$\dot{\theta}_j = \omega_j + kR(t) \sin(\psi - \theta_j) \quad (3.2.3)$$

where ψ is the global phase of the whole system and kR is the new effective coupling strength.

This is an Euler differential equation, that can be mapped –in the continuum limit for large N – into a continuity equation¹

$$\frac{\partial P}{\partial t} + \frac{\partial}{\partial \theta} \{P [\omega + kR \sin(\psi - \theta)]\} = 0 \quad (3.2.4)$$

where $P(\theta, \omega, t)$ is the density of oscillators of phase θ and characteristic frequency ω at time t , obeying the normalization condition,

$$\int_{-\pi}^{\pi} P(\theta, \omega, t) = 1 \quad (3.2.5)$$

This equation has the trivial solution $P = \frac{1}{2\pi}$, $R = 0$, that corresponds to an equally phase distribution of the oscillators in $[-\pi, \pi]$. We are interested in the non-trivial stationary solution of $P(\theta, \omega)$ which generate a non-zero value of R . Thus, it can be possible to take the condition $v = \omega - kR \sin(\theta - \psi)$, wherein v (the drift velocity) is a constant, as stationary solution of Eq. (3.2.4) and, in particular, let us choose the case $v = 0$ –by simply fiddling with the rotating reference frame– for the coupled ones, turning it into $\theta - \psi = \arcsin(\frac{\omega}{kR})$. From its domain, it is easy to see that: (i) the coupling oscillators are in an interval $[-\frac{\pi}{2}, \frac{\pi}{2}]$ and, (ii) those with frequency $\omega > |kR|$ cannot be possibly in phase.

Such a state of partial synchronization should fulfill the form,

$$P(\theta, \omega, t) = \begin{cases} \delta[\theta - \psi - \arcsin(\frac{\omega}{kR})] H(\cos \theta) & \omega < |kR| \\ \frac{C}{|\omega - kR \sin(\theta - \psi)|} & \omega > |kR| \end{cases} \quad (3.2.6)$$

properly normalized, being C a normalization constant, and $H(x)$ the Heaviside step function.

¹That is very similar in spirit to a mapping from a Langevin equation to a Fokker-Planck -in the Itô sense- in the limiting case $\sigma = 0$. Remember (or see chapter 1) that a general stochastic equation $\dot{x} = A(x) + C\xi(t)$ is equivalent to $\dot{P}(x, t) = -\frac{\partial}{\partial x} A(x) P(x, t) + \frac{1}{2} C^2 \frac{\partial^2}{\partial x^2} P(x, t)$.

✖ **Inferring the critical point** In all this sight, we have considered the continuum limit for large N and, the density of oscillators of phase θ and characteristic frequency ω at time t , $P(\theta, \omega, t)$. Assuming a probability distribution of natural frequencies, $g(\omega)$, the complex order parameter can be expressed as,

$$Z = Re^{i\psi} = \int_{-\infty}^{+\infty} d\omega \int_{-\pi}^{\pi} d\theta P(\theta, \omega, t) g(\omega) e^{i\theta} \quad (3.2.7)$$

replacing the form of $P(\theta, \omega, t)$ (Eq. (3.2.6)) and considering the condition $P(\theta, \omega) = P(\theta + \pi, -\omega)$ and thus, neglecting the terms with $\omega > |kR|$, the above equation becomes²,

$$R = \int_{-\infty}^{+\infty} g(\omega) d\omega \int_{-\pi/2}^{\pi/2} d\theta e^{i(\theta-\psi)} \delta \left[\theta - \psi - \arcsin \left(\frac{\omega}{kR} \right) \right] = \int_{-\pi/2}^{\pi/2} g(\omega) d\omega e^{i(\sin^{-1}(\frac{\omega}{kR}))} \quad (3.2.8)$$

which, imposing that the distribution of frequencies should be an even function, i.e. $g(\omega) = g(-\omega)$, centered on $\omega = 0$, then we are left with nothing but the real part of the complex exponential, giving us,

$$R = Rk \int_{-\pi/2}^{\pi/2} \cos^2 \theta g(kR \sin \theta) d\theta \quad (3.2.9)$$

or, simply

$$R = \int_{-kR}^{kR} \sqrt{1 - \left(\frac{\omega}{kR} \right)^2} g(\omega) d\omega \quad (3.2.10)$$

Let us take a close look at these equations. The trivial solution $-R = 0$ always present— corresponds to a random distribution of the oscillators in the unit circle ($P = \frac{1}{2\pi}$). Also, there is a solution of partial synchronization that can lead to the critical value of the coupling strength, k_c . Only by taking the limit $R \rightarrow 0^+$ in Eq. (3.2.9), it comes to be,

$$k_c = \frac{2}{\pi g(0)} \quad (3.2.11)$$

separating the incoherent phase from the coherent one.

²Employing the next property of the Dirac delta function, $\int_{-\infty}^{+\infty} \delta(x-a) f(x) dx = f(a)$.

Even though it gives us the precise value for any symmetric distribution, it does not tell us nothing about the nature of the underlying synchronization transition. All this information lies behind the self-consistency equation (Eq. (3.2.9)), which prompt both first order and second order phase transitions [11]. Indeed, for unimodal and symmetric distributions, with non-zero second derivative, a second order phase transition emerges, forming a seed that grows monotonically with k beyond the critical point (in the coherent phase). By contrast, first order phase transition emerges when the distributions shows a plateau at the maximum or even for bimodal distributions. In these cases, all the oscillators in the plateau contributes to form the seed, and it becomes in a macroscopic effect in the order parameter.

Looking back briefly to the derivation of the critical point, with no more than insert the Taylor series expansion of $g(kR \sin \theta)$ –around $\omega = 0$ – in the previous self-consistency equation (Eq. (3.2.9)) and assuming that it is unimodal and has a maximum in $\omega = 0$, it can be seen that, in the vicinity of the critical point, the growth of the order parameter is proportional to the square root of its distance, $R \propto (k - k_c)^{1/2}$, i.e. with critical exponent $\frac{1}{2}$. This supports the existence of a second-order phase transition and the universality class associated to the MF approached threatened here [56]. Furthermore, this validity fulfill the hole ensemble of unimodal and symmetric distributions –if the Taylor expansion exists– and it is of great help to characterize the critical behavior of the MF system. Notwithstanding, not to go on so long with this reflection, all this behaviors are carefully studied below.

3.2.2

The Ott-Antonsen ansatz

Further analytical insight –in the “all-to-all” case with heterogeneous frequencies– can be obtained using the celebrated Ott-Antonsen (OA) ansatz [52], which allows for a projection of the high-dimensional dynamics onto an evolution equation for $Z(t)$, i.e. a dimensional reduction of the problem. Despite showing it in a context of globally coupled oscillators, this perspective transcends the MF approach, and is very useful in other contexts, as networks of networks or time-delays, among others [52].

From Eqs. (3.2.2) and (3.2.3) the next equality can be obtained,

$$\begin{aligned}\dot{\theta}_j &= \omega_j + kR \sin(\psi - \theta_j) = \omega_j + k \operatorname{Im} \left(Z e^{-i\theta_j} \right) \\ &= \omega_j + \frac{k}{2i} \left(Z e^{-i\theta_j} - \bar{Z} e^{i\theta_j} \right)\end{aligned}\quad (3.2.12)$$

and now search –in the continuum limit– the stationary solution of

$$\frac{\partial f}{\partial t} + \frac{\partial}{\partial \theta} \{ f [\omega + kR \sin(\psi - \theta)] \} = 0 \quad (3.2.13)$$

being $f(\theta, \omega, t) = g(\omega) P(\theta, \omega, t)$, which is no more than the density of oscillators of phase θ and characteristic frequency ω at time t .

However, this equation does not imply a simplification of our problem, because, as it can be seen, an N -dimensional problem is replaced with an infinite dimensional one. But, the Ott-Antonsen ansatz, with the purpose to reduce the dimensionality of the problem, assumes that $f(\theta, \omega, t)$ can be expanded in Fourier series as,

$$f(\theta, \omega, t) = \frac{g(\omega)}{2\pi} \left[1 + \sum_{n=1}^{\infty} \left(\hat{f}_n(\omega, t) e^{in\theta} + \hat{f}_n^*(\omega, t) e^{-in\theta} \right) \right] \quad (3.2.14)$$

and that $\hat{f}_n(\omega, t)$ should verify the form $\hat{f}_n(\omega, t) = [\alpha(\omega, t)]^n$ with $|\alpha(\omega, t)| \leq 1$, to avoid divergence of the series and, being $\operatorname{Im}(\omega) < 0$ and $|\alpha(\omega, t)| \rightarrow 0$ when $\operatorname{Im}(\omega) \rightarrow -\infty$. These properties are verified in both Kuramoto model stationary states, the incoherent and the partially synchronous. Thus, the continuity equation is transformed into another one for the order parameter. After some calculations, plugging Eq. (3.2.14) into (3.2.13), it can be shown that (see appendix C.1),

$$\dot{\alpha} + i\omega\alpha + \frac{k}{2} \left(Z\alpha^2 - \bar{Z} \right) = 0 \quad \bar{Z} = \int_{-\infty}^{+\infty} d\omega g(\omega) \bar{\alpha}(\omega, t) \quad (3.2.15)$$

providing the general result for the dimensional reduction of the problem and enabling us to study the phase transition in terms of the frequency distribution.

3.2.3

The role of the frequency distribution: $g(\omega)$

As we have seen, the frequency distribution of the set of oscillators plays a crucial role in the phase transition of the system, entailing the main source of frustration that has been considered until now. Indeed, the results covered in the globally coupled case –by the MF description or the Ott-Antonsen ansatz– completely depend on the frequency distribution of natural frequencies (for example, giving rise to first-order and second-order phase transitions). Here, some results for those archetypal distributions are presented, highlighting and threshing its role on the emergent synchronization phenomena.

3.2.3.1 Cauchy-Lorentz distribution

The Cauchy-Lorentz distribution of natural frequencies

$$g(\omega) = \frac{\gamma}{\pi [\gamma^2 + (\omega - \Omega_0)^2]} \quad (3.2.16)$$

is a case for which explicit analytical predictions can be done. It provides, employing Eq. (3.2.11), a critical point $k_c = 2\gamma$. On another note, the Ott-Antonsen ansatz can be applied here (for the entire derivation, see appendix C.1.1), giving rise to the next two differential equations,

$$\begin{cases} \dot{\psi} = \Omega_0 \\ \dot{R} = -\gamma R + \frac{1}{2}kR(1 - R^2) \end{cases} \quad (3.2.17)$$

The first of these equations is trivial and it has only a fixed point at $\Omega_0 = 0$. Rather, the second one has a first stable fixed point in $R_1^* = 0$ until $k = 2\gamma$, and a stable fixed point after $k = 2\gamma$, $R_2^* = \sqrt{1 - \frac{2\gamma}{k}}$. Similarly, circles of variable radius R –coming from the complex order parameter $Z = X + iY$ – appear in the coherent phase.

The excellent agreement between theory and simulation can be appreciated in Figure 3.2.2, in which the analytical prediction for the critical point and the analytical function derived from the Ott-Antonsen equations are one on top of the other. Besides, the standard deviation of the averaged order parameter, σ_R , rescaled by a factor \sqrt{N} coming from a direct application of the central limit theorem ($\chi = \sigma_R\sqrt{N}$), shows a pronounced peak located at the size-dependent critical point, growing anomalously with N , indicating the presence of a legitimate critical point. Meanwhile, Figure 3.2.3 shows the expected emergent circles in the phase portrait of the complex Kuramoto order parameter, traces of the coherent state that arises in the system.

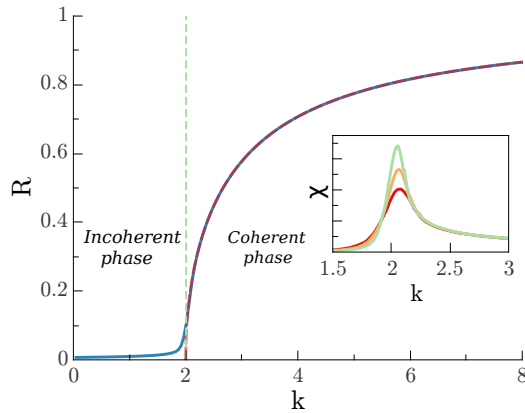


Figure 3.2.2: Order parameter R as a function of the coupling strength k for analytical and computational (for a size of $N = 16000$ oscillators) perspectives. Observe that the critical point sort out the absorbing (or incoherent) from the active (or coherent) phase growing continuously. Inset: Standard deviation of the averaged order parameter multiplied by \sqrt{N} , $\chi = \sigma_R \sqrt{N}$ for different system sizes ($N=4000, 8000$ and 16000). The point of maximal variability displays the location of the critical point depending on the system size.

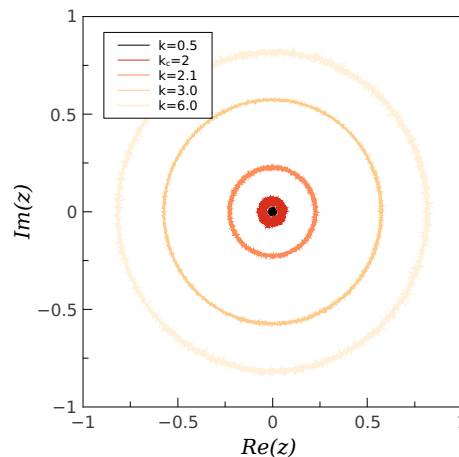


Figure 3.2.3: Phase portrait showing circles in the Kuramoto model beyond the critical point (coherent phase). In the incoherent phase, there is no evidence of synchronous activity (a point can be appreciated for $k < k_c$) but, just in the critical point (at $k_c = 2$, see red line), a seed of synchronization is formed and grows shaping out circles in the coherent phase until the state with $R = 1$ has been reached.

3.2.3.2 Uniform distribution

Another simple and especially illustrative case is that of an uniform distributions of frequencies, but ensuring that the aforementioned conditions are satisfied,

$$g(\omega) = \frac{1}{2\gamma} \quad \omega \in (-\gamma, \gamma) \quad (3.2.18)$$

which provides, through the Eq. (3.2.11), a critical point in $k_c = \frac{4\gamma}{\pi}$. Besides, by employing Eq. (3.2.10) it is possible to derive the next self-consistency equation,

$$R = \frac{1}{2} \sqrt{1 - \left(\frac{\gamma}{kR}\right)^2} + \frac{kR}{2\gamma} \arcsin\left(\frac{\gamma}{kR}\right) \quad (3.2.19)$$

There is only a real solution for $kR \geq \gamma$, giving in the limiting case a particular value of $R_c = \frac{\pi}{4}$. Thus, in this case, we have a gap in the value of the order parameter from the incoherent state to the coherent one, which generate a sudden change in the order parameter. Hence, a first order phase transition emerges in this situation. Figure 3.2.4 shows the discrete jump of high $\frac{\pi}{4}$ in the order parameter derived from the analytical prediction. Besides, it also reflects the remarkable compromise between theory and simulation, showing a discontinuity located at the critical point, as expected in first-order phase transitions.

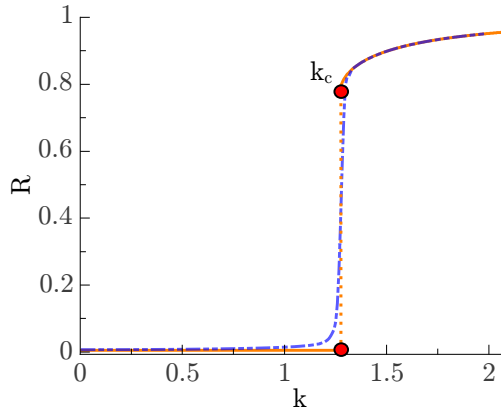


Figure 3.2.4: Order parameter R as a function of the coupling strength k for analytical (orange line, solution of the self-consistency Eq. (3.2.19)) and computational (blue line, for a size of $N = 16000$ oscillators) perspectives. A (discontinuous) gap of size $\frac{\pi}{4}$ appears together with the coherent phase of synchronized oscillators.

3.2.4

Chimera states: getting frustration and metastability

According to the Greek mythology, the chimera was a hybrid three-headed monster, a fire breathing creature, with lion's head and body a goat's head in his back and a serpent's tail. Figuratively, Abrams and Strogatz coined this term –broadly employed now in the field of synchronization phenomena– to define a synchronized state with incongruous interconnected parts, in which regions of coherent and incoherent oscillators coexist [1, 3, 43, 53]. It stems from the study of the Kuramoto-Sakaguchi model, that –in the MF case– only includes an additional intrinsic repulsion term with respect to Kuramoto, namely,

$$\dot{\theta}_j = \omega_j + \frac{k}{N} \sum_{l=1}^N \sin(\theta_l - \theta_j + \alpha) \quad (3.2.20)$$

where α is a repulsion term between oscillators.

The derivation of the critical coupling strength could be done under identical assumptions as those for the original Kuramoto one,

$$k_c = \frac{2}{\pi g(0) \cos \alpha} \quad (3.2.21)$$

which clearly leads to a growing level of frustrated synchronization, i.e. the value of the critical coupling separating the coherent phase from the incoherent one is bigger and bigger until it reaches –for values of $\alpha > \frac{\pi}{2}$ – a negative coupling scheme scenario. But, in particular, in the limiting case with $\alpha = \frac{\pi}{2}$, it is clear that both phases –coherent and incoherent– coexist for any k value. This leads to a divergence of the coupling strength (see Eq. (3.2.21)) shown in the Figure 3.2.5, where the critical coupling strength value is estimated through the point of maximal variability of the standard deviation in an ensemble of $N = 4000$ oscillators.

Although not in the “all-to-all” extremely simple case, but rather adding a slight variation of the coupling scheme with two clusters, thwarting even more the complete synchronization of the whole system, Abrams and Strogatz depicted the existence of this research topic [3]. Indeed, they develop some interesting analytical calculations employing the Ott-Antonsen ansatz in that two-cluster system of identical oscillators, uncovering the existence of chimera states, and defining it as follows [53],

Definition 3.1 (Chimera state)

“a spatio temporal pattern in which a system of identical oscillators is split into coexisting regions of coherent (phase and frequency locked) and incoherent (drifting) oscillations.”

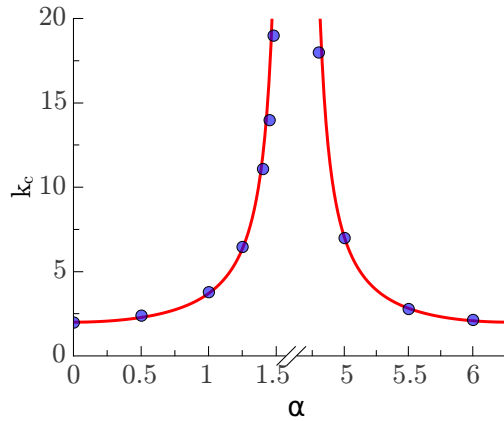


Figure 3.2.5: Critical value of the coupling strength as a function of the repulsion term, α . Analytical curve is plotted in red, and computationally estimated values as blue points (for $N = 4000$ oscillators). Note the break in the x-axis, due to the region of order with negative couplings obtained for some particular values of α .

Even if it is true that this intriguing phenomenon was explored in a large variety of underlying topologies, like clustered networks, rings, torus, spheres, and so on (see [53] and references therein), the all-to-all case was also recently revealed both analytically [75] and experimentally in a four globally coupled system of oscillators [57]. Likewise, two successful stable experimental chimeras are recently reported [32, 67]. Besides, it is of particular interesting the real application of unihemispheric sleep in many species of birds, dolphins, whales or sea lions (a half of the brain sleeps while the other half remains awake) [55].

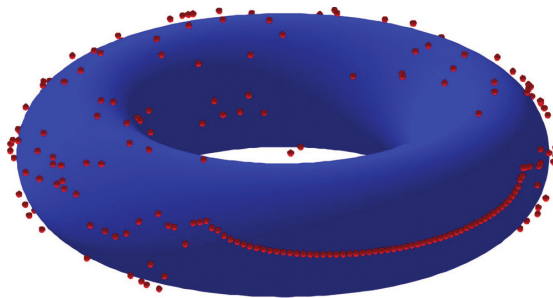


Figure 3.2.6: Chimera state in the surface of a torus. Radial coordinate involves the spatial coordinate while the radial one stands for the phase of each oscillator. From: Abrams and Strogatz (2006) [2].

Complex networks coupling

We have analyzed the simple “all-to-all” coupling scheme. However, the forthcoming step –coming back to the general Eq. (3.2.1)– is to consider the system in a general network [6], represented by a coupling matrix, \mathbf{W} , and scrutinize the results for the well-known general case of random couplings.

The general equation for the Kuramoto model can be reformulated as,

$$\dot{\theta}_j = \omega_j + \sum_{l=1}^N \sigma_{jl} a_{jl} \sin(\theta_l - \theta_j) \quad (3.3.1)$$

where a_{jl} represents the (binary or weighted) connectivity matrix and σ_{jl} stands for the coupling strength, that should be redefined in terms of the network coupling. The normalization of the coupling between oscillators must be carefully defined. The choice³ in which the coupling strength is intensive, has serious issues now because, except in the case of some particular nodes in scale-free networks, the connectivity of each node never scales with the system size, nullifying the effective coupling in the infinite size limit. Consequently, there are two possible choices, namely to consider local properties of each node or some general properties of the network [6]. The first one is defined by $\sigma_{jl} = \frac{k}{\kappa_j}$, where κ_j is the specific connectivity (or degree) of each node and k the usual coupling strength of the model. This choice –obviously intensive– makes a clean sweep of the nodes matching the hubs and the periphery, and it is able to mask the heterogeneities in the network. On the other hand, there is the possibility of take a general property of the network, as the mean-connectivity $\langle \kappa \rangle$ or the maximum connectivity κ_{max} , among others. But, in this simple case, in which σ is a constant that does not depend on the local properties of each node, we can appreciate that the interaction term (non-intensive in some cases) can diverge in the infinite-size limit.

Either way, for simplicity, we will now consider the second one for the analytical results described below but, on subsequent computational analysis we consider a proper intensive normalization ($\sigma_{jl} = \frac{k}{\kappa_j}$) without observing any qualitative change in the phenomenology.

³The all-to-all case is recovered in the particular case of $a_{jl} = 1 \forall j \neq l$ and $\sigma_{jl} = \frac{k}{N}$.

At this point, it is interesting to estimate the critical point of a homogeneous network. To this end, as indicated in [6], it is necessary to define a local order parameter (r_j) as,

$$r_j(t)e^{i\psi_j(t)} = \sum_{l=1}^N a_{jl}e^{i\theta_l(t)} \quad (3.3.2)$$

where r_j and ψ_j capture the mean amplitude and phase of the local field in the vertex j of our network. From this equation, we obtain,

$$\dot{\theta}_j = \omega_j + \sigma r_i \sin(\psi_j - \theta_l) \quad (3.3.3)$$

and after some calculations (see appendix C.2.1), the critical point is given by,

$$\sigma_c = k_c \frac{\langle \kappa \rangle}{\langle \kappa^2 \rangle}$$

where k_c is the all-to-all critical point of Eq. (3.2.11), and $\langle \kappa^i \rangle$ stand for the i -th moment of the network degree distribution. This highlights the vanishing σ – *value* (and thus, these networks are always synchronous) in the particular case of diverging $\langle \kappa^2 \rangle$, i.e. in power-law degree distributions of the form $P(\kappa) \sim \kappa^{-\gamma}$ with $\gamma \leq 3$, present in many real biological networks [9, 10].

Also, it is clear that the underlying topology of the network induces heterogeneities, non-existent in the all-to-all case. As pointed out by *Um et al.* [69] this type of disorder induces dramatic changes in the nature of the synchronization transition, reaching the point that the first-order phase transition becomes a second-order phase transition in a quenched Erdős–Rényi network (see Figure 3.3.1). And, in particular, the same mean-field exponents of the all-to-all case can emerge, for all types of frequency distributions.

These results reveal that the underlying topology is crucially important, beyond the (usually nonlinear) dynamical process adopted in each particular case. It has profound implications, stretching the usual approach of theoretical model developing to the study of the spatial systems in which they are embedded. In fact, as recently shown [48], the specific –hierarchical-modular– organization of structural brain networks can induce strongly disturbances in neural dynamics [39, 44, 76, 77].

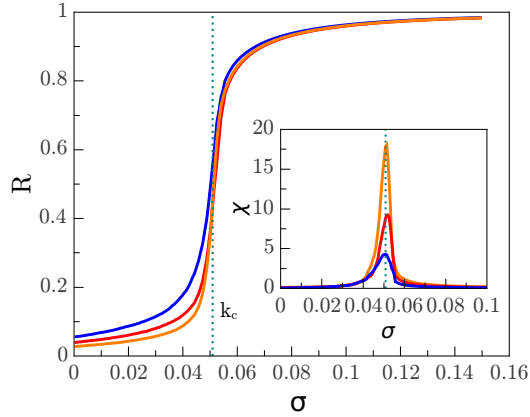


Figure 3.3.1: Synchronization phase transition in an Erdős–Rényi network with $\langle \kappa \rangle = 25$ and a uniform and symmetric frequency distribution $g(\omega) = U(-1, 1)$ for different system sizes ($N = 256$, blue line; $N = 256$, red line; and $N = 1024$, orange line). The dotted line stands for the analytical result for the critical point in this particular case, $\sigma_c \approx 0.051$, showing a good match between theory and simulations. It has to be emphasized the emergence of a second-order phase transition due to the network heterogeneities.

3.4

The Human Connectome

Once established all the tools needed to understand the behavior of the Kuramoto model, now we change the underlying topology –‘all to all’ or Erdős–Rényi– to a realistic ones,



Figure 3.4.1: (a) Cumulative degree distribution (see inset for the non-cumulative). The blue line represent a Weibull distribution [31], $f(\kappa; \lambda, \zeta) = \frac{\zeta}{\lambda} \left(\frac{\kappa}{\lambda}\right)^{\zeta-1} e^{-(\kappa/\lambda)^\zeta}$ $\kappa \geq 0$, with mean equal to the expected mean connectivity $\langle \kappa \rangle \approx 36$ of the Human Connectome (i.e. $\lambda \approx 41$) and $\zeta \approx 2.3$. (b) Adjacency matrix, with 998 nodes, of the Human Connectome network [33], employing a reverse Cuthill-McKee reordering algorithm. Connections between nodes are plotted in blue. Pay close attention to the structure in boxes along the diagonal, which can be seen by the naked eye. (c) Dendrogram of the human connectome, red lines shows a partition in twelve communities, that is the optimal partition into disjoint communities, i.e. the partition maximizing the modularity parameter [50].

which is the Human Connectome network (HC) [33], as depicted in Figure 3.4.1b. It comprises 998 non-directed nodes, organized in a clear modular structure (as can be seen from the structure in boxes along the diagonal). Also, the degree distribution of the network consists in a Weibull distribution [31] for the probability density function and therefore a “stretched” exponential in the cumulative distribution function (Figure 3.4.1a). At last, as shown in Figure 3.4.1c, note that the dendrogram of the HC –on its first hierarchy levels– shows a very rich landscape of interspersed moduli.

We perform a computational study of the Kuramoto model, running it on top of the Human Connectome (HC) network, unveiling the existence of an intermediate regime placed between the coherent and the incoherent phase (see Figure 3.4.2). This is characterized by broad quasi-periodic temporal oscillations of $R(t)$ which wildly depend upon the realization of intrinsic frequencies [5, 8]. Anomalously large sampling times would be required to extract good statistics for the actual mean values and variances. Besides, collective oscillations of $R(t)$ are a straightforward manifestation of partial synchronization (as can be appreciated in the raster plot of individual phases in Figure 3.4.2) and they are robust against changes in the frequency distribution (e.g. Gaussian, Lorentzian, uniform, etc.) whereas the location and width of the intermediate phase depend upon details.

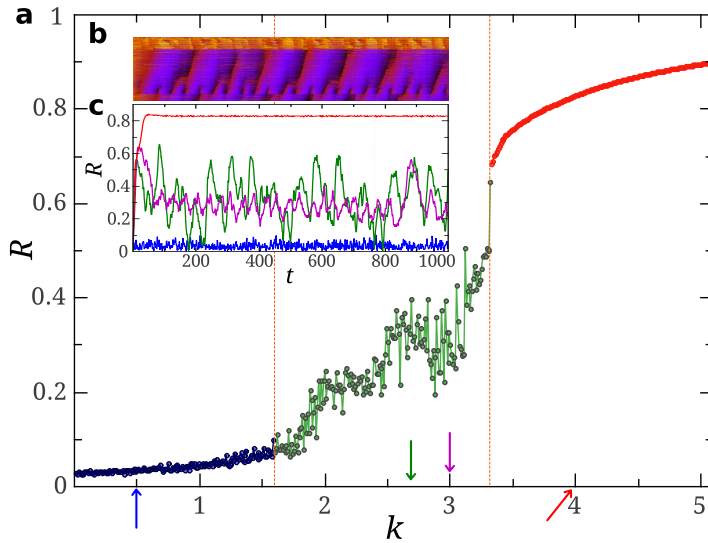


Figure 3.4.2: Time average of the order parameter $R(t)$, for Kuramoto dynamics on the HC network employing a $N(0, 1)$ Gaussian distribution set of frequencies. Observe that the synchronous phase (for high values of k) is separated from the incoherent phase by a broad intermediate regime, in which coherence increases with k in an intermittent fashion, and with strong dependence on the frequency realization. (b) Raster plot of individual phases (vertical axis) versus time showing local rather than global synchrony and illustrating the coexistence of coherent and incoherent nodes ($k = 2.7$). (c) Temporal series of the order parameter, $R(t)$, for four selected values of k (arrows in the main plot).

With the aim of quantifying the observed variability of R in the intermediate phase, we take a particular realization of frequencies (extracted from a Gaussian

$g(\omega)$) and, starting from an initial –uniformly distributed– random configuration of individual phases, $\{\theta_i(t=0)\}_{i=1}^N$, to measure the temporal standard deviation of the global coherence parameter R (after the transient) up to a maximum time $T = 10^4$, which we will call “*time variability*”⁴,

$$\sigma = \left(\langle (R - \langle R \rangle_t)^2 \rangle_t \right)^{1/2} \quad (3.4.1)$$

as a function of the coupling strength k .

As we have seen a great variability in the intermediate region, it suggests the existence of several possible attractors. So, the ergodicity may be broken and thus, different initial conditions may lead to different attractors of the dynamics. Therefore we also average σ over 10^2 different independent realizations of the dynamical process. Figure 3.4.3 illustrates the diagram of the order parameter obtained for this particular (averaged) realization of $g(\omega)$.

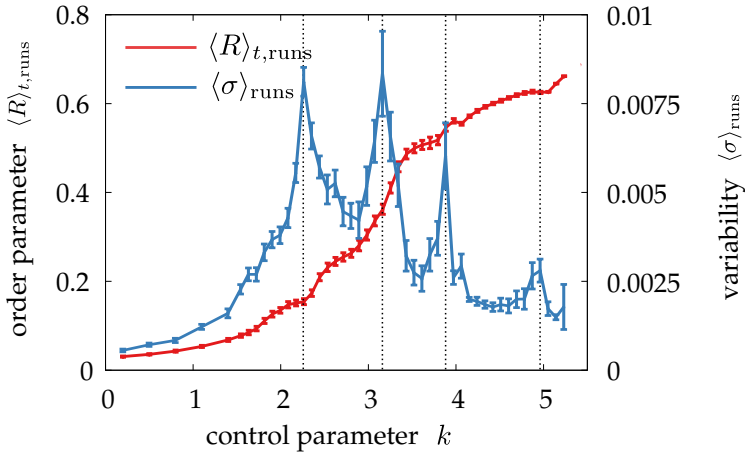


Figure 3.4.3: Time-averaged order parameter $R = \langle R(t) \rangle$ (blue curve) standard deviation of time-series, averaged over realizations with different –uniformly distributed– initial conditions. Maximal variability is found in the intermediate phase, where the system is neither too unsynchronized nor too coherent. Several peaks in the variability can be distinguished (dashed lines), which appear at values of the control parameter k for which the system experiments a fast increase in global synchronization. Statistical sampling of different realizations indicate that error-bars are larger in the intermediate region, suggesting the existence of several attractors depending on the initial conditions.

⁴Notice that this definition of σ , that we call, ‘*time variability*’ is closely related to the chimera index that will be introduced afterward (and originally by Shanahan [58]). In this case, σ is defined at the global level and records fluctuations of the global order parameter, while chimera indices are averaged between individual network moduli to highlight the onset of local coherence.

Let us stress the following salient aspects from the “*time variability*” of the system:

- i) Averaged time variabilities are small in the non-coherent ($k \lesssim 1$) as well as in the coherent ($k \gtrsim 5$) phases, whereas much larger variabilities are found in the intermediate region ($1 \lesssim k \lesssim 5$).
- ii) The curve of time variabilities presents several peaks for the intermediate region, lying in the vicinity of values of the control parameter at which the system experiences a change in its level of coherence (see the corresponding jumps in the derivative of the order parameter).
- iii) And finally, error bars are also larger in the intermediate phase; this variability of time variabilities means that different initial conditions can lead to different types of time-series, suggesting a large degree of metastability in the intermediate regime.

As there are clues that this phenomenology may be reminiscent of a Griffiths phases –posed in between order and disorder and stemming from the existence of semi-isolated regions [48, 49, 70]– it is natural to investigate how the HC hierarchical modular structure affects synchronization dynamics. Besides, as one can deduce from a simple visual inspection of Figure 3.4.1, there exists a modular organization of the network and thus, we expect that the different moduli must play an important role in this emergent new phase.

On the other hand, it is not so hard to envision the fact that any network with perfectly isolated and independently synchronized moduli trivially exhibits oscillations of $R(t)$, with amplitude peaking at times when maximal mutual synchronization happens to be incidentally achieved. Such oscillations can become chaotic if a finite and relatively small number of different coherent moduli are coupled together [54]. Thus, in a connected network without delays or other additional ingredients, oscillations in the global coherence are the trademark of strong modular structure with weakly interconnected moduli.

As shown before (see Figure 3.4.1), strong modular organization into distinct hierarchical levels is indeed present in the HC and it has been already discussed in the literature (see e.g. [48] and references therein). For instance, we have found –employing standard community detection algorithms [28, 37]– that the optimal partition into disjoint communities –i.e. the partition maximizing the modularity parameter [50]– corresponds to a division in 12 communities (see Figures 3.4.1 and 3.4.4c) while, at a higher hierarchical level, a separation into just 2 moduli –the 2 cerebral hemispheres– is obtained [36] (Figure 3.4.4). Obviously, these 2 coarser moduli include the 12 above as sub-moduli. Although more levels of hierarchical partitioning could be inferred (see e.g. [13] and refs. therein), for the sake of simplicity we focus on these two levels l , $l = 1$ and $l = 2$ with 12 and 2 moduli, respectively.

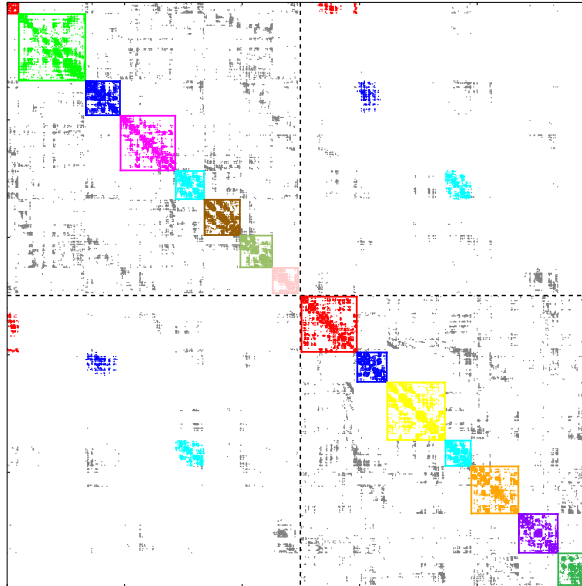


Figure 3.4.4: Adjacency matrix of the HC network with 998 nodes [33, 36] ordered to emphasize its modular structure as highlighted by a community detection algorithm, showing also the partition into the 2 hemispheres (dashed lines). 12 moduli can be distinguished (each plotted with a different color); 4 of them correspond to one of the two hemispheres, 5 to the other, and only 3 moduli overlap with both hemispheres (cyan, blue and red moduli). Inter-modular connections (grey) are limited to small subsets, acting as interfaces or connectors between moduli.

Now we analyze the local properties of the different moduli –and hierarchical scales– just analyzed. Fig. 3.4.5 shows numerical results for the local order parameter, $r^{(l)}$, for some of the moduli at the 2 hierarchical levels, $l = 1$ and $l = 2$ in the HC network. It reveals that (Fig. 3.4.5a) local coherences exhibit oscillatory patterns in time (with characteristic frequencies typically between 0.01 and $0.1Hz$) and that (Fig. 3.4.5b) the transition to local coherence at progressively higher hierarchical level occurs at progressively larger values of k ; i.e. coherence seems to emerge out of a hierarchical bottom-up process. Also, Fig. 3.4.5 reveals that the ordering process in the hierarchical modular HC may be non-monotonous: coherence does not systematically grow with k .

Indeed, the emergence of local order in some community may hinder or reduce coherence in others, inducing local “desynchronization” and reflecting the metastable nature of the emerging states.

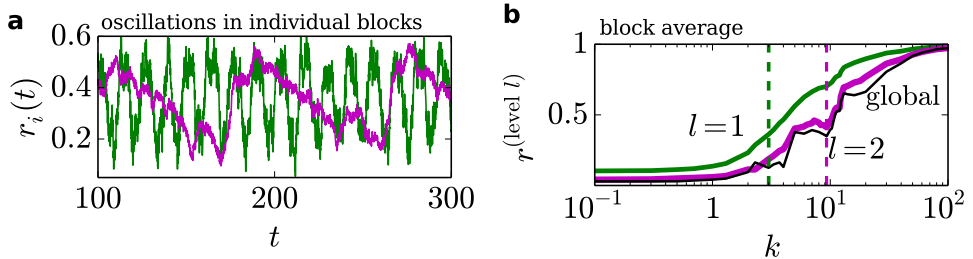


Figure 3.4.5: Local synchronization in the human connectome: (a) Oscillations of the local order parameters in one particular modulus in the partitions of the HC into 12 (green, $l = 1$, and $k = 3$) and 2 (magenta, $l = 2$, and $k = 10$) moduli, respectively. The characteristic frequency of these oscillations is typically between 0.01 and 0.1 Hz (a range which coincides with slow modes detected in brain activity; see e.g. [15]). (b) Average of the local order parameter over all moduli.

To better illustrate the role played by internal network modularity on global synchronization, Figure 3.4.6 portrays the trajectories of the parameter $Z(t)$ in the complex plane for different values of the control parameter k , measured at different hierarchical levels: two (out of the existing 12) different small moduli (violet and orange curves), the two hemispheres (red and green), and the overall brain (blue). In the incoherent phase (panel a), the real and imaginary parts of Z fluctuate around zero at all scales in the hierarchy. On the other hand, in the coherent phase (panel d), all nodes are synchronized, and trajectories are circles with radii close to unity at all hierarchical levels

A much richer behavior is found in the intermediate region: panel b (left) illustrates a situation in which one modulus (orange) is mostly coherent, while the other (violet) is not; however, hemispheres and global dynamics remain mostly unsynchronized (panel b (right)). In panel c (left), we have slightly increased the control parameter with respect to panel b, with a subsequent increase of the coherence for all hierarchical levels. Interestingly, as not all moduli exhibit the same state of coherence, chaotic-like oscillations of the order parameter are observed at the global scale.

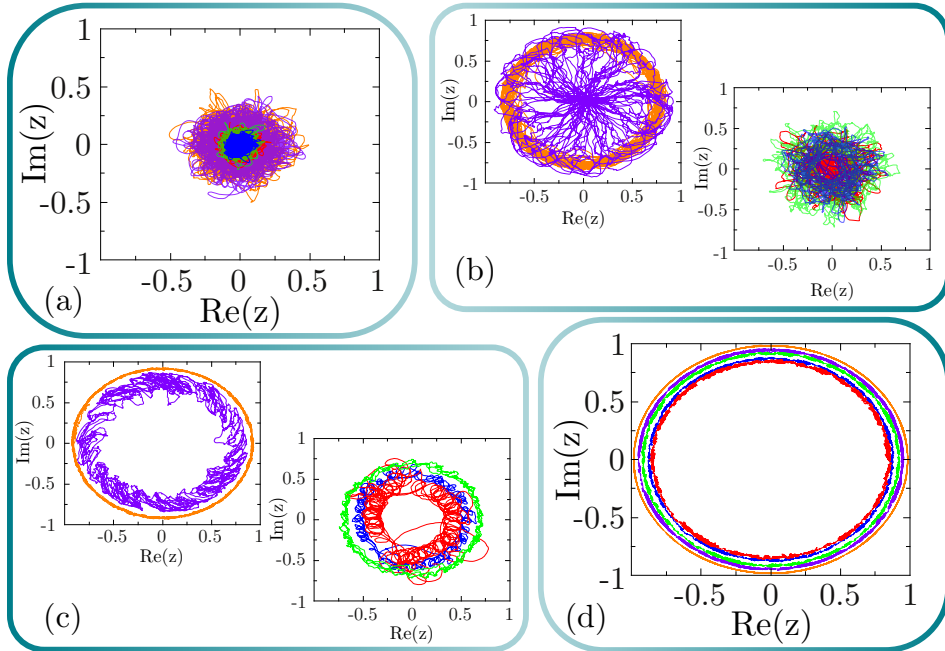


Figure 3.4.6: Phase portraits of the complex order parameter $Z(t)$, measured at different scales in the hierarchy for a Gaussian $g(\omega)$: two of the existing moduli are plotted in violet and orange, respectively, the two hemispheres in red and green, and the global scale in blue. Panels (a)-(d) correspond to values of the control parameter $k = 1, 3, 5$ and 8 , respectively (panels (b) and (c) have been split into two to enhance clarity). (a) In the non-ordered phase, the real and imaginary components of Z fluctuate around zero, not exhibiting synchronization at any scale. (b) In the early region of the intermediate phase, a few moduli are coherent (as the one in orange) but most of them remain unsynchronized (violet), and the system does not present coherence for upper scales in the hierarchy. (c) Increasing k , more heterogeneity of synchronization among moduli is found, and the system exhibits complex trajectories for the intermediate (hemispheres) and global scale. (d) In the coherent phase, all moduli are synchronized, and trajectories are concentric circles.

3.4.1

Chimeras

Local oscillations and states of partial synchronization, mixed with a high degree of frustration and an extraordinary plethora of emergent properties in the intermediate phase, closely resembles to the chimeras that had been introduced earlier (see section 3.2.4 on page 91).

To answer the question as to whether or not there are chimeras in our case, we must examine some type of index that provides us such information. A good possibility is the chimera index, $\chi^{(l)}$, that is introduced as a measure of partial synchronization at the community level l [58, 73]. Besides, it could be foreseeable that at any hierarchical level l , the HC network, in a fractal-like way can be divided into a set of communities. Thus, following [58], $\chi^{(l)}$ is defined as follows:

- i) In the steady (oscillatory) state, and for each time t , local order parameters $r_i^{(l)}(t)$ for each community i are calculated and their variance across communities $\sigma_{\text{chi}}^{(l)}(t)$ is stored.
- ii) The chimera index is computed as the time average $\chi^{(l)} = \langle \sigma_{\text{chi}}^{(l)}(t) \rangle_t$. Having $\chi^{(l)} > 0$ at a given hierarchical level l implies that local order is only partial as $r_i^{(l)}$ fluctuates, giving rise to a chimera-like state. On the other hand, $\chi^{(l)} = 0$ means that each local order parameter at that level is $r_i^{(l)} \approx 1$, and local order has been attained.

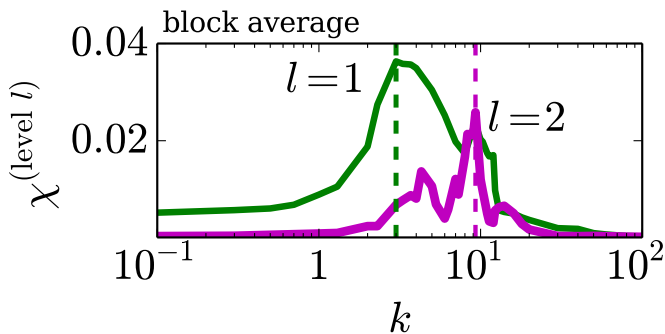


Figure 3.4.7: Chimera index for moduli at levels as a function of k , in one particular modulus in the partitions of the HC into 12 (green, $l = 1$) and 2 (magenta, $l = 2$) moduli, respectively. Global order emerges only after local order is attained at lower levels.

Figure 3.4.7 shows that at each l ($l = 1$ and $l = 2$) a peak in the corresponding $\chi^{(l)}$ marks the onset of the local synchronization processes: as soon as the peak vanishes upon increasing k , local order at that level is attained. The sequence of separated peaks in $\chi^{(l)}$ for increasing values of l is the direct evidence of a hierarchical synchronization process.

Concluding, the fact that the average variance of local coherences (called chimera index, χ) [58] exhibits a marked peak –reflecting maximal configurational variability– indicates a transition point for the corresponding level. It should be added that similar intra-modular oscillatory patterns –dubbed *chimera states*– have been recently found [1, 3, 58, 73] in Kuramoto models in which explicit phase lags induce a different kind of frustration, hindering global synchronization. Strictly speaking, chimeras are defined in systems of identical oscillators. In such a case, a non-zero phase lag term is essential for partial synchronization to occur. Realistic models of the brain, however, require oscillators to be heterogeneous. States of partial synchronization in empirical brain networks with frequency heterogeneity have been found for Kuramoto models with explicit time delays [19]. In contrast, the chimera-like states put forward here have a purely structural origin, as they arise from the network topology. It was noted in the past that synchronization in a synthetic network with hubs could be limited to those hubs by tuning clustering properties, and global order could be attained in a monotonous step-like fashion upon increasing k [46].

One important question remains, namely, to carefully select the essential ingredients to achieve this prolific phenomenology in synthetic networks. Henceforth, on the basis that a modular network forms the cornerstone of all this, one of the latest steps is to develop a model –with increasing complexity– able to reproduce all these behaviors.

Modeling the HC

To shed further light on the properties of synchronization on the HC, we revisit the existing analytical approaches for networks with a community structure of coupled oscillators, and after that a very simple network model is developed –allowing for analytical understanding– which constitute the elementary “building-block” for subsequent more complex analyses. The subsequent step is the inclusion of simple modular networks, examining very attentively what elements are lacking in this structures to resemble to the HC. Definitely, hierarchic modular networks –containing a huge variety of modules of different sizes in a fractal way– will constitute the optimal solution to reproduce the behavior observed in the HC topology.

3.5.1

Communities

Once the procedure for the original Ott-Antonsen approach has been presented, the generalization to the case of community structured networks is rather straightforward. The original idea was formulated by themselves and developed by Skardal and Restrepo [63] and consists in assuming that nodes in community σ interact with nodes in community σ' with a Kuramoto coupling $k_{\sigma\sigma'}$. In the presence of C communities in a network of total size N , nodes are relabeled in such a way that their phases are written as θ_i^σ , referring to the phase of node i in the community σ of size N_σ . The Kuramoto equations thus read

$$\dot{\theta}_j^\sigma = \omega_j^\sigma + \frac{k_{\sigma\sigma'}}{N} \sum_{\sigma'=1}^C \sum_{l=1}^{N_{\sigma'}} \sin(\theta_l^{\sigma'} - \theta_j^\sigma). \quad (3.5.1)$$

Still, in a hierarchical modular network all connected nodes interact with the same k , it constitutes a first approach to explore the analytical understanding of the effects of a separation in simple communities. But, in our case, this means that $k_{\sigma\sigma'}$ is either zero or one, depending on whether communities σ and σ' are connected. The basic idea behind the community model is that, in spite of the fact the mean field approach is not exact system-wide, it is inside each community, so that the goal is to coarse-grain all communities and end up with a system of C coupled equations employing the Ott-Antonsen ansatz (in the way of Eq. (3.2.15)) expressing the interaction between C complex oscillators.

To this end we define the local order parameter of community σ as

$$z_\sigma = r_\sigma e^{i\psi_\sigma} = \frac{1}{N_\sigma} \sum_{j=1}^{N_\sigma} e^{i\theta_j^\sigma}, \quad (3.5.2)$$

so that the global order parameter is simply the weighted average $Z = \sum_\sigma (N_\sigma/N) z_\sigma$. We can thus rewrite Eq. (3.5.1) in terms of local r_σ and ψ_σ as

$$\dot{\theta}_i^\sigma = \omega_i^\sigma + \sum_{\sigma'=1}^C \mathcal{K}_{\sigma\sigma'} r_{\sigma'} \sin(\psi_{\sigma'} - \theta_i^\sigma), \quad (3.5.3)$$

where the effective coupling constants are given by

$$\mathcal{K}_{\sigma\sigma'} = (N_{\sigma'}/N) k_{\sigma\sigma'}. \quad (3.5.4)$$

This last result is crucial. Even if $k_{\sigma\sigma'}$ is one between all linked communities (as in our case), the effective coupling between linked communities depends on their size. That is to say, if two communities of different sizes interact between them, the bigger one affects the smaller one more than it is affected by it. However, Skardal and Restrepo assume that all N_σ are large enough as to allow the usual continuum approximation, defining the Eulerian drift term for each community

$$v_\sigma = \omega^\sigma + \frac{1}{2i} \sum_{\sigma'} \mathcal{K}_{\sigma\sigma'} \left(z_{\sigma'} e^{-i\theta^\sigma} - \bar{z}_{\sigma'} e^{i\theta^\sigma} \right), \quad (3.5.5)$$

which is aware of the interactions with other communities thanks to the cross terms with $\sigma \neq \sigma'$, and since the density of oscillators per community $f_\sigma(\theta^\sigma, \omega^\sigma, t)$ is conserved, its form will simply be

$$\frac{\partial}{\partial t} f_\sigma(\theta^\sigma, \omega^\sigma, t) + \frac{\partial}{\partial \theta^\sigma} [f_\sigma(\theta^\sigma, \omega^\sigma, t) v_\sigma] = 0. \quad (3.5.6)$$

For each f_σ , we can write the Fourier decomposition

$$f_\sigma(\theta^\sigma, \omega^\sigma, t) = \frac{g(\omega^\sigma)}{2\pi} \left[1 + \sum_{n=1}^{\infty} \left(\hat{f}_{\sigma,n}(\omega^\sigma, t) e^{in\theta^\sigma} + \hat{f}_{\sigma,n}^*(\omega^\sigma, t) e^{-in\theta^\sigma} \right) \right]. \quad (3.5.7)$$

and employ the respective Ott-Antonsen ansatz, $\hat{f}_{\sigma,n}(\omega^\sigma, t) = a_\sigma^n(\omega^\sigma, t)$, leading to

$$\dot{a}_\sigma + i\omega^\sigma a_\sigma + \frac{1}{2} \sum_{\sigma'=1}^C \mathcal{K}_{\sigma\sigma'} (\bar{z}_{\sigma'} a_\sigma^2 - \bar{z}_{\sigma'}) = 0, \quad (3.5.8)$$

$$z_\sigma = \int_{-\infty}^{+\infty} d\omega^\sigma \int_0^{2\pi} d\theta^\sigma f_\sigma(\theta^\sigma, \omega^\sigma, t). \quad (3.5.9)$$

We assume that characteristic frequencies in each community σ are distributed following a Lorentzian $g_\sigma(\omega^\sigma; \Omega_\sigma, \gamma_\sigma)$ so that Eq. (3.5.9) leads to

$$z_\sigma = \bar{a}_\sigma(\Omega_\sigma - i\gamma_\sigma, t) \quad (3.5.10)$$

that replaced in each (Eq. (3.5.8)) finally yields the evolution equations for each community

$$\dot{z}_\sigma + (\gamma_\sigma - i\Omega_\sigma)z_\sigma + \frac{1}{2} \sum_{\sigma'=1}^C \mathcal{K}_{\sigma\sigma'} (\bar{z}_{\sigma'} z_\sigma^2 - z_{\sigma'}), \quad (3.5.11)$$

or, separating real and imaginary part,

$$\dot{\psi}_\sigma = \Omega_\sigma + \frac{1+r_\sigma^2}{2r_\sigma} \sum_{\sigma'=1}^C \mathcal{K}_{\sigma\sigma'} r_{\sigma'} \sin(\psi_{\sigma'} - \psi_\sigma) \quad (3.5.12)$$

$$\dot{r}_\sigma = -\gamma_\sigma r_\sigma + \frac{1-r_\sigma^2}{2} \sum_{\sigma'=1}^C \mathcal{K}_{\sigma\sigma'} r_{\sigma'} \cos(\psi_{\sigma'} - \psi_\sigma). \quad (3.5.13)$$

This result states that, irrespective of the details of the topology of the network at hand and provided that a decomposition of the type in Eq. (3.5.1) can be performed, in which each of the C communities behaves in a mean-field way, the time evolution of Kuramoto dynamics is described by the set of $2C$ differential equations depicting the evolution of the local phase and coherence of each community. An important point is that, by virtue of Eq. (3.5.1), all nodes in community σ are in interaction with all nodes in community σ' through a coupling constant $\mathcal{K}_{\sigma\sigma'}$. Allowing $\mathcal{K}_{\sigma\sigma'}$ to vary by small amounts, as done by Skardal and Restrepo, accounts for a weak community structure, where pair interactions are almost of mean-field type. This is generally not the case in networks where communities introduce sparsity and isolation, in which case $\mathcal{K}_{\sigma\sigma'}$ should be allowed to vary substantially, being zero for disconnected community pairs. Interestingly, the Human Connectome falls in this category.

3.5.2

The two-block model

The first model that we develop, is a very simple network model –that might be dealt analytically– which will constitute the elementary “building-block” for subsequent more complex analyses.

This consists of a few blocks with very large internal connectivity and very sparse inter-connectivity. Each block is composed by a bulk of $M \gg 1$ nodes that share no connection with the outside and a relatively small “interfacial” set that connects with nodes in other blocks. For instance, in the simplest realization, consisting of just two blocks connected by a single pair of nodes

(Figure 3.5.1), each block is endowed with local coherence $r_{A,B}$, average phase $\psi_{A,B}$, and average characteristic frequency $\omega_{A,B}$, while 1-node interfaces have perfect coherence $r = 1$, phase $\varphi_{A,B}$, and characteristic frequency $\nu_{A,B}$. In this case, $N = 2M + 2$, and the OA ansatz can be safely applied to each block (large M) but not to single-node interfaces. The Kuramoto coupling will simply be $k_{\sigma\sigma'} = k$ between linked communities and 0 otherwise. In the particular case in which $g(\omega)$ are zero-mean Lorentz distributions $g(\omega) = \frac{1}{\pi} \frac{\delta}{\omega^2 + \delta^2}$ (convenient for analytical treatment) with spreads $\delta_{A,B}$, the resulting set of OA equations is

$$\begin{cases} \dot{\psi}_A = \omega_A + k \frac{1+r_A^2}{2r_A} \sin(\varphi_A - \psi_A) \\ \dot{r}_A = -\delta_A r_A + k \frac{1-r_A^2}{2} [Mr_A + \cos(\varphi_A - \psi_A)] \\ \dot{\varphi}_A = \nu_A + k [Mr_A \sin(\psi_A - \varphi_A) + \sin(\varphi_B - \varphi_A)] \end{cases} \quad (3.5.14)$$

(and $r = 1$ for each 1-node interface), and a symmetric set ($A \leftrightarrow B$) for block B.

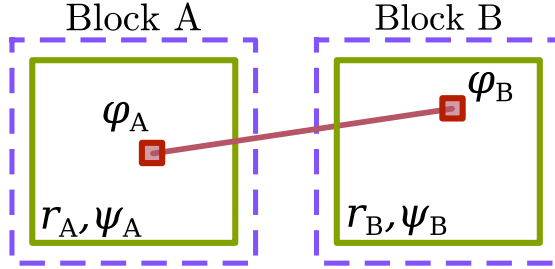


Figure 3.5.1: Sketch of the two-block model.

The solution of Eq. (3.5.14) –displayed in Figure 3.5.2– reveals a transition to local coherence within each block at a certain threshold value of $k \approx 0.02$. As soon as local order is attained, $r_{A,B} \approx 1$ and $\dot{\psi}_{A,B} \approx 0$, from Eq. (3.5.14) the mutual synchronization process obeys

$$\dot{\varphi}_A \approx (\nu_A + M\omega_A) + k \sin(\varphi_B - \varphi_A) \quad (3.5.15)$$

and a symmetrical equation for $\dot{\varphi}_B$. For small k , the right-hand side is dominated by $\nu_A + M\omega_A$: whereas the average value ω_A becomes arbitrarily small within blocks (assuming that M is large), the frequency ν_A does not. Consequently, synchronization between the two blocks through the interfacial link is frustrated: each block remains internally synchronized but is unable to achieve coherence with the other over a broad interval of coupling strengths. This interval is delimited above by a second transition at $k \sim \max\{M|\omega_{A,B}|, \nu_{A,B}\}$, where

k is large enough as to overcome frustration and global coherence emerges. This picture is confirmed by numerical integration of the full system of N coupled Kuramoto equations as well as by its OA approximation (Eq. (3.5.14)), both in remarkably good agreement. Therefore, local and global coherences have their onsets at two well-separated transition points [63] and –similarly to the much more complex HC case– R oscillates in the intermediate regime (Figure 3.5.2). The existence of two distinct (local and global) transitions had already been reported in a recent study of many blocks with much stronger inter-moduli connections than here [63] (even if, owing to this difference, no sign of an intermediate oscillatory phase was reported).

Our two-block model shows that the presence of “structural bottlenecks” between moduli combined with heterogeneous frequencies at their contact nodes (interfaces) are essential ingredients to generate a broad region of global oscillations in R . Still, it is obviously a too-simplistic model to account for all the rich phenomenology emerging on the HC. As a main example, local oscillations were not present in the two-block model. This suggests that the 12 moduli in the HC are on their turn composed of finer sub-moduli and that structural frustration, as introduced above, affects all hierarchical levels.

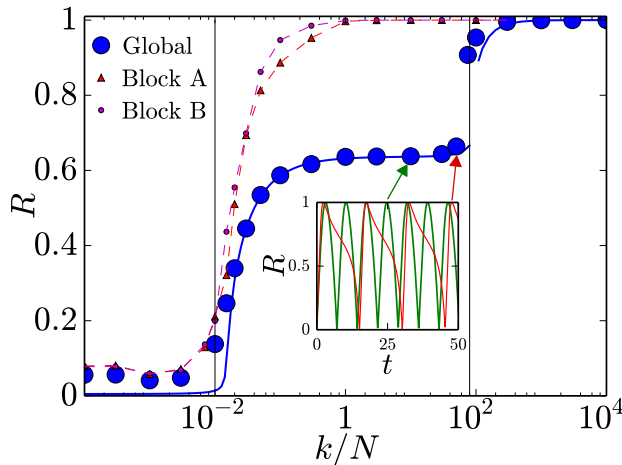


Figure 3.5.2: Global order parameter for the two-block model with $M = 128$. Results of the numerical integration of the 256 Kuramoto equations (blue points) are in strikingly good agreement with the integration of Eq. (3.5.14) (solid blue line). Local block-wise order parameters are shown for comparison (small symbols; dashed lines are guides to the eye). A first transition, where local order emerges, occurs at $k \approx 2$, while global coherence is reached at a larger value of k . In the intermediate region, the global $R(t)$ oscillates (inset), revealing the lack of global coherence.

3.5.3

Simple-modular network

Similar results are expected to hold for versions of the model with more than two moduli, e.g. 4 in a single-level modular network. This simple extension consider four Erdős–Rényi blocks, randomly connected with probability $p = \beta \frac{\langle k \rangle}{N}$, where β is an additional parameter much smaller for inter-block connections. Additionally, all the results presented from now on are completely numerical.

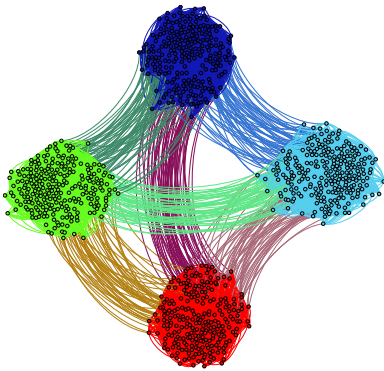


Figure 3.5.3: 4-block modular network, with similar features to the network of the HC.

	HC	4-block
$\langle k \rangle$	35.8	25.9
l_G	3.072	2.96
Modularity	0.469	0.722

Table 3.1: Structural properties of both networks: mean connectivity, average path length (l_G) and modularity index. The latter is larger in our synthetic network.

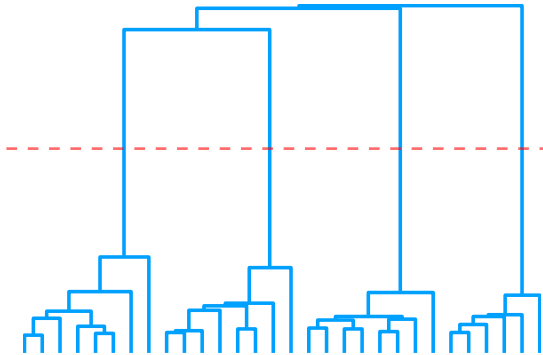


Figure 3.5.4: Dendrogram of the 4-block modular network. Note that the four communities could be clearly appreciated, and there is a great gap with the lower hierarchical levels, that presents a random coupling with very large internal connectivity.

Thus, running the Kuramoto model on top of this particular network, we can recover the intermediate regime with complex oscillations observed in the HC, and placed between the coherent and the incoherent phase, as shown in Figure 3.5.5. Again, it is characterized by broad quasi-periodic temporal oscillations of $R(t)$ which wildly depend upon the realization of intrinsic frequencies, but with partial synchronization and being robust against changes in the frequency distribution (e.g. Gaussian, Lorentzian, uniform, etc.)

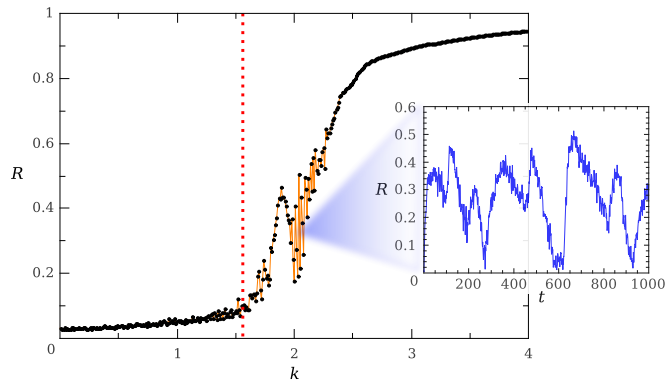


Figure 3.5.5: Time average of the order parameter $R(t)$, for Kuramoto dynamics on the four-block network employing a $N(0, 1)$ Gaussian distribution set of frequencies (red dotted line stands for the mean-field predicted critical point). Observe that the synchronous phase (for high values of k) is separated from the incoherent phase by an intermediate regime, in which the temporal series of the order parameter, $R(t)$, shows an huge variability.

3.5.3.1 Anomalous dynamics in the human connectome

In order to focus specifically on structural effects, let us to fix all intrinsic frequencies to be identical. Thus, we consider, without loss of generality, the simple case $\omega_i = 0$, and define the “activity” $\rho = 1 - \langle R \rangle$. In this case, perfect asymptotic coherence should emerge for all values of k but, as illustrated in Figure 3.5.6a, the convergence towards $\rho = 0$ turns out to be extremely slow (much slower than exponential, like in the case of the single-level modular network).

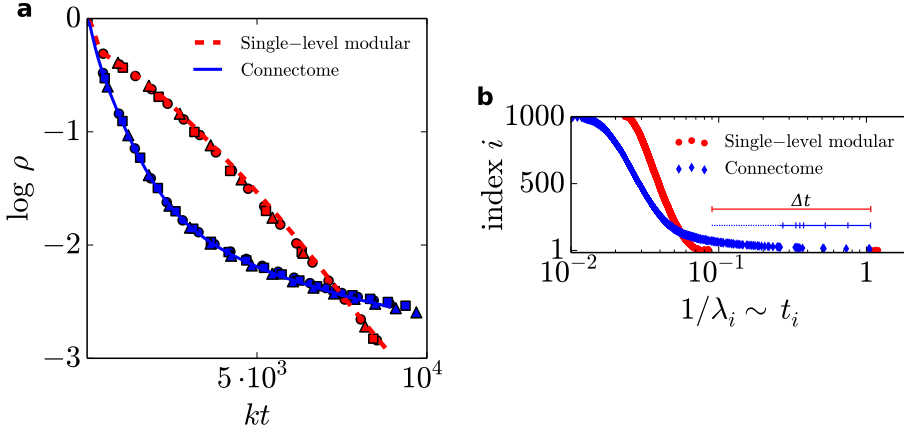


Figure 3.5.6: (a) Average decay of activity ρ for identical frequencies $\omega = 0$ in the HC network and comparison with a single-level modular network (made up of 4 similar random moduli at a single hierarchical level) of the same size and average connectivity as the HC network. Symbols stand for different values of k . (b) Characteristic decay times corresponding to the inverse of the first 1000 non-trivial eigenvalues of the Laplacian matrix (x axis) as a function of their respective ordered indexes (y axis), for networks as in (a). The stretched exponential behavior in (a) is the result of the convolution of slow time scales associated with small eigenvalues in (b).

This effect can be analytically investigated assuming that, for large enough times, all phase differences are relatively small. Then, up to first order, $\dot{\theta}_i = -k \sum_j L_{ij} \theta_j$ where $L_{ij} = \delta_{ij} \sum_l W_{jl} - W_{ij}$ are the elements of the Laplacian matrix [21, 27]. Solving the linear problem (see complete derivation on appendix C.2.2), $\theta_i(t) = \sum_{l,j} e^{-k\lambda_l t} v_i^l v_j^l \theta_j(0)$, where λ_l denotes the l -th Laplacian eigenvalue ($0 = \lambda_1 < \lambda_2 < \dots < \lambda_N$) and v_i^l the i -th component of the corresponding eigenvector. Since the averaged order parameter can be written as $Z(t) \approx \frac{1}{N} \sum_j (1 + i\theta_j - \frac{1}{2}\theta_j^2)$, averaging over initial conditions, and considering that (as the Laplacian has zero row-sums [27]) $\lambda_1 = 0$, we obtain

$$\rho(t) = \frac{\sigma^2}{2} \sum_{l=2}^N e^{-2k\lambda_l t}, \quad (3.5.16)$$

where σ is the standard deviation of the initial phases. This expression holds for any connected network. As usual, the larger the spectral gap λ_2 , the more “entangled” [27] the network and thus the more difficult to divide it into well separated moduli ($\lambda_2 = 0$ only for disconnected networks) [21, 27].

For large spectral gaps all timescales are fast, and the last expression can be approximated by its leading contribution, ensuing exponential relaxation to $\rho = 0$, as in fact observed in well-connected network architectures (Erdős-Rényi, scale free, etc. [50]). This is not the case for the HC matrix, for which a tail of small non-degenerate eigenvalues is encountered (see Figure 3.5.6b and [48]). Each eigenvalue λ_i in the tail corresponds to a natural division of moduli into sub-moduli [27], and the broad tail reflects the heterogeneity in the resulting modular sizes. As a consequence, each of these eigenvalues –with its associated large timescale, $t_i = 1/\lambda_i$ – contributes to the sum above, giving rise to a convolution of relaxation processes, entailing anomalously-slow dynamics, which could not be explained by a single-level modular network (see Figure 3.5.6a-b): slow dynamics necessarily stems from the existence of a hierarchy of moduli and structural bottlenecks. As explained, in the case of the HC the convolution of different times scales gives rise to stretched-exponential decay, which is an obvious flaw of this single-level modular structure should be reproduced in some way. It was noted in the past that strongly modular networks exhibit isolated eigenvalues in the lower edge of the Laplacian spectrum. Synchronization would develop in a step-wise process in time, where each transient would be given by each isolated eigenvalue [7]. In our case, the depth of the hierarchical organization and the strength of topological disorder produce instead a quasi-continuous tail of eigenvalues, and the step-wise process is replaced by an anomalous stretched-exponential behavior.

3.5.4

Hierarchic-modular network

Now, we go beyond the single-level modular network model and study hierarchical modular networks (HMN) in which moduli exists within moduli in a nested way at various scales [17, 37, 38, 47, 64, 76]. HMN are assembled in a bottom-up fashion: local fully-connected moduli (e.g. of 4 nodes) are used as building blocks. They are recursively grouped by establishing additional inter-moduli links in a level-dependent way as sketched in Figure 3.5.7 (top) [48, 71].

✖ **Building a Hierarchic-modular network** A model to construct synthetic hierarchical and modular networks (HMN) have been devised with s hierarchical levels, comprising L links (mimicking synapses) and N nodes (mimicking neurons), with a variable structure with the aim to resemble real neural networks [48]. They are built in a bottom-top procedure; to begin with, at hierarchical level 1, 2^s basal fully connected blocks of size M are linked pairwise into super-blocks by establishing a fixed number α of random unweighted links between the elements of each ($\alpha = 2$ in the Figure 3.5.7). Newly formed blocks are then linked iteratively with the same α up to level s , i.e. the number of connections

between blocks is fixed a priori, until the network becomes connected, avoiding double connections and self-loops between nodes. There is an inherent stochasticity when connections are assigned even though both, the degree distribution of the network and the total number of connections, are fixed initially. Finally, it is important to mention that the networks exhibit an exponential degree distribution with a characteristic connectivity. Besides, the network is characterized by,

$$\begin{cases} N = M2^s \\ k = (M - 1) + \frac{2\alpha}{M} (1 - 2^{-s}) \end{cases} \quad (3.5.17)$$

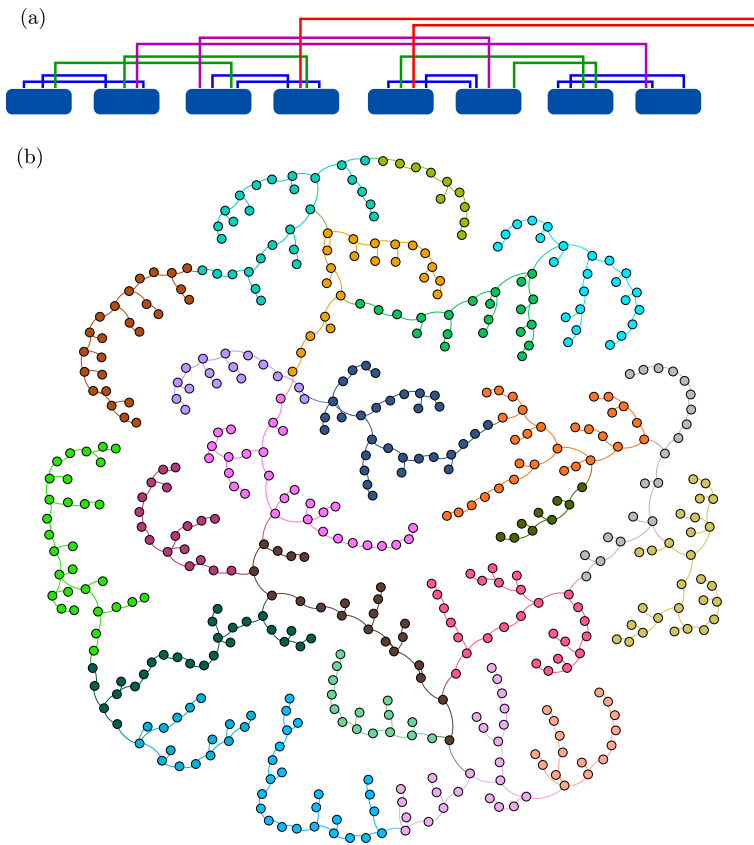


Figure 3.5.7: (a) Sketch of a HMN network bottom-up grouping. (b) Graph representation of a HMN with $N = 512$ and $s = 9$ hierarchical levels ($\alpha = 1$, $M = 2$).

In a similar vein, implementing the Kuramoto model on top of this synthetic topology, an intermediate regime placed between the coherent and the incoherent phase emerges (see Figure 3.5.8). Patterns akin to the broad quasi-periodic temporal oscillations of $R(t)$ are present now, with Gaussian $g(\omega)$, and they are also robust against changes in the frequency distribution whereas the location and width of the intermediate phase depend upon details. Also, Figure 3.5.8 shows that –through the local order parameter, $r^{(l)}$, for different hierarchical levels ($l = 1$ to $l = 5$)– the transition to local coherence at progressively higher hierarchical level occurs at progressively larger values of k ; i.e. coherence emerges out of a hierarchical bottom-up process. Identically, the ordering process is non-monotonous and coherence could decrease momentarily with k , due to that the emergence of local order in some communities hinder or reduce coherence in others, inducing local “desynchronization” and frustration in the burgeoning global order, and reflecting the metastable fractal-like nature of the emerging states. This metastable nature is revealed by the study of the “chimera index” for this networks, presenting a clear peak in the corresponding $\chi^{(l)}$ for each hierarchical level, that marks the “matrioshka-doll” synchronization processes: the sequence of separated peaks in $\chi^{(l)}$ for increasing values of l reflect the direct evidence of the hierarchical synchronization process, being local order attained in a bottom-up process.

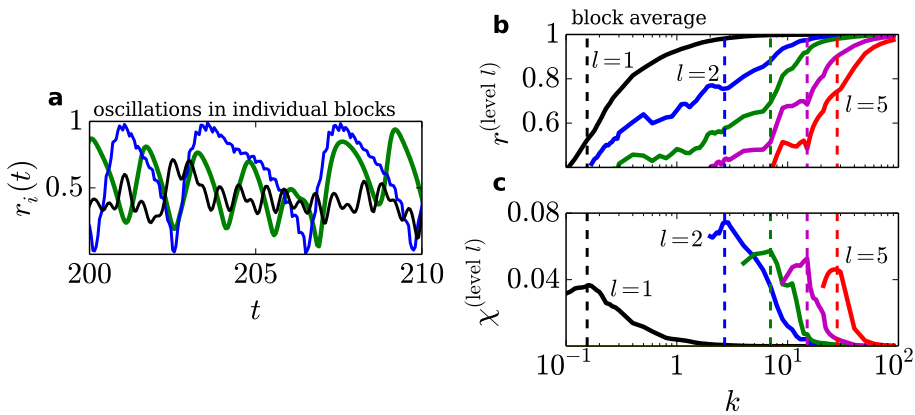


Figure 3.5.8: Results for a HMN with $N = 512$, $s = 5$, and $\alpha = 4$. Hierarchical levels are $i = 1 \rightarrow 5$ in black, blue, green, magenta and red respectively (as in the previous sketch, not all shown in a) for clarity). (a) Temporal series with broad oscillations of the local order parameter, $r_i(t)$, for 3 selected hierarchical levels (arrows in the main plot). (b) Average of the local order parameter over each hierarchical level. (c) Chimera index for different levels as a function of k . As in the HC, global order emerges only after local order is attained at lower levels.

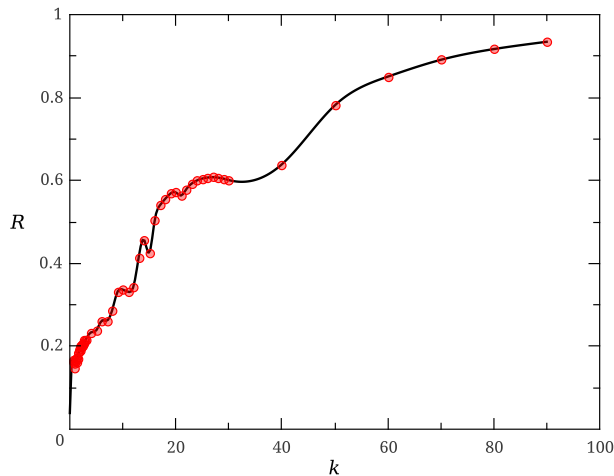


Figure 3.5.9: Time-averaged order parameter $R = \langle R(t) \rangle$ for a HMN with $N = 512$, $s = 5$, and $\alpha = 4$.

3.5.4.1 Lifshitz tails and stretched-exponential asymptotic behavior

In sparse HMNs, the lower end of the Laplacian spectrum is characterized by an exponential tail in the density of states $p(\lambda) \sim e^{-1/\lambda^a}$ for $N \rightarrow \infty$, with $a \approx 1$, known as Lifshitz tail [48]. In graphs, Lifshitz tails signal the existence of non-trivial heterogeneous localized states governing the asymptotic synchronization dynamics at very large times t . We have shown that in the absence of frequency heterogeneity, the $t \rightarrow \infty$ behavior of the activity is given –taking the continuum limit of Eq. (3.5.16)– by $\rho(t) \approx \frac{\sigma^2}{2} \int d\lambda p(\lambda) e^{-2k\lambda t}$, which can be evaluated with the saddle-point method (details in appendix C.2.2), yielding

$$\rho(t) \approx \frac{\sigma^2}{2} \exp \left[-(1+a) a^{-\frac{a}{1+a}} (2kt)^{\frac{a}{1+a}} \right]. \quad (3.5.18)$$

Substituting $a \approx 1$, as empirically found in HMNs [48], leads to

$$\rho(t) \sim e^{-\sqrt{8kt}}, \quad (3.5.19)$$

i.e. anomalous stretched-exponential asymptotic behavior, in excellent agreement with computational results (see Figure 3.5.10). Therefore, hierarchical modular networks constitute a parsimonious and adequate model for reproducing all the complex synchronization phenomenology of the HC.

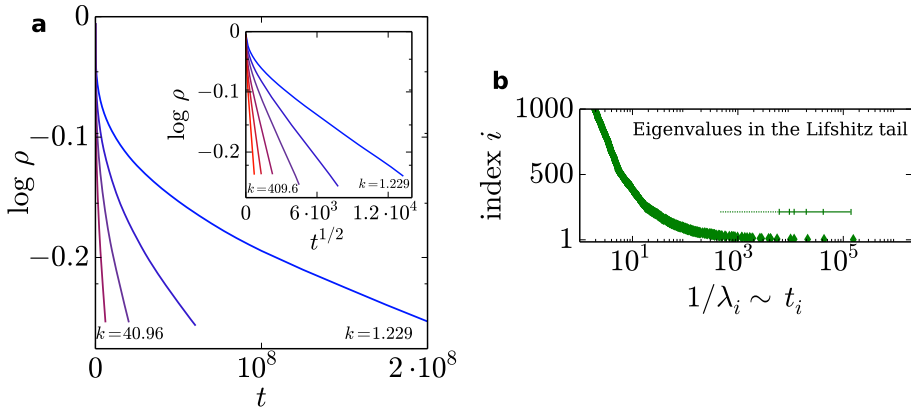


Figure 3.5.10: (a) Time relaxation of activity ρ for homogeneous characteristic frequencies $\omega = 0$, for logarithmically equally spaced values of k . Averages over 10^6 realizations of HMNs with $N = 4096$ and $s = 11$. Inset: as in the main plot (a), but representing as a function of $t^{1/2}$ and confirming the predicted stretched exponential behavior. (b) Inverse tail-eigenvalues for a HMN.

Thus, our computational analyses of the Kuramoto dynamics on HMN substrates (Figures 3.5.8 and 3.5.10) reveal the striking similarity between both networks, HC and HMNs, specifically:

- i) A sequence of synchronization transitions for progressively higher hierarchical levels at increasing values of k .
- ii) Chimera-like states at every hierarchical level, resulting in a hierarchy of metastable states with maximal variability at the corresponding transition points.
- iii) Extremely slow relaxation toward the coherent state when all internal frequencies are identical. Furthermore, anomalies in the Laplacian spectrum analogous to those of the HC network are observed for HMN matrices.

It is clear that a crucial role in the emergence of such behavior is played by disorder. One would be tempted to believe that all networks characterized by a finite spectral dimension could potentially give rise to this phenomenology. This is obviously not the case for a regular lattice, where the spectral gap is always well defined. A fractal lattice or an ordered tree, on the other hand, could exhibit a hierarchy of discrete low eigenvalues, whose multiplicities reflect system symmetries. The introduction of disorder, as in HMNs, is then necessary in order to transform such hierarchy of discrete levels into a continuous Lifshitz tail, leading eventually to the behavior predicted by Eq. (3.5.19).

3.6

Metastability and noise effects

Our previous results vividly illustrate the existence of an intermediate region in which the HC exhibits maximal dynamical variability at the global scale, suggesting metastable behavior. In order to explore more directly whether metastable states exist, we now assess if the dynamics may present different attractors and, for some values of the control parameter k and noise amplitudes, if the system may switch between different global attractors with different levels of coherence.

For this purpose, an additional term must be added to Eq. (3.2.1) to implement a noisy Kuramoto dynamics,

$$\dot{\theta}_j(t) = \sigma \eta_j(t) + \omega_j + k \sum_{l=1}^N W_{jl} \sin [\theta_l(t) - \theta_j(t)], \quad (3.6.1)$$

where the new term, $\eta_i(t)$, is a zero-mean delta-correlated Gaussian noise, tuned by the real-valued amplitude σ .

Figure 3.6.1 shows a time series of the global parameter, for a fixed realization of internal frequencies –with Gaussian $g(\omega)$ – and initial phases. It clearly illustrates how the HC spontaneously switches between two different attractors. These type of events, however, are not easy to observe in the HC network. Due to the coarse-grained nature of the HC mapping, different attractors may actually have comparable average values of the coherence R , which makes their discrimination especially difficult at the global scale.

Remarkably, such events are easier to spot in synthetic hierarchical modular networks (HMN), such as proposed to model brain networks in an efficient way, since the effects of modularity and hierarchy are much enhanced, as they develop across a larger number of hierarchical levels than the one allowed by current imaging techniques for empirically obtained connectomes. Also, figure 3.6.1 illustrates the bi-stable nature of the global parameter in the intermediate phase for a HMN, in which metastability can be very well appreciated. This switching behavior closely resembles “up and down” states, which are well known to appear in certain phases of sleep or under anesthesia (see [29] and refs. therein).

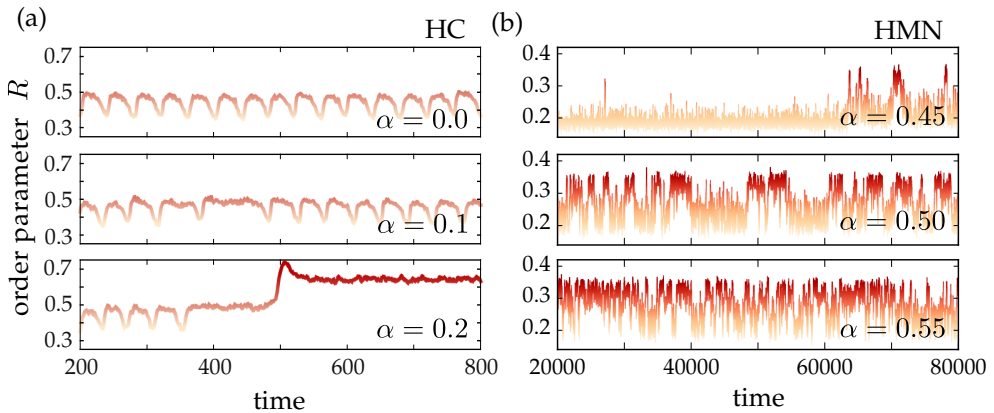


Figure 3.6.1: Time series exhibit metastability of the global synchronization in the HC and in HMNs, in the intermediate region. (a) In the HC—in the intermediate region—the system remains in the same attractor for low noise amplitudes ($\sigma = 0$ and 0.1). But, for large values, such as $\sigma = 0.2$, it is able to “jump” to another more coherent attractor, where it settles. (b) In HMNs (size $N = 1024$, $s = 9$), we observe the same phenomenology, but much enhanced: when noise is very low ($\sigma \leq 0.45$), the system tends to remain stable in a certain attractor (with a few exceptions after very large waiting times). Choosing a higher σ ($\sigma \geq 0.5$), it exhibits bi-stable behavior, switching intermittently between two different attractors. For large enough σ ($\sigma \geq 0.55$), the dynamics becomes too erratic to appreciate metastability.

We hypothesize that hierarchical modular networks in general (and the HC in particular) enable the possibility of a large repertoire of attractors, with different degrees of coherence and stability. Such metastability can be made evident and quantified by performing the following type of numerical test. Starting from a fixed random initial condition and considering a vanishing noise amplitude (i.e. $\sigma = 0$), the system might deterministically fall into a number of different attractors, each of them with an associated value of the global coherence depending on the initial conditions, the network structure, and the choice of natural frequencies. Once this attractor A is reached, the system is perturbed by switching on a non-vanishing noise amplitude ($\sigma > 0$) during a finite time window. The system may remain stable in the same attractor A if the noise is weak enough ($\sigma \ll 1$). However, if larger values of the noise amplitude are chosen, the system may jump into another close, more stable, attractor. If the noise amplitude is very large ($\sigma \gg 1$), the system can in principle jump to any attractor, but, very likely, will also escape from it, wandering around a large fraction of the configuration space.

After the perturbation time-window is over, we let the system relax once again, and check if the new resulting steady state B has changed with respect to A. In that case, we can conclude that the systems was in a metastable state A before the perturbation, and has reached another state B after it – potentially a metastable state itself.

We have carried out this type of test using an artificial HMN (see Figure 3.6.2) for a specific value of the control parameter, k , belonging in the intermediate region. Natural frequencies are sampled from the a Lorentzian distribution $g(\omega)$ (as above, our main results are not sensible to this choice). Starting from a random initial configuration of phases, we integrate Eq. (3.6.1) up to time 500 with $\sigma = 0$. After this, we introduce the external perturbation by switching the noise coefficient σ to a certain non-zero value during a time window of duration 100. Finally we revert to $\sigma = 0$ and continue the integration up to time $t = 1000$. The last steady state value is averaged over 10^4 realizations of initial conditions, networks, and intrinsic frequencies.

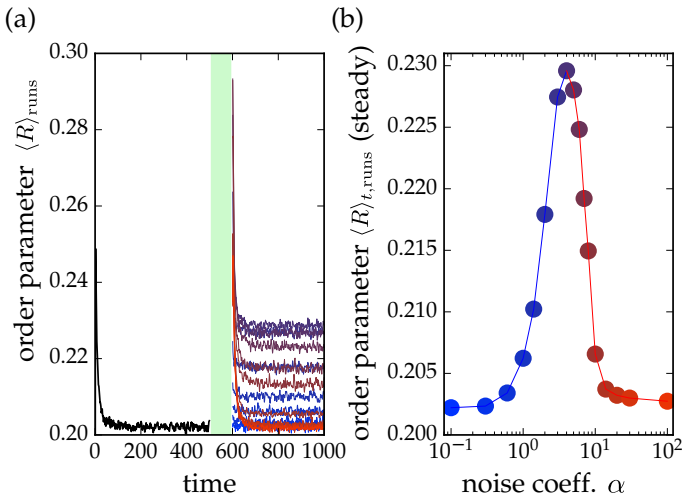


Figure 3.6.2: Perturbations can lead the system to more coherent attractors in the intermediate non-coherent phase. (a) Order parameter R averaged in time over 10^4 realizations. A noise pulse of amplitude σ is applied during the green interval. This same protocol is repeated for different values of σ . (b) Average order parameter in the final steady state (after the noise pulse) as a function of σ . For intermediate values of σ , a resonant peak emerges for $1 < \sigma < 10$, illustrating that the system can jump to a close, more coherent on-average attractor. Simulations are run on HMN networks of size $N = 1024$, with 9 hierarchical levels.

As illustrated in Figure 3.6.2, for low as well as for high values of the noise amplitude, the system has the same average order parameter close to $\langle R \rangle_{t, \text{runs}} \simeq 0.2$, as could have been anticipated. However, a resonant peak emerges for intermediate values of the noise, where the system switches to states with different levels of coherence. This plot explicitly illustrates the existence of metastability and noise-induced jumps between attractors. As noise is enhanced, progressively more stable states are found, but above some noise threshold, the system does not remain trapped in a single attractor but jumps among many, resulting in a progressive decrease of the overall coherence.

3.7

Conclusions

Simple models of synchronization dynamics exhibit an unexpectedly rich phenomenology when operating on top of empirical human brain networks. This complexity includes oscillatory behavior of the order parameter suggesting the existence of relatively isolated structural communities or moduli, that –as a matter of fact– can be identified by using standard community detection algorithms. Even more remarkably, oscillations in the level of internal coherence are also present within these moduli, suggesting the existence of a whole hierarchy of nested levels of organization, as also found in the recent literature relying on a variety of approaches [13, 17, 18, 37, 38, 47, 64, 76]. Aimed at unveiling this complex behavior we have introduced a family of hierarchical modular networks and studied them in order to assess what structural properties are required in order to reproduce the complex synchronization patterns observed in brain networks.

In the absence of frequency dispersion, perfect coherence is achieved in synthetic hierarchical networks by following a bottom-up ordering dynamics in which progressively larger communities –with inherently different timescales– become coherent (see [7]). However, this hierarchically nested synchronization process is constrained and altered by structural bottlenecks –as carefully described here for the simpler two-block toy model– at all hierarchical levels. This structural complexity brings about anomalously-slow dynamics at very large timescales. Observe that the HC, in spite of being a coarse-grained mapping of a brain network, already shows strong signals of this ideal hierarchical architecture as reflected in its anomalously slow synchronization dynamics as well as in the presence of non-degenerate eigenvalues in the lower edge of its Laplacian spectrum, acting as a fingerprint of structural heterogeneity and complexity. We stress that such a complex phenomenology would be impossible to obtain in networks with stronger connectivity patterns (e.g. with the small world property) such as scale free-networks or high-degree random graphs. Even the generic presence of simple communities may not be sufficient to grant the emergence of frustration: the uniqueness of the human connectome, and of hierarchical modular networks in general, resides in the strong separation into distinct levels, which the synchronization dynamics is able to resolve only at well-separated values of the coupling k .

On the other hand, in the presence of intrinsic frequency heterogeneity, the described slow ordering process is further frustrated. Actually, for small values of the coupling constant k the system remains trapped into metastable and

chimera-like states with traits of local coherence at different hierarchical levels. In this case, inter-moduli frequency barriers need to be overcome before weakly connected moduli achieve mutual coherence. This is clearly exemplified by the separation between distinct peaks in the chimera index $\chi^{(l)}$ in Figures 3.4.7–3.5.8, each one signaling the onset of an independent synchronization process at a given level. The result is a complex synchronization landscape, which is especially rich and diverse in the intermediate regime put forward here. If a hierarchical modular network is loosely connected, this type of “matryovska-doll” synchronization process is constrained at all levels by structural bottlenecks, bringing about anomalously-slow synchronization dynamics.

Including other realistic ingredients such as explicit phase frustration [58] or time delays [19, 73] to our simplistic approach should only add complexity to the structural frustration effect reported here. It is also expected that more refined models –including neuro-realistic ingredients leading to collective oscillations– would generate similar results and provide a finer description of brain activity, but this remains to be explored in future works.

Addition of noise to the Kuramoto dynamics allows the system to escape from metastable states, in which the loose connectivity between some moduli does not allow them to overcome intrinsic-frequency differences and achieve coherence. Stochasticity can overcome the “potential barriers” between mutually incoherent moduli as well as re-introduce “desynchronization” effects. These combined effects can make the system able to explore the nested hierarchy of attractors, allowing one to shed some light into the complex synchronization patterns in real brain networks. Actually, spontaneous dynamical fluctuations have been measured in the resting state of human brains [14]; these are correlated across diverse segregated moduli and characterized by very slow fluctuations, of typical frequency $< 0.1Hz$, in close agreement with those found here (Figure 3.4.5). While persistence in metastable states may extend indefinitely, it has been suggested that the brain is routinely exploring different states or attractors [24] and that –in order to enhance spontaneous switching between attractors– brain networks should operate close to a critical point, allowing for large intrinsic fluctuations which on their turn entail attractor “surfing” and give access to highly varied functional configurations [20, 24, 34, 60, 61] and, in particular, to maximal variability of phase synchrony [74]. The existence of multiple attractors and noise-induced surfing is largely facilitated in the broad intermediate regime first elucidated here, implying that a precise fine tuning to a critical point might not be required to guarantee functional advantages usually associated with criticality [12, 20, 59]: the role usually played by a critical point is assumed by a broad intermediate region in hierarchically architected complex systems [48].

We have shown that a simple description of neural coherence dynamics based on the noisy Kuramoto model may suffice to reproduce a very rich phe-

nomenology, in hierarchical modular networks and in particular in the human connectome. The introduction of small fluctuations (exemplifying external perturbations, stimuli, or intrinsic stochasticity) allow the system to escape from metastable states and sample the configuration space, proving a paradigmatic modeling tool for the attractor surfing behavior suggested by experiments. Finally, let us remark that our results might also be of relevance for other hierarchically organized systems such as gene regulatory networks [68] for which coherent activations play a pivotal role [51].

References

- [1] ABRAMS, D. M., MIROLLO, R., STROGATZ, S. H. & WILEY, D. A. «Solvable model for chimera states of coupled oscillators». *Phys. Rev. Lett.* **101**, 084103 (2008).
- [2] ABRAMS, D. M. & STROGATZ, S. H. «Chimera states in a ring of nonlocally coupled oscillators». *Int. J. Bifurc. Chaos* **16**, 21–37 (2006).
- [3] ABRAMS, D. M. & STROGATZ, S. H. «Chimera states for coupled oscillators». *Phys. Rev. Lett.* **93**, 174102 (2004).
- [4] ACEBRÓN, J. A., BONILLA, L. L., PÉREZ-VICENTE, C. J., RITORT, F. & SPIGLER, R. «The Kuramoto model: A simple paradigm for synchronization phenomena». *Rev. Mod. Phys.* **77**, 137–185 (2005).
- [5] ACEBRÓN, J. & BONILLA, L. «Asymptotic description of transients and synchronized states of globally coupled oscillators». *Physica D* **114**, 296–314 (1998).
- [6] ARENAS, A., DÍAZ-GUILERA, A., KURTHS, J., Y. MORENO, Y. & ZHOU, C. «Synchronization in complex networks». *Phys. Rep.* **469**, 93–153 (2008).
- [7] ARENAS, A., DÍAZ-GUILERA, A. & PÉREZ-VICENTE, C. «Synchronization reveals topological scales in complex networks». *Phys. Rev. Lett.* **96**, 114102 (2006).
- [8] ARENAS, A. & VICENTE, C. P. «Exact long-time behavior of a network of phase oscillators under random fields». *Phys. Rev. E* **50**, 949 (1994).
- [9] BARABÁSI, A.-L. & ALBERT, R. «Emergence of scaling in random networks». *Science* **286**, 509–512 (1999).
- [10] BARABASI, A.-L. & OLTVAI, Z. N. «Network biology: understanding the cell's functional organization». *Nat. Rev. Gen.* **5**, 101 (2004).
- [11] BASNARKOV, L. & URUMOV, V. «Phase transitions in the Kuramoto model». *Phys. Rev. E* **76**, 057201 (2007).
- [12] BEGGS, J. M. «The Criticality Hypothesis: How Local Cortical Networks Might Optimize Information Processing». *Phil. Trans. R. Soc. A* **366**, 329–343 (2008).

-
- [13] BETZEL, R. *et al.* «Multi-scale community organization of the human structural connectome and its relationship with resting-state functional connectivity». *Netw. Sci.* **1**, 353–373 (2013).
- [14] BISWAL, B., ZERRIN YETKIN, F., HAUGHTON, V. & HYDE, J. «Functional connectivity in the motor cortex of resting human brain using echo-planar mri». *Magn. Reson. Med.* **34**, 537–541 (1995).
- [15] BREAKSPEAR, M., HEITMANN, S. & DAFFERTSHOFER, A. «Generative models of cortical oscillations: neurobiological implications of the kuramoto model.». *Front. Hum. Neurosci.* **4** (2010).
- [16] BREAKSPEAR, M. & STAM, C. J. «Dynamics of a neural system with a multiscale architecture». *Phil. Trans. R. Soc. Lond. B* **360**, 1051–1074 (2005).
- [17] BULLMORE, E. & SPORNS, O. «Complex brain networks: graph theoretical analysis of structural and functional systems». *Nat. Rev. Neurosci.* **10**, 186–198 (2009).
- [18] BUZSÁKI, G. *Rhythms of the Brain* (Oxford University Press, New York, 2006).
- [19] CABRAL, J., HUGUES, E., SPORNS, O. & DECO, G. «Role of local network oscillations in resting-state functional connectivity.». *NeuroImage* **57**, 130–139 (2011).
- [20] CHIALVO, D. R. «Emergent complex neural dynamics». *Nat. Phys.* **6**, 744–750 (2010).
- [21] CHUNG, F. R. K. *Spectral graph theory*. No. 92 in Reg. Conf. Series in Maths (AMS, Providence, 1997).
- [22] CUMIN, D. & UNSWORTH, C. «Generalising the Kuramoto model for the study of neuronal synchronisation in the brain». *Physica D* **226**, 181–196 (2007).
- [23] DAVID, O. & FRISTON, K. J. «A neural mass model for MEG/EEG:: coupling and neuronal dynamics». *NeuroImage* **20**, 1743–1755 (2003).
- [24] DECO, G. & JIRSA, V. K. «Ongoing Cortical Activity at Rest: Criticality, Multistability, and Ghost Attractors». *J. Neurosci.* **32**, 3366–3375 (2012).
- [25] DECO, G., JIRSA, V. K. & MCINTOSH, A. R. «Emerging concepts for the dynamical organization of resting-state activity in the brain». *Nat. Rev. Neurosci.* **12**, 43 (2011).

-
- [26] DONETTI, L., HURTADO, P. I. & MUNOZ, M. A. «Entangled networks, synchronization, and optimal network topology». *Phys. Rev. Lett.* **95**, 188701 (2005).
- [27] DONETTI, L., NERI, F. & MUÑOZ, M. A. «Optimal network topologies: expanders, cages, Ramanujan graphs, entangled networks and all that». *J. Stat. Mech. Theory Exp.* **2006**, P08007 (2006).
- [28] DUCH, J. & ARENAS, Á. «Community detection in complex networks using extremal optimization». *Phys. Rev. E* **72**, 027104 (2005).
- [29] ECKMANN, J. P. *et al.* «The physics of living neural networks». *Phys. Rep.* **449**, 54–76 (2007).
- [30] FREEMAN, W. «Models of the dynamics of neural populations.». *Electroen. Clin. Neuro.* 9–18 (1978).
- [31] GASTNER, M. T. & ÓDOR, G. «The topology of large Open Connectome networks for the human brain». *Sci. Rep.* **6**, 27249 (2016).
- [32] HAGERSTROM, A. M. *et al.* «Experimental observation of chimeras in coupled-map lattices». *Nat. Phys.* **8**, 658 (2012).
- [33] HAGMANN, P. *et al.* «Mapping the structural core of human cerebral cortex». *PLoS Biol.* **6**, e159 (2008).
- [34] HAIMOVICI, A., TAGLIAZUCCHI, E., BALENZUELA, P. & CHIALVO, D. R. «Brain Organization into Resting State Networks Emerges at Criticality on a Model of the Human Connectome». *Phys. Rev. Lett.* **110**, 178101 (2013).
- [35] HONEY, C. J. & SPORNS, O. «Dynamical consequences of lesions in cortical networks». *Hum. Brain Mapp.* **29**, 802–809 (2008).
- [36] HONEY, C. J. *et al.* «Predicting human resting-state functional connectivity from structural connectivity». *Proc. Natl. Acad. Sci. USA* **106**, 2035–2040 (2009).
- [37] IVKOVIĆ, M., AMY, K. & ASHISH, R. «Statistics of Weighted Brain Networks Reveal Hierarchical Organization and Gaussian Degree Distribution». *PLoS ONE* **7**, e35029 (2012).
- [38] KAISER, M. «A tutorial in connectome analysis: topological and spatial features of brain networks». *NeuroImage* **57**, 892–907 (2011).
- [39] KAISER, M., GOERNER, M. & HILGETAG, C. «Criticality of spreading dynamics in hierarchical cluster networks without inhibition». *New J. Phys.* **9**, 110 (2007).

-
- [40] KANDEL, E. R., SCHWARTZ, J. H. & JESSELL, T. M. *Principles of Neural Science* (McGraw-Hill, New York, 2000).
- [41] KOMIN, N., MURZA, A. C., HERNÁNDEZ-GARCÍA, E. & TORAL, R. «Synchronization and entrainment of coupled circadian oscillators». *Interface Focus* **1**, 167–176 (2011).
- [42] KURAMOTO, Y. «Self-entrainment of a population of coupled nonlinear oscillators». *Lect. Notes Phys.* **39**, 420–422 (1975).
- [43] LAING, C. R. «Chimera states in heterogeneous networks». *Chaos* **19**, 013113 (2009).
- [44] M. KAISER, C. H. «Optimal Hierarchical Modular Topologies for Producing Limited Sustained Activation of Neural Networks». *Front. in Neuroinform.* **4**, 14 (2010).
- [45] MALAGARRIGA, D., VILLA, A. E., GARCIA-OJALVO, J. & PONS, A. J. «Mesoscopic segregation of excitation and inhibition in a brain network model». *PLoS Comp. Biol.* **11**, e1004007 (2015).
- [46] MCGRAW, P. N. & MENZINGER, M. «Clustering and the synchronization of oscillator networks». *Phys. Rev. E* **72**, 015101 (2005).
- [47] MEUNIER, D., LAMBIOTTE, R. & BULLMORE, E. «Modular and hierarchically modular organization of brain networks». *Front. Neurosci.* **4**, 200 (2010).
- [48] MORETTI, P. & MUÑOZ, M. A. «Griffiths phases and the stretching of criticality in brain networks». *Nat. Comm.* **4**, – (2013).
- [49] MUÑOZ, M. A., JUHÁSZ, R., CASTELLANO, C. & ÓDOR, G. «Griffiths Phases on Complex Networks». *Phys. Rev. Lett.* **105**, 128701 (2010).
- [50] NEWMAN, M. «The Structure and Function of Complex Networks». *SIAM Review* **45**, 167–256 (2003).
- [51] NYKTER, M. *et al.* «Gene expression dynamics in the macrophage exhibit criticality». *Proc. Natl. Acad. Sci. USA* **105**, 1897–1900 (2008).
- [52] OTT, E. & ANTONSEN, T. M. «Low dimensional behavior of large systems of globally coupled oscillators». *Chaos* **18**, 037113 (2008).
- [53] PANAGGIO, M. J. & ABRAMS, D. M. «Chimera states: coexistence of coherence and incoherence in networks of coupled oscillators». *Nonlinearity* **28**, R67 (2015).

- [54] POPOVYCH, O. V., MAISTRENKO, Y. L. & TASS, P. A. «Phase chaos in coupled oscillators». *Phys. Rev. E* **71**, 065201 (2005).
- [55] RATTENBORG, N. C., AMLANER, C. & LIMA, S. «Behavioral, neurophysiological and evolutionary perspectives on unihemispheric sleep». *Neurosci. Biobehav. Rev.* **24**, 817–842 (2000).
- [56] ROSENBLUM, M. G., PIKOVSKY, A. & KURTHS, J. *Synchronization – A universal concept in nonlinear sciences* (Cambridge University Press, Cambridge, 2001).
- [57] SCHMIDT, L., SCHÖNLEBER, K., KRISCHER, K. & GARCÍA-MORALES, V. «Coexistence of synchrony and incoherence in oscillatory media under nonlinear global coupling». *Chaos* **24**, 013102 (2014).
- [58] SHANAHAN, M. «Metastable chimera states in community-structured oscillator networks». *Chaos* **20**, 013108 (2010).
- [59] SHEW, W. L. & PLENZ, D. «The Functional Benefits of Criticality in the Cortex». *The Neuroscientist* **19**, 88–100 (2013).
- [60] SHEW, W. L., YANG, H., PETERMANN, T., ROY, R. & PLENZ, D. «Neuronal Avalanches Imply Maximum Dynamic Range in Cortical Networks at Criticality». *J. Neurosci.* **29**, 15595–15600 (2009).
- [61] SHRIKI, O. *et al.* «Neuronal Avalanches in the Resting MEG of the Human Brain». *J. Neurosci.* **33**, 7079–7090 (2013).
- [62] SIVASHINSKY, G. «Diffusional-thermal theory of cellular flames». *Combust. Sci. Technol.* **15**, 137–145 (1977).
- [63] SKARDAL, P. S. & RESTREPO, J. G. «Hierarchical synchrony of phase oscillators in modular networks». *Phys. Rev. E* **85**, 016208 (2012).
- [64] SPORNS, O. *Networks of the Brain* (MIT Press, Cambridge, 2010).
- [65] STEINMETZ, P. N. *et al.* «Attention modulates synchronized neuronal firing in primate somatosensory cortex». *Nature* **404**, 187–190 (2000).
- [66] STROGATZ, S. H. «From Kuramoto to Crawford: exploring the onset of synchronization in populations of coupled oscillators». *Physica D* **143**, 1–20 (2000).
- [67] TINSLEY, M. R., NKOMO, S. & SHOWALTER, K. «Chimera and phase-cluster states in populations of coupled chemical oscillators». *Nat. Phys.* **8**, 662 (2012).

- [68] TREVIÑO III, S., SUN, Y., COOPER, T. F. & BASSLER, K. «Robust Detection of Hierarchical Communities from Escherichia coli Gene Expression Data». *PLoS Comp. Biol.* **8**, e1002391 (2012).
- [69] UM, J., HONG, H. & PARK, H. «Nature of synchronization transitions in random networks of coupled oscillators». *Phys. Rev. E* **89**, 012810 (2014).
- [70] VOJTA, T. «Rare region effects at classical, quantum and nonequilibrium phase transitions». *J. Phys. A* **39**, R143–R205 (2006).
- [71] WANG, S.-J., HILGETAG, C. C. & ZHOU, C. «Sustained activity in hierarchical modular neural networks: SOC and oscillations.». *Front. Comp. Neurosci.* **5**, 30 (2011).
- [72] WIESENFELD, K., COLET, P. & STROGATZ, S. H. «Synchronization transitions in a disordered Josephson series array». *Phys. Rev. Lett.* **76**, 404 (1996).
- [73] WILDIE, M. & SHANAHAN, M. «Metastability and chimera states in modular delay and pulse-coupled oscillator networks». *Chaos* **22**, 043131+ (2012).
- [74] YANG, H., SHEW, W. L., ROY, R. & PLENZ, D. «Maximal Variability of Phase Synchrony in Cortical Networks with Neuronal Avalanches». *J. Neurosci.* **32**, 1061–1072 (2012).
- [75] YELDESBUY, A., PIKOVSKY, A. & ROSENBLUM, M. «Chimeralike states in an ensemble of globally coupled oscillators». *Phys. Rev. Lett.* **112**, 144103 (2014).
- [76] ZHOU, C., ZEMANOVÁ, L., ZAMORA-LÓPEZ, G., HILGETAG, C. & KURTHS, J. «Hierarchical Organization Unveiled by Functional Connectivity in Complex Brain Networks». *Phys. Rev. Lett.* **97** (2006).
- [77] ZHOU, C., ZEMANOVÁ, L., ZAMORA-LÓPEZ, G., HILGETAG, C. C. & KURTHS, J. «Structure–function relationship in complex brain networks expressed by hierarchical synchronization». *New J. Phys.* **9**, 178–178 (2007).

Reactive and noisy dynamics in simple neural systems: avalanches far away of the critical point

4.1	Introduction	133
4.2	Demographic noise and balanced logarithmic potentials . . .	135
4.2.1	A simple calculation for the branching process . . .	136
4.2.2	Random walks in a logarithmic potential	138
4.3	Reactive and noisy dynamics in the Wilson-Cowan model . .	143
4.3.1	Phenomenology	145
4.3.2	Criticality and balance	145
4.3.3	The roles played by the noise	149
4.4	Reactive dynamics in the Tsodyks-Markram model	154
4.5	Conclusions	157
	References	159

Introduction

“If you have a hammer, use it everywhere you can, but, although I wish, I do not claim that everything is critical.”

Adapted from B. Mandelbrot

Scale-invariance has been proven to be ubiquitous in nature. Power-law distributed avalanches of activity are reported in very diverse phenomena, from earthquakes and microfracturing phenomena, to solar flares, rainfall, or type II superconductors [2, 22, 59, 76]. Very often such a scale-invariant behavior is considered as the fingerprint of underlying criticality. Groundbreaking experimental evidence by Beggs and Plenz, revealed the existence of scale-invariant episodes of electrochemical activity in neural tissues *in vitro*, thereafter named *neural avalanches*. Subsequently, neural avalanches were detected in a wide range of experimental settings, tissues and species both *in vitro* [4, 5, 23, 43, 60] and *in vivo* [6, 30, 56, 58].

Such a scale-invariant organization has been taken as an indicator that cortical dynamics operates close to a critical state, endowing the system with huge sensitivity to stimuli, large spatio-temporal correlations and fluctuations, optimal transmission of information, etc [52, 68], and theoretical models have actually proposed a link to self-organized criticality (or variants of it) [9, 40, 41, 48, 65]. Nevertheless, the criticality hypothesis in cortical networks is still controversial [71] and some authors have highlighted that it is not clear whether the available empirical evidences actually call for criticality or alternative origins could be invoked, such as noise, bistability or neutral theories [23, 47, 67, 71]. Moreover the optimal properties that have been attributed to criticality are often related to scale invariance and consequently they can be ascribed, to the same extent, to other mechanisms originating heavy-tailed observables.

Thus, in order to focus on alternative scenarios for the emergence of neuronal avalanches we should first specify the most fundamental and particular aspects that give rise to such scale-invariant behavior. In such a way, is essential the comprehension and reassessment of simple non-equilibrium phase transitions with absorbing states. In particular, one of the most representative case between an active phase and an absorbing phase, the quintessential Directed Percolation one. Despite its straightforward definition, it cannot be solved even

in one dimension, but provides a robust universality class with well-defined scale-invariant avalanches explaining, for example, spreading of infectious disease. It is also has been related (for high-dimensional systems [14, 49]) with the experimental exponents of neuronal avalanches founded (originally) by Beggs and Plenz together with the theory of critical branching processes ([31, 38]).

Otherwise, beyond and active/quiescent phase transition, the emergence of highly irregular bursts of activity has often been reported in association with balance between excitatory and inhibitory activity [13, 75], but it is not always clear whether or not implementing a balanced condition can be interpreted as tuning the system close to the point of transition between two distinct phases. In this context, Benayoun et al. in [7] introduced an intriguingly puzzling, with very general mechanisms, giving rise to the emergence of self-similar bursts of activity in finite-size systems of spiking neurons. Thus, indicating that the system, poised in a regime of balance between excitation and inhibition, results in an avalanching-like behavior.

Our aim is to uncover the interplay between the factors concurring to the appearance of non-critical avalanches of activity in [7] as well as to extend these results to regularly mechanisms other than inhibition.

In order to explain the phenomenon, we will recover the mathematical rationale of “non-normal” forms and in particular we will study the transient behavior of “reactive” systems and try to explain the emergence of a non-differentiable manifold (a “scar”) close to the fixed point. Also, this framework allows to precisely survey the relationship that exists between “balance” and “criticality” and to explain that the system being close to the transition between two phases is not a necessary nor sufficient condition for the emergence of the phenomenon. Although the specific meaning of the two concepts of “balance” and “criticality” might vary in other contexts, clarifying the differences between them in a simple framework, may give a hint on how they can be correctly interpreted in more complex setups. Moreover we give specific quantitative insights on the exponents of the power laws, measured at a mesoscopic level and relate them to two different types of noise (multiplicative and additive, playing a key role in many physical systems [66]), that become dominant at different scales.

Finally we show that the described mechanism is not a peculiarity of the excitatory/inhibitory underlying structure, but it applies to a wider scenario: a similar non-critical scale-invariance can be obtained by changing the regulatory mechanism that drives the dynamics, i.e. excluding inhibition and introducing synaptic plasticity.

Demographic noise and balanced logarithmic potentials

Directed percolation (DP) is the paradigmatic example of a very large class of systems –including catalytic reactions, growing interfaces in random media, damage spreading, epidemic dynamics, and turbulence, to name but a few– exhibiting a phase transition separating a quiescent or absorbing state from an active one [28, 31, 32, 42, 46, 54]. The essence of this very robust universality class –which, curiously enough, had to wait long for experimental backing [70]– is parsimoniously encoded in the following Langevin equation [27, 28, 32, 37, 54]

$$\dot{\rho}(\mathbf{r}, t) = a\rho(\mathbf{r}, t) - b\rho^2(\mathbf{r}, t) + D\nabla^2\rho(\mathbf{r}, t) + \sqrt{\rho(\mathbf{r}, t)}\eta(\mathbf{r}, t), \quad (4.2.1)$$

where $\rho(\mathbf{r}, t)$ is the density of activity at coordinates \mathbf{r} and time t , a is the control parameter regulating the distance to the critical point, b and D are constants, and $\eta(t)$ is a Gaussian white noise of variance σ^2 . Critical exponents, scaling functions, and, in general, all critical features can be obtained using Eq.(4.2.1) as a starting point. The most preponderant aspect of this equation, distinguishing it from other classes, as for instance the Ising class [8], is the $\sqrt{\rho}$ factor in the noise amplitude. This square-root noise term stems from the “demographic” nature of the particle-number fluctuations; and it imposes that there are no fluctuations in the absence of activity, as corresponds to the absorbing state¹.

The same type of demographic noise also appears in other slightly different universality classes, such as:

- i) the *voter-model* or neutral class describing the dynamics of neutral theories in which two symmetric competing states are possible [1, 18, 20, 42]; in this class there is no deterministic force except for diffusion, and the noise amplitude is different from zero only at the interfaces separating the two absorbing states e.g. at $\rho = 0$ and $\rho = 1$, i.e. $\dot{\rho}(\mathbf{r}, t) = D\nabla^2\rho(\mathbf{r}, t) + \sqrt{\rho(\mathbf{r}, t)(1 - \rho(\mathbf{r}, t))}$ [1];

¹Another group of universal behavior is that of systems with noise proportional to the activity (rather than to the square-root of the activity); these encode a different type of processes where the most dominant fluctuations are not demographic, but associated to spatio-temporal variability in the overall parameters [25, 29, 49].

- ii) the *dynamical percolation* class [26, 36] –in which re-activation of sites cannot occur and, as a consequence, the non-linear term in Eq.(4.2.1) needs to be replaced by a non-Markovian term $-\rho(\mathbf{r}, t) \int_{-\infty}^t dt' \rho(\mathbf{r}, t')$ keeping track of past activity while the noise term remains unchanged, and
- iii) the *Manna* class of systems with many absorbing states such as sandpiles in which an additional conservation law –that can be encapsulated in an additional term $-\rho(\mathbf{r}, t) \int_{-\infty}^t dt \nabla^2 \rho(\mathbf{r}, t)$ [10, 74]– exists, while the noise term remains as in directed percolation.

As previously discussed in chapter 1, all systems with absorbing states exhibit scale-invariant avalanches at criticality, distributed as $P(S) \sim S^{-\tau}$ and $P(T) \sim T^{-\alpha}$. Of course, such behavior include these four classes and some other more infrequent ones, not specified here. Remember also that, in particular, for avalanches propagating in high dimensional systems (or in densely connected networks) mean-field exponent values $\tau = 3/2$, $\alpha = 2$ and $\gamma = 2$ are obtained for all systems with absorbing states.

In order to explicitly compute these exponent values, textbooks usually resort to the (Galton-Watson) branching process [21, 31, 42, 77]. In this, each node of a tree has two branches emerging out of it; from an occupied/active node at time/generation n each of its two out-branches (at time/generation $n+1$) are occupied/active with probability p or left empty with complementary $(1-p)$. Observe that this is just a variant of directed percolation running on a regular tree (see Figure 4.2.1). For completeness, we now present a very simple derivation of its associated avalanche distribution functions.

4.2.1

A simple calculation for the branching process

To compute $P(S)$ –where S is the total number of occupied/active nodes before the process comes to its end– one just needs to evaluate the total number of connected trees of size S , which is nothing but the Catalan number [33]

$$C(S) = \frac{1}{S} \binom{2S}{S-1}, \quad (4.2.2)$$

and multiply it for the probability of each one to occur, $p^{S-1}(1-p)^{S+1}$. Evaluating the resulting expression $P(S, p) = (2S)!/((S+1)!S!)p^{S-1}(1-p)^{S+1}$ in the Stirling approximation for $S \gg 1$, one readily obtains

$$P(S, p) = \frac{\mathcal{N}}{\sqrt{\pi}} S^{-3/2} (4p(1-p))^S, \quad (4.2.3)$$

where \mathcal{N} is a normalization constant; in particular, this becomes a power law at the critical point $p = 1/2$: $P(S, 1/2) = \frac{\mathcal{N}}{\sqrt{\pi}} S^{-3/2}$, implying $\tau = 3/2$.

The exponent γ can also be derived using the statistics of branch lengths in Catalan trees of a given size [16], leading readily to the result $\gamma = 2$; and from this, using the scaling relation Eq.(1.2.13), one obtains $\alpha = 2$.

These results for the branching-process avalanche statistics can be derived in a more systematic way –for different types of underlying regular or random tree topologies– within the generating function formalism [61, 63, 79]; indeed, already back in 1949 Otter computed the solution for the case of a Poissonian distribution of branches per node [55].

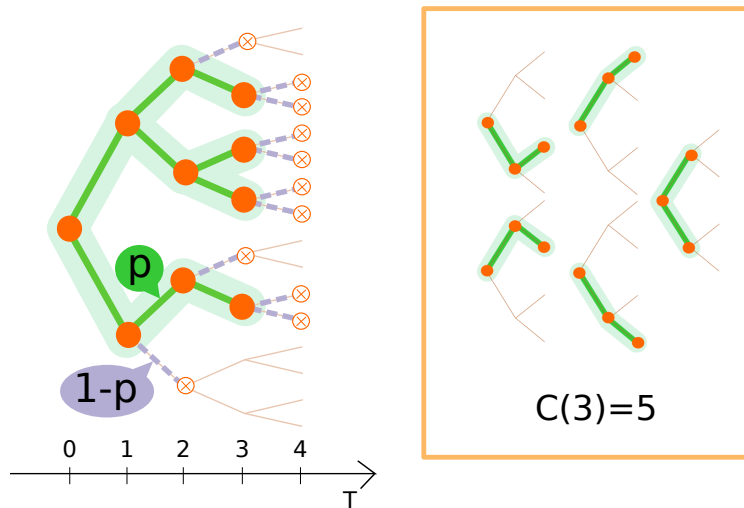


Figure 4.2.1: Left: Illustration of a realization of the un-biased branching process, showing (highlighted) an avalanche of size $S = 10$ and duration $T = 3$, together with the structure of the underlying rooted binary tree on top of which it unfolds. Right: Visualization of the 5 possible paths of $S = 3$ as counted by the Catalan number $C(3) = 5$.

Given that the result, e.g. a power-law with exponent $3/2$ for the size distribution, is much more general than any specific branching process in any specific tree-like topology, it is appealing from a theoretical point of view to derive an even more general proof of these results, covering all cases at once. From a slightly different perspective, relying on field theory and scaling arguments [35, 50, 51] the whole set of exponent values can be obtained for each specific universality class, but again, the result –being common to all classes, i.e. *super-universal*– should be amenable for a more generic explanation.

4.2.2

Random walks in a logarithmic potential

The common feature shared by all the Langevin equations of the different classes of systems with absorbing states, as already mentioned above, is the presence of a demographic, square-root, noise amplitude. As a matter of fact –as illustrated in more detail in appendix (D.1)– in the mean-field limit it is easy to derive a common and unique effective Langevin equation for all classes of systems with absorbing states at criticality, as

$$\dot{\rho} = \sqrt{\rho} \xi(t), \quad (4.2.4)$$

where ρ is the overall activity and $\xi(t)$ is a Gaussian white noise with zero mean and $\langle \xi(t)\xi(t') \rangle = 2\sigma^2\delta(t-t')$ which needs to be interpreted in the Itô sense in order to guarantee that $\rho = 0$ is an absorbing state [24, 72]. We refer to Eq.(4.2.4) as “demographic random walker” (DRW). To avoid the complications of the Itô calculus, we write the equivalent equation in the Stratonovich interpretation (see appendix A.1 or [24, 72] for a detailed discussion):

$$\dot{\rho} = -\frac{\sigma^2}{2} + \sqrt{\rho}\eta(t) \quad (4.2.5)$$

where now $\langle \eta(t)\eta(t') \rangle = \frac{\sigma^2}{2}\delta(t-t')$. Using now standard calculus to change variables to $x = \sqrt{\rho}$ directly gives²

$$\dot{x} = -\frac{\sigma^2}{4x} + \eta(t). \quad (4.2.6)$$

The resulting equation is just a particular case of a one-dimensional random walker (RW) moving in a logarithmic potential $U(x) = \lambda \log x$, i.e.

$$\frac{dx}{dt} = -\frac{dU(x)}{dx} + \eta(t) = -\frac{\lambda}{x} + \eta(t), \quad (4.2.7)$$

where λ is a positive constant and, in general, $\langle \eta(t)\eta(t') \rangle = 2\mu\delta(t-t')$, with μ a generic positive constant. Observe that Eq.(4.2.6) corresponds to the particular case, $\lambda = \mu = \sigma^2/4$ –that we call *balanced*– in which the ratio between the amplitudes of the logarithmic potential and the noise-correlation amplitude, μ , is equal to unity: $\beta \equiv \lambda/\mu = 1$. This perfect balance between the deterministic-force and stochastic coefficients is essential for what follows, as we shall see.

²An alternative approach to analyze Langevin equations such as Eq.(4.2.4) consists in re-absorbing the noise amplitude into the time-scale, leading to a standard random walk with a different “clock” [64]. Another interesting possibility is deriving these results from a more general fractional Brownian motion [19].

More in general, let us remark that, in the presence of an external field –allowing for the spontaneous generation of activity at a fixed rate h – Eq.(4.2.5) needs to be complemented with an additional $+h$ term. Upon changing variables, this implies $\beta = 1 \rightarrow 1 - h/\mu$, in Eq.(4.2.7) and thus, in the presence of external driving, the perfect balance between coefficients breaks down.

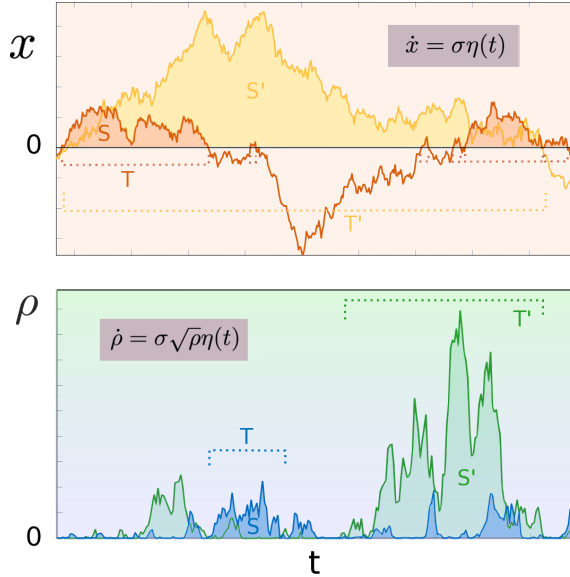


Figure 4.2.2: Illustration of the time evolution of a standard random walk (RW) and a demographic random walk (DRW); each color corresponds to a different realization. Upper panel: standard RW that, in principle, can freely cross the origin. Avalanches start and end when the walker crosses the origin. Lower panel: the DRW can be represented as a stochastic RW moving in a balanced logarithmic potential that keeps the walker bounded to the origin. Since the variable is always strictly positive, the avalanches can be defined as the activity over a threshold $\epsilon \rightarrow 0$.

To compute avalanche exponents from Eq.(4.2.7), let us define an avalanche as a random walk $x(T)$, starting at $x(t=0) = 0^+$ and returning for the first time to the origin at time T , $x(T) = 0$ (see Figure (4.2.2)). The distribution or its return times is nothing but $P(T)$ as defined above. The problem of computing such a return-time distribution for the random walk in a logarithmic potential, i.e. by Eq.(4.2.6), was solved by A. Bray [12] and revisited by F. Colaiori in the context of Barkhausen crackling noise [15]. The solution requires writing

down the equivalent Fokker Planck equation for the Langevin dynamics, with a delta-like initial condition centered at a value slightly larger than $x = 0$, and computing the probability flux F at the origin as a function of the time T (more detailed sketch of the analysis is presented in Appendix D.2 for the sake of completeness). The resulting first-return probability distribution function is

$$P(T) = \frac{4\mu\epsilon^{2\nu}}{\Gamma(\nu-1)}(1+\beta)(4\mu T)^{-\nu-1}e^{-\frac{x^2}{4\mu T}} \\ \sim T^{-\nu-1} = T^{-\frac{3+\beta}{2}}, \quad (4.2.8)$$

where $\nu = (1 + \beta)/2$, implying $\alpha = \frac{3+\beta}{2}$. Observe that, in the limit of vanishing potential amplitude, $\lambda = 0$, this result reproduces the statistics of a freely-moving random walk, $P(T) \sim T^{-\frac{3}{2}}$, while in the opposite perfectly-balanced limit, $\lambda = \mu$ (i.e. $\beta = 1$) the result is $P(T) \sim T^{-2}$ in agreement with the expectations for the un-biased branching process. It is noteworthy that –despite the fact that the random walk in a logarithmic potential gives a non-universal avalanche duration exponent– for the undriven DRW case, in which the logarithmic potential derives from a change of variables in Itô calculus, there exists a perfect balance between the coefficients of the equation; they both depend on the noise amplitude and, compensating each other, they generate the universal value $\alpha = 2$. However, in the presence of an external field, $\beta = 1 - h/\mu$ breaking down the perfect balance between coefficients, non-universal continuously-varying avalanche exponents appear (see Figure 4.2.3); in particular,

$$\alpha = 2 - \frac{h}{2\mu}. \quad (4.2.9)$$

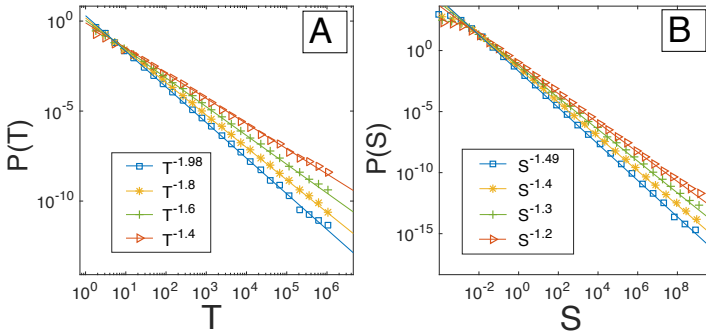


Figure 4.2.3: Size-avalanche and duration-avalanche distributions for the un-driven demographic random walk as described by Eq.(4.2.4), as well as for diverse values of the external driving field (marked with symbols) $h = 0.01$ (blue squares), $h = 0.1$ (yellow stars), $h = 0.2$ (green crosses) and $h = 0.3$ (red triangles), with reference curves (solid lines) $t^{-2+h/(2\mu)}$ and $s^{-3/2+h/(4\mu)}$ (as derived in the text), respectively, illustrating the agreement with theoretical predictions.

In any possible discrete/particle model with absorbing states, this change of exponents stems from the fact that –owing to the external driving– avalanches from different initial seeds (each of them spontaneously generated by the external driving field) can merge, which allows their combination to survive longer and be larger, leading to smaller effective exponents α and τ (see Table 4.1).

Turning back to the general discussion, using the above result together with simple scaling, we can readily derive the associated avalanche size exponent, τ . In order to have a unified notation let us use a generic variable $v(t)$, which can be in particular, $x(t)$ for the RW, or $\rho(t)$ for the DRW. The size of any given avalanche is defined as the area under the curve defined by the random walk, i.e. $S = \int_0^T v(t) dt$, and we are interested in the distribution of such sizes as a function of T , $P(S|T)$. Given that the typical displacement of a random walk in time t scales as $v \sim \sqrt{t}$, for the DRW (for which there is an additional square-root factor) we have $v \sim \sqrt{v}\sqrt{t}$, and thus, $v \sim t$; hence, we can write, in general, $v \sim t^\phi$, with $\phi = 1/2$ and $\phi = 1$ for the RW and the DRW (either driven or undriven), respectively.

It is natural to define a new rescaled variable $\tilde{v}(t/T) = v(t)/T^\phi$ which describes a random excursion in the interval $[0, 1]$. In these terms,

$$S = \int_0^T v(t)dt \sim T^{\phi+1} \int_0^1 \tilde{v}(z)dz. \quad (4.2.10)$$

Thus, the average avalanche size, $\langle S \rangle$ obtained averaging over all possible avalanche shapes, $\tilde{v}(z)$, scales also with $T^{\phi+1}$, implying $\gamma = \phi + 1$.

Using the previous result, $P(S|T)$ can be written as a scaling form $P(S|T) = T^{-\gamma} \mathcal{G}(S/T^\gamma)$ where the factor $T^{-\gamma}$ comes from the normalization condition, and the unspecified scaling function \mathcal{G} obeys $\mathcal{G}(z) \geq 0$ for all z and $\int_0^\infty \mathcal{G}(z)dz = 1$. Having computed the conditional probability $P(S|T)$, we can obtain $P(S)$ as

$$\begin{aligned} P(S) &= \int_0^\infty dT P(S|T)P(T) \\ &\sim C \int_0^\infty dT T^{-\gamma} T^{-\alpha} \mathcal{G}(S/T^\gamma) \\ &\sim CS^{-(\gamma+\alpha-1)/\gamma} \int_0^\infty du u^{\frac{(\alpha-1)}{\gamma}} \mathcal{G}(u), \end{aligned} \quad (4.2.11)$$

and, thus, $\tau = (\gamma + \alpha - 1)/\gamma$ (which is nothing but the scaling relation Eq. (1.2.13)). Plugging the value of α and γ derived above one obtains the well-known result $\tau = 4/3$ for the standard random walk³ and, for the DRW,

$$\tau = \frac{3}{2} - \frac{h}{4\mu}, \quad (4.2.12)$$

which reduces to the well-known result $\tau = 3/2$ for the un-driven case.

³In the case of the standard RW case the scaling function \mathcal{G}_{RW} has been exactly derived (see e.g. [44]), but its specific form is not essential for our purposes here.

A summary of the exponents for the different cases is contained in Table 4.1.

	Unbiased RW	Demographic RW	Driven Demographic RW
$P(T) \sim T^{-\alpha}$	$\alpha = 3/2$	$\alpha = 2$	$\alpha = 2 - h/2\mu$
$P(S) \sim S^{-\tau}$	$\tau = 4/3$	$\tau = 3/2$	$\tau = 3/2 - h/4\mu$
$P(S T) \sim T^{-\gamma}$	$\gamma = 3/2$	$\gamma = 2$	$\gamma = 2$

Table 4.1: Summary of the avalanche exponents for the standard RW, the demographic RW, and the driven demographic RW (in the presence of an external field, allowing for the spontaneous generation of activity at a fixed rate h).

Results beyond critical exponents have also been obtained in the literature, for example, the average shape of random-walk excursions is a semi-circle for standard un-biased random walkers [3] while it is a parabola for demographic walkers [57]. This can be easily seen by rescaling the walks to \tilde{v} and the times to t/T to collapse curves as described above. In this way $\tilde{v}(t/T) = \mathcal{F}(t/T)$ where $\mathcal{F}(t/T)$ is a scaling function. Given that, $v(t) \sim t^{\gamma-1}$, dividing by $T^{\gamma-1}$, $\tilde{v}(t/T) \sim (t/T)^{\gamma-1}$, at least for small times, $t \ll T$. Considering that a similar relation holds for the reverse time walk starting from $t/T = 1$, then the avalanche shape is $\mathcal{F}(t/T) = [(t/T)(1 - t/T)]^{\gamma-1}$ which is a semicircle for $\gamma = 3/2$ (RW) and a parabola for $\gamma = 2$ (DRW and driven DRW).

In summary, we have explicitly shown that the mean-field values of avalanche exponents in systems with absorbing states can be computed in a general way by mapping them into a random walk confined by a logarithmic potential, Eq.(4.2.6). Of course, this same conclusion could have been reached by arguing in a heuristic way that all of high-dimensional processes involving absorbing states should be effectively described by an un-biased branching process, and then constructing a continuous description of it (i.e. a Fokker-Planck or equivalently a Langevin equation) which would be nothing but Eq.(4.2.4).

An interesting corollary is that the exponents do change in the presence of spontaneous creation of activity, even if the rate is arbitrarily small. This result could be relevant to understand empirical results; for instance in cortical networks, avalanches of neural activity have been reported to exhibit branching process statistics [5]; still inspection of some of the most careful estimations reveals possible deviations from $\tau = 3/2$ [68], which could be potentially ascribable to a non-vanishing inherent spontaneous-activation. Thus, special care should be taken to ensure that such (theoretical) power laws are a fingerprint of criticality, because the spontaneous creation of activity (h) leads to generic power laws across the entire absorbing phase. The picture is not entirely negative since, just at the critical point, true scale-invariant avalanches are present (in a spatial extended system) and the well-known fingerprints of criticality (e.g. long-range correlations, among others) are retrieved.

Reactive and noisy dynamics in the Wilson-Cowan model

Following [7], we consider the Wilson-Cowan mean field description of a large-scale neocortical homogeneous population of excitatory and inhibitory neurons [78] (that has already been used in appendix B.1 to explain a particular case of the synchronization transition of chapter 2). The equations describing the dynamics of the activity (density of active neurons) for the two subpopulations E and I read [78]:

$$\begin{cases} \frac{dE}{dt} = -\alpha E + (1 - E) f(s) \\ \frac{dI}{dt} = -\alpha I + (1 - I) f(s), \end{cases} \quad (4.3.1)$$

where $f(s)$ is a sigmoid arbitrary response function, that for simplicity we fix to

$$f(s) = \begin{cases} \tanh(s) & s \geq 0 \\ 0 & s < 0 \end{cases}$$

and s is the incoming current

$$s = \omega_E E - \omega_I I + h.$$

which is simply the sum of all synaptic inputs, i.e. the sum of the whole excitatory and inhibitory activity weighted by their respective synaptic efficacy (ω_E and ω_I), plus an external small constant input current h . These simple equations state that for low incoming currents the activity of each population decays exponentially with a time scale specified by $1/\alpha$; on the other hand the activity grows up to a maximum saturation value ($E, I = 1$) as a function of the incoming current s . According to this mean field approach, the connections between the cells within the described populations are assumed to be random and dense enough so that spatial heterogeneity can be neglected.

Despite its simplicity, the Wilson-Cowan model encompasses a plethora of different possible scenarios, depending on the parameter values. The possibility to visually display and readily understand those scenarios using phase plane methods (together with the feasibility to analytically approach some issues) granted a big success to the model, considering that its collection of behaviors turned out to be very effective in describing a striking variety of experimentally observed neural behaviors, concerning both spontaneous and evoked activity, such as the existence of multiple stable states (Up-Down states), oscillatory

behavior, simple and multiple hysteresis loops, together with the prediction that a weak stimulus produces dumped propagating waves whereas a stronger stimulus generates a more localized response [11, 34, 78]. Leaving aside fancy behaviors, the model can be further simplified and reduced to an elementary setting, where only one stable fixed point exists and depending on whether excitation or inhibition dominates, the steady state is respectively active or inactive. More specifically, by considering that the coupling constants depend uniquely on the pre-synaptic cell type, i.e. $\omega_{EE} = \omega_{EI} = \omega_E$ and $\omega_{II} = \omega_{IE} = \omega_I$ (and fixing the decay constant α and the small external current h) the system is left with a two dimensional parameter space, which consists of the excitatory and inhibitory synaptic strengths. Under this symmetry, the unique steady state only depends on $\omega_0 = \omega_E - \omega_I$. In Fig.4.3.1 we plot the value of the fixed point, in the variable $\Sigma = (E + I)/2$, for different values of ω_0 , while keeping $\omega_s = \omega_E + \omega_I$ constant. The system shows a phase transition in the critical value $\omega_0 = 0$ separating an active (excitation dominated) from an inactive (inhibition dominated) phase. Note that since a small external field h is present, the fixed point does not lose its stability at criticality.

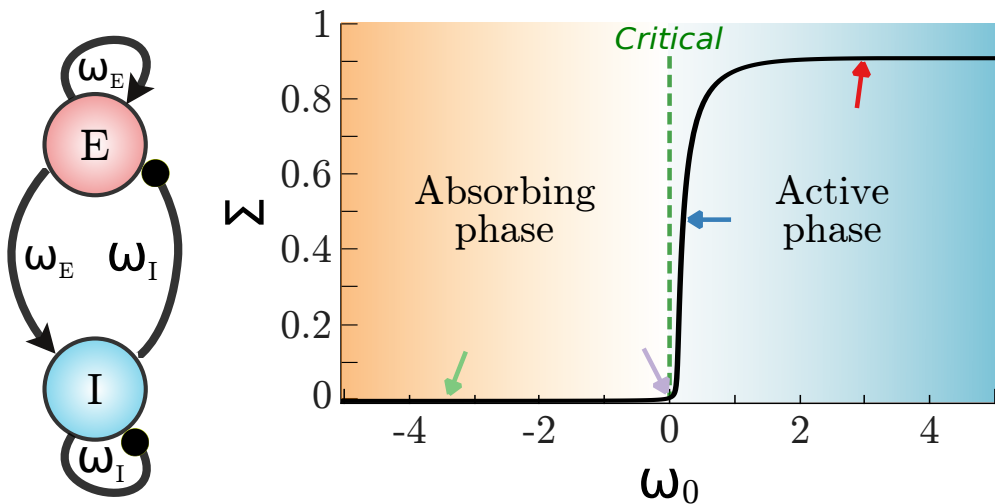


Figure 4.3.1: Left figure: sketch of the Wilson Cowan model. The excitatory population interacts with a single parameter, ω_E and the same applies to the inhibitory population, with ω_I . Right figure: Phase transition for the model, the phase of the system depends on the difference $\omega_0 = \omega_E - \omega_I$; if $\omega_0 > 0$ the system is in the active phase. From left to right the system is in the 'down' state, critical point, a 'low-stable' up state and in the 'up' state (green, purple, blue and red, respectively).

Strikingly, this remarkably simple and intuitive behavior is overturned when finite size effects are taken into account. In [7], Benayoun et al considered a simple (all-to-all) spiking neuron model such that (i) each neuron is either active or quiescent (ii) the probability that each quiescent neuron becomes active depends on (a sigmoid function of) the total synaptic input and (iii) each active neuron decays at a constant rate. Starting from this microscopic simple binary-neuron rate model Benayoun et al were able to recover Wilson-Cowan (mesoscopic) dynamics, through a Van Kampen system-size expansion [72]. Thus they determined the correct stochastic term to be added to Eq. (4.3.1) to consider the effects of the finiteness of the population described. After a coarse graining of the master equation, the full stochastic equations read

$$\begin{cases} \frac{dE}{dt} = -\alpha E + (1 - E) f(s) + \sigma \sqrt{\alpha E + (1 - E) f(s)} \eta_E \\ \frac{dI}{dt} = -\alpha I + (1 - I) f(s) + \sigma \sqrt{\alpha I + (1 - I) f(s)} \eta_I \end{cases} \quad (4.3.2)$$

where $\eta_{E,I}$ are Gaussian white variables and the stochastic term is a demographic noise (given by the second moment of the jump probabilities), which decays with system-size and vanishes in the thermodynamic limit.

4.3.1

Phenomenology

Benayoun et al [7] showed that, in a regime of *balance between excitation and inhibition*, or equivalently, when the difference between excitatory and inhibitory synaptic weights is very small with respect to their sum $\omega_0 \ll \omega_s$, low levels of noise (i.e. large but not infinite system sizes) generate highly bursty (pseudo-scale-invariant) behavior. This seems to be in outstanding counter-trend with respect to the mean field case, which would predict a single sustained steady state, instead of shows an alternation of highly bursty time intervals –interspersed with periods of silence– extremely reminiscent of the experimental evidences showing self-similar bursts of activity in the resting state of cortical dynamics. In fact a measure of the avalanches size and duration, defined in complete analogy with the experimental setup, gives power-law distributions.

4.3.2

Criticality and balance

As a starting point, we address the problem of fully specifying the difference between "critical" and "balanced". First of all we should better talk about "quasi-criticality" [9], given both the inherent limitedness of the system size and the existence of a small external field h . The condition for the system to be quasi-critical is $\omega_0 \ll 1$, while the system is balanced when $\omega_0 \ll \omega_s$, thus quasi-criticality is not necessary nor sufficient for balance.

In order to clarify this issue and discriminate the effects of criticality and balance we plot in Fig.4.3.2 the phase plane of the deterministic system (Eq.4.3.1).

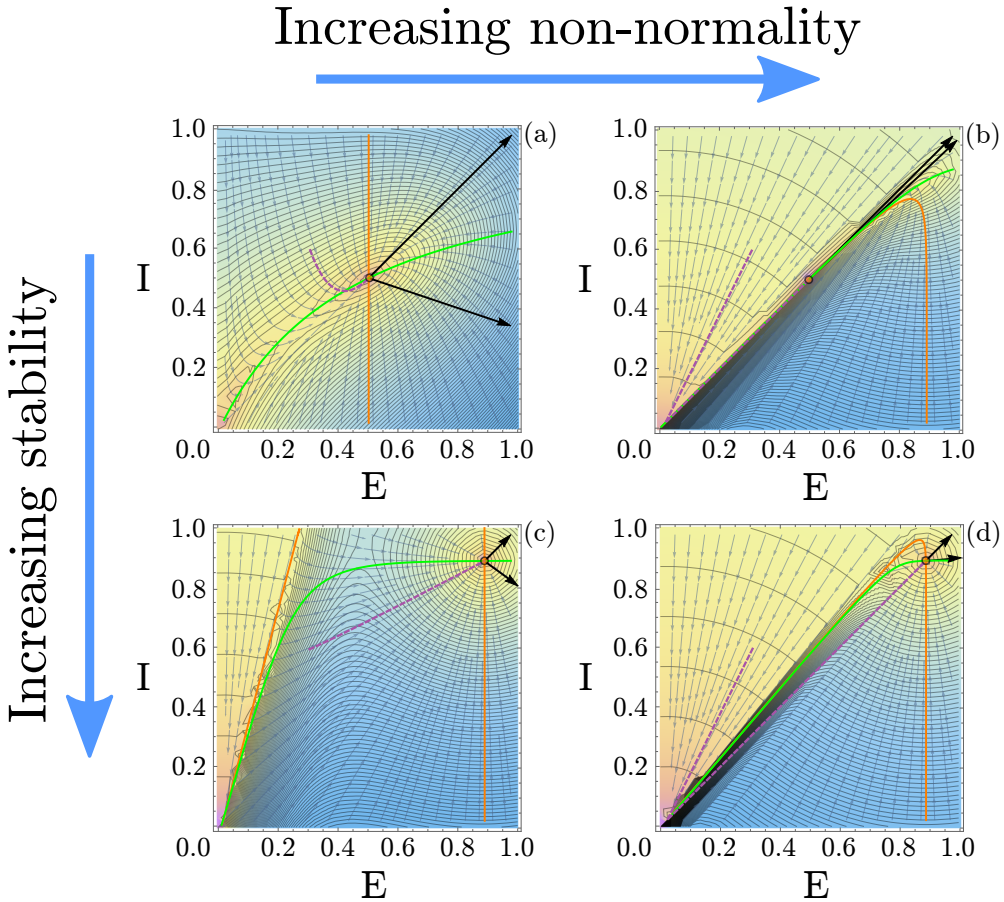


Figure 4.3.2: (a) E-I phase portrait for a stable state near the critical point ($\omega_E = \frac{1}{5}$, $\omega_I = 0$). The stable fixed point –wherein the nullclines intersect– is represented as a circle. At last, the eigenvectors direction in the stable ‘up’ state are indicated by black arrows, (b) E-I phase portrait for a balanced-amplification condition ($\omega_E = 7$, $\omega_I = \frac{34}{5}$). The nullclines are in close proximity to each other, in contrast with the former case, (c) E-I phase portrait for a stable state far from the critical point ($\omega_E = 4$, $\omega_I = 1$). and, (d) E-I phase portrait for the same situation in the active phase but, with ($\omega_E = 20$, $\omega_I = 17$). The proximity between the nullclines make it easy to look that the systems evolves, near the critical point, around a $(1 + \epsilon)$ -dimensional movement; i.e. any small perturbation resulted in great dynamical fluctuations.

In the first row (Fig.4.3.2a and b) the parameters set the system in a (close to) critical state, (the stable fixed point, i.e. the point where the nullclines intersect, is evidenced with a dot) corresponding to the blue arrow in Fig.4.3.1, while in the second row (Fig.4.3.2c and d) the deterministic system spontaneously evolves towards a stable highly active phase (red arrow in Fig.4.3.1). Moreover, the first column (Fig.4.3.2a and c) shows non-balanced configurations (i.e. small values of the sum ω_s) while the second column (Fig.4.3.2b and d) shows balanced ones.

At this heuristic level we can remark that in the balanced case there is some sort of "scar" in the phase portrait, such that two shear stresses flowing in opposite directions, coexist very close to each other. In other words, the vector field (\vec{E}, \vec{I}) shows a discontinuity all along a manifold (a line in this case) that corresponds to a whole (infinite) set of (unstable –or marginally stable–) points in which the nullclines superimpose. As we shall explain in further details in what follows, this "scar" is responsible for the amplification of the fluctuations around the fixed point introduced by demographic noise: as soon as a small noise drives the system "slightly" away from the fixed point (i.e. outside of its local basin of attraction), these strong flows hardly pull the system towards very low (or very high) levels of activity. Conversely, in the case of a critical, but non-balanced system (Fig. 4.3.2a) it is immediately evident that another completely different mechanism generates large fluctuations.

4.3.2.1 Linearized dynamics is non-normal

Following Murphy et al. [53] this phenomenon can be explained under the rationale of *non-normal* or *reactive* dynamics. Considering that the dynamics in the balanced case naturally determines a preferential direction along the diagonal [7], let us change variables to $\Sigma = (E + I)/2$, $\Delta = (E - I)/2$. Thus, Eq. 4.3.1 becomes

$$\begin{cases} \frac{d\Sigma}{dt} = -\alpha\Sigma + (1 - \Sigma) f(\theta) \\ \frac{d\Delta}{dt} = -\Delta(\alpha + f(\theta)) \end{cases} \quad (4.3.3)$$

with $\theta = \omega_0\Sigma + (\omega_s) \Delta + h$. Elementary algebra can be employed to verify that the fixed point lays in $(\Sigma_0, 0)$, i.e. always in the diagonal in the (E, I) reference frame. A standard linear stability analysis around the fixed point gives the Jacobian

$$J = \begin{pmatrix} -\lambda_1 & \omega_{ff} \\ 0 & -\lambda_2 \end{pmatrix} \quad (4.3.4)$$

where the eigenvalues are $\lambda_1 = (\alpha + f(\theta_0)) + (1 - \Sigma_0)\omega_0 f'(\theta_0)$ and $\lambda_2 = (\alpha + f(\theta_0))$ and $\omega_{ff} = (1 - \Sigma_0)(\omega_E + \omega_I) f'(\theta_0)$.

Note that, near the critical point, where ω_0 is small and positive, immediately λ_1 and λ_2 are also small [7], inducing a *weakly stable* fixed point. Therefore, such

“weakness” of the stability of the fixed point is related –at first glance– to the distance to the critical point (ω_0). Nevertheless, the structure of the Jacobian makes it visible that its diagonal does not enclose all the information of the dynamics, as the out-diagonal term (the so-called *feed-forward* term) cannot be eliminated⁴. Triangular matrices such as J are called *non-normal*, meaning that $J^*J \neq JJ^*$, where J^* is the conjugate transpose of J ⁵. The effect of a big feed-forward term in Eq.(4.3.4) is straightforward to verify since, when operating on a small perturbation along the Δ direction, the linearized dynamics gives a small response in the same direction plus a much bigger response along the Σ direction, corresponding to the strong shear flows clearly visible in Fig. 4.3.2. Non-normal matrices also have the property of being “reactive” [73], since the dynamics they describe can show unusually long-lasting transient behavior, i.e. the system can be strongly driven away from the fixed point before coming to its steady state. Thus, in this case, the stability of the fixed point has to be compared with the feed-forward term ω_{ff} . A big feed-forward term is able to strongly affect the dynamics when the stability of the fixed point is weak *with respect to the feed-forward component* (even if the eigenvalues are not close to zero), i.e. when the non-normality is big with respect to the stability. Since the eigenvalues depend on the control parameter through ω_0 –while ω_{ff} only depends on ω_s – the requirement for the appearance of the mechanism is the balanced condition $\omega_0 \ll \omega_s$ even far from the quasi-critical condition $\omega_0 \gtrsim 0$.

✱ **On the eigenvectors of the Jacobian** We should remark that the change of variables $(E, I) \rightarrow (\Sigma, \Delta)$, that we performed for evident convenience, turns out to be a Schur transformation⁶, indeed generating a triangular Jacobian. The (non-orthogonal) basis of eigenvectors in the variables (Σ, Δ) is

$$\begin{pmatrix} 1 \\ 0 \end{pmatrix}, \begin{pmatrix} 1 \\ \xi \end{pmatrix}$$

with $\xi = \frac{\omega_0}{(\omega_E + \omega_I)}$, leading to almost equal eigenvectors for $\xi \rightarrow 0$.

Moreover, the weight of the non-normality is basically the weight of the feed-forward interaction with respect to the eigenvalues, which means that, fixing ω_0 , it grows with ω_s (going –very– roughly as $1 - \mathcal{O}(\omega_0)/\mathcal{O}(\omega_s)$). In other words the balance condition $\omega_0 \ll \omega_s$ means exactly that the non-normality is big with respect to the stability of the fixed point. From the balanced condition of Figure 4.3.2 we can imagine that, if we perturbed the stable fixed point one step further from the basin of attraction, the trajectory would perform a big transient excursion in the direction of the scar.

⁴Triangular matrices are not diagonalizable.

⁵Note that in the quantum mechanics all non-normal matrices are “explicitly forbidden”, since all physical operators are Hermitian and all Hermitian matrices are normal.

⁶The Schur decomposition is a matrix decomposition $A = MJM^{-1}$ where M is a unitary matrix and J is an upper triangular matrix (the Schur form) of A .

4.3.3

The roles played by the noise

By numerical simulation of Eqs.(4.3.2), when the system is endowed with some tiny noise (see upper panel of Figure 4.3.3), it is confirmed the existence of a fixed (stable) point Σ^* . Little bigger values of noise produce fluctuations around such stable fixed point but, beyond some particular value of the noise amplitude, σ , the stability is disturbed and the system is able to reach to the origin. Thus, the dynamics keeps wandering, and noise-induced fluctuations are strongly amplified –under balance conditions– by the mechanism of reactivity along the Σ direction (i.e. along the diagonal in the (E, I) reference-frame of Fig.4.3.2). In particular, intermediate values of σ give rise to up and down states, reminiscent of experimental findings of cortical areas in the brain. Even more, one can appreciate that the higher the value of the noise the more time elapses the system close to the origin, showing excursions to the 'up' state; such fluctuations most closely resembles to the emergence of avalanches of activity, growing, spreading and coming back to the absorbing state.

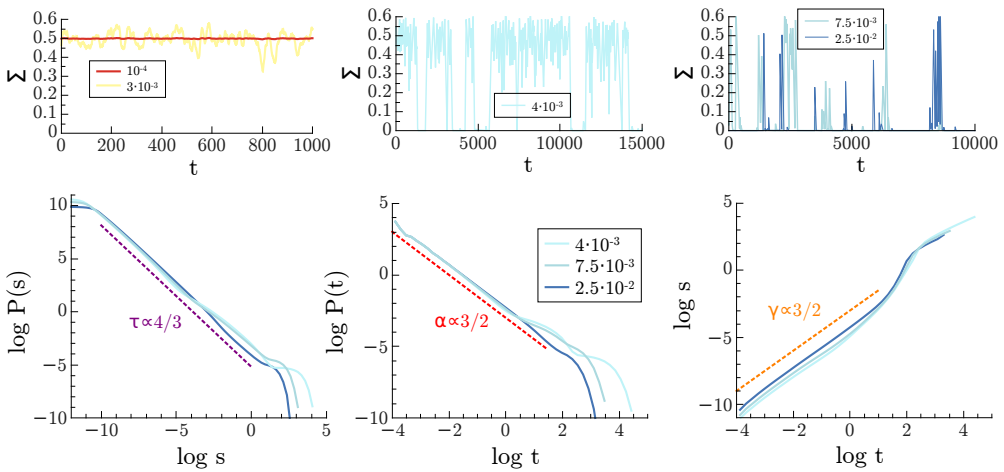


Figure 4.3.3: Up figure: Temporal series of Σ in a balanced-amplification condition ($\omega_E = 7$, $\omega_I = \frac{34}{5}$) for increasing levels of noise (from left to right). Above a certain threshold the system is allowed to reach the absorbing state, showing an avalanching behavior for high values of noise. Down figure: Probability of different types of avalanches for different values of the noise amplitude (σ , see Legend); size avalanches, time avalanches and, size versus time avalanches. Note that, in the three cases, the nature of the avalanches highly depends on the noise amplitude. Other parameter values: $\alpha = 0.1$, $h = 10^{-3}$

From such avalanche-like dynamics, defining duration and size of the activity over a small threshold, it is possible to confirm the result of [7] on the scale-invariance of the activity, i.e. both follow a power law of the form $P(T) \sim T^{-\alpha}$ and $P(S) \sim S^{-\tau}$, where α and τ are the corresponding exponents (see lower panel of Figure 4.3.3). Furthermore, it allows for an accurate analysis of the exponent of the power-laws. Although the power law is composed by a mixture of different trends, for high values of the noise (or at least for small avalanche sizes), the exponents are compatible with the well known exponents for a standard random walk, i.e. $\alpha = 3/2$ and $\tau = 4/3$.

Despite the fact that the mechanism that generates large fluctuations has been defined, the system shows large silent time-intervals (with extremely low activity as shown in Fig.4.3.3), whose existence is a necessary condition in order to define avalanches. However, the origin of such –highly probable– silent intervals is misunderstood yet but, as indicated by the temporal series it is related and (probably) induced by high values of noise.

4.3.3.1 The reduced system

The empirical observation that the system keeps wandering along the diagonal in the (E, I) reference-frame suggests to study a reduced one variable system, where the dynamics is strictly constrained to evolve along the diagonal (i.e. $\Delta = 0, E = I = \Sigma$). Since in this approximation θ is small, it is possible to take the Taylor expansion $\tanh(\theta) \approx \theta$ and, thus, the reduced system in the variable ρ reads

$$\frac{d\rho}{dt} = h + (-\alpha - h + \omega_0)\rho - \omega_0\rho^2 + \sigma\sqrt{(\omega_0 + \alpha - h)\rho - \omega_0\rho^2 + h}\eta_\rho, \quad (4.3.5)$$

where η_ρ is a Gaussian white variable. For very low levels of activity ($\rho \approx 0$), the noise amplitude in Eq.(4.3.5) is dominated by the square root term and the reduced dynamics is approximately equivalent to the Langevin equation for the Contact Process in a fully connected network (considering $\sqrt{\rho + \bar{h}} \approx \sqrt{\bar{\rho}}$, already presented in the above section or in chapter 1)

$$\dot{\rho} = h + a\rho - b\rho^2 + \tilde{\sigma}\sqrt{\rho}\eta, \quad (4.3.6)$$

with $a = (-\alpha - h + \omega_0)$, $b = \omega_0$ and $\tilde{\sigma} = \sigma\sqrt{(\omega_0 + \alpha - h)}$.

Previously, it has been shown that Eq.(4.3.6) can be mapped into a random walk confined by a logarithmic potential, attracting the dynamics of the system to the noise-induced singularity in the origin. This would explain the unusually large permanence times of the original two-variable system into low activity regimes, responsible for the avalanching behavior.

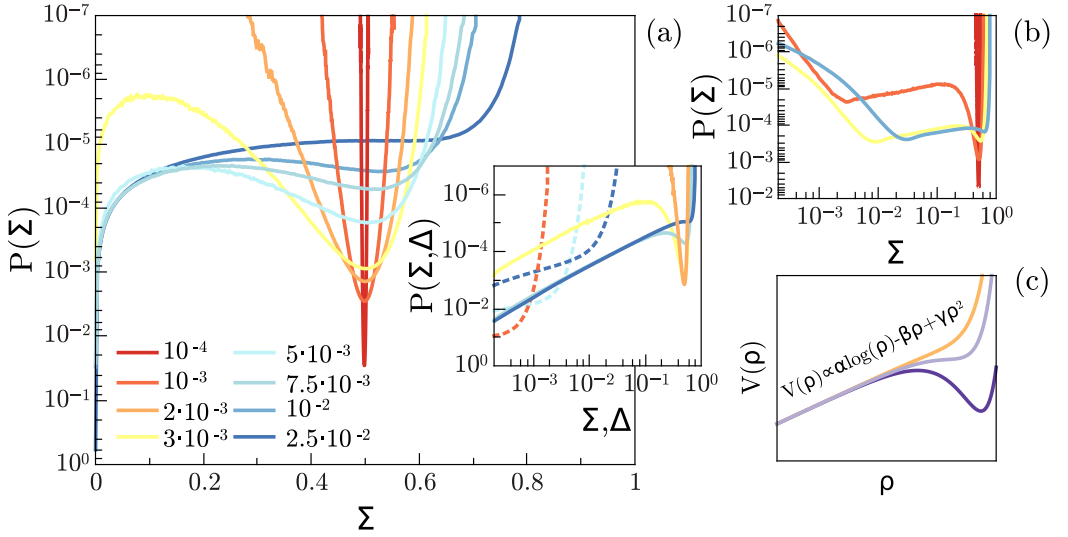


Figure 4.3.4: (a) Log-normal scale, y-axis is inverted. Histogram of the Σ – signal of one Wilson-Cowan column for different values of the noise amplitude (σ , see legend). The potential change from a single potential well (for low noise, not shown) to a bistable situation alternating between ‘up’ and ‘down’ states and, finally, to a new single potential focused on the ‘down’ state Inset: same data but in log-log scale. Dashed lines corresponds to Δ – potential, showing extremely small and parabolic-like potentials. (b) Histogram of the Σ – signal of one Wilson-Cowan column for the additive noise case and different values of the noise amplitude (σ , same color code). (c) Theoretical potential from previous one-dimensional effective equations in ρ . The similarity among them is undeniable. Parameter values: $\omega_E = 7$, $\omega_I = \frac{34}{5}$, $\alpha = 0.1$, $h = 10^{-6}$

The original dynamics of Eq.(4.3.2) can be directly compared with the simplified one introduced above (Fig.4.3.4). On one hand, the time series of the dynamics of the complete system (resulting from a numerical integration of the model) defines the effective bivariate probability distribution $P(\Sigma, \Delta)$. Marginalizing over Δ , one obtains the stationary distribution of the dynamics along the diagonal $P(\Sigma) = \int_0^\infty P(\Sigma, \Delta) d\Delta$, from which it is straightforward to define (the projection along the diagonal of) an effective potential, as $V_{eff}(\Sigma) = -\ln P(\Sigma)$. On the other hand, the stationary potential for the reduced dynamics in ρ can be calculated through a Fokker-Planck approach (as stated in chapter 1) giving rise to

$$V(\rho) \propto \left(\left(1 - \frac{2h}{\sigma^2}\right) \ln \rho - \frac{2a}{\sigma^2} \rho + \frac{b}{\sigma^2} \rho^2 + c \right) \quad (4.3.7)$$

In Fig.4.3.4 the effective potentials deriving from the complete and the reduced dynamics are shown to be fairly similar. Also, the bivariate probability distribution $P(\Sigma, \Delta)$ for a system with additive noise confirms such hypothesis, because it shows no signs of being singular at the origin. Thus we can conclude that the bistability of the potential, causing the system to remain tightly trapped when it is close to the origin, is generated by the square root multiplicative noise term. The presence of a small driving h makes sure that the system never falls into the absorbing state, but keeps trying to escape from the logarithmic potential well.

Also, for the reduced system in Eq.(4.3.6), the avalanche distributions have been fully determined above from the first return time to the origin of the random walk confined to the logarithmic potential. They are power-law distributed, with continuously varying non-universal exponents that depend on the driving (h) and on the noise amplitude (σ), that are $\alpha = 2 - 2h/\sigma^2$ and $\tau = 1.5 - h/\sigma^2$. However, the avalanche distributions of the Wilson-Cowan dynamics under the balance condition (enclosed in Eq.(4.3.2)) does not follow such critical exponents (as shown in Fig. 4.3.3). This is due to the neglected term $\sqrt{\rho + h}$; note that vanishing values of ρ , we always have an additive noise with amplitude \sqrt{h} , leading to the observed random walk exponents.

4.3.3.2 Beyond the diagonal

As shown in Fig.4.3.3 the statistics of avalanches in the full system are composed by a mixture of different trends, showing bumps and following the exponents for a standard random walk. Also, the temporal series provide “up and down” states, as well as certain degree of avalanching behavior depending on the noise amplitude. A possible reason for this can be figured out observing the vector field (\vec{E}, \vec{I}) in Fig.4.3.2. Indeed, the whole semi-plane $I > E$ is attracted to the origin by a (roughly) parabolic potential with a noise-induced minimum close to the origin, that joins discontinuously along the diagonal with the other half system, which is another attractive potential with another deterministic minimum, i.e. the up-state.

Therefore, when inhibition dominates ($I > E$), the system is rapidly trapped very close to the origin (by the logarithmic potential sketched above). On the contrary, when the activity is excitatory dominated ($E > I$), the system is strongly pulled towards high activity states. Such behavior suggests some type of “tunneling effect” between both minima.

In order to test this hypothesis, and corroborate our conjecture on the role played by the various ingredients (i.e. non-normal dynamics, multiplicative and additive noise) cooperating to produce the noise induced bursty behavior in Wilson-Cowan balanced system, we propose a simple effective model, that contains an essential version of all the mechanisms described.

4.3.3.3 Minimal model

Enclosing the all the dynamics described above, we propose a minimal one-dimensional model to mimic the behavior of the system,

- i) The system follows the next system of effective equations for the activity with multiplicative/additive noise, separated by some arbitrary small threshold value (T)

$$\begin{cases} \dot{\rho} = h + a\rho - b\rho^2 + \sigma\sqrt{\rho}\eta & \rho > T \\ \dot{\rho} = -a\rho + \sigma\eta & \rho < T \end{cases} \quad (4.3.8)$$

- ii) The system can instantly take the value $\rho = 0$ or $\rho = \frac{a}{b}$ with probability p , mimicking the shear flow close to the diagonal and allowing some type of “*tunneling effect*”.

Setting up the system in the active phase (i.e. with $a > 0$) this “toy” model are able to reproduce the complex behavior of the avalanches shown in Fig.4.3.3. In this sense, Fig. 4.3.5 shows the avalanche size and duration probability distributions for different values of p . Just as our original model, there is a region with a power-law behavior following the Random Walk universality class, and (sometimes) a “bump” that reflects the existence of an (weakly) up stable state. Finally, for huge avalanches there exists an exponential cut-off.

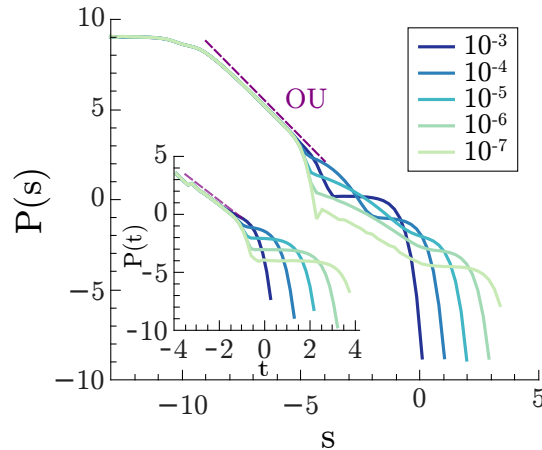


Figure 4.3.5: Avalanches for the $(1 + \epsilon)$ -dimensional model. Avalanche size distribution for different values of p . There is a region of random walk movement, followed by a bump related to the tunneling effect. Inset: Same behavior for the avalanche duration distribution. Parameters values: $a = 0.5$, $b = 1$, $\sigma = 10^{-3}$, $h = 10^{-3}$, $T = 2.5 \cdot 10^{-4}$.

4.4

Reactive dynamics in the Tsodyks-Markram model

With the aim to generalize the –just described– mechanism of “*balanced amplification*” to another neural dynamics, we hypothesize that inhibition is not the only regulatory mechanism that induces a reactive behavior: non-normal forms –and more in general, noise-induced behavior– might be a common trait in neurophysics. In particular, a balanced-like system must therefore be found in the proposed Landau-Ginzburg model (widely described in chapter 2).

In this way, the inhibition is now withdrawn from the picture, and Short-Term Synaptic Plasticity (STP), encoded by the combined effect of synaptic depression and synaptic recovery [45], is considered. This mechanism, under some homeostatic conditions represented here by particular choices of synaptic and neuronal timescales, should show a nontrivial reactive behavior.

We employ similar equations to those that have been proposed in appendix B.1, i.e. a density (Wilson Cowan-like) variable (ρ), that describes the excitatory activity of the network, and a synaptic density variable (R), describing the (short term) dynamic behavior of the synapses,

$$\begin{cases} \dot{\rho} = -\alpha\rho + (1 - \rho)S[\rho R - \Theta] + \sigma\sqrt{\rho}\eta + h \\ \dot{R} = \frac{1}{\tau_R}(\xi - R) - \frac{1}{\tau_D}\rho R \end{cases} \quad (4.4.1)$$

where $S(\rho)$ is a sigmoid (transduction) function (in particular, $S(\rho) = \tanh(\rho)$), Θ is a small threshold value, τ_R (resp. τ_D) is the characteristic recovery (depletion) time, ξ is the baseline level of non-depleted synaptic resources, h is an external driving field and $\alpha > 0$ controls the spontaneous decay of activity. Also, η is a (zero-mean, unit-variance) Gaussian noise.

By similarity with the Wilson-Cowan model, where only one fixed active/i-nactive point exists (depending on whether excitation or inhibition dominates, respectively), the specific parameters of the Landau-Ginzburg model are chosen to be consistent with the case B described above. In such a case, between the up and the down states, an intermediate regime of bistability including three fixed points is found for intermediate values of ξ (in between two saddle-node bifurcations): the up and the down ones, as well as an unstable fixed point in between.

Thus, it is just in such intermediate regime where the reactive dynamics is present. In particular, this specific case is achieved by taking the limit of small

(but non-vanishing) values of Θ , α , τ_D and τ_R and also, with some extra fine tuning (i.e. the condition $\frac{\tau_D}{\tau_R} \ll 1$ and $\frac{1}{\tau_D} \approx \alpha$, where the last one represents some equilibrium between the synaptic depression timescale and the neuronal decay timescale) to reach the non-normal condition shown in Figure 4.4.1a. As in the Wilson-Cowan model, there exists an stable 'up' state with a characteristic "shear" flow surrounding the stable fixed point and dropping the system (in a noise-induced phenomenon) to the 'down' state. Of course, if the dynamics of the system is non-reactive the fixed point presents an incoming flow in all directions (see Figure 4.4.1b).

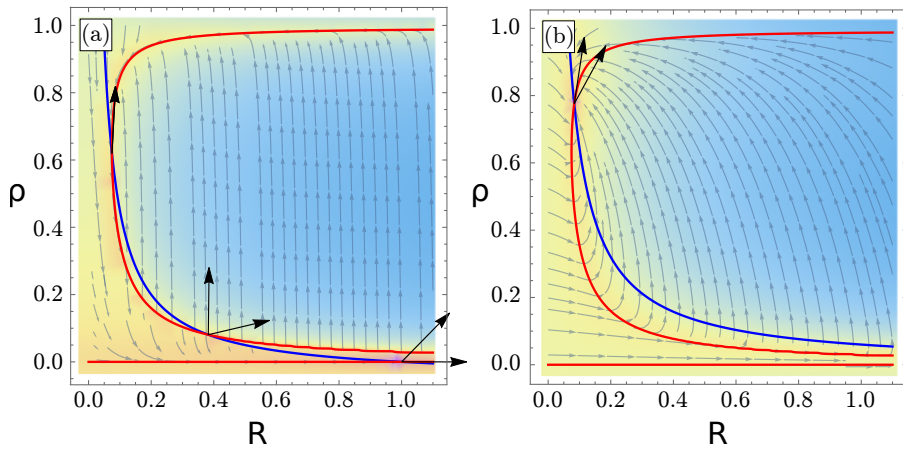


Figure 4.4.1: Phase portrait for the “balanced” TM model. (a) Non-normal condition with two fixed points with reactive dynamics. A characteristic “shear” flow surrounds the two stable fixed points, ‘up’ and ‘down’. Parameters: $h = 10^{-6}$, $\Theta = 0.03$, $\alpha = 0.01$, $\tau_D = 100$, $\tau_R = 2000$, $\chi = 1$ (b) Stable fixed point with incoming flow in all directions. Parameters: $h = 10^{-6}$, $\Theta = 0.03$, $\alpha = 0.01$, $\tau_D = 0.2$, $\tau_R = 1000$, $\chi = 13$.

By numerical simulation of Eqs.(4.4.1), there exists a clear distinction between the two cases indicated in Figure 4.4.1. As shown in Figure (4.4.2) both cases have two stable states –‘up’ and ‘down’– in the intermediate regime but for the first case, the “weak” stable “up” state for low amplitudes of the noise can be easily destabilized for intermediate values of the noise. It also produces a clear bursty quasi-periodic dynamics –with amplified fluctuations– when the amplitude is even greater. Otherwise, for the second one (see Figure (4.4.2)b) the ‘up’ state is tightly stable and equal values of the noise amplitude slightly disturb the dynamics of the system around the ‘up’ state, with no trace of noise-induced fluctuations. In this way, we have shown that the reactive dynamics can

also play a key role in the emergence –or the source of– large fluctuations in the well-known Tsodyks-Markram model for synaptic plasticity, and can be key of multiple noise-induced phenomena in neuroscience.

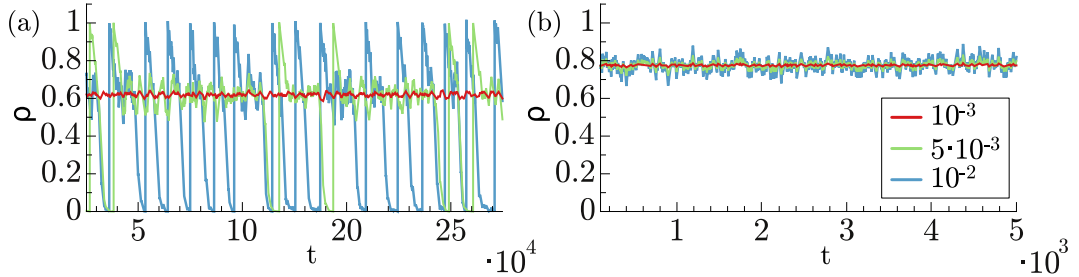


Figure 4.4.2: Temporal series for both cases shown in the above figure. (a) Reactive system for different values of the noise amplitude (detailed in the legend). For the lower one (red line) the system feature a stable 'up' state, that can be destabilized (green line) up to generate bursty dynamics (blue line) for increasing values of noise amplitude. Such fluctuations are no more than excursions between the two metastable states. (b) For identical values of the noise amplitude, only an 'up' stable state exists. The lack of non-normal effects around the stable state prevents noise-induced fluctuations.

4.5 Conclusions

We hope that the brief summary on the generation of avalanches in the Directed Percolation universality class will help in interpreting empirical results considering the possibility of non-universal continuously-varying exponents, even though most of the results derived here appear in the literature as independently derived for individual universality classes or for the branching process itself. Such continuously-varying exponents stems from the presence of small external driving, that might induce avalanche merging and, to the best of our knowledge, has not been noticed in the past. Also, we believe that such simple and unified perspective can help to shed light on the frequent confusion (mostly in the neuroscience literature) within the concepts developed in this chapter about branching processes and their relation with random walks, and in particular to:

- i) clarify the overall picture,
- ii) underline the superuniversality of the behavior as well as the dependence on external driving, and
- iii) avoid the common existing confusion between unbiased branching processes (equivalent to a random walker in a balanced logarithmic potential) and standard (unconfined) random walkers.

Thereby, empirical findings have reported size and lifetime exponents for neuronal avalanches compatibles with those of the universality class of a critical branching process (i.e. $\tau = \frac{3}{2}$ and $\alpha = 2$) [5, 6, 23, 43, 56, 58]. However, in some specific empirical analysis particular exponents could be compatible with those of an unbiased random walk [39, 62] (i.e. $\tau = \frac{4}{3}$ or $\alpha = \frac{3}{2}$) and, therefore, in no way implies a critical behavior of the system. In particular, due to the similarity of τ in both cases, α can be a better distinctive and empirically verifiable feature as well as some perils of thresholding must be avoided (see appendix B.3.2 for a further explanation).

Likewise, special care should be taken to ensure that the emergence of power laws constitutes a fingerprint of criticality (it is a necessary, but not a sufficient condition). As first counter-example, the generic power laws –across the entire absorbing phase– are produced by the spontaneous creation of activity (h). Thus, even if true scale-invariant avalanches emerge (in a spatial extended system) if the system is poised at criticality, other factors must also be present (e.g. long-range correlations, divergent susceptibility or maximum dynamic range).

In this sense, the mechanism of balanced amplification, recently proposed by Benayoun et al. [7], and thoroughly scrutinized here provides a (non-critical) candidate to model some features of neuronal avalanches. Thus, the Wilson-Cowan model for excitatory and inhibitory neuron populations, placed in a condition of an exquisite balance between excitatory and inhibitory couplings, is able to describe (without any need of fine tuning to a critical point) transitions between up (active) and down (quiescent) states as they occur in the brain during sleep or under anesthesia [17, 69], as well as large fluctuations that closely resembles the empirical scale-free avalanches of brain dynamics [5].

Theoretical analysis shows that such mechanism requires the existence of a stable fixed point (even far away from the critical point) with a “non-normal” stability matrix (i.e. with eigenvectors that does not form an orthonormal basis) in concomitance with inherent stochasticity. Thus, the “balanced amplification” condition is able to generate some type of discontinuous “scar” in the directions of the (reactive) dynamical evolution of the system producing very large noise-induced fluctuations. However, temporal series suggests that the system, in order to show avalanching behavior, remains trapped very close to the origin, that is the effect of the logarithmic potential along the balanced dynamical trajectory, i.e. the one-dimensional trajectory where excitatory and inhibitory activity are completely equal. Deviations from such diagonal drop the system from minimum to minimum, mimicking something similar to a “tunneling effect”, and where the remaining time in each one depend on their relative depth. Additionally, such depth is fully determined by the intensity of the noise.

Nevertheless, unlike the microscopical mechanism proposed by Benayoun et al. [7], the mean-field description shows scale-free avalanches composed either by a mixture of different trends or (for high values of the noise) showing compatible exponents with the well known standard random walk universality class, i.e. $\alpha = 3/2$ and $\tau = 4/3$. Thus, although reactive dynamics may be of key importance in neural mechanisms (such as in up and down states) and in fostering large fluctuations, it does not seem a plausible candidate to account for a large number of the founded empirical results already outlined in previous chapters.

On the other hand we have shown that the reactive dynamics applies to a wider scenario extensible to further neural mechanisms, which includes synaptic plasticity such as encoded in the Tsodyks-Markram model, showing dynamics very similar to the aforementioned up and down states because of the destabilization of the stable (active) states of the system.

References

- [1] AL HAMMAL, O., CHATÉ, H., DORNIC, I. & MUÑOZ, M. A. «Langevin description of critical phenomena with two symmetric absorbing states». *Phys. Rev. Lett.* **94**, 230601 (2005).
- [2] BAK, P., CHRISTENSEN, K., DANON, L. & SCANLON, T. «Unified scaling law for earthquakes». *Phys. Rev. Lett.* **88**, 178501 (2002).
- [3] BALDASSARRI, A., COLAIORI, F. & CASTELLANO, C. «Average shape of a fluctuation: Universality in excursions of stochastic processes». *Phys. Rev. Lett.* **90**, 060601 (2003).
- [4] BEGGS, J. M. «The criticality hypothesis: how local cortical networks might optimize information processing». *Philos. Trans. A Math. Phys. Eng. Sci.* **366**, 329–343 (2008).
- [5] BEGGS, J. M. & PLENZ, D. «Neuronal avalanches in neocortical circuits». *J. Neurosci.* **23**, 11167–11177 (2003).
- [6] BELLAY, T., KLAUS, A., SESHADRI, S. & PLENZ, D. «Irregular spiking of pyramidal neurons organizes as scale-invariant neuronal avalanches in the awake state». *Elife* **4**, e07224 (2015).
- [7] BENAYOUN, M., COWAN, J. D., VAN DRONGELEN, W. & WALLACE, E. «Avalanches in a stochastic model of spiking neurons». *PLoS Comp. Biol.* **6**, e1000846 (2010).
- [8] BINNEY, J., DOWRICK, N., FISHER, A. & NEWMAN, M. *The Theory of Critical Phenomena* (Oxford University Press, Oxford, 1993).
- [9] BONACHELA, J. A., DE FRANCISCIS, S., TORRES, J. J. & MUNOZ, M. A. «Self-organization without conservation: are neuronal avalanches generically critical?». *J. Stat. Mech. Theory Exp.* **2010**, P02015 (2010).
- [10] BONACHELA, J. A. & MUÑOZ, M. A. «Self-organization without conservation: true or just apparent scale-invariance?». *J. Stat. Mech.* **2009**, P09009 (2009).
- [11] BORISYUK, R. M. & KIRILLOV, A. B. «Bifurcation analysis of a neural network model». *Biol. Cyber.* **66**, 319–325 (1992).
- [12] BRAY, A. «Random walks in logarithmic and power-law potentials, nonuniversal persistence, and vortex dynamics in the two-dimensional XY model». *Phys. Rev. E* **62**, 103 (2000).

-
- [13] BRUNEL, N. «Dynamics of Sparsely Connected Networks of Excitatory and Inhibitory Spiking Neurons». *J. Comp. Neurosci.* **8**, 183–208 (2000).
- [14] BUICE, M. A. & COWAN, J. D. «Field-theoretic approach to fluctuation effects in neural networks». *Phys. Rev. E* **75**, 051919 (2007).
- [15] COLAIORI, F. «Exactly solvable model of avalanches dynamics for Barkhausen crackling noise». *Adv. Phys.* **57**, 287–359 (2008).
- [16] DERSHOWITZ, N. & RINDERKNECHT, C. «The Average Height of Catalan Trees by Counting Lattice Paths». *Math. Mag.* **88**, 187–195 (2015).
- [17] DESTEXHE, A. «Self-sustained asynchronous irregular states and up-down states in thalamic, cortical and thalamocortical networks of nonlinear integrate-and-fire neurons». *J. Comp. Neurosci.* **27**, 493 (2009).
- [18] DICKMAN, R. & TRETYAKOV, A. Y. «Hyperscaling in the Domany-Kinzel cellular automaton». *Phys. Rev. E* **52**, 3218 (1995).
- [19] DING, M. & YANG, W. «Distribution of the first return time in fractional Brownian motion and its application to the study of on-off intermittency». *Phys. Rev. E* **52**, 207–213 (1995).
- [20] DORNIC, I., CHATÉ, H., CHAVE, J. & HINRICHSSEN, H. «Critical Coarsening without Surface Tension: The Universality Class of the Voter Model». *Phys. Rev. Lett.* **87**, 045701 (2001).
- [21] FELLER, W. «Two singular diffusion problems». *Ann. Math.* 173–182 (1951).
- [22] FIELD, S., WITT, J., NORI, F. & LING, X. «Superconducting vortex avalanches». *Phys. Rev. Lett.* **74**, 1206 (1995).
- [23] FRIEDMAN, N. *et al.* «Universal critical dynamics in high resolution neuronal avalanche data». *Phys. Rev. Lett.* **108**, 208102 (2012).
- [24] GARDINER, C. W. *Handbook of stochastic methods: for physics, chemistry and the natural sciences; 3rd ed.* Springer Series in Synergetics (Springer, Berlin, 2004).
- [25] GENOVESE, W., MUÑOZ, M. A. & SANCHO, J. M. «Nonequilibrium transitions induced by multiplicative noise». *Phys. Rev. E* **57**, R2495 (1998).
- [26] GRASSBERGER, P. «On the critical behavior of the general epidemic process and dynamical percolation». *Math. Bio.* **63**, 157–172 (1983).

- [27] GRASSBERGER, P. «On phase transitions in Schlögl's second model». *Z. Phys. B.* **47**, 365–374 (1982).
- [28] GRINSTEIN, G. & MUÑOZ, M. A. «The Statistical Mechanics of Systems with Absorbing States». In GARRIDO, P. & MARRO, J. (eds.) *Fourth Granada Lectures in Computational Physics*, vol. 493 of *Lecture Notes in Physics*, 223 (1996).
- [29] GRINSTEIN, G., MUÑOZ, M. A. & TU, Y. «Phase structure of systems with multiplicative noise». *Phys. Rev. Lett.* **76**, 4376 (1996).
- [30] HAHN, G. *et al.* «Neuronal avalanches in spontaneous activity in vivo». *J. Neurophysiol.* **104**, 3312–3322 (2010).
- [31] HARRIS, T. E. *The theory of branching processes* (Courier Corporation, 2002).
- [32] HENKEL, M., HINRICHSSEN, H. & LÜBECK, S. *Non-equilibrium Phase Transitions: Absorbing phase transitions*. Theoretical and mathematical physics (Springer, Berlin, 2008).
- [33] HILTON, P. & PEDERSEN, J. «Catalan numbers, their generalization, and their uses». *Math. Intell.* **13**, 64–75 (1991).
- [34] HOPPENSTEADT, F. C. & IZHIKEVICH, E. M. *Weakly connected neural networks*, vol. 126 (Springer Science & Business Media, 2012).
- [35] JANSSEN, H. K. «Survival and percolation probabilities in the field theory of growth models». *J. Phys. Cond. Matter* **17**, S1973 (2005).
- [36] JANSSEN, H. K. «Renormalized field theory of dynamical percolation». *Z. Phys. B.* **58**, 311–317 (1985).
- [37] JANSSEN, H. K. «On the nonequilibrium phase transition in reaction-diffusion systems with an absorbing stationary state». *Z. Phys. B.* **42**, 151–154 (1981).
- [38] LARREMORE, D. B., CARPENTER, M. Y., OTT, E. & RESTREPO, J. G. «Statistical properties of avalanches in networks». *Phys. Rev. E* **85**, 066131 (2012).
- [39] LARREMORE, D. B., SHEW, W. L., OTT, E., SORRENTINO, F. & RESTREPO, J. G. «Inhibition causes ceaseless dynamics in networks of excitable nodes». *Phys. Rev. Lett.* **112**, 138103 (2014).
- [40] LEVINA, A., HERRMANN, J. M. & GEISEL, T. «Phase Transitions towards Criticality in a Neural System with Adaptive Interactions». *Phys. Rev. Lett.* **102**, 118110 (2009).

-
- [41] LEVINA, A., HERRMANN, J. M. & GEISEL, T. «Dynamical synapses causing self-organized criticality in neural networks». *Nat. Phys.* **3**, 857–860 (2007).
- [42] LIGGETT, T. *Interacting Particle Systems*. Classics in Mathematics (Springer, New York, 2004).
- [43] LOMBARDI, F., HERRMANN, H., PERRONE-CAPANO, C., PLENZ, D. & DE ARCANGELIS, L. «Balance between excitation and inhibition controls the temporal organization of neuronal avalanches». *Phys. Rev. Lett.* **108**, 228703 (2012).
- [44] MAJUMDAR, S. N. & COMTET, A. «Airy distribution function: from the area under a Brownian excursion to the maximal height of fluctuating interfaces». *J. Stat. Phys.* **119**, 777–826 (2005).
- [45] MARKRAM, H. & TSODYKS, M. «Redistribution of synaptic efficacy between pyramidal neurons». *Nature* **382**, 807–810 (1996).
- [46] MARRO, J. & DICKMAN, R. *Nonequilibrium Phase Transition in Lattice Models* (Cambridge University Press, Cambridge, 1999).
- [47] MARTINELLO, M. *et al.* «Neutral theory and scale-free neural dynamics». *Phys. Rev. X* **7**, 041071 (2017).
- [48] MILLMAN, D., MIHALAS, S., KIRKWOOD, A. & NIEBUR, E. «Self-organized criticality occurs in non-conservative neuronal networks during 'up' states». *Nat. Phys.* **6**, 801–805 (2010).
- [49] MUÑOZ, M. A., COLAIORI, F. & CASTELLANO, C. «Mean-field limit of systems with multiplicative noise». *Phys. Rev. E* **72**, 056102 (2005).
- [50] MUÑOZ, M. A., DICKMAN, R., VESPIGNANI, A. & ZAPPERI, S. «Avalanche and spreading exponents in systems with absorbing states». *Phys. Rev. E* **59**, 6175 (1999).
- [51] MUÑOZ, M. A., GRINSTEIN, G. & TU, Y. «Survival probability and field theory in systems with absorbing states». *Phys. Rev. E* **56**, 5101 (1997).
- [52] MUÑOZ, M. A. «Colloquium: Criticality and dynamical scaling in living systems». *arXiv preprint arXiv:1712.04499* (2017).
- [53] MURPHY, B. K. & MILLER, K. D. «Balanced Amplification: A New Mechanism of Selective Amplification of Neural Activity Patterns». *Neuron* **61**, 635–648 (2009).

-
- [54] ÓDOR, G. *Universality in Nonequilibrium Lattice Systems: Theoretical Foundations* (World Scientific Publishing, Singapore, 2008).
- [55] OTTER, R. «The multiplicative process». *Ann. Math. Stat.* **20**, 206–224 (1949).
- [56] PALVA, J. M. *et al.* «Neuronal long-range temporal correlations and avalanche dynamics are correlated with behavioral scaling laws». *Proc. Natl. Acad. Sci. USA* **110**, 3585–3590 (2013).
- [57] PAPANIKOLAOU, S. *et al.* «Universality beyond power laws and the average avalanche shape». *Nat. Phys.* **7**, 316–320 (2011).
- [58] PETERMANN, T. *et al.* «Spontaneous cortical activity in awake monkeys composed of neuronal avalanches». *Proc. Natl. Acad. Sci. USA* **106**, 15921–15926 (2009).
- [59] PETERS, O., HERTLEIN, C. & CHRISTENSEN, K. «A complexity view of rainfall». *Phys. Rev. Lett.* **88**, 018701 (2001).
- [60] PLENZ, D. & THIAGARAJAN, T. C. «The organizing principles of neuronal avalanches: cell assemblies in the cortex?». *Trends Neurosci.* **30**, 101–110 (2007).
- [61] PLISCHKE, M. & BERGERSEN, B. *Equilibrium statistical physics* (World Scientific, Singapore, 2006).
- [62] POIL, S.-S., HARDSTONE, R., MANSVELDER, H. D. & LINKENKAER-HANSEN, K. «Critical-state dynamics of avalanches and oscillations jointly emerge from balanced excitation/inhibition in neuronal networks». *J. Neurosci.* **32**, 9817–9823 (2012).
- [63] REDNER, S. *A guide to first-passage processes* (Cambridge University Press, Cambridge, 2001).
- [64] RUBIN, K. J., PRUESSNER, G. & PAVLIOTIS, G. A. «Mapping multiplicative to additive noise». *J. Phys. A* **47**, 195001 (2014).
- [65] RUBINOV, M., SPORNS, O., THIVIERGE, J.-P. & BREAKSPEAR, M. «Neurobiologically realistic determinants of self-organized criticality in networks of spiking neurons». *PLoS Comp. Biol.* **7**, e1002038 (2011).
- [66] SAN MIGUEL, M. & TORAL, R. «Stochastic effects in physical systems». *Instabilities and nonequilibrium structures VI* **5**, 35–127 (2000).
- [67] DI SANTO, S., BURIONI, R., VEZZANI, A. & MUÑOZ, M. A. «Self-Organized Bistability Associated with First-Order Phase Transitions». *Phys. Rev. Lett.* **116**, 240601 (2016).

- [68] SCHUSTER, H. G., PLENZ, D. & NIEBUR, E. *Criticality in neural systems* (John Wiley & Sons, New Jersey, 2014).
- [69] STERIADE, M., NUNEZ, A. & AMZICA, F. «A novel slow (< 1 Hz) oscillation of neocortical neurons in vivo: depolarizing and hyperpolarizing components». *J. Neurosci.* **13**, 3252–3265 (1993).
- [70] TAKEUCHI, K. A., KURODA, M., CHATÉ, H. & SANO, M. «Directed percolation criticality in turbulent liquid crystals». *Phys. Rev. Lett.* **99**, 234503 (2007).
- [71] TOUBOUL, J. & DESTEXHE, A. «Can power-law scaling and neuronal avalanches arise from stochastic dynamics?». *PLoS ONE* **5**, e8982 (2010).
- [72] VAN KAMPEN, N. G. *Stochastic processes in physics and chemistry* (Elsevier, North-Holland, 1992).
- [73] VERDY, A. & CASWELL, H. «Sensitivity Analysis of Reactive Ecological Dynamics». *Bull. Math. Biol.* **70**, 1634–1659 (2008).
- [74] VESPIGNANI, A., DICKMAN, R., MUÑOZ, M. A. & ZAPPERI, S. «Driving, conservation, and absorbing states in sandpiles». *Phys. Rev. Lett.* **81**, 5676 (1998).
- [75] VAN VREESWIJK, C. & SOMPOLINSKY, H. «Chaos in Neuronal Networks with Balanced Excitatory and Inhibitory Activity». *Science* **274**, 1724–1726 (1996).
- [76] WANG, F. & DAI, Z. «Self-organized criticality in X-ray flares of gamma-ray-burst afterglows». *Nat. Phys.* **9**, 465–467 (2013).
- [77] WATSON, H. W. & GALTON, F. «On the probability of the extinction of families». *J. Roy. Anthropol. Inst.* **4**, 138–144 (1875).
- [78] WILSON, H. R. & COWAN, J. D. «Excitatory and inhibitory interactions in localized populations of model neurons». *Biophys. J.* **12**, 1 (1972).
- [79] ZAPPERI, S., LAURITSEN, K. B. & STANLEY, H. E. «Self-organized branching processes: mean-field theory for avalanches». *Phys. Rev. Lett.* **75**, 4071 (1995).

*Dynamics of sparse gene networks
under noisy conditions*

5.1	Introduction	167
5.2	Boolean network approach	170
5.3	Adaptive evolution of boolean gene-regulatory networks	174
5.4	Emergent properties	183
5.4.1	Convergence times and phases of learning networks	183
5.4.2	Noisy conditions	187
5.4.3	Empirical networks	190
5.5	Conclusions	193
	References	196

5.1 Introduction

“Evolution is not just “chance caught on the wing”. It is not just a tinkering of the ad hoc, of bricolage, of contraption. It is emergent order honored and honed by selection.”

Stuart A. Kauffman

The central dogma of molecular biology is that each single gene is transcribed into RNA, which in turn is translated into a protein, which –usually in cooperation with other proteins– can regulate the expression of other genes, giving rise to a complex network of regulatory interactions [16]. Genetic regulation, protein-protein interactions, as well as cell metabolic and signaling pathways are essential biological processes that can all be represented as networks [13]. The network picture encapsulates the complexity of cellular processes and provides us with a natural framework for a systems-perspective approach to extremely complicated biological problems. As a matter of fact, the study of information processing in living systems has shifted from the analysis of single pathways to increasingly complex regulatory networks, allowing for a visualization of the collective effects of a host of units acting at unison. Since the pioneering work of Kauffman [5, 18, 31, 35, 36], genetic regulatory systems have been modeled as random Boolean networks, in which the expression level of each gene is represented by a binary (on/off) variable and where mutual regulatory interactions are described as arbitrary random Boolean functions operating synchronously at discrete time steps. Even if admittedly simplistic and limited in a number of ways (e.g. gradual levels of gene expression might be essential to understand some cellular processes), such a binary description is particularly useful when dealing with large networks because it simplifies the overwhelming complexity of the original system to a problem with a logical structure. In particular, the Boolean approach has shed light on important conceptual problems such as the possibility of diverse (phenotypic) states emerging from a unique given genetic network, as well as the possibility of transitions among them (as happens in cell differentiation and reprogramming), and the emergence of cycles in cell states. More specifically, the trajectory of the segment polarity network in the fly *Drosophila melanogaster* [1] and the yeast cell cycle [42] are two specific examples in which the most relevant features have been fully elucidated on the basis of Boolean models [12] (for a broad discussion we refer to [4, 18, 20, 31, 36]).

Random Boolean networks (RBNs) can operate in different regimes including ordered and chaotic phases as well as a critical point (or line or surface) separating them. Ordered or frozen phases (typically obtained for small network connectivities) are characterized by a small set of stable attractors which are largely robust to perturbations, while in the disordered or chaotic phase (typically obtained for densely connected networks) perturbations rapidly proliferate all through the network. As formalized mathematically by Derrida and Pomeau, separating these two phases there is a critical line (that used to be called the “edge of chaos”) at which perturbations propagate marginally [19]. It was conjectured some time ago that critical RBNs might be optimal to represent actual biological networks; the underlying idea is that operating at criticality might provide such systems with an optimal trade-off between being exceedingly ordered/stable –and thus barely responsive to environmental changes, signals and clues– and too disordered/noisy –and thus enormously sensitive to the effects of noise, lacking the required robustness and accuracy that biological machinery demands [37]; the criticality hypothesis states that the marginal situation between these two impractical tendencies –that we shall call subcritical and supercritical, respectively, in what follows– constitutes an excellent compromise. This conjecture, which was developed in the machine-learning and neural-network community [11, 40, 45], proposes that –by operating nearby criticality– networks exhibit an optimal trade-off between stability to perturbations and sensitivity/responsiveness to signals and –at larger timescales– between robustness and evolvability [3, 56], and allows for an optimization of information storage and transmission [39, 50], response and sensitivity, computational capabilities, and a number of other functional advantages [3, 15, 25, 37–39, 54, 56, 61].

Remarkably, the development of powerful experimental high-throughput technologies in molecular biology has paved the way to experimental analyses of gene-expression patterns in large regulatory networks. Recent empirical results, analyzing hundreds of micro-array experiments to infer regulatory interactions among genes and implementing these data into Boolean models, seem to support the hypothesis that regulatory networks of *S. cerevisiae*, *E. coli*, *B. subtilis*, the macrophage, as well as some subnetworks of *D. melanogaster* and *A. thaliana* are indeed very close to criticality (in the sense of marginal propagation of perturbations) [9, 46], while some other empirical analyses leave the door open to regulatory networks being ordered [37, 55].

Recent work, aimed at rationalizing why and how criticality might come about in living systems, relies on adaptive/evolutionary models, in which communities of agents –each of them modeled as a Boolean network– are selected for if they succeed at performing some complex tasks which may change in time. For instance, Hidalgo et al. [34] showed –by employing an information theoretic approach– that critical networks may emerge as optimal solutions in such a setting (however, the networks employed as a specific example in [34] where fully

connected and thus lacked the structural richness of usual RBNs). Similarly, Goudarzi *et al.* [29] considered an ensemble of RBN's able to experience "mutations" in their topological structure and employed a genetic algorithm to select for those able to perform a given computational task; i.e. networks which have learned have a larger fitness than those that have not. Under these conditions the ensemble of networks converges to a state in which all networks operate close to criticality. In other words, critical networks emerge as the optimal solution out of the combined selective pressures of having to learn different tasks (i.e. having to produce different outcomes/attractors) and being able to readily shift among them following changes in the inputs in real time.

Given that living cells typically possess very low copy numbers of important regulatory molecules (e.g. for the 80% of genes in *E. coli* genome the copy number of their associated proteins is less than 100 [33]) stochastic effects are unavoidable and ubiquitous in gene regulatory networks [53]. Even if noise is usually assumed to be detrimental to reliable information transfer and, more in general, to cell functioning, stochastic effects can lead to beneficial outcomes; for instance, noise accounts for the observed (phenotypic) variability in identical (isogenic) populations [23] and can help cells to adapt to fluctuating environments [6, 22, 43, 60]. Within the framework of RBN the role of stochasticity and noise has been addressed in a number of works (e.g. [17, 49, 58]).

Here, we further delve in the problem of investigating the mechanisms and the conditions under which networks may become critical (or not), focusing on the role played by noise, and ask the question whether—in the presence of strongly noisy conditions—regulatory networks, modeled as RBNs having to perform some complex computational task, should operate in ordered, critical or supercritical regimes. In other words: what is the role of noise in the emergence of criticality? Does it foster or hinder critical behavior? In order to gauge the effect of noise on the dynamics of RBNs having to perform a complex task we consider a setting very similar to that of Goudarzi *et al.* [29] as described above, but including different additional sources of stochasticity. In particular, our approach differs from the previous one in three main aspects: (i) we consider asynchronous updating [28, 30, 52] rather than the usual deterministic one, thus introducing the effect of stochasticity in the updating timings, (ii) both the structure and the dynamics of the networks are subjected to noise (be it intrinsic or external), and (iii) we do not consider an evolutionary algorithm to search for the best possible network connectivity, but rather we work in a constant-connectivity ensemble and explore how the network performance depends on the network connectivity, i.e. on the network dynamical state.

As we shall illustrate, criticality emerges as the solution providing the fastest route to learning complex tasks even in the presence of asynchronous updating, but, on the other hand, once additional sources of stochasticity are explicitly taken into account ordered dynamical states perform better than critical ones.

5.2

Boolean network approach

As said before, the pioneering work of Kauffman [5, 18, 31, 35, 36] paved the way to employ a Boolean modeling for genetic regulatory systems. In this approach, a binary variable –with possible values 0 or 1 (off/on), $\sigma_i = \{0, 1\}$ – are the expression level of a gene, while the (direct) links stand for the regulatory interactions, activation or repression (Figure 5.2.1 shows two examples of real gene-regulatory networks). Side by side, there exists an ensemble of possible states for the N nodes, or a realization of possible states, which comprise the attractors of the dynamics, emulating the cellular states.

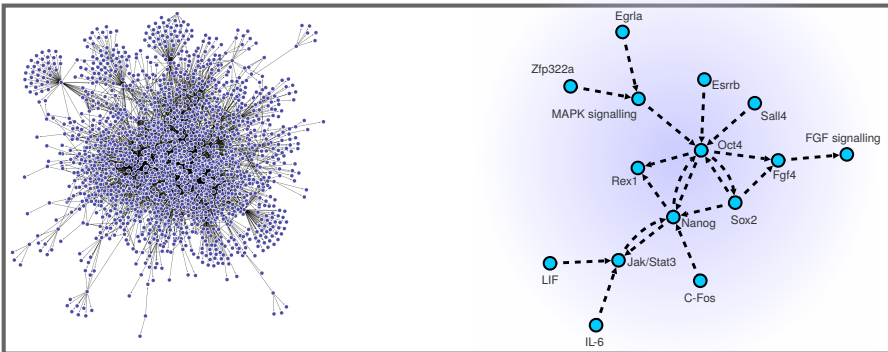


Figure 5.2.1: Large scale gene-regulatory network of *E. Coli* (left, [27]) and small gene regulatory network for the mouse embryonic stem-cell subnetwork (right, [48]). Genes are represented as nodes and gene regulatory interactions as links. Observe that these networks are directed and genes can have gradual levels of gene expression regulating another downstream genes.

Also, the evolution of the state of each node is given by a Boolean function, which also depends on the state of the K_{in} neighbor nodes regulating it, mimicking the dynamics of mutual regulatory interactions [20, 31]. At the same time, nodes contribute to regulating the state of K_{out} out-neighbors (see Table in Figure 5.2.2 for an example of a random Boolean function).

Thus, nodes are updated according to:

$$\sigma_i(t+1) = f_i(\sigma_{n_1^i}(t), \sigma_{n_2^i}(t), \dots, \sigma_{n_{K_{\text{in}}^i}}(t)), \quad (5.2.1)$$

where n_j^i identifies the j -th neighbor of node i , time is incremented, and the process is iterated. The updating process can be arbitrary operating synchronously (i.e. updating all the nodes simultaneously) at discrete time steps or not (updating one variable—randomly or with some predefined sequence—at every step $\Delta t = 1/N$), but, in any case a time step of the dynamics corresponds to update all the nodes, on average.

In particular, considering the case of a regular network (in which every vertex has the same number of neighbors), it is clear that there are 2^{2^K} possible coupling functions. Hence, depending on the specific situation, there are different ways to assign the Boolean functions (randomly selected, choosing a subset, etc.), but it is specially important the case of taking a random bias toward “on” or “off” states, p , as the averaged fraction of 1’s in the outputs of the random Boolean function, that can be fixed a priori and acts as a control parameter.

If that is the case, in the infinite size limit, Random Boolean Networks (RBNs) are known to exhibit a critical point—in the sense of marginal propagation of perturbations [19, 31]—at a value of the connectivity

$$K_C(p) = \frac{1}{2p(1-p)}, \quad (5.2.2)$$

being ordered/subcritical for $K < K_C(p)$ and disordered/supercritical otherwise. In particular, in the unbiased case, $p = 1/2$, $K_C = 2$ (see Figure 5.2.2) which is often quoted as “the” critical connectivity for RBNs.

✱ **The Hamming distance as a mark of the dynamical state** In order to move towards a custom measure of the dynamical states of the network, let us bear in mind two initial states, defined as,

$$\Sigma_0 = \{\sigma_1(0), \sigma_2(0), \dots, \sigma_N(0)\}, \quad \tilde{\Sigma}_0 = \{\tilde{\sigma}_1(0), \tilde{\sigma}_2(0), \dots, \tilde{\sigma}_N(0)\}$$

and, on this basis, it is possible to define a proper measure based in a “damage spreading” algorithm to elucidate the dynamical state of a RBN. In particular, consider Σ_0 and $\tilde{\Sigma}_0$ two set of identical states, except for a flipped node, and compute its Hamming distance, defined as,

$$H(\Sigma_0, \tilde{\Sigma}_0) = \frac{1}{N} \sum_{i=1}^N |\sigma_i - \tilde{\sigma}_i| \quad (5.2.3)$$

Thus, in order to determine the dynamical state of any specific network—and to quantify possible deviations from criticality—we explicitly compute whether

individual site perturbations do grow or shrink on average. This is quantified by measuring the branching parameter, B , defined as the averaged Hamming distance after one timestep, between the original and all possible network perturbations at one site; branching parameters $B > 1$ (resp. $B < 1$) reflect supercritical (resp. subcritical) networks while the marginal case $B = 1$ is the trademark of criticality [19, 31]. In brief:

- If $B > 1$ the Hamming distance grows exponentially. The network is disordered (chaotic phase).
- If $B = 1$ the perturbations propagate marginally. The network is critical.
- If $B < 1$ the trajectories converge and the network is ordered (frozen phase).

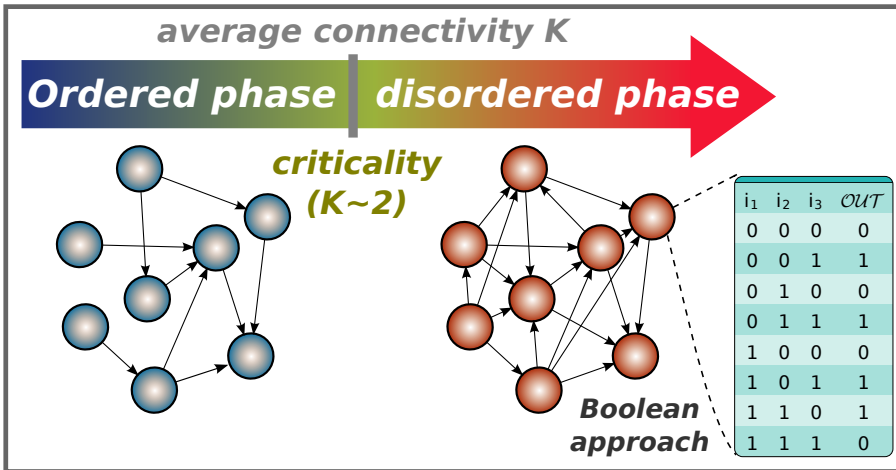


Figure 5.2.2: Sketch of a Boolean network. Dynamical phases depends on the mean connectivity of the network, from ordered (or frozen) phase for low connectivity to disordered (or chaotic) phase for high connectivity, separated by a critical point lying in $K_c = 2$ for the particular case $p = 1/2$. The table shows an example –for one node– of logical operations.

✳ **Assessing the network dynamical state in Erdős-Rényi networks.** However, all this is applicable to the simple case of regular networks. A first target must be the estimation of the scaling of the critical point as function of the system size in an Erdős-Rényi (ER) generic network with N nodes, L directed links, and averaged connectivity or degree $K = L/N$. Whereas this network comes from a binomial degree distribution ($P(k)$), the two first central moments are $\mu = \bar{k}$ and $\sigma^2 = \bar{k} - \frac{\bar{k}^2}{N}$. On the other hand, a correction in the critical point –measured

by the recently explained Derrida curve method— comes from effects due to second neighbors (or higher orders). Namely, the number of second neighbors, z_2 , and the number of neighbors, z_1 , are defined by $z_2 = \langle k^2 \rangle - \langle k \rangle$ and $z_1 = \langle k \rangle$, respectively. Straight away, in our case, $z_2 = \bar{k} - \frac{\bar{k}^2}{N}$ and thus, considering the critical point from Eq. (5.2.2),

$$\sqrt{z_2} = \sqrt{\bar{k} - \frac{\bar{k}^2}{N}} = \frac{1}{2p(1-p)} \quad (5.2.4)$$

which in turn, taking a Taylor series expansion in N , the corrections of k_c follows the form,

$$K_c = K_c^{MF} + \mathcal{O}(N^{-1}) \quad (5.2.5)$$

i.e. critical values are shifted —for finite networks— toward slightly larger connectivity values by corrections of order $\mathcal{O}(N^{-1})$.

As shown in Figure 5.2.3, the critical point of an Erdős–Rényi Boolean network —with $p = \frac{1}{2}$ and measured employing the method explained above— converges towards $K_c = 2$ in the infinite size limit. Also, the finite size effects follows the expected behavior $\varepsilon N^{-\beta}$ with $\varepsilon = 4.4(1.1)$, $\beta = -1.00(4)$ in the asynchronous updating, and $\varepsilon = 2.3(0.1)$, $\beta = -1.02(2)$ in the synchronous one (regardless of the updating scheme, in the infinite size limit).

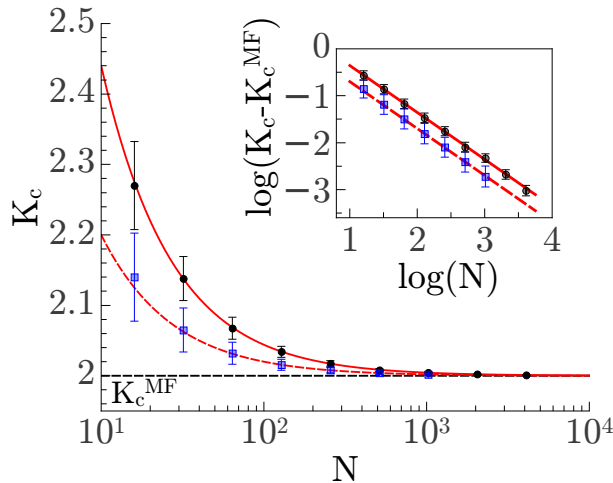


Figure 5.2.3: Variation of the critical point measured employing the branching parameter, B , for an Erdős–Rényi network versus system size (blue points: synchronous updating and black points: asynchronous updating). Inset: Distance to the mean-field critical point ($K_c = 2$) versus system size, in log-log scale.

5.3

Adaptive evolution of boolean gene-regulatory networks

As said above, we consider a setting very similar to that of [29] to train Random Boolean networks to perform a computational task, but we introduce a number of changes –to be detailed in this section– devoted mostly to implement stochasticity in various ways. In this central work [29], Goudarzi et al. train an ensemble of RBN, representing bacterias or specific gene regulatory networks and predefining some input and readout nodes, to synthesize information from the environment and provide a response. By allowing a genetic algorithm with random mutations in the structure of the networks they showed that the closer to criticality the better the way to process the information and successfully attain the imposed computational tasks. Thus, criticality emerges in a highly changing environment, i.e. when a lot of tasks must be reproduced.

✱ **Network architecture and dynamics.** In order to implement computational tasks or learning rules in RBNs we consider a slight variation of the just-described general architecture, in which some predefined input and output nodes are included (see Figure 5.3.1). By construction, input nodes are imposed to have $K_{in} = 0$, so that they are not influenced by others and $K_{out} > 0$, so that they are not isolated, while –on the contrary– output nodes have $K_{out} = 0$ and $K_{in} \geq 1$ (in particular, we take $n_{input} = 3$ input nodes and one single output or readout node ($n_{output} = 1$)). The set of $(N - n_{input})$ non-input nodes is called the network core. Self-loops and multiple edges with the same directionality linking two nodes are explicitly excluded, and otherwise the wiring pattern is randomly set. In the same way, a bias $p = 1/2$ is taken as initial condition in all analyses here, i.e. all the network core and the readout node have random boolean functions of its signaling nodes. Additionally, in contrast with most studies of RBNs and in order to implement a first source of stochasticity, nodes are updated in an *asynchronous* way [28, 30, 52], i.e. a given node is randomly selected with homogeneous probability and its state is updated according to a Boolean function depending on the state of the input nodes.

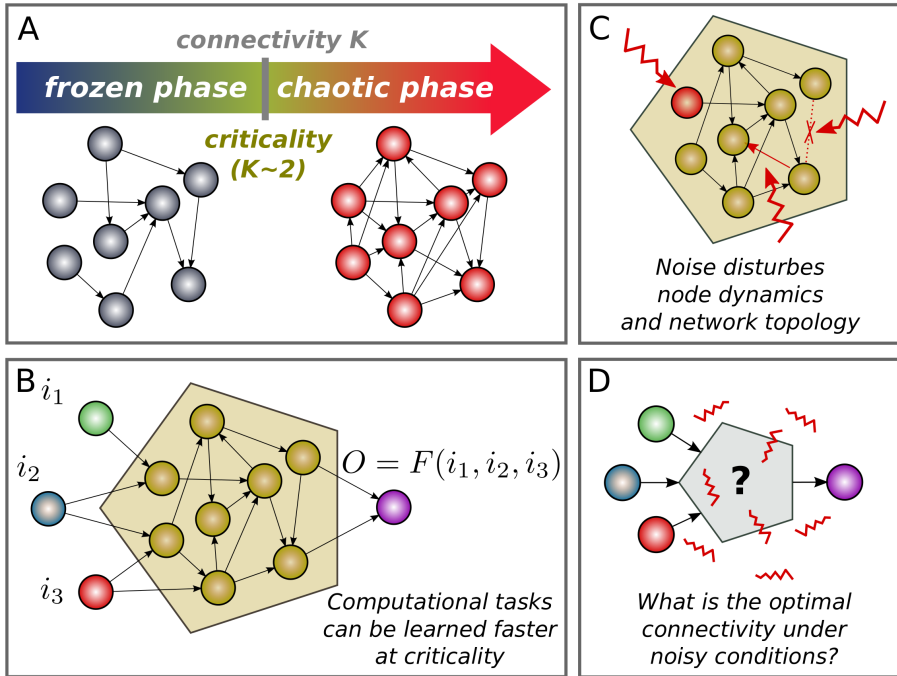


Figure 5.3.1: Network training sketch. (A) Dynamical phases in general random Boolean networks (RBNs) in the case for which $K_C \approx 2$ ($p = 1/2$). (B) Constrained network architecture: three input nodes are imposed ($i_{1,2,3}$) to receive information from the environment and one output/readout node (O) to produce a response. The overall computational task to be learned can be summarized in a predefined truth table $\mathcal{O} = F(i_1, i_2, i_3)$ where \mathcal{O} is the output state and $i_{1,2,3}$ the input ones. (C) During the network dynamics and adaptive evolution, there can be noise sources (internal or external) disturbing the network states as well as its topological structure. (D) The aim is to find the optimal connectivity to learn and perform successfully the computational tasks either in the absence of additional stochasticity as well as in the presence of noise.

✱ **Assessing network criticality.** We employ the standard method of plotting the Derrida curve –as described above– in order to determine the dynamical phase of any specific RBN –specified by its topology and the set of its Boolean functions– and assess how far it operates from criticality.


Let us remember, however, that the method is based in damage spreading dynamics and involves the next steps:

- i) Take a network M in one specific state, and a copy of it M' in which a single randomly chosen node has inverted its state.

- ii) Compute the Hamming distance, H , [19, 31] between these two networks after one time step ($t = 1$; nodes are updated following the same random order in both cases).
- iii) Average the Hamming distance for many different “flipped” nodes.
- iv) Average the previous result over network states. The *branching parameter*, B , is defined as the averaged H after perturbing the different nodes in the network (in some cases, we present results for perturbations only at input/core nodes). If $B < 1$ perturbations shrink on average and the network is said to be subcritical (or in the ordered phase), while if $B > 1$ perturbations proliferate and grow on average and the network is supercritical (chaotic or disordered phase). Finally, in the intermediate case, $B = 1$, in which perturbations propagate marginally, the network is critical.

Observe that in networks with some fixed input and output nodes, we can measure B in different ways, depending on whether we flip inputs nodes or not and on whether we compute the Hamming distance in the whole network or just in the core (excluding input nodes); therefore the concept of criticality might refer to just the core or to the full network. Finally, in order to determine the critical regime of an ensemble of networks –and not just an individual one– it is necessary to measure the ensemble average, \bar{B} , of B .

✱ **Computational tasks.** The task to be learned can be codified in a “truth table”, i.e. for each specific input (out of a total of $I = 2^{n_{\text{input}}}$) there is an output value to be reproduced. A given truth table defines a specific computational task. An example is the odd-even classifier (rule $R150$ in in the Wolfram’s classification of cellular automata [62]), which assigns a Boolean variable to each input accounting for its parity. Another examples that we consider are rules number $R51$ and $R60$ in Wolfram’s classification (as shown in Figure 5.3.2). These rules can be categorized accordingly to their “complexity”, understanding as such, the number of nodes in the input that do change the output state when altered (and how often do so for different values of the remaining nodes). In particular, out of the three rules that we study here, the most complex one is the odd-even classifier ($R150$) whose output obviously depends on all input nodes, $R60$ is an intermediate case, while the less complex one is $R51$ whose output is the opposite of one particular input unit, being insensitive to the others. A more precise definition on how to quantify task complexity –unnecessary for our purposes here– is discussed in [29].



Rule 51			
i_1	i_2	i_3	OUT
0	0	0	1
0	0	1	1
0	1	0	0
0	1	1	0
1	0	0	1
1	0	1	1
1	1	0	0
1	1	1	0

Rule 60			
i_1	i_2	i_3	OUT
0	0	0	0
0	0	1	0
0	1	0	1
0	1	1	1
1	0	0	1
1	0	1	1
1	1	0	0
1	1	1	0

Rule 150			
i_1	i_2	i_3	OUT
0	0	0	0
0	0	1	1
0	1	0	1
0	1	1	0
1	0	0	1
1	0	1	0
1	1	0	0
1	1	1	1

Figure 5.3.2: The task to be learned can be codified in a “truth table”. Computational tasks in increasing order of complexity (R51, R60 and R150, respectively).

✱ **Network fitness.** The goal of the trained networks is to produce –for each specific input configuration i – a time-averaged value of the output state, $\langle \sigma_{\text{output}}(i) \rangle$, which is as close as possible to the desired output, $\sigma_{\text{output}}^*(i)$; the difference between these two values, $|\langle \sigma_{\text{output}}(i) \rangle - \langle \sigma_{\text{output}}^*(i) \rangle|$, –which is a real number– is a measure of the network performance, conditioned to a given input state. The overall *network fitness* is defined as the average of such difference for $I = 2^{n_{\text{input}}}$ inputs:

$$F = 1 - \frac{1}{I} \sum_{i=1}^I |\langle \sigma_{\text{output}}(i) \rangle - \langle \sigma_{\text{output}}^*(i) \rangle|. \quad (5.3.1)$$

✱ **Network training.** The network is trained to “learn” to produce the correct output when exposed to each of the $I = 2^{n_{\text{input}}}$ specific input states; i.e. the network learns the computational task as defined by a given truth table. To implement this, we sequentially expose the network to I randomly chosen inputs. The resulting random order of inputs can be viewed as a form of stochasticity, mimicking environmental variability. Moreover, the environment is assumed to change rapidly so that, in order to cope with that, networks are trained to reach the correct output within just $t_{\text{max}} = 10$ timesteps, after which the input is changed (while the network state is left unaltered). The first half of this time interval allows for the network to converge, while in the second half we measure the average state of the output node $\langle \sigma_{\text{output}} \rangle$ and compute the network fitness, F .

✖ **Network mutations.** Having established the fitness of a given network, M , we now allow it to “mutate” by rewiring some existing link –thus preserving its overall connectivity K – and generate a slightly modified network M' . Described in detail, the mutation process follows the succeeding scheme:

- i) Given a original network, M , we perform a rewiring, which consists in choosing a link (say from node i to node j), removing it, and introducing a new one (from i to j') assuming this one did not exist before (and keeping the topological constraints described above).
- ii) This change of the network topology, requires of some modifications in the random Boolean functions f_j and $f_{j'}$ (see Figure 5.3.3). For f_j one needs to eliminate the input σ_i ; thus f_j changes from being a function of $K_{\text{in}}(j)$ arguments to a function of $K_{\text{in}}(j) - 1$. The new function coincides with the original one fixing $\sigma_i = 0$, i.e. for the case when the driving node i was off. After this, each output in its table is chosen for mutation with probability $1/2$ and selects a new random value, defining the “mutated” Boolean function. Similarly, for node j' a new argument, σ_i , is introduced to the Boolean function $f_{j'}$: all values for $\sigma_i = 1$ (“on” i node) are assigned randomly, while for $\sigma_i = 0$ (the new input is off) we keep the preexisting Boolean-function values.
- iii) This whole rewiring process is performed the first time with prob. one; after that a second rewiring is attempted with prob. $1/2$; if it occurs, then a third one happens with prob. $1/3$ and so on, giving rise to a mutated network, M' . This allows for the possibility of large mutations, involving many re-wirings.

Observe that this “mutation process” keeps the out degree sequence, as well as the overall connectivity K fixed, so it can be understood as a sort of “micro-canonical ensemble” [10]. Note that this differs from previous studies [29] where the overall network connectivity is allowed to change along the evolutionary dynamics. Our approach permits us to analyze the network performance as a function of network connectivity.

	σ_{i_2}	$\overset{\times}{\sigma_{i_1}}$	σ_{i_0}	σ_{out}		σ_{i_2}	σ_{i_1}	σ_{i_0}	σ_{out}
0	0	0	0	0/ \square	0	0	0	0	0
1	0	0	1	1/ \square	1	0	0	1	1
$\times 2$	0	1	0	1	2	0	1	0	1
$\times 3$	0	1	1	0	3	0	1	1	0
4	1	0	0	1/ \square	4	1	0	0	\square
5	1	0	1	0/ \square	5	1	0	1	\square
$\times 6$	1	1	0	1	6	1	1	0	\square
$\times 7$	1	1	1	0	7	1	1	1	\square

(a) (b)

Figure 5.3.3: Examples of Boolean functions modification –initially with 3 inputs– by adding or removing an input node: (a) Link i_1 is removed (the connectivity K_{in} decreases from 3 to 2) the rows 2, 3, 6, and 7 (corresponding to $\sigma_{i_1} = 1$) are canceled out (marked with \times and reddish color); the outputs in rows 0, 1, 4, and 5 can be flipped with probability $p = 0.25$; (b) Addition of a new link corresponding to input i_2 (green color; K_{in} increases from 2 to 3): outputs for rows 4, 5, 6, and 7 are randomly chosen (represented as \square). Color code: white cells remain fixed, reddish ones are removed, and blueish ones involve a random choice.

✱ **Network evolution and convergence.** The network with the largest fitness value, between M and M' , is selected (while the original one is kept if the two fitnesses coincide). This mutation and selection process defines an *evolutionary time step* (to be distinguished from a time step of the dynamics; there is a factor $t_{max}I$ between both). The evolutionary process is iterated until F reaches its maximal possible value $F = 1$. Observe, however, as the I inputs are randomly chosen at each evolutionary step, observation of $F = 1$ at a given step does not necessarily imply $F = 1$ at successive time. Therefore, in order to impose that the network robustly “learns” the computational task, we continue to measure its fitness, when exposing it to a much large number of randomly chosen inputs ($100I$, instead of just I as in the fitness-computation Eq. (5.3.1)); if $F = 1$ all across this long checking time window, the network is classified as having learned. Otherwise, the mutation/selection process is restarted until an optimally performing network is found. The final number of evolutionary steps required to reach an optimal network is called convergence time, T .

✱ **Ensemble averages.** Keeping fixed specific values of the network size N and connectivity K , the previous evolutionary process is iterated a large number of times (typically from 10^3 to $5 \cdot 10^5$) giving rise to an ensemble of trained networks. The ensemble averaged convergence time, $\bar{T} = \bar{T}(N, K)$, is a proxy for the network performance: the best network ensemble is the one with the smallest

\bar{T} . In this set of networks –once they have been trained– we also measured the ensemble-average of the branching parameter, \bar{B} . In the approach [29], K is allowed to change during the evolutionary process; thus the fastest learning networks are selected for; instead, we explore different fixed- K ensembles and determine a posteriori which is the optimal one. Both approaches are obviously equivalent to determine the optimal connectivity K .

✖ **Dynamics under noisy conditions.** To investigate the effect of fluctuations in the system dynamics, we allow the dynamics to be exposed to noise. In particular, we consider that either

- i) with a small probability, η , nodes can invert their state every time they are updated (accounting for errors/fluctuations in gene expression levels) or
- ii) with some small probability, ξ , (which is proportional to the network connectivity) the network topology experiences a mutation process at each evolutionary step, and the mutated network is selected regardless of its fitness value (this describes physical damage in the network produced, for example, by the lack or excess of some regulatory factors).

For the sake of simplicity, we refer to the first possibility as “dynamical” noise and to the second one as “structural” noise.

In the former case, considering a general ER network with dynamical noise, (η , the probability of flip a node once its state is updated) the critical point can be analytically inferred. Let D the Hamming Distance between two networks, M and M' , where M' is identical to M but D nodes ($i = 1, 2, 3, \dots, D$) –being D small, $D \sim \frac{1}{N}$, to ensure that two perturbed nodes are not connected– have been flipped. The damage spreading process follows the equation,

$$\begin{aligned}
 & D(t + \frac{1}{N}) - D(t) \\
 = & D \left[\frac{K}{N} 2p(1-p)(1-2\eta) + \frac{2\eta K}{N} (1-2p(1-p)) - \frac{1}{N} (1-2\eta) \right] + \frac{2\eta}{N} (1-D) \\
 = & \frac{1}{N} [D(2kp(1-p) + 2\eta k(1-4(1-p))) - 1 + 2\eta] + 2\eta(1-D) \\
 =_{D=\frac{1}{N}} & \frac{1}{N} \left[\frac{1}{N} (2Kp(1-p) + 2\eta K(1-4(1-p))) - 1 + 2\eta \right] + 2\eta - \frac{2\eta}{N} \\
 = & \frac{1}{N} \left[\frac{k}{N} 2p(1-p) + 2\eta K(1-4(1-p)) - \frac{1}{N} + 2\eta \right] \quad (5.3.2)
 \end{aligned}$$

where the first term reflects the probability of choose a site pointed by a i perturbed site, changing its state and incrementing D in one unit with probability $\frac{k}{N} 2p(1-p)$ (and flipping it again with probability η in M and η in M').

The second term reflects the probability of choose a node pointed by a i perturbed site, that doesn't change its state –with probability $\frac{k}{N}(1 - 2p(1 - p))$ – without noise, but finally the node change the state with probability 2η . Last term reflects the probability of choose a i node and “save” it (each one with probability $\frac{1}{N}$) but, the node can be flipped again with probability 2η . Finally, it should be considered the probability of change a node that is not pointed by a i node (with probability 2η). So, by taking $D(t + \frac{1}{N}) = D(t)$,

$$K_c^{eff} = \frac{1 - 2\eta N}{2p(1 - p) + 2\eta(1 - 4(1 - p))} \quad (5.3.3)$$

In the particular case with $p = \frac{1}{2}$,

$$K_c^{eff} = K_c^{MF} - 2K_c^{MF}\eta N \quad (5.3.4)$$

However, if $p \neq \frac{1}{2}$, we can take the Taylor series expansion of η around $\eta = 0$,

$$K_c^{eff} = K_c^{MF} - 2K_c^{MF}\eta N - K_c^{MF}\frac{(1 - 2p)^2}{p(1 - p)}\eta \quad (5.3.5)$$

In Figure 5.3.4 we show the theoretical prediction and simulation of an ER network with noise and $p = \frac{1}{2}$, following the inferred Eq. (5.3.4).

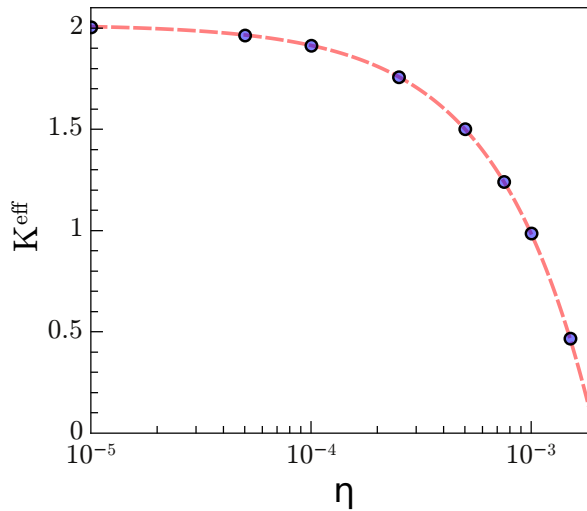


Figure 5.3.4: Effective critical point for an ER network of size $N = 256$ as function of the level of dynamical noise. Observe the excellent fit between the theoretical prediction (red dashed line) and computational prediction (blue points) of the critical point employing the Derrida curve method.

This result only shows the simple case between $D(t+1)$ and $D(t)$. But, what happens when the network go on S Monte Carlo steps? Taking, for simplicity, the usual case with $p = \frac{1}{2}$,

$$\dot{D} = D \left(\frac{K}{2N} - \frac{1}{N} \right) + \frac{2\eta}{N} \quad (5.3.6)$$

$$\begin{aligned} D(t+1) - D(t) &= D(t) \left(\frac{K}{2N} - \frac{1}{N} \right) + \frac{2\eta}{N} \\ D(t+1) &= D(t) \underbrace{\left[\frac{K}{2N} - \frac{1}{N} + 1 \right]}_{g(K)} + \underbrace{\left[\frac{2\eta}{N} \right]}_b \end{aligned} \quad (5.3.7)$$

Iterating,

$$\begin{aligned} D(t+S) &= D(0) [g(K)]^2 + \sum_{i=0}^{S-1} b g(K) = \\ &= D(0) [g(K)]^2 + b \frac{1 - [g(K)]^M}{1 - g(K)} \end{aligned} \quad (5.3.8)$$

And finally, take into account that –in the critical point– $D(t+S) = D(t) = D(0) = D^*$,

$$D^* = \frac{b}{1 - g(K)} = \frac{2\eta/N}{-\frac{K}{2N} + \frac{1}{N}} \xrightarrow{D^* = \frac{1}{N}} \frac{K}{2N} = \frac{1}{N} - 2\eta \quad (5.3.9)$$

$$K_c^{eff} = 2 - 4\eta N \quad (5.3.10)$$

which is the same previous result with $K_c^{MF} = 2$, i.e. with $p = \frac{1}{2}$.

Consequently, for further analysis, it should be noted that the critical point diminishes linearly with the level of noise and system size. However, take present that this effect is really insignificant for the size of networks discussed below (up to $N = 64$) (in the light of the Figure 5.3.4, that shows the critical connectivity for an ER with $N = 256$ nodes as function of the level of noise) and thus, the possible effects of the emergent sparsity should be carefully analyzed.

Emergent properties

5.4.1

Convergence times and phases of learning networks

Even in the absence of explicit noise sources, the dynamics based on asynchronous updating –which is the one we adopt here– has a stochastic component (i.e. nodes are updated in a random order), which could be more adequate to represent real genetic networks than synchronously updated RBNs as it avoids spurious effects associated with perfectly synchronous updating [30].

We consider a complex computational task –the odd-even classifier– and analyze networks of variable N and K . We let them evolve to learn this task and measure the average convergence time, \bar{T} , to do so (ensemble averages performed over up to $5 \cdot 10^5$ network realizations). Results are shown in Figure 5.4.1 for sizes from $N = 6$ to $N = 64$ as a function of the network connectivity K (from $K = 0.5$ to $K = 3.5$). First of all (upper Fig. 5.4.1B), observe that for all values of N , \bar{T} exhibits a characteristic (pseudo)parabolic shape with a minimum at some optimal connectivity value, K_T , at which networks learn the computational task in the fastest possible way. It is important to stress that networks with connectivities other than K_T also learn, even if after longer evolutionary times. In Fig. 5.4.1A the same data are represented, but rescaling \bar{T} for each N with its minimum, $\bar{T}_{\min}(N)$ (this is done to help the eye to compare the location of the different minima). In Fig. 5.4.1C we plot $|K_T - 2|$ as a function of N (blue squares); the value $K = 2$ corresponds to the usually accepted critical connectivity for RBNs in the infinite size limit. Observe that the optimal connectivities seem to converge to this value, $K = 2$, as a power-law function of N . The precision of our numerics does not allow us to discriminate if the convergence is exactly to $K = 2$ or to a nearby value (within 2.00 ± 0.05). In the same plot, we also present results for the branching parameter, \bar{B} (as defined above), for the same network ensembles. Importantly, \bar{B} is computed in the ensemble of networks that have learned –and not in the Erdős-Rényi ensemble– and Hamming distance measurements are restricted to the network core (excluding input nodes, which do not change in the course of the dynamics). In particular, dotted lines in Fig. 5.4.1A stand for measurements of \bar{B} , after perturbing nodes in the core, while dashed-dotted lines correspond to perturbations at input nodes. Observe that these two sets of curves exhibit qualitatively different behaviors.

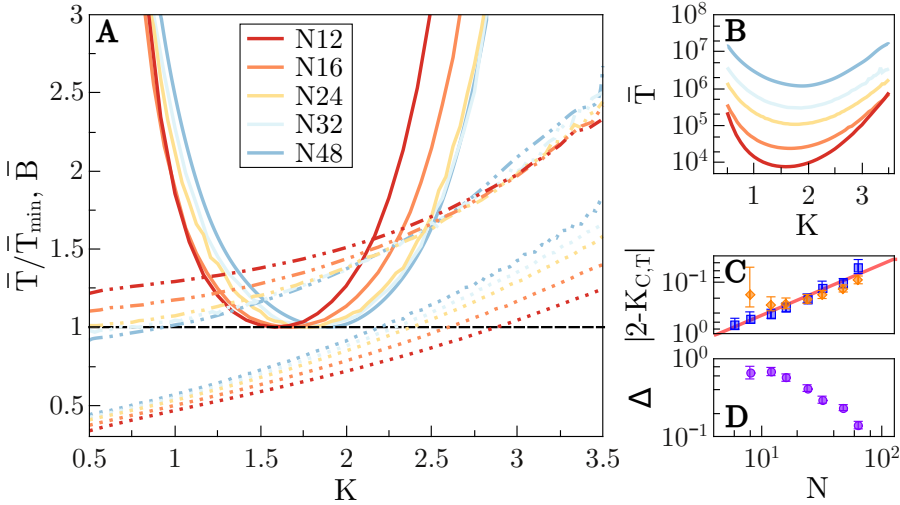


Figure 5.4.1: (A) Averaged convergence time, \bar{T} , divided by its minimum value \bar{T}_{\min} plotted as a function of the network connectivity K for different network sizes N (solid lines). Similarly, the non-normalized convergence times are plotted in (B). Discontinuous lines in (A) represent the value of the branching parameter, \bar{B} as measured in the network after the learning process is completed; dashed-dotted lines stand for \bar{B} averaged after perturbing only input nodes, while dotted lines have been obtained after perturbing nodes in the network core. Note that as \bar{T}/\bar{T}_{\min} and \bar{B} are both dimensionless quantities, they have been plotted in the same scale; the same color code has been used for all curves. (C) Scaling of the connectivity at which the minimum \bar{T} is obtained, K_T , as a function of N (blue squares), plotted together with the position of the critical point K_C as estimated from the condition $\bar{B} \approx 1$ (orange diamonds). In both cases, there is a convergence toward a value close to 2 in the large N limit (blue squares) (the red line is a guide to the eye and corresponds to a decay $\mathcal{O}(N^{-1})$ toward 2). (D) $\Delta = K_C - K_T$ plotted as a function of N showing explicitly that the distance to criticality diminishes with network size; i.e. the larger the network the closer to criticality the fastest learning networks.

We have chosen to present results in this way to stress the fact that –after learning– networks are not homogeneous, and not all nodes respond in the same way; in particular, the network is more responsive to input perturbations than to core ones. For example, networks with connectivity $K = 2$ are supercritical to input perturbations (fostering network sensitivity to external changes) and subcritical for core perturbations (as required for a robust convergence to the attractor/output).

To obtain the overall branching parameter \bar{B} (given N and K) –for all nodes in the network– we need to average these two contributions (weighted with $n_{\text{input}} = 3$ and $N - 3$ nodes, respectively). For these averaged curves (which are not explicitly shown in Fig. 5.4.1A for the sake of clarity) the crossing $B = 1$ indicates overall critical dynamics, and corresponds to a critical connectivity K_C . As shown in Fig. 5.4.1C (orange diamonds), K_C is larger than $K = 2$ and shifts toward lower connectivity values as N grows; indeed, its distance to $K = 2$ decreases with N , suggesting that learning networks have critical connectivity $K \approx 2$ (within our resolution) in the infinite size limit, as happens with random networks.

Moreover, we have measured the difference $\Delta = K_C - K_T$ to gauge how far optimal connectivities (in the sense of achieving the fastest possible learning) are from critical dynamics (in the sense of the branching parameter as close as possible to 1). As shown in Fig. 5.4.1D (magenta circles), Δ decreases monotonously upon increasing N , indicating that –for sufficiently large networks– the optimal connectivity is as close to criticality as desired, but for any finite size they are slightly subcritical ($\Delta > 0$). Thus optimal learning occurs for slightly subcritical networks, but as close as criticality as wanted for sufficiently large system sizes.

Figure 5.4.2A illustrates results for other, less complex (see above) computational tasks. As before, there is a well-defined minimum for \bar{T} in all cases, but these times are significantly shorter for lesser complex tasks. Observe also that for the simplest, *R51* rule, \bar{T} hardly depends on K (Fig. 5.4.2C), indicating that, as the task complexity decreases K progressively becomes a lesser relevant parameter. Observe also (Fig. 5.4.2D) that the distance of optimal networks to criticality, Δ , decreases with increasing network complexity. Therefore, it is reasonable to conjecture that for more complex tasks than the ones we considered (e.g. involving larger values of n_{input}), the benefits derived from operating at optimality/criticality are progressively more crucial.

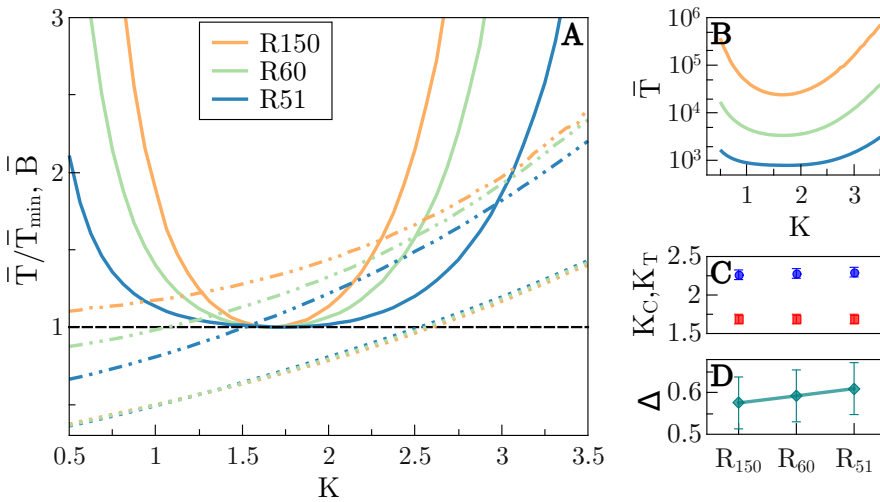


Figure 5.4.2: Figure analogous to Fig. 5.4.1, but obtained for different computational tasks of different complexity (from the most complex R_{150} to the intermediate R_{60} and the simplest R_{51} rule; the names come from Wolfram’s classification of cellular automata [62]). (A) \bar{T}/\bar{T}_{\min} for $N = 16$ (solid lines) and the 3 considered rules. Discontinuous lines are as in Fig. 5.4.1. (different colors stand for different rules). (B) Non-normalized \bar{T} for $N = 16$; the same color code has been used for all curves. (C) Optimal-time connectivities for fast learning, K_T (red squares) and critical connectivities K_C (blue circles) for the different rules. Observe that in all cases, optimal networks are slightly subcritical for this relatively small size $N = 16$. As shown in (D) the distance to criticality decreases upon increasing the task complexity.

Summing up, in order to achieve the fastest possible learning of complex tasks, RBNs with a connectivity such that their dynamics turns out to be critical (or slightly subcritical for finite sizes) are the best possible option.

The larger the network size and the more complex the task, the more convenient to be close to criticality.

5.4.2

Noisy conditions

5.4.2.1 Dynamical noise

Figure 5.4.3 is analogous to Figure 5.4.1 but has been obtained in the presence of dynamical noise, $\eta \neq 0$ (results for $\eta = 0$ are also plotted for the sake of comparison). Observe that we present results for a fixed size $N = 16$ and variable noise strengths (from $\eta = 10^{-5}$ to $\eta = 10^{-3}$).

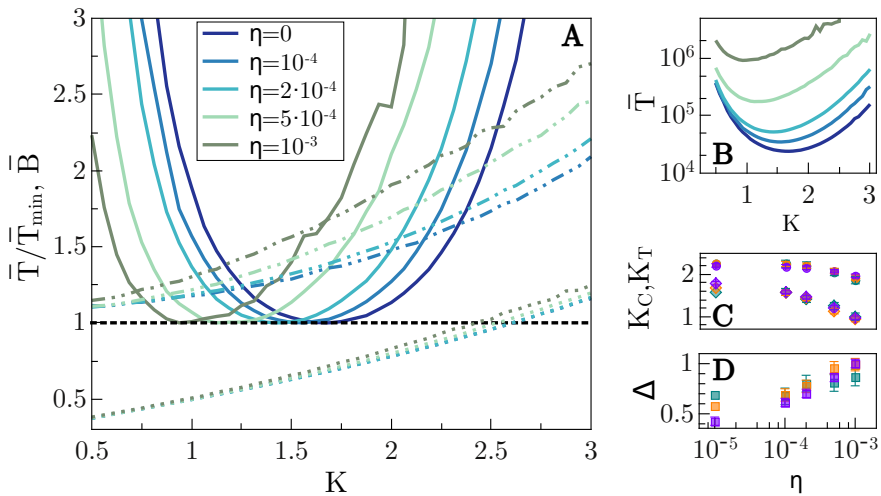


Figure 5.4.3: Figure analogous to Fig. 5.4.1 and Fig. 5.4.2 but for analyzing the dependence on the strength η of the dynamical noise. (A) \bar{T}/\bar{T}_{\min} for $N = 16$ (solid lines) as a function of K for different values of η (different colors). Discontinuous lines are as in Figs. 5.4.1 and 5.4.2 (however, different colors stand now for different η values). (B) Non-normalized \bar{T} for $N = 16$; the same color-code has been used for all curves. (C) Optimal-time connectivities for fast learning, K_T , (diamonds) and critical connectivities K_C (circles) for the different values of η and various network sizes ($N = 12$ blue, $N = 16$ orange, $N = 24$ purple). In all cases, optimal networks are slightly subcritical for this relatively small sizes. However, in contrast with the noiseless cases above, here (D) the distance to criticality Δ does not decrease upon enlarging the size (except for exceedingly small noise strengths, e.g. 10^{-5} , for which noise effects are not visible in the time windows we consider) actually it remains almost constant or –for large values of η such as 10^{-3} – it grows with N , and in any case, it grows with the noise strength (same color code used in C and D).

It is noteworthy that for larger values of η (e.g. 0.01) the dynamics is so noisy that the probability for the networks –resulting out of the evolutionary process– to pass the robustness filter we have imposed (i.e. to have fitness $F = 1$ for $100I$ evolutionary steps) is exceedingly small. Therefore, networks do not achieve perfect learning in such extremely noise conditions. On the other hand, for exceedingly small noise strengths, we essentially see the same results as for $\eta = 0$, within the simulation checking time windows we consider. For intermediate noise-strength levels (such as the ones reported in Fig. 5.4.3) networks are more likely to pass the filter. In such cases, (see Fig. 5.4.3B), the optimal connectivity is observed to shift toward lower values of K as the noise level is increased (see also Fig. 5.4.3C where K_T is plotted as a function of η for various system sizes). In parallel, the convergence times, \bar{T} (Fig. 5.4.3B), also grow with noise.

On the other hand, the branching parameter measured by perturbing core nodes does not show a strong dependence on η (see dotted lines in Fig. 5.4.3A) while the values of \bar{B} obtained by perturbing just the inputs (dashed-dotted lines in Fig. 5.4.3A) are more severely affected. The resulting critical points obtained by averaging these two contributions are plotted in Fig. 5.4.3C, and always close to $K = 2$ (for the considered sizes). Comparing these values with the optimal connectivities for learning, i.e. measuring, $\Delta = K_C - K_T$, one observes (see Fig. 5.4.3D) that Δ increases monotonously with η . This occurs for the different system sizes we studied allowing us to conclude that

it takes longer to learn in more noisy conditions and that the larger the dynamical-noise strength the more subcritical the optimal networks.

5.4.2.2 Structural noise

Figure 5.4.4 shows results analogous to those in Fig. 5.4.3. We present results for a fixed size $N = 16$ and variable noise strengths (from $\xi = 10^{-3}$ to $\xi = 10^{-2}$). In parallel with the site-noise case, there is a noise intensity threshold above which the mutation probability is exceedingly high for the networks to learn, while for too small strengths, the same results as for $\xi = 0$ are observed within the operational checking time windows we have. For intermediate noise amplitudes, the larger ξ the longer the learning process takes (see Fig. 5.4.4B). In these cases, the optimal connectivity is observed to shift toward lower values of K as the noise level is increased (see Fig. 5.4.4D where K_T is plot as a function of ξ). Also, as above, the branching parameter, \bar{B} does not have a strong dependence on ξ (Fig. 5.4.4A). The associated critical point K_C is slightly above $K = 2$ for small noises, and moves progressively to smaller connectivity values as ξ grows.

Also, as in the previous case, Δ increases monotonously with η , so that, as above,

we can safely conclude that, in general, the larger the structural noise strength the more subcritical the optimal networks.

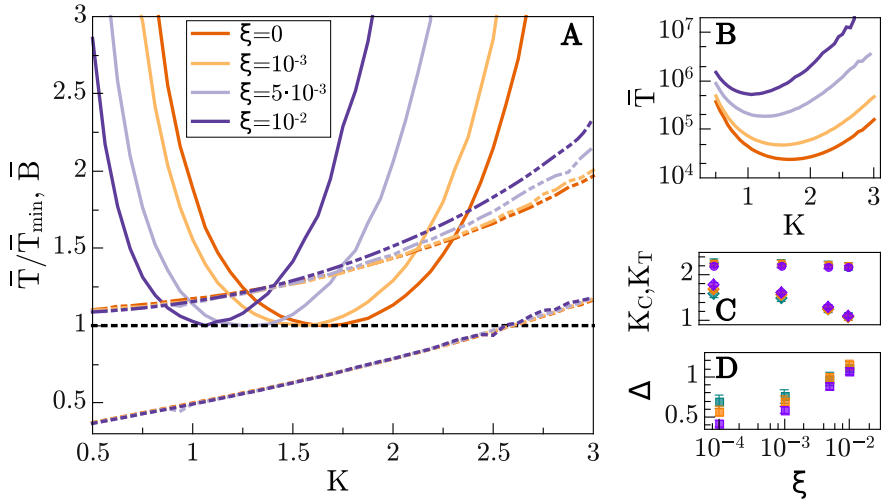


Figure 5.4.4: Figure analogous to Fig. 5.4.3. but analyzing the dependence on the strength ξ of the structural noise. (A) \bar{T}/\bar{T}_{\min} for $N = 16$ (solid lines) as a function of K for different values of ξ (different colors). Discontinuous lines are as in Fig. 5.4.3. (different colors stand now for different ξ values). (B) Non-normalized \bar{T} for $N = 16$ (C) Optimal-time connectivities for fast learning, K_T (diamonds) and critical connectivities K_C (circles) for the different values of ξ and various network sizes ($N = 12$ blue, $N = 16$ orange, $N = 24$ purple). Observe that in all cases, optimal networks are slightly subcritical for this relatively small sizes. However, in contrast with the noiseless cases above, and in parallel with the case of dynamical noise, here (D) the distance to criticality Δ does not decrease upon enlarging the size (except for extremely low values of the noise, as in Fig.5.4.3), actually it remains almost constant and, in any case, it grows with the noise strength. Same color code used in C and D.

Summing up, we conclude that while in the case of noiseless dynamics the optimal solution –to achieve the fastest possible learning– is obtained at connectivities for which the network is about critical (actually slightly subcritical, but closer and closer to criticality as the network size and/or the complexity of the task are increased), the situation is different in the presence of additional stochasticity, be it dynamical or structural noise. Under noisy conditions, the optimal solutions lie clearly well within the ordered/subcritical phase. A straightforward interpretation of this result is that the network dynamics needs to compensate for the excess of noise, and does so by reducing its internal level of uncertainty, i.e. by shifting deep into the ordered/subcritical phase.

5.4.3

Empirical networks

We have collected a set of empirical data from the literature and compiled a set of real directed networks. This includes public empirical datasets with biological genetic regulatory networks [57], and networks of metabolic interactions [24]. Specific examples of networks collected from the literature are the metabolic networks of *C.reinhardtii* ($K = 2.05$) [14]), and *B.subtilis* ($K = 1.03$) [47], and the gene regulatory networks of *E.coli* ($K = 1.24$, $K = 2.32$) [7, 49], *A.thaliana* ($K = 2.755$) [44], *M.tuberculosis* ($K = 1.19$, $K = 1.98$) [8, 51], *P.aeruginosa* ($K = 1.48$) [26], and *S.cerevisiae* ($K = 1.85$) [32]. Figure 5.4.5 presents a scatter plot of all networks in our dataset, representing the averaged connectivity K and network size N of each one. As it can be seen, the averaged connectivity of this dataset is well below the value $K = 2$, the critical connectivity for large random networks, suggesting that they could operate in subcritical regimes. It is noteworthy that it has been suggested that some empirical networks with high connectivity values (such as some of the outliers in Fig. 5.4.5) might result from systematic errors in correlation analyses (giving rise to false positives) [41].

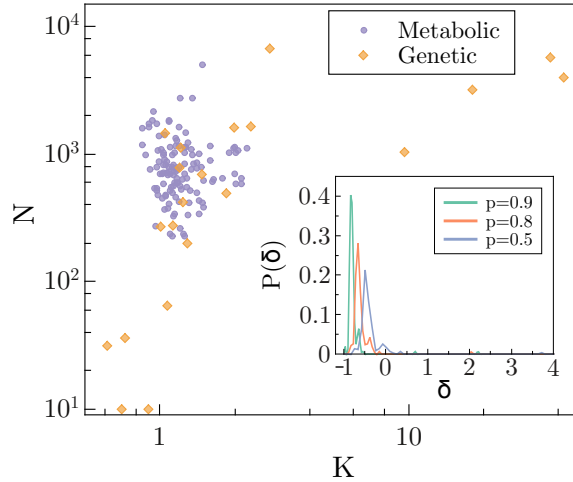


Figure 5.4.5: Size N versus mean connectivity K for empirical biological networks of different types. In particular, it includes genetic and metabolic networks of species such as *Escherichia coli*, *Saccharomyces cerevisiae*, *Pseudomonas aeruginosa*, *Bacillus subtilis*, etc. Observe that all networks are significantly sparse, with most mean connectivities lying between $K = 1$ and $K = 2$. The outliers, with $K > 10$ come all from BioGRID [57]; the most extreme case has $K = 41.90$ and corresponds to the genetic network of “*Escherichia coli K-12 W3110*” (but, it might be that these networks are plagued with false-positive connections [41]). In the inset, we plot the probability that a network from our empirical ensemble is at a certain relative distance to the critical point of a random Boolean model with its corresponding connectivity, i.e. $\delta = (K - K_c(p))/K_c(p)$, assuming a fixed value of the bias p (in particular, we show results for $p = 1/2$, $p = 0.8$ and 0.9); observe that regardless of the value of the considered bias (which in general is unknown to us) most of the networks lie within the subcritical regime (assuming their dynamics was random).

Being more precise –given the absence of knowledge on dynamical aspects of the specific dynamics of each empirical network– it is not possible to properly ascertain the dynamical state (critical or not) of each of them. For instance, in random Boolean networks the critical point is located as discussed above at $K_C = \frac{1}{2p(1-p)}$ [4, 20, 31]; thus the minimal possible critical connectivity is $K = 2$ (corresponding to the unbiased case $p = 1/2$). Note that for finite random networks, the critical connectivity shifts to values slightly larger than 2 (positive corrections of order N^{-1}). Therefore, if the collected (finite) empirical network obeyed random Boolean dynamics –at the light of Figure 5.4.5– almost all of them would be certainly subcritical. However, we know that the dynamics of real

networks may involve, for instance, canalizing updating functions and for such networks the critical connectivity can be smaller than $K = 2$ [20]. Therefore, even if no definite conclusion can be extracted from these empirical data about the possible criticality (or absence of it), we can certainly conclude that empirical networks are quite sparse (significantly sparser than critical random networks) suggesting that –in the absence of further information about their dynamics– the most likely scenario would be that they operate in ordered regimes (however, see below for a critical discussion).

Conclusions

The hypothesis that living systems may operate in the vicinity of critical points of their internal dynamics has inspired and tantalized scientists for some time. In particular, it has been claimed that genetic regulatory networks might operate close to criticality, achieving in this way an optimal balance between sensitivity to signals and stability to noise, and/or between adaptability and robustness on large evolutionary scales. A few works have recently explored different mechanisms allowing for network to self-organize or evolve to critical or quasi-critical dynamics.

Here –inspired by the set up proposed by Goudarzi et al. [29]– we have shown that random Boolean network models that are trained to perform a given computational task, can learn it much faster if they have a connectivity K such that they are close to criticality, as defined by a marginal averaged propagation of perturbations. This does not mean that networks far from criticality cannot learn; indeed they do, but it takes much longer to do so. Two important differences between the present work and previous ones are as follows. First, we work with networks with constant connectivity, i.e. the allowed mutations keep K constant, while in [29] there is no such a constraint. These makes that the evolutionary process implemented there converge directly to the optimal connectivity K_T , as the fastest learning networks, have sooner large fitness value and are this selected for. On the other hand, by studying the constant-connectivity ensemble, we are able to put forward that learning is compatible with rather diverse connectivity patterns, compatible with the network being critical, subcritical or supercritical. The second important difference is that we implement a stochastic updating scheme, which introduces stochasticity in the dynamics; we find, however, that results are mostly insensitive to this change. Moreover, we have seen that in all cases, the distance to criticality of the optimal-connectivity networks diminishes monotonously upon enlarging system size and upon enlarging the task complexity. Indeed, very simple tasks, establishing simple relationships between (a few) inputs and the output, can be readily learned by networks in the ordered/subcritical regime, where such a direct correspondence can be robustly realized. On the other hand, complex tasks, in which the output is sensitive to many different possible changes in the input nodes, requires of much larger responsiveness/susceptibility, and thus, shift the network optimal connectivity toward larger values, closer and closer to criticality. In any case, we do not find under any circumstances the optimal connectivity to lie within

the disordered/supercritical regime; it seems as if the requirement to learn a task was incompatible with the network being disordered.

Biological systems must have homeostasis, i.e. the capacity to maintain their internal conditions even in the presence of fluctuations and noise, be it internal or external. In the second part of our study posed ourself the question of how do these results depend upon the explicit introduction of noise. To this end, we have introduced more extreme forms of noise, be it dynamical or structural, within the same RBN model.

Dynamical noise allows network nodes to invert their dynamical state with a small probability each time they are updated, introducing perturbations that can potentially propagate through the system, compromising the network performance. Similarly, structural noise, implying that the network topology itself is exposed to random changes with some small probability, also producing potential damage in the learned patterns. Both of these noise sources have clear correspondence with stochastic effects in real biological networks. In both cases, there is a threshold in noise strength above which networks do not learn the computational task in a reliable and robust way; i.e. they end up being plagued with errors, hindering network learning. Such thresholds clearly depend on the criterion imposed to declare that networks have learned; put differently, if the time in which one checks for network robustness are increased, i.e. if the criterion becomes more stringent, the noise-strength thresholds diminish. Remarkably, in both of the cases, dynamical and structural noise, we find that the optimal connectivity to achieve the fastest possible learning lies deep-inside the subcritical region, far away from criticality, and the distance to criticality increases upon enlarging the noise strength and does not diminish upon increasing the system size (as happens in the absence of explicit noise).

Our results suggest that real biological networks, in order to perform the complex tasks required for information processing and survival in a noisy world, should operate in sub-critical regimes rather than in critical ones as it has been argued. As a matter of fact, the collection of empirical (genetic and metabolic) networks that we have compiled from the recent literature shows a rather sparse averaged connectivity in most cases, with only a few outlier networks. If the dynamics underlying these networks could be modeled by random Boolean functions, one could safely conclude that they are typically subcritical. However, in most cases, the dynamics remains mostly unknown, and a clear cut conclusion about the dynamical state of each specific network instance cannot be derived. To fill this gap, recent analyses have employed high throughput data from hundreds of microarray experiments to infer regulatory interactions among genes. This type of approach leads to more detailed information on dynamical aspects (e.g. switching off a given gene it is possible to follow the cascade of modifications it generates through the whole network). The resulting data, implemented into Boolean models, seem to support the hypothesis that regulatory networks

for a number of species (*S. cerevisiae*, *E. coli*, etc) are close to criticality [9, 46], but some other analyses leave the door open for the networks to operate in an ordered/subcritical phase [37, 55]. Therefore, given the present state of affairs, one can only conclude that more accurate and extensive experimental approaches would be extremely valuable to shed further light on this fascinating problem.

An important observation to be made is that the tasks we have employed to be learned are relatively simple (as they only involve a maximum of 3 input nodes and a single readout). Thus, one can wonder what would happen if a more extensive use of the network potentiality was necessary (by employing for instance, two or more tasks simultaneously, of involving a much larger number of inputs in each single task).

Following our results for the noiseless case –where we found that upon considering far more complex tasks, involving many more input and output nodes, the dynamics becomes progressively more critical– it would not be surprising that if one could analyze much more complex tasks –as the ones probably controlling real biological networks– the dynamics could become closer to criticality even in the presence of noise. Furthermore, in such more complex cases, one should also relax the criterion to declare that networks have learned, and look for “fuzzy” types of learning (i.e. accept networks with fitnesses slightly smaller than one). The combination of much more complex rules together with less rigid criteria for learning, could very likely shift the optimal solutions toward more critical states. A detailed analysis of these issues is left as an open challenge for future analyses.

It is also noteworthy that –even if network topology is known to play a very important role in the outcome of RBNs [2, 3, 21, 41, 56, 59], here we have focused mostly on random Erdős-Rényi networks and left the analysis of important topological features of empirical networks –such as scale-free connectivity distributions, and hierarchical and modular organization– for future work. These aspects might also play an important role in determining the network dynamical state. Finally, we also plan to extend the studies beyond the limit of the Boolean approach and to implement more complex and biologically realistic tasks. Our summary, of the obtained results is that the criticality hypothesis remains as a valid and fascinating possibility, but that it needs to be critically evaluated under each set of specific circumstances, avoiding making exceedingly general claims.

References

- [1] ALBERT, R. & OTHMER, H. G. «The topology of the regulatory interactions predicts the expression pattern of the segment polarity genes in *drosophila melanogaster*». *J. Theor. Biol.* **223**, 1–18 (2003).
- [2] ALDANA, M. «Boolean dynamics of networks with scale-free topology». *Physica D* **185**, 45–66 (2003).
- [3] ALDANA, M., BALLEZA, E., KAUFFMAN, S. & RESENDIZ, O. «Robustness and evolvability in genetic regulatory networks». *J. Theor. Biol.* **245**, 433–448 (2007).
- [4] ALDANA, M., COPPERSMITH, S. & KADANOFF, L. P. «Perspectives and problems in nonlinear science». 23–89 (Springer-Verlag, New York, 2003).
- [5] ALON, U. *An introduction to systems biology: design principles of biological circuits* (CRC press, London, 2006).
- [6] BALÁZSI, G., VAN OUDENAARDEN, A. & COLLINS, J. J. «Cellular decision making and biological noise: from microbes to mammals». *Cell* **144**, 910–925 (2011).
- [7] BALÁZSI, G., BARABÁSI, A.-L. & OLTVAI, Z. N. «Topological units of environmental signal processing in the transcriptional regulatory network of *escherichia coli*». *Proc. Natl. Acad. Sci. USA* **102**, 7841–7846 (2005).
- [8] BALÁZSI, G., HEATH, A. P., SHI, L. & GENNARO, M. L. «The temporal response of the mycobacterium tuberculosis gene regulatory network during growth arrest». *Mol. Sys. Biol.* **4** (2008).
- [9] BALLEZA, E. *et al.* «Critical dynamics in genetic regulatory networks: examples from four kingdoms». *PLoS One* **3**, e2456 (2008).
- [10] BEN-NAIM, E., FRAUENFELDER, H. & TOROCZKAI, Z. *Complex networks*, vol. 650 (Springer, Berlin Heidelberg, 2004).
- [11] BERTSCHINGER, N. & NATSCHLAGER, T. «Real-time computation at the edge of chaos in recurrent neural networks». *Neural Comput.* **16**, 1413–1436 (2004).
- [12] BORNHOLDT, S. «Less is more in modeling large genetic networks». *Science* **310**, 449 (2005).
- [13] BUCHANAN, M. *Networks in cell biology* (Cambridge University Press, Cambridge, 2010).

-
- [14] CHANG, R. L. *et al.* «Metabolic network reconstruction of chlamydomonas offers insight into light-driven algal metabolism». *Mol. Sys. Biol.* **7**, 518 (2011).
- [15] CHATÉ, H. & MUÑOZ, M. «Insect swarms go critical». *Physics* **7**, 120 (2014).
- [16] CRICK, F. «Central dogma of molecular biology». *Nature* **227**, 561–563 (1970).
- [17] DARABOS, C., TOMASSINI, M. & GIACOBINI, M. «Dynamics of unperturbed and noisy generalized boolean networks». *J. Theor. Biol.* **260**, 531–544 (2009).
- [18] DE JONG, H. «Modeling and simulation of genetic regulatory systems: a literature review». *J. Comp. Biol.* **9**, 67–103 (2002).
- [19] DERRIDA, B. & POMEAU, Y. «Random networks of automata: a simple annealed approximation». *Europhys. Lett.* **1**, 45 (1986).
- [20] DROSSEL, B. «Random boolean networks». In SCHUSTER, H. G. (ed.) *Reviews of nonlinear dynamics and complexity*, vol. 1, chap. 3, 69–110 (Wiley VCH, Weinheim, 2008).
- [21] DROSSEL, B. & GREIL, F. «Critical boolean networks with scale-free in-degree distribution». *Phys. Rev. E* **80**, 026102 (2009).
- [22] ELДАР, A. & ELOWITZ, M. B. «Functional roles for noise in genetic circuits». *Nature* **467**, 167–173 (2010).
- [23] ELOWITZ, M. B., LEVINE, A. J., SIGGIA, E. D. & SWAIN, P. S. «Stochastic gene expression in a single cell». *Science* **297**, 1183–1186 (2002).
- [24] FEIST, A. M., HERRGÅRD, M. J., THIELE, I., REED, J. L. & PALSSON, B. Ø. «Reconstruction of biochemical networks in microorganisms». *Nat. Rev. Microbiol.* **7**, 129–143 (2009).
- [25] FURUSAWA, C. & KANEKO, K. «Adaptation to optimal cell growth through self-organized criticality». *Phys. Rev. Lett.* **108**, 208103 (2012).
- [26] GALÁN-VÁSQUEZ, E., LUNA, B. & MARTÍNEZ-ANTONIO, A. «The regulatory network of pseudomonas aeruginosa». *Microb. Inform. Exp.* **1**, 3–3 (2011).
- [27] GAMA-CASTRO, S. *et al.* «Regulondb version 9.0: high-level integration of gene regulation, coexpression, motif clustering and beyond». *Nucleic Acids Res.* **44**, D133–D143 (2015).

- [28] GERSHENSON, C. «Proceedings of the eighth international conference on artificial life». 1–8 (The MIT Press, Cambridge, 2002).
- [29] GOUDARZI, A., TEUSCHER, C., GULBAHCE, N. & ROHLF, T. «Emergent criticality through adaptive information processing in boolean networks». *Phys. Rev. Lett.* **108**, 128702 (2012).
- [30] GREIL, F. & DROSSEL, B. «Dynamics of critical kauffman networks under asynchronous stochastic update». *Phys. Rev. Lett.* **95**, 048701 (2005).
- [31] GROS, C. *Random Boolean networks* (Springer, Berlin Heidelberg, 2011).
- [32] GUELZIM, N., BOTTANI, S., BOURGINE, P. & KÉPÈS, F. «Topological and causal structure of the yeast transcriptional regulatory network». *Nat. Genet.* **31**, 60–63 (2002).
- [33] GUPTASARMA, P. «Does replication-induced transcription regulate synthesis of the myriad low copy number proteins of escherichia coli?». *Bioessays* **17**, 987–997 (1995).
- [34] HIDALGO, J. *et al.* «Information-based fitness and the emergence of criticality in living systems». *Proc. Natl. Acad. Sci. USA* **111**, 10095–10100 (2014).
- [35] KAUFFMAN, S. «Metabolic stability and epigenesis in randomly constructed genetic nets». *J. Theor. Biol.* **22**, 437–467 (1969).
- [36] KAUFFMAN, S. A. *The origins of order: Self-organization and selection in evolution* (Oxford university press, New York, 1993).
- [37] KAUFFMAN, S., PETERSON, C., SAMUELSSON, B. & TROEIN, C. «Random boolean network models and the yeast transcriptional network». *Proc. Natl. Acad. Sci. USA* **100**, 14796–14799 (2003).
- [38] KINOUCHI, O. & COPELLI, M. «Optimal dynamical range of excitable networks at criticality». *Nat. Phys.* **2**, 348–351 (2006).
- [39] KRAWITZ, P. & SHMULEVICH, I. «Basin entropy in boolean network ensembles». *Phys. Rev. Lett.* **98**, 158701 (2007).
- [40] LANGTON, C. G. «Computation at the edge of chaos: phase transitions and emergent computation». *Physica D* **42**, 12–37 (1990).
- [41] LECLERC, R. D. «Survival of the sparsest: robust gene networks are parsimonious». *Mol. Sys. Biol.* **4** (2008).

-
- [42] LI, F., LONG, T., LU, Y., OUYANG, Q. & TANG, C. «The yeast cell-cycle network is robustly designed». *Proc. Natl. Acad. Sci. USA* **101**, 4781–4786 (2004).
- [43] LOSICK, R. & DESPLAN, C. «Stochasticity and cell fate». *Science* **320**, 65–68 (2008).
- [44] MA, S., GONG, Q. & BOHNERT, H. J. «An arabidopsis gene network based on the graphical gaussian model». *Genome Res.* **17**, 1614–1625 (2007).
- [45] MAASS, W., NATSCHLÄGER, T. & MARKRAM, H. «Real-time computing without stable states: A new framework for neural computation based on perturbations». *Neural Comput.* **14**, 2531–2560 (2002).
- [46] NYKTER, M. *et al.* «Gene expression dynamics in the macrophage exhibit criticality». *Proc. Natl. Acad. Sci. USA* **105**, 1897–1900 (2008).
- [47] OH, Y.-K., PALSSON, B. O., PARK, S. M., SCHILLING, C. H. & MAHADEVAN, R. «Genome-scale reconstruction of metabolic network in bacillus subtilis based on high-throughput phenotyping and gene essentiality data». *J. Biol. Chem.* **282**, 28791–28799 (2007).
- [48] PARFITT, D.-E. & SHEN, M. M. «From blastocyst to gastrula: gene regulatory networks of embryonic stem cells and early mouse embryogenesis». *Phil. Trans. R. Soc. B* **369**, 20130542 (2014).
- [49] PEIXOTO, T. P. «Emergence of robustness against noise: A structural phase transition in evolved models of gene regulatory networks». *Phys. Rev. E* **85**, 041908 (2012).
- [50] RIBEIRO, A. S., KAUFFMAN, S. A., LLOYD-PRICE, J., SAMUELSSON, B. & SOCOLAR, J. E. «Mutual information in random boolean models of regulatory networks». *Phys. Rev. E* **77**, 011901 (2008).
- [51] SANZ, J. *et al.* «The transcriptional regulatory network of mycobacterium tuberculosis». *PLoS One* **6**, e22178 (2011).
- [52] SCHMAL, C., PEIXOTO, T. P. & DROSSEL, B. «Boolean networks with robust and reliable trajectories». *New J. Phys.* **12**, 113054 (2010).
- [53] SCHWIKOWSKI, B., UETZ, P. & FIELDS, S. «A network of protein–protein interactions in yeast». *Nat. Biotechnol.* **18**, 1257–1261 (2000).
- [54] SHEW, W. L. & PLENZ, D. «The functional benefits of criticality in the cortex». *Neuroscientist* **19**, 88–100 (2013).

- [55] SHMULEVICH, I., KAUFFMAN, S. A. & ALDANA, M. «Eukaryotic cells are dynamically ordered or critical but not chaotic». *Proc. Natl. Acad. Sci. USA* **102**, 13439–13444 (2005).
- [56] SOSA, C. T., HUANG, S. & ALDANA, M. «Criticality is an emergent property of genetic networks that exhibit evolvability». *PLoS Comp. Biol.* **8**, e1002669 (2012).
- [57] STARK, C. *et al.* «Biogrid: a general repository for interaction datasets». *Nucleic Acids Res.* **34**, D535–D539 (2006).
- [58] STERN, M. D. «Emergence of homeostasis and “noise imprinting” in an evolution model». *Proc. Natl. Acad. Sci. USA* **96**, 10746–10751 (1999).
- [59] SZEJKA, A. & DROSSEL, B. «Evolution of boolean networks under selection for a robust response to external inputs yields an extensive neutral space». *Phys. Rev. E* **81**, 021908 (2010).
- [60] TKAČIK, G. & WALCZAK, A. M. «Information transmission in genetic regulatory networks: a review». *J. Phys. Condens. Mat.* **23**, 153102 (2011).
- [61] TORRES-SOSA, C., HUANG, S. & ALDANA, M. «Criticality is an emergent property of genetic networks that exhibit evolvability». *PLoS Comp. Biol.* **8**, e1002669 (2012).
- [62] WOLFRAM, S. *A new kind of science*, vol. 5 (Wolfram media, Champaign, 2002).

Emergence of universal topological features: from gene regulatory to Linux modular networks

6.1	Introduction	203
6.2	Debian as “mirror” model	206
6.2.1	Evolutionary process of Debian networks	208
6.2.2	Network information and the size of packages.	214
6.3	Conclusions	217
	References	221

6.1 Introduction

*“An infinite number of monkeys
typing into GNU emacs would never
make a good program.”*

Linus Torvalds

Large-scale DNA-sequencing techniques and proteomics methods have allowed to dissect and understand deeply the basic components –genes and proteins– of the cellular processes. Nevertheless, each cell is an integrated device conformed by large amounts of interacting genes, proteins and metabolites. Thus, in order to understand the emergent properties of cellular function we must allow for a global outlook, rather than the study of its isolated individual components and interactions [4, 48]. But even so, together with the dynamics of the system, i.e. its temporal behavior, the study of synthetic biology is of particular interest, at it requires the comprehension of the structure of the system, i.e. the interactions and biochemical pathways that took place there in, as well as the understanding of their effect in the emergent properties of the cell function [30, 31].

Recently, interesting gene knock-out experiments (silencing individual genes and following the cascade of differences between two replicas) have allowed to highlight some types of “avalanches”, representing cascading failures, that were reported to follow a power law size distribution. For example, on those gene knock-out experiments, the total number of affected genes [42], as well as the number of affected metabolite ions [18], seems to decay with an exponent compatible with $\tau = 3/2$ entailing the possibility of collective effects of a host of units acting at unison.

On the basis of a reductionist position, the central dogma of molecular biology states that each isolated gene, which constitute the basic unit of heredity, is transcribed into RNA, which, in turn, is translated into a protein, which can regulate the expression of other genes, usually inter-related with other proteins conforming a complex network of regulatory interactions [12] entailing causal topological relations and the transfer of sequential information between such genes. Thereby, genetic regulation, protein-protein interactions, as well as cell metabolic and signaling pathways are essential biological processes that can all be represented as (directed) networks [10].

Many biological and real data have been represented by networks for some time now. For example, this approach has pervaded other fields like neuroscience

[23], ecological [44], epidemic networks [40], among many examples [37] and, specifically, those in which we are interested, gene-regulatory, protein-protein and metabolic networks [7, 26]. Thus, the complexity of cellular processes is depicted in such networks providing a systems-perspective approach to extremely complicated biological problems. In fact, the study of information processing in living systems has benefited from the complex perspective rather than the analysis of single pathways, providing a richer understanding through the emergent collective phenomena from a large number of basic inter-related units.

In particular, an important progress to understand the cell regulatory mechanisms was the discovery of the scale-free structure of most of the internal networks of the cell such as metabolic, protein-protein or gene-regulatory networks [7]. However, there also exists networks within the cell that are not scale-free. For instance, most of the genetic networks shows a mixed scale-free and exponential structure for the outgoing distribution (indicating the number of regulated genes) and the ingoing distribution (indicating the number of interacting genes and entailing a finite capacity of information processing), respectively. Most networks within the cell shows further properties such as a small-world effect (arising from the small average path length), a highly modular structure and an outstanding response to external stimuli, as well as dynamical and structural robustness [7].

On the other hand, the pioneering ideas of Kauffman [22, 27, 28], paved the way to the identification of cellular states as attractors of the dynamics of genetic regulatory systems, being modeled as random Boolean networks, in which the genes are the network nodes and the mutual regulatory interactions are described by direct links involving arbitrary random Boolean functions. Such simple setup has shed light on important conceptual problems such as the emergence of different phenotypes (or states) from a unique genetic network, the existence of transitions among them (as exemplified in cell differentiation and reprogramming), and the emergence of cycles in cell states. On this point, two real examples are the predicted expression patterns of the fly *Drosophila melanogaster* [2] and the yeast cell cycle [33].

In either case, it seems clear that gene-regulatory networks, composed by a large number of specific interactions, involve some type information transmission (or flow) encoded in mutual regulatory interactions, determining the cellular response to different stimuli [7, 45]. Thus, it is foreseeable that the analysis and study of interacting systems with such information flow can shed light onto the particular structure and emergent properties of genetic systems.

Nevertheless, all of the empirical founded networks, that have been generated over millions of year of evolution, can only reflect a static evolutionary stage. Thus, it would be interesting to identify and scrutinize some examples of how its dynamical evolution operates, as well as having certain synthetic self-organized networks able to reproduce some properties that of gene networks. For this

purpose, free software networks of packages, constituting a software ecosystem, are an excellent model for the study of the evolution of such systems, as highlighted in the recent literature [16, 17, 39, 46]. Such networks are composed by packages (acting as nodes and conforming the basic unit of software) that are inter-related due to the need to reuse code of others in order to work properly (the so-called dependencies; i.e. package i needs some neighbor packages to be functional). A crucial question in such systems is the convergence (or not) between the solutions found by software networks and real gene regulatory networks to achieve an optimal storage and transmission of information through the particular topology of the networks.

In this chapter, we first characterize the evolving structure of the network of dependencies between software packages in the different Debian GNU/Linux distributions released to date. After that, we explore the emergent properties and vulnerability of such networks and their role in the functionality of the system. In parallel, it is also interesting to see the parallelisms between the architecture and emergent properties of software networks and that of regulatory interactions between genes.

6.2

Debian as “mirror” model

Debian is an open-source operating system that has evolved –in a relatively short period of time– through the contribution of many developers, forming an intricate structure between a vast number of packages, which conform the basic unit of software in the whole operating system. Such packages must decrypt the information coming from another packages¹, in order to satisfy the so-called dependencies, i.e. pieces of software relying on another one.

Thus, each node represents a package whose dependence on certain (neighbor) nodes is symbolized by directed links [16]. One specific example, represented in Figure 6.2.1 and extracted from Buzz 1.1, shows different dependences between packages. In order to build such dependency network, in particular, we have employed the relationships between the binary *x86* packages included in Debian GNU/Linux from its beginning, for the available 14 distributions (from Buzz 1.1 to Stretch 9). However, for this purpose, beyond the dependencies, reflecting requirements, there exists additional relations between packages named conflicts, which reflect incompatibilities between them [24], that also needs to be considered.

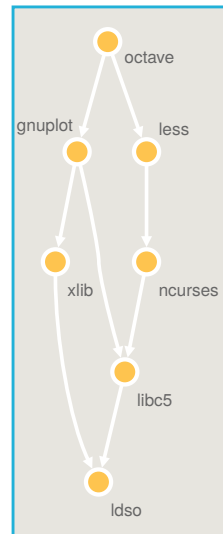


Figure 6.2.1: Subgraph showing particular dependences between packages from Buzz distribution

To fix this problem we must take into account a special type of package, called “*virtual*”, which provides functionalities in our network (e.g. both *firefox* and *konqueror* provide the same service, *www-browser*, if necessary). Interestingly, as explained in the Debian Policy Manual [25] conflicts are used (in many cases) to avoid duplications in virtual facilities of the system. So, in order to

¹It can be easily argued a shift in the links direction according to the interpretation, i.e. in terms of dependencies or information transmission.

exclude such duplications, we should only select a particular (random) choice of each “virtual” package, averaging over them, to explore the whole ensemble of networks. Now we can safely say that we have generated the Debian potential network indicating the requirements (or dependency network) between the different packages.

On the other hand, since its very beginnings, with the humble Buzz distribution with 486 packages, Debian has shown an spectacular (exponential) growth in the total number of packages conforming each stable distribution (as shown in Figure 6.2.2), until reach a surprisingly large number of packages ($\sim 4.9 \cdot 10^4$) in the last distribution, Stretch. One of our main purposes is to scrutinize the evolutionary process related to such growth, as well as the structural emergent properties (or those that already exist) of Debian networks.

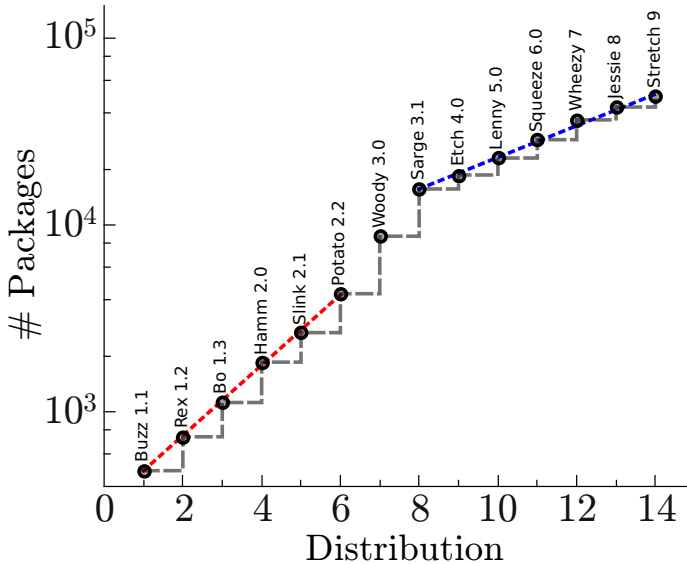


Figure 6.2.2: Evolution of the total number of packages represented on a logarithmic scale (vertical axis) for the different Debian distributions (horizontal axis). It follows an exponential growth appear, of the form $N(R) \propto e^{\frac{R}{\tau_i}}$, where N is the total number of packages, R is the release number of each distribution, and τ_i the particular growth rate. Two exponential growths, separated by Woody distribution can be appreciated with $\tau_1 = 2.306(1)$ and $\tau_2 = 5.132(1)$, respectively.

6.2.1

Evolutionary process of Debian networks

The selection between random choices of “virtual” packages is done over 10^4 realizations for every distribution, giving us the possibility of analyze, for now, the averaged incoming and outgoing degree distributions. As shown in Fig.6.2.3b and Fig.6.2.3c, the incoming cumulative degree distribution follows a power law, $P(k) \sim k^{-\alpha+1}$ with characteristic exponent α and the outgoing degree distribution fits very well to a stretched (or compressed) exponential², $P(k) \sim \exp(-(\frac{k}{\tau})^\beta)$ with characteristic exponent β .

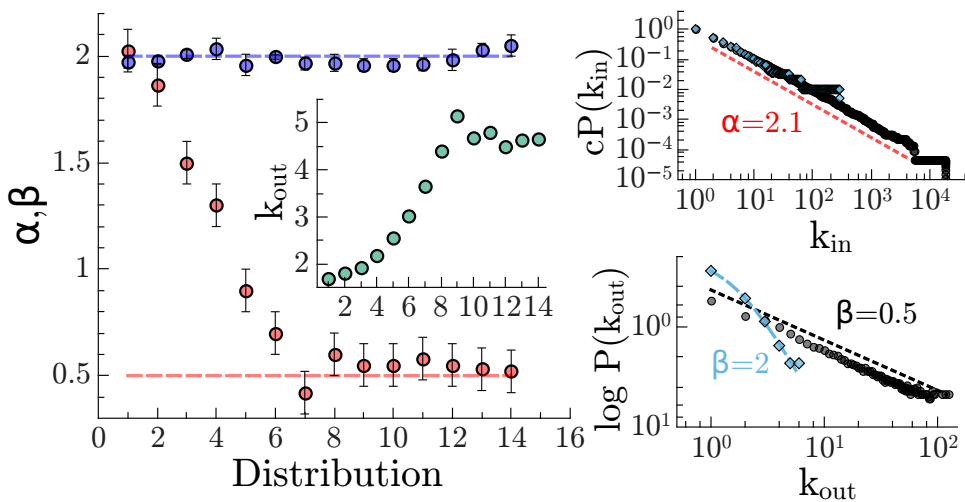


Figure 6.2.3: a) Exponent of the power law fit for the incoming degree distribution of dependencies (blue circles) and for the stretched exponential one (red circles). Inset: Mean out-degree for all distributions from Buzz to Stretch. b) Cumulative degree distribution for the incoming dependencies for the first distribution of Debian (Buzz) and for the last one (Stretch) in log-log scale and, c) logarithm of the degree distribution for the outgoing dependencies for the Buzz and Stretch distributions, showing a half-normal distribution decay ($\beta = 2$) for Buzz and a stretched exponential distribution ($\beta = 0.5$) for the stretched distribution.

In the evolutionary process of the Debian network, is expected some trend of both exponents, as reflected in Fig.6.2.3a. Observe that the incoming degree distribution has a stable behavior and its exponent remains very close to $\alpha = 2$

²We have employed a Levenberg–Marquardt algorithm to curve-fitting the cumulative distribution function in the power law case, $P(k) \sim k^{-\alpha}$, and the stretched exponential for the outgoing distribution, $P(k) \sim \exp(-(\frac{k}{\tau})^\beta)$.

for all distributions (blue points). However, the exponent of outgoing degree distribution – arising from a normal decay with $\beta = 2$ in Buzz – reaches a stationary state after the 8th distribution (Sarge) with $\beta \approx 0.5$ (red points). At last, we should ask ourselves what happens with the mean out-degree connectivity, $\langle k_{out} \rangle$, of the different networks. As can be seen in the inset of the Fig.6.2.3a, Debian software networks are very sparse networks, with $\langle k_{out} \rangle$ between 1.5 and 5. Also, it can be appreciated a sustained growth of the mean connectivity, a trend that leads to an apparent stationary state after 8th distribution with a mean out-connectivity between 4.5 – 5.

This features are very close to those observed for real gene-regulatory networks, which present an interesting (biological) example of mixed scale-free and exponential characteristics in the outgoing and incoming degree distributions with similar exponents [3, 10, 26], respectively. In the same way, they also are very sparse networks, with mean incoming connectivity (associated to the exponential distribution) around 1.5 – 3.5 in most of the cases, as outlined in Figure 5.4.5 of the previous chapter.

6.2.1.1 Emergence of a non-trivial structure

Even though the networks have a non-trivial scale-free structure, it is to be expected that the different functional areas play a key role in the evolutionary process. In all cases, the modular structure seems really significant, and the modularity index³ (Q , averaged over 10^4 realizations) grows continuously in the last six distributions (from 9th “Etch” and after, see blue points in Fig. 6.2.4a). Nevertheless, we should explore the possibility that such modularity can be an artifact of the degree sequence. For this, the network is “swapped” by changing links between random nodes under certain rules, giving us a randomized structure to compare. To that end, from the original degree sequence of a Debian network (D), we select a copy (D') and a swapping process is performed in this one to maintain both the ingoing and the outgoing connectivity unaltered. This swap of links cover the next steps:

- i) Select randomly a package A and one of its dependences a .
- ii) Select, all different, a random package B and one of its dependences b with the conditions: (i) A cannot depend on b and (ii) B cannot depend on a .
- iii) Swap both links, i.e. A depends on b and B depends on a .
- iv) Iterate the process until randomize the whole network.

³The measure of the modularity index (Q) is done through the Louvain method [9] on directed networks [14], and the average path length on the graph employing the *igraph R* package.[13]

Such “swapped” networks shows a sustained decrease of the modularity index until 7th-8th distributions “Woody” and “Sarge”, as shown in Fig. 6.2.4a (red points), and its standard deviation (σ) decrease monotonically with the system size (upper inset). In a different manner, the standard deviation of the original networks shows a pronounced peak around such distributions, suggesting a strong change in the network structure. At last, we have measured the Z-score of the modularity index⁴, in order to estimate the difference between modularity indexes regarding to the standard deviation of the ensemble of possible networks, a measure that shows a dramatic increase over time. As a corollary we can state categorically that the (emergent) modular structure plays an important role in the development of software networks and that not a simple artifact of the particular degree distribution of the networks.

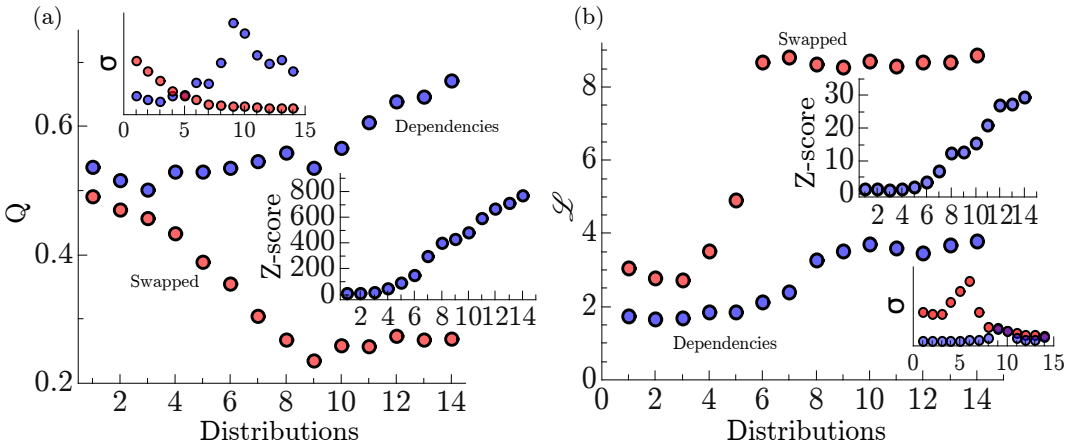


Figure 6.2.4: (a) Modularity index (Q) of the different Debian distributions (blue points) and the ensemble of networks preserving the degree sequence (“swapped”, red points). A monotonic increase of the modularity index can be appreciated over time, while Q decreases for the swapped ones. Together with these results, the standard deviation of the modularity index shows an abrupt increase around 7th-8th distribution and a sustained decrease for the “swapped” networks (upper inset). Consequently, the Z-score, shows a steep rise until $z = 800\sigma$ in the last distribution “Stretch” (lower inset) (b) Average path length (\mathcal{L}) of the different Debian distributions (blue points) and the “swapped” networks (red points). It shows a small increase for the original networks and an abrupt change in the “swapped” ones, together with a pronounced peak in the standard deviation for the “swapped” networks around the 6th-7th distributions (upper inset). Additionally, Z-score also grows after this abrupt change in the ensemble of networks.

⁴The Z-score of a quantity is defined as difference with the mean in terms of the standard deviations, $z = \frac{x-\mu}{\sigma}$.

Another useful insight is the evolution of the average path length (\mathcal{L}) over the different distributions (also averaged over 10^4 realizations). It can be seen in Figure 6.2.4b a small increase in this quantity (blue points), featuring that its value remains constrained between 2 and 4, suggesting some type of small world effect allowing to the neighbors to be genuinely close and facilitating the transfer of information. Pay close attention that, in the “swapped” networks (blue points in Fig. 6.2.4b), the average path length shows a great increase around 6th-7th distributions “Potato” and “Woody” (red points), together with a pronounced peak on its standard deviation (see lower inset) suggesting some type of dramatic structural reorganization of the ensemble of networks. It also should be noted that the Z-score for the average path length grows monotonically after 7th distribution “Woody”.

For these particular observables, we have analyzed the gene-regulatory networks of *E.Coli*, *M. Tuberculosis*, *B.Subtilis*, *P.Aeruginosa* and *S.Cerevisiae* [1, 5, 19, 34] getting values of Q and \mathcal{L} between (0.55 – 0.8) and (2.0 – 3.5), respectively (data not represented properly on a graph). Again, such values bear an acceptable resemblance to the measured values of Debian dependency networks. Such high modularity values have been hypothesized to play a key role in gene regulation [47], fostering the flow of information and providing effective responsiveness to external stimuli [6, 43].

✱ **Loosing hierarchy.** Beyond the importance of the modularity [16], it has been highlighted the relevance of a high hierarchical organization in information flow networks [49]. Thus, in order to analyze the evolution of the hierarchical structure of the networks, we define three levels of hierarchy: (i) “sinks” that are those packages that only depend on another packages (ii) “middle nodes” which depend on another packages and some packages depend on them and finally, (iii) “sources”, that are packages with no dependences, and which may be interpreted as information containers.

At this point, the fraction of such type of packages can be monitored over the different releases. As shown in Figure 6.2.5, the “source” packages only represent a small fraction of the whole network and, more interestingly, the “sinks” –which constitute most of the network in the first distributions– decrease astoundingly quickly for successive releases, demonstrating a clear loose of the (pronounced) hierarchical structure of the initial distributions.

An even greater hierarchical structure is prominent in real gene networks [43, 49] (where more than 85% of the nodes are “sinks”), which has been hypothesized to confer an effective and robustness way to transfer information and coordinate processes [49].

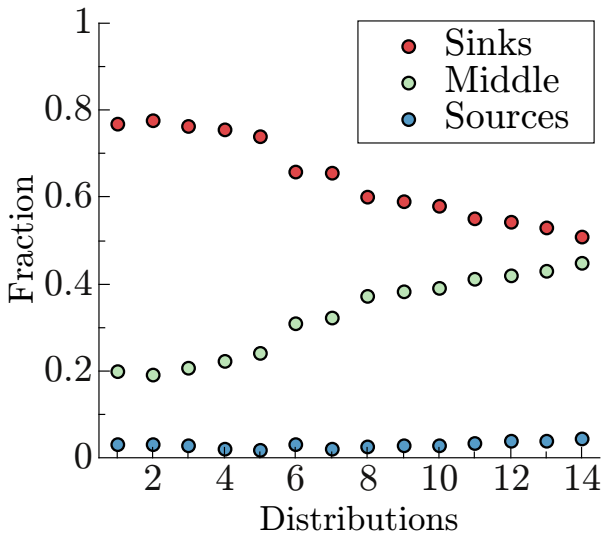


Figure 6.2.5: Evolution of the three main hierarchies identified in the network: “sinks”, “middle nodes” and “sources” (see legend). Observe that the “sources” of information, i.e. nodes that not depend on another nodes, constitute a small fraction of the network. However the “sinks”, situated in the lowest point of the hierarchy are being lost over time, very probably due to the reuse of packages.

✱ **Evolution of resilience in Debian networks.** One plausible assumption in the traveled way of Debian releases is that the network should be driven toward a resilience, non-breakable, target, and that, the structural changes observed above satisfy this process of improvement. To check this possibility, we propose to carry out the next experiment: to attack a small fraction of the network (making 1% of the total number of packages unusable) and to observe what happens with its dependent packages. That is to say, once a package is damaged, all the packages that depend on this one cause a cascading failure affecting to some fraction of the whole network. This proportion of the whole network that has been damaged is called the “*vulnerability*” and it is computed over the different distributions. Figure 6.2.6a shows the different values of the vulnerability across the evolution of Debian, exhibiting –again– a big increase of it around the 7th-8th distributions, where the major changes on the modularity index (Q), the average path length (\mathcal{L}) and the stationary state of the outgoing degree distribution turned up for it. But then, apparently, Debian networks are becoming less and less resilient over time. We are asking ourselves, what is being optimized, or where is going, the evolutionary dynamics of such software networks?

But before going into such issue, a similar analysis, mimicking empirical gene knockout experiments, i.e. a study of avalanches of damage, can be performed by attack a single node of each network, and following the cascade of failures. Results of such damage spreading are shown in Figure 6.2.6b, where it may be seen the emergence (or convergence) to a power law distribution, with an exponent close to $\tau = 1.5$, of the total number of damaged packages for the last distributions and, in particular, exemplified for Etch (blue line). Perhaps surprisingly, the scale-free behavior shown by the distribution of failures for the last distributions bears a very close resemblance to the real gene knockout experiments recently reported [18, 42] (and shown in Figure 6.2.6b).

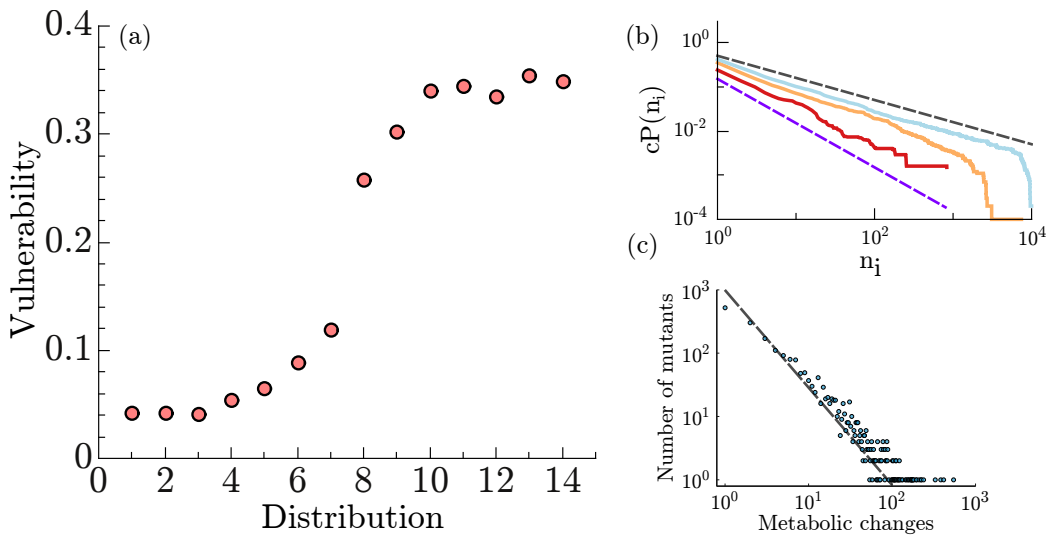


Figure 6.2.6: (a) Vulnerability index for the different Debian distributions. An abrupt increase of the vulnerability can be appreciated around the 7th-8th distributions affecting to a large fraction of the network and, possibly, making it totally unusable in practice if there are any problems. (b) Scale-free avalanches of damage after attack one random node of the network for Bo (red), Woody (orange) and Etch (blue) distributions. Dashed lines are guides to the eye (black, $\tau = 1.5$ and violet, $\tau = 2$) and (c) Total number of metabolite changes for different mutants replica (i.e. with single-gene deletions) of *E. Coli*. It seems to follow a power law distribution with exponent $\tau \approx 3/2$ (the dashed lines are guides to the eye). Data from [26].

6.2.2

Network information and the size of packages.

As we have seen, there exists an important and apparent contradiction with the (reasonable) evolution toward a resilient target in concomitance with an optimal information flow across the network. An important property –beyond the structure of the network– emerge from the study of the information about the size of the different packages, concerning the total amount of information that is present in the Debian potential network. In this sense, it can be analyzed the evolution of the total size of the network according to the system size. Thereby, Figure 6.2.7 shows the increase of the size of the system with the number of packages. A linear growth can be estimated for the first distributions, as well as a clear slowing down for this trend after 7th distribution (as a comparison, a square-root dependence is depicted). As a direct consequence, this implies that twice the number of packages, not twice the total information contained in the network.

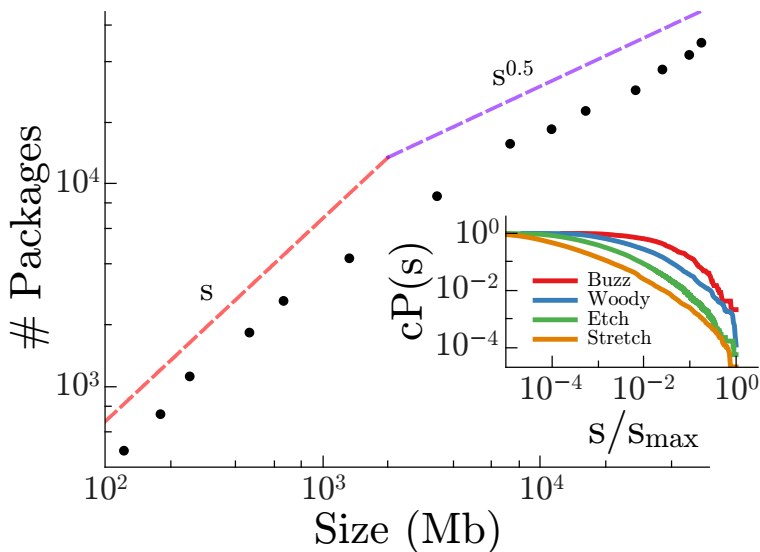


Figure 6.2.7: Total number of packages versus total system size for each Debian distribution (black dots). An initial linear growth, presenting a clear slowing down can be appreciated as a general trend. Dashed lines are guides to the eye showing a linear growth (reddish one) and a square-root growth (purplish one). Inset: Cumulative distribution of the size of individual packages across different distributions featuring a tendency to an ever larger size.

To understand this a little better, there are new aspects of the isolated package structure that need further explanations to address an accurate and precise knowledge of the issue. The Debian software package format, in particular, in the same way as further package management systems, consists of payload data (the software in itself) together with extra control information encapsulated in particular control files, which contains meta-information (the dependences needed, as well as mechanisms designed to avoid errors during unpacking and installation processes) ensuring a proper transmission of information [32]. Really, these control files are what comprise and ensure the resilience of the network, minimizing risks in the transmission of the information of the system and thus, doing not matter the growth of the vulnerability appreciated in Figure 6.2.6a.

This raises a clear analogy with cellular organisms and viruses, for which the *C-value* of an organism is defined as the amount of DNA per haploid nucleus in the genome. In essence, a measure of the genome size of an organism. Such relation between the total number of genes and the genome size is of common wisdom and has been known for a long time in biology for many living things [21], from prokaryotes to eukaryotes and plasmids, as well as viruses. The growth of the total amount of information for living systems was expected to exhibit some type of constancy or relationship with the number of genes of an organism but, as shown in Figure 6.2.8 it bears no relationship with the genome size of living things, giving place to the *C-value paradox* or, more recently, to the *C-value enigma*. The paradox surrounds the next question: why genome size does not correlate with the complexity of an organism? Or in other words, it seems clear that the more complex the organism the larger the genomes should be, but it is not the case for eukaryotes. They not correlate properly and, hence, the cells of those organisms contains much more DNA than expected. This apparently paradox was solved in 1971 with the discovery of the non-coding DNA in eukaryotes [38], i.e. a DNA sequence that do not encode protein sequences. However, the functionality and role of such non-coding DNA has not been fully elucidated and its utility or futility are still under discussion [11] provoking controversy and promoting the enigma.

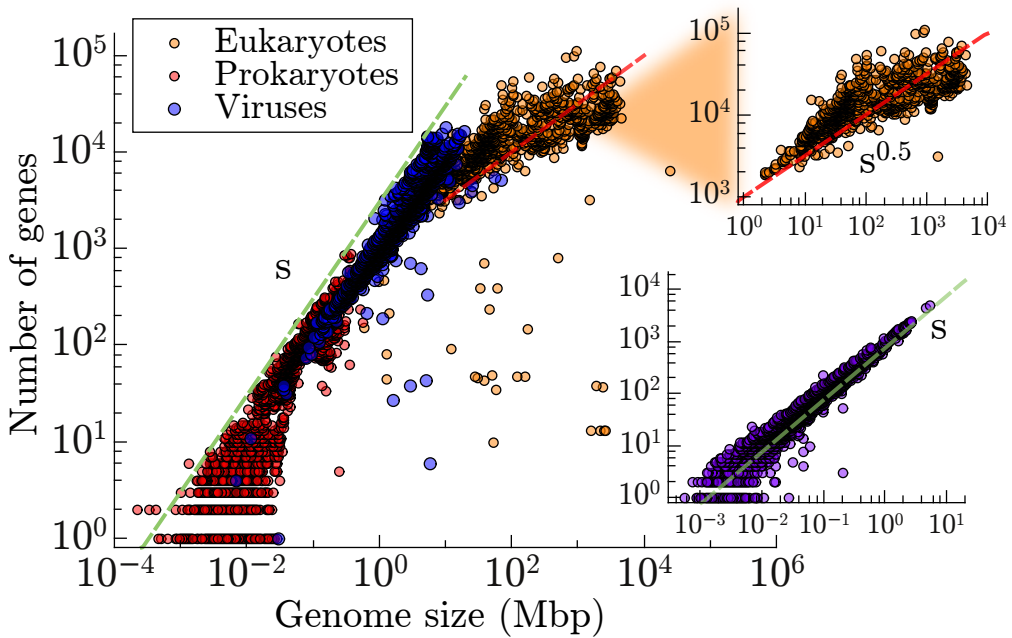


Figure 6.2.8: Genome size as function of the total number of genes (in log-log scale) for many living things. Data from NCBI database [21]. Observe the linear scaling associated to prokaryotes and viruses (red and blue dots, respectively), as well as to plasmids (lower inset, violet dots). Pay close attention to the slowing-down of such growth for eukaryotic organisms (orange dots, enlarged in the upper inset). Lines are guides to the eye indicating linear a root-squared scaling, in green and red, respectively.

Conclusions

With the aim of developing artificial systems able to mimic the mechanisms operating in living systems, new grounds have been broken in the fields of biomedical therapies, biosensing modular circuits and biosynthetic pathways [8, 29, 41]. At this stage, various disciplines such as systems biology, biophysics and evolutionary biology play a key role, so the clarification of the collective properties stemming from the interactions of a large number of units such as genes, proteins or metabolites should provide insight into further developments in the field. Regarding this, a pioneering creation of a genetic toggle switch and a synthetic oscillatory network entailed a significant contribution showing the potential of this branch [15, 20]. Further particular applications, such as biosensing, mimicking the myriads of regulatory circuits of the cell to process external stimuli, require a thorough understanding of the different regulatory interactions at the transcriptional, translational and post-translational levels [29], as well as fully elucidate their collective properties and features. Since the current knowledge still has some serious flaws [36], more exhaustive empirical measurements and analytical theory/modeling would be needed.

Here, employing the software network of the Debian operating system, we have scrutinized its evolutionary dynamics, as well as the specific emergent properties achieved through the collective action of thousand of developers. Based on causal topological relations and the transfer of sequential information, the software ecosystem of Debian networks –whose evolution has occurred on a very short evolutionary time, approximately 20 years– constitute an excellent analogy with gene networks. In particular, Debian networks are quite sparse and show a mixed scale-free and exponential structure for the ingoing distribution (representing the number of dependent packages) and the outgoing distribution (representing the number of processing packages and entailing a finite capacity of information processing), respectively. Especially interesting is the increase of the modular structure of the networks for the different releases that have been proposed to be an effective strategy for allowing, at the same time, the growth of resilient networks, minimizing the risk of collapse if some packages experience failures [16]. In turn, the evolutionary trend confirms a clear loss of the hierarchy of the networks, probably coming from the reuse of code as the new software develops. In this way, the reuse of code (or software) to optimize the development of the operating system must be part of a concerted action with the effective and robust transfer of information and coordination processes that

the hierarchy confer. Additionally, the small average path length can be taken as an indication of small-world effects.

On the other hand, as might be expected, the cascading failure resulting from individual package deletion follow a power law size distribution but, interestingly, its slope converge to $3/2$ in the last distributions of Debian. Likewise, the vulnerability of the system from a random attack to a fraction of it shows a sharp increase around the Woody distribution, in accordance with all the major (and mostly dramatic) changes that have taken place throughout the evolutionary dynamics of Debian systems. Last but not least, Debian seems to be reaching some type of stationary state –after undergoing major changes close to Woody distribution– as emerging of the different properties in the last distributions.

Also, in the light of the increasing amount of information per package in high complexity networks of the last distributions, bearing no relationship with the total number of packages, we hypothesize an increasing relevance of the control files as an effective strategy in order to minimize the disruptions during the information processing, that allows for an emergent optimized structure for the information flow throughout the network.

Inspired by previous works [16, 17, 49] we have found that software synthetic networks are able to recreate many of the emergent properties observed in real gene regulatory processes. For instance, the particular structure of the (ingoing and outgoing) degree distribution, a high level of modularity that has emerged throughout its evolution, as well as similar values of the -small- average path length indicating small-world effects. In turn, both systems show a highly hierarchical structure (much more pronounced in genetic networks) that has been hypothesized to confer an effective and robustness way to transfer information and coordinate processes [49]. The counterintuitive trend found in Debian networks, promoting the loss of hierarchy throughout their evolution, is thus of particular interest. This aspect raises an important question, how can the system lose hierarchical structure and increase modularity at the same time?

Regarding gene knockout experiments, showing identical behavior to the experiments done in the software networks, it is possible to provide an explanation relying on structural effects only. The dynamics may play no role whatsoever, in what appears to be an emergent topological property.

On the other hand, although a great effort has been made to understand the role of the non-coding DNA, it is actually perceived as the dark-matter of the genome [11], since its particular function remains still unknown. In this sense, it has provoked extended discussions about its functionalities or its futility [35]. Thus, our analogy can support the vision that, at least one of its roles, can be the monitoring and minimization of gene disruption during the transcriptional process. However, further work is needed on the analogy with the non-coding DNA, in order to clarify the biological function of the “dark matter” of the genome.

In either case, it seems that common solutions emerge, both in synthetic networks and in real biological networks, to the general problem designing circuitry that optimizes storage, information processing (of both internal and external stimuli), and robustness. Thus, it might be of interest to consider the suggestion of borrowing and implementing some features and strategies coming from real gene regulatory networks in operating systems, maybe contributing to optimize software networks in future developments.

References

- [1] ALBERGANTE, L., BLOW, J. J. & NEWMAN, T. J. «Buffered qualitative stability explains the robustness and evolvability of transcriptional networks». *Elife* **3**, e02863 (2014).
- [2] ALBERT, R. & OTHMER, H. G. «The topology of the regulatory interactions predicts the expression pattern of the segment polarity genes in drosophila melanogaster». *J. Theor. Biol.* **223**, 1–18 (2003).
- [3] ALDANA, M., BALLEZA, E., KAUFFMAN, S. & RESENDIZ, O. «Robustness and evolvability in genetic regulatory networks». *J. Theor. Biol.* **245**, 433–448 (2007).
- [4] ALON, U. *An introduction to systems biology: design principles of biological circuits* (CRC press, London, 2006).
- [5] ARRIETA-ORTIZ, M. L. *et al.* «An experimentally supported model of the bacillus subtilis global transcriptional regulatory network». *Mol. Sys. Biol.* **11**, 839 (2015).
- [6] BABU, M. M., LUSCOMBE, N. M., ARAVIND, L., GERSTEIN, M. & TEICHMANN, S. A. «Structure and evolution of transcriptional regulatory networks». *Curr. Opin. Struct. Biol.* **14**, 283–291 (2004).
- [7] BARABASI, A.-L. & OLTVAI, Z. N. «Network biology: understanding the cell's functional organization». *Nat. Rev. Gen.* **5**, 101–113 (2004).
- [8] BENNER, S. A. & SISMOUR, A. M. «Synthetic biology». *Nat. Rev. Gen.* **6**, 533–543 (2005).
- [9] BLONDEL, V. D., GUILLAUME, J.-L., LAMBIOTTE, R. & LEFEBVRE, E. «Fast unfolding of communities in large networks». *J. Stat. Mech. Theory Exp.* **2008**, P10008 (2008).
- [10] BUCHANAN, M. *Networks in cell biology* (Cambridge University Press, Cambridge, 2010).
- [11] CAREY, N. *Junk DNA: A Journey Through the Dark Matter of the Genome* (Columbia University Press, New York, 2015).
- [12] CRICK, F. «Central dogma of molecular biology». *Nature* **227**, 561–563 (1970).
- [13] CSARDI, G. & NEPUSZ, T. «The igraph software package for complex network research». *InterJournal, Complex Systems* **CX.18:1695**, 1–9 (2006).

-
- [14] DUGUÉ, N. & PEREZ, A. *Directed Louvain: maximizing modularity in directed networks*. Ph.D. thesis, Université d'Orléans (2015).
- [15] ELOWITZ, M. B. & LEIBLER, S. «A synthetic oscillatory network of transcriptional regulators». *Nature* **403**, 335–338 (2000).
- [16] FORTUNA, M. A., BONACHELA, J. A. & LEVIN, S. A. «Evolution of a modular software network». *Proc. Natl. Acad. Sci. USA* **108**, 19985–19989 (2011).
- [17] FORTUNA, M. A. & MELIÁN, C. J. «Do scale-free regulatory networks allow more expression than random ones?». *J. Theor. Biol.* **247**, 331–336 (2007).
- [18] FUHRER, T., ZAMPIERI, M., SÉVIN, D. C., SAUER, U. & ZAMBONI, N. «Genomewide landscape of gene–metabolome associations in escherichia coli». *Mol. Sys. Biol.* **13**, 907 (2017).
- [19] GAMA-CASTRO, S. *et al.* «Regulondb version 9.0: high-level integration of gene regulation, coexpression, motif clustering and beyond». *Nucleic Acids Res.* **44**, D133–D143 (2015).
- [20] GARDNER, T. S., CANTOR, C. R. & COLLINS, J. J. «Construction of a genetic toggle switch in escherichia coli». *Nature* **403**, 339–342 (2000).
- [21] GEER, L. Y. *et al.* «The ncbi biosystems database». *Nucleic Acids Res.* **38**, D492–D496 (2009).
- [22] GROS, C. *Random Boolean networks* (Springer, Berlin Heidelberg, 2011).
- [23] HAGMANN, P. *et al.* «Mapping the structural core of human cerebral cortex». *PLoS Biol.* **6**, e159 (2008).
- [24] HERTZOG, R. & MAS, R. *The Debian Administrator's Handbook, Debian Wheezy from Discovery to Mastery* (2014).
- [25] JACKSON, I. *et al.* «Debian policy manual». Available in <http://www.debian.org/doc/manuals/debian-policy> v4.1.1.1 (2017).
- [26] JEONG, H., TOMBOR, B., ALBERT, R., OLTVAI, Z. & BARABASI, A. «The large-scale organization of metabolic networks». *Nature* **407**, 651 (2000).
- [27] KAUFFMAN, S. «Metabolic stability and epigenesis in randomly constructed genetic nets». *J. Theor. Biol.* **22**, 437–467 (1969).
- [28] KAUFFMAN, S. A. *The origins of order: Self-organization and selection in evolution* (Oxford university press, New York, 1993).

- [29] KHALIL, A. S. & COLLINS, J. J. «Synthetic biology: applications come of age». *Nat. Rev. Gen.* **11**, 367–379 (2010).
- [30] KITANO, H. «Systems biology: a brief overview». *Science* **295**, 1662–1664 (2002).
- [31] KITANO, H. «Computational systems biology». *Nature* **420**, 206–210 (2002).
- [32] KRAFFT, M. F. *The Debian system: concepts and techniques* (No Starch Press, San Francisco, 2005).
- [33] LI, F., LONG, T., LU, Y., OUYANG, Q. & TANG, C. «The yeast cell-cycle network is robustly designed». *Proc. Natl. Acad. Sci. USA* **101**, 4781–4786 (2004).
- [34] MA, S., KEMMEREN, P., GRESHAM, D. & STATNIKOV, A. «De-novo learning of genome-scale regulatory networks in *s. cerevisiae*». *PLoS One* **9**, e106479 (2014).
- [35] MERCER, T. R., DINGER, M. E. & MATTICK, J. S. «Long non-coding rnas: insights into functions». *Nat. Rev. Gen.* **10**, 155–159 (2009).
- [36] MUÑOZ, M. A. «Colloquium: Criticality and dynamical scaling in living systems». *arXiv preprint arXiv:1712.04499* (2017).
- [37] NEWMAN, M. E. «The structure and function of complex networks». *SIAM Rev.* **45**, 167–256 (2003).
- [38] OHNO, S. «So much "junk" dna in our genome.». In *Brookhaven symposia in biology*, vol. 23, 366–370 (1972).
- [39] PANG, T. Y. & MASLOV, S. «Universal distribution of component frequencies in biological and technological systems». *Proc. Natl. Acad. Sci. USA* **110**, 6235–6239 (2013).
- [40] PASTOR-SATORRAS, R. & VESPIGNANI, A. «Epidemic spreading in scale-free networks». *Phys. Rev. Lett.* **86**, 3200 (2001).
- [41] PURNICK, P. E. & WEISS, R. «The second wave of synthetic biology: from modules to systems». *Nat. Rev. Mol. Cell Biol.* **10**, 410–422 (2009).
- [42] RÄMÖ, P., KESSELI, J. & YLI-HARJA, O. «Perturbation avalanches and criticality in gene regulatory networks». *J. Theor. Biol.* **242**, 164–170 (2006).

-
- [43] RAVASZ, E., SOMERA, A. L., MONGRU, D. A., OLTVAI, Z. N. & BARABÁSI, A.-L. «Hierarchical organization of modularity in metabolic networks». *Science* **297**, 1551–1555 (2002).
- [44] SOLE, R. V. & MONTROYA, M. «Complexity and fragility in ecological networks». *Proc. R. Soc. Lond. B Biol. Sci.* **268**, 2039–2045 (2001).
- [45] TKAČIK, G., CALLAN, C. G. & BIALEK, W. «Information flow and optimization in transcriptional regulation». *Proc. Natl. Acad. Sci. USA* **105**, 12265–12270 (2008).
- [46] VALVERDE, S. & SOLÉ, R. V. «Logarithmic growth dynamics in software networks». *Europhys. Lett.* **72**, 858 (2005).
- [47] WAGNER, G. P., PAVLICEV, M. & CHEVERUD, J. M. «The road to modularity». *Nat. Rev. Gen.* **8**, 921–931 (2007).
- [48] WATSON, J. D. *et al.* *Molecular biology of the gene* (Pearson, New York, 2008), 7 edn.
- [49] YAN, K.-K., FANG, G., BHARDWAJ, N., ALEXANDER, R. P. & GERSTEIN, M. «Comparing genomes to computer operating systems in terms of the topology and evolution of their regulatory control networks». *Proc. Natl. Acad. Sci. USA* **107**, 9186–9191 (2010).

Conclusions

7.1	Concluding remarks	227
7.2	Papers derived from this thesis	233
	References	235

Concluding remarks

“Things happen by revolutions, not gradually, precisely because dynamical systems are poised at the critical state.”

Per Bak

The criticality hypothesis frames a fascinating idea, living systems may operate in the vicinity of a phase transition, i.e. at the borderline between order and disorder, shedding much light on the comprehension of several collective natural phenomena and, more recently, in specific features of real biological systems. Likewise, it has revealed its rapport with many functional benefits crucial for the survival, proliferation and refinement of living matter evolving by natural selection.

On this basis, throughout this thesis we have delved deeper into the idea of possible clues of criticality in living matter, as well as their emergent collective phases and phenomena. In particular, we have considered particular real biological systems –neural and genetic– susceptible to be analyzed together with specific quantitative features, i.e. experiments, trying to elucidate –in them– how far and how accurate the criticality hypothesis is.

✖ **Neural dynamics operates at the edge of a synchronization phase transition**

In the context of neural systems, criticality hypothesis conjectures that the underlying dynamics of cortical networks is such that it is posed at the edge of a continuous phase transition, separating qualitatively different phases or regimes, with different degrees of order [2, 9, 20, 41]. However, what these phases are, and what the nature of the putative critical point is, are questions that still remain to be fully settled.

In this sense, the Landau-Ginzburg model of cortical dynamics –focused on a regulatory dynamics controlled by synaptic plasticity or inhibition– allow us to classify the possible emerging phases of cortical networks under very general conditions by the consideration of intrinsic stochasticity and spatial dependence. Even though Buice and Cowan developed a very similar approach based on continuous phase transitions from a quiescent to an active phase [6], we believe that this scenario does not properly capture the essence of cortical dynamics as, in actual networks of spiking neurons, there are spike-integration mechanisms, i.e. many inputs are required to trigger further activity. Indeed, as the Wilson-Cowan model captured, the threshold of the sigmoid response function precludes

the existence of a continuous quiescent/active phase transition. Moreover, based on the “spiking” nature of the activity dynamics, our theory underlies the fundamental role of oscillations and partial synchronization –suggesting that kind of phase transition– in neural dynamics.

From an experimental viewpoint, our model constitutes –in a specific case– a sound description of the cortex during deep sleep or during anesthesia, when up and down transitions are observed [10, 44]. But, better yet, just at the synchronization critical point, our model shows the best performance reproducing empirically observed resting-state networks [43], the existence of long-range temporal correlations in alpha oscillations [28], as well as power-law distributed avalanche sizes and durations with the same statistics as in empirical networks, i.e. the critical exponents compatible with those of an unbiased branching process [2]. Moreover, our results are compatible with the amazingly detailed model put together by the Human Brain Project consortium [29], in which the calcium concentration is well-known to modulate the level of available synaptic resources setting the network state. Additionally, our model is able to reproduce remarkably well empirical in vitro results for neural cultures with different levels of mesoscopic structural heterogeneity [37].

✱ The architecture of cortical networks induces an extended critical-like synchronization region In the spirit of neural field models, and to preserve the essence of a minimal design, we show that simple models of synchronization dynamics (the Kuramoto model), operating on top of empirical human brain networks, exhibit an unexpectedly rich phenomenology.

Such phenomenology is a broad critical-like region (reminiscent of a Griffiths phase [33]) with oscillatory behavior of the order parameter, which stems from the existence of relatively isolated structural communities or moduli. Even more remarkably, oscillations in the level of internal coherence are also present within these moduli, suggesting the existence of a whole hierarchy of nested levels of organization, as also found in the recent literature [7, 32, 43, 46].

In this respect, in the absence of frequency dispersion, perfect coherence is achieved in hierarchical networks by following a “matryoshka doll” (i.e. bottom-up) ordering dynamics, which is further frustrated in the presence of intrinsic frequency dispersion. This allows the system to remain trapped into metastable and chimera-like states with traits of local coherence at different hierarchical levels, rendering accessible –in a robust though flexible way– a large variety of functional attractors and dynamical repertoires without ad hoc fine-tuning to a critical point. In addition, stochasticity allows the system to wander in such complex synchronization landscape overcoming the “potential barriers” between mutually incoherent moduli as well as re-introducing “desynchronization” effects, leading to an even more enriched dynamics.

Interestingly, such intermediate broad regime reproduce the real dynamics found in alpha oscillations and in the resting state of human brains [4, 28], characterized by very slow fluctuations, of typical frequency $< 0.1\text{Hz}$. Also, the attractor “surfing” behavior, that has been suggested to give access to highly varied functional configurations in real neural dynamics [9, 18, 41] is largely facilitated in the broad intermediate regime, without any need of fine-tuning of a critical point to guarantee the functional advantages usually associated with criticality. Likewise, it justifies the observed critical-like regions in different models of neural dynamics [13, 21, 40].

✖ **Non-critical mechanisms of power laws** From a theoretical viewpoint, critical exponents of an unbiased branching process have been founded to be fully compatible with the empirical scale-free avalanches discovered by Beggs and Plenz [2]. Since all systems with absorbing states can exhibit avalanche behavior, turning out to be scale invariant at critical points, and simple quiescent-to-active phase transitions show the branching-process exponent values [19, 30], they can be used to account for the neural scale-free avalanches. In this sense, we hope that the brief summary exposed here helps avoiding frequent confusions in the neuroscience literature, as well as underlining the superuniversality of the directed percolation universality class, which, in fact, is also related with synchronization effects [35, 39].

On the other hand, at the very least, we intended to highlight the relevance of showing the lifetime exponent in empirical/theoretical findings, as well as to avoid misleading measures of avalanches over temporal series.

Conversely, as counterpoint, we have shown the emergence of generic (non-critical) power laws in a theoretical model with small external driving [5]. Also, in a more realistic way, we have thoroughly understood the “balanced amplification” mechanisms proposed by Benayoun et al. [3, 36] in populations of excitatory and inhibitory neurons, as well as to present the same phenomena by employing synaptic plasticity as the chief regulatory mechanism. In essence, such non-critical mechanisms requires the existence of a stable active fixed point, enriched with a reactive dynamics allowing for very large noise-induced fluctuations leading the system to get trapped into the origin by the effect of a logarithmic potential. Thus, “balanced amplification” provides a (non-critical) candidate to model up and down states, such as those occurring in the brain during sleep or under anesthesia [10, 44].

Nevertheless, despite the “balanced amplification” mechanism is able to show scale-free avalanches, their exponents are compatible with the random walk universality class. Thus, although reactive dynamics may be of key importance in neural mechanisms (such as in up and down states) and in fostering large fluctuations, it does not seem a plausible candidate to account for the large number of founded empirical findings explained by different theoretical approaches.

✱ **The dynamics of GRN is ordered or critical but not chaotic** Genetic regulatory networks constitute another sound suggested case that might operate close to criticality, exploiting its many benefits.

Thus, we have shown that random Boolean network models –with an inherent stochastic updating dynamics [16] and mimicking real gene regulatory networks [15, 17, 22, 23]– that are trained to perform a given computational task, can learn it much faster if they have a connectivity K such that they are close to criticality. In this sense, from an evolutionary point of view, although the learning process is compatible with being subcritical, critical or supercritical, for sure criticality is fostered in a system whose evolution is guided by natural selection.

Biological systems must have homeostasis, i.e. the capacity to maintain their internal conditions even in the presence of fluctuations and noise. So, in the same set up, we have added extreme forms of dynamical or structural noise, mimicking dynamical perturbations or physical damages in the transcriptional network. Under this effects, we find that the optimal connectivity to achieve the fastest possible learning lies deep-inside the subcritical region, far away from criticality, and the distance to criticality increases upon enlarging the noise strength and does not diminish upon increasing the system size. That is to say, real biological networks surviving in a noisy world, should operate in sub-critical regimes rather than in a critical one.

Furthermore, we have collected many empirical (genetic and metabolic) networks which show a rather sparse connectivity, leading to subcritical dynamics if the dynamics underlying these networks is assumed to be modeled by random Boolean functions [11, 24]. Our results seems compatible with the Kauffman net model for eukaryotic cells [42], as well as for the yeast transcriptional network [25].

Hence, the criticality hypothesis remains as a valid and fascinating possibility, but it needs to be critically evaluated under each set of specific circumstances, avoiding making exceedingly general claims. Also, together with the need of more accurate and extensive experimental approaches, one can only conclude that better and more accurate dynamical models are needed to model gene regulatory networks, as well as to infer the impact of important topological features (such as hierarchical and modular organization) of empirical networks.

✱ **Mimicking and shedding light on the regulatory circuitry of cell organisms** The comprehension of the structure (and the evolution) of real gene networks is key for the emergent collective properties of the cell function [26, 27]. For this purpose, Debian networks, as collective information flow networks, offer a unique opportunity to study the evolution and the emergent properties of gene networks [12, 45].

We have found that such software synthetic networks are able to recreate many of the emergent properties observed in real gene regulatory processes [1]. For instance, the particular structure of the (ingoing and outgoing) degree distribution, a high level of modularity that has emerged throughout network evolution, as well as similar values of the -small- average path length indicating small-world effects. In turn, both systems shows a high hierarchical structure (much more pronounced in genetic networks) that has been hypothesized to confer an effective and robust way to transfer information and coordinate processes.

Also, they are able to reproduce the power laws founded in gene 'knock-out' experiments [14, 38], allowing for a compelling explanation (without any sign of critical dynamics) relying only on structural effects. In the same way, Debian synthetic networks can support the conjecture that, at least, one of the roles of the non-coding DNA in eukaryotic cells [8, 31] can be the monitoring and minimization of gene disruption during the transcriptional process. In essence, playing a similar role to the control files in Debian packages.

✖ **How living matter works** Certainly, the criticality hypothesis is a tantalizing and powerful solution to the mystery of how collective properties (ubiquitously) emerge in concomitance with the large amount of functional benefits required by living systems.

In this sense, we do not aim to fully elucidate the accuracy of this central controversy, but hopefully we have contributed to shedding light on the (synchronization) phase transition in which the cortex might operate, and that, as far as we are concerned, is able to reproduce all chief empirical findings for neural avalanches. It also represents an example of a phase transition far away of the archetypal active/quiescent one, very interesting for systems with ceaseless activity or dynamics. But, even better, such edge of synchronization can be stretched whether heterogeneous or modular structures are present, suggesting a broad living region –that is relevant for other hierarchically organized systems– rather than the narrow line that SOC proposes.

Likewise, the empirical evidence was regarded as essential in order to provide a theoretical approach that goes further than an abstract hypothesis, i.e. beyond a simple qualitative view. The criticality hypothesis must provide a large number of quantitative measures and predictions (along with the already discovered, which, in our opinion, are not fully convincing enough). To that end, larger systems, more accurate and integral experiments –arising from an interdisciplinary perspective– are needed. In particular, the quest for a “smoking gun”, which might be brain function, is a priority objective to duly justify the criticality hypothesis. In particular, we hope that our Landau-Ginzburg model does its part in the quest for such “holy grail” of criticality.

Therefore, the criticality hypothesis should not be magnified yet. It is an undeniable fact that living things cannot be too quiescent, nor can they be too variable: in order for the criticality hypothesis to be considered as a valid explanation, many specific quantitative features should arise from this perspective. Otherwise, it merely suggests a tautology, i.e. that our limited models –in which the most complex dynamics arise at criticality– provide complex analogies to the most complex systems we know, the living matter of Earth. We indeed believe that criticality hypothesis is accurate in several cases (see [34] for more specific examples), but biology is rich enough to foster living matter also operating in different phases (beyond criticality, we should not forget that such phases emerge from a collective action of an enormous host of acting units, that already is a fascinating and captivating issue). For instance, we have serious doubts –in the light of the Boolean approach– about the critical dynamics in gene regulatory networks, which are exposed to numerous external stress factors. In the same way, gene knock-out experiments are still far from being an evidence of critical dynamics in gene networks, because they are susceptible of alternative (and compelling) interpretations. This only reinforces the idea that more accurate and integral experiments are needed in order to clarify how successful the criticality hypothesis is.

Thus, in our view, this thesis points to further work on how adaptive, homeostatic or self-regulatory mechanisms can account for the brain to operate in the edge of a synchronization phase transition, as well as for the role of more realistic spatial dependences and dynamical models of neural dynamics (with explicit time delays, for example). In the same way, the possibility of a synchronization transition related with neural dynamics should be clarified and carefully analyzed both from the experimental and the theoretical viewpoint, and ideally through the correct definition of a universality class. On the other hand, we should explore the development of dynamical models that can –as closely as possible– replicate the gene regulation dynamics (maybe) at criticality. Likewise, the charming idea of broad critical-like regions allowing for very rich dynamical repertoires and stemming from the modular structure of further biological systems, as possibly gene regulatory networks, should be scrutinized and clarified. Indeed, only the design, replication and framing of more experimental findings and evidences –supporting or refuting the criticality hypothesis in living matter– is, per se, a major challenge and a great source of work.

Finally, we believe that the criticality hypothesis might be able to elucidate why Nature, and living matter is complex, as well as to account for quantitative features of living matter, solving a key mystery with huge implications. After all, in agreement with Russell and Dirac, if a theory possesses some beauty (and, certainly, criticality does) it should also possess some truth. Although, it may also be that –the also complex– God, under the (highly unlikely) assumption that it exists, is a statistical physicist.

Papers derived from this thesis

- [1] VILLEGAS, P., MUÑOZ, M. A. & BONACHELA, J. A. «Unveiling the emergent structure of grn from debian networks». *In preparation* (2018).
- [2] DI SANTO, S., VILLEGAS, P., BURIONI, R. & MUÑOZ, M. A. «Self-organized bistability: is it a relevant concept for brain dynamics?». *In preparation* (2018).
- [3] DI SANTO, S., VILLEGAS, P., BURIONI, R. & MUÑOZ, M. A. «On a misleading definition of neural avalanches». *In preparation* (2018).
- [4] VILLEGAS, P., DI SANTO, S., BURIONI, R. & MUÑOZ, M. A. «Reactive and noisy dynamics in simple models of neural systems». *Submitted* (2018).
- [5] DI SANTO*, S., VILLEGAS*, P., BURIONI, R. & MUÑOZ, M. A. «Landau-Ginzburg theory of cortex dynamics: scale-free avalanches emerge at the edge of synchronization». *Proc. Natl. Acad. Sci. USA* (2018). (*Joint 1st authors).
- [6] DI SANTO, S., VILLEGAS, P., BURIONI, R. & MUÑOZ, M. A. «Simple unified view of branching process statistics: Random walks in balanced logarithmic potentials». *Phys. Rev. E* **95**, 032115 (2017).
- [7] VILLEGAS, P., RUIZ, J. M., HIDALGO, J. & MUÑOZ, M. A. «Intrinsic noise and deviations from criticality in Boolean gene-regulatory networks». *Sci. Rep.* **6**, 34743 (2016).
- [8] VILLEGAS, P., HIDALGO, J., MORETTI, P. & MUÑOZ, M. A. «Complex synchronization patterns in the human connectome network». In BATTISTON, S., DE PELLEGRINI, F., CALDARELLI, G. & MERELLI, E. (eds.) *Proceedings of ECCS 2014: European Conference on Complex Systems*, 69–80 (Springer International Publishing, Cham, 2016).
- [9] MOGLIA, B., ALBANO, E. V., VILLEGAS, P. & MUÑOZ, M. A. «Interfacial depinning transitions in disordered media: revisiting an old puzzle». *J. Stat. Mech. Theory Exp.* **2014**, P10024 (2014).
- [10] VILLEGAS, P., MORETTI, P. & MUÑOZ, M. A. «Frustrated hierarchical synchronization and emergent complexity in the human connectome network». *Sci. Rep.* **4**, 5990 (2014).

✱ Contributions to conferences

- [1] VILLEGAS, P., MORETTI, P. & MUÑOZ, M. A. «Kuramoto dynamics, glassy synchronization and rare regions in the human connectome». In *Quantitative Laws II: From physiology to ecology, from interaction structures to collective behavior* (Como, (Italy), 2016).
- [2] VILLEGAS, P., MORETTI, P. & MUÑOZ, M. A. «Neuronal avalanches: synchronization and criticality in the brain». In *I Conferences for young researchers: fostering the interdisciplinarity* (Granada, (Spain), 2016).
- [3] VILLEGAS, P., HIDALGO, J., MORETTI, P. & MUÑOZ, M. A. «Complex synchronization patterns in the human connectome network». In *FISES 2015* (Badajoz, (Spain), 2015).
- [4] VILLEGAS, P., HIDALGO, J., MORETTI, P. & MUÑOZ, M. A. «Hierarchical synchronization and complex patterns in the human connectome network». In *13th Granada Seminar on Computational and Statistical Physics* (La Herradura, (Spain), 2015).

References

- [1] BARABASI, A.-L. & OLTVAI, Z. N. «Network biology: understanding the cell's functional organization». *Nat. Rev. Gen.* **5**, 101–113 (2004).
- [2] BEGGS, J. M. & PLENZ, D. «Neuronal avalanches in neocortical circuits». *J. Neurosci.* **23**, 11167–11177 (2003).
- [3] BENAYOUN, M., COWAN, J. D., VAN DRONGELEN, W. & WALLACE, E. «Avalanches in a stochastic model of spiking neurons». *PLoS Comp. Biol.* **6**, e1000846 (2010).
- [4] BISWAL, B., ZERRIN YETKIN, F., HAUGHTON, V. & HYDE, J. «Functional connectivity in the motor cortex of resting human brain using echo-planar mri». *Magn. Reson. Med.* **34**, 537–541 (1995).
- [5] BRAY, A. «Random walks in logarithmic and power-law potentials, nonuniversal persistence, and vortex dynamics in the two-dimensional XY model». *Phys. Rev. E* **62**, 103 (2000).
- [6] BUICE, M. A. & COWAN, J. D. «Field-theoretic approach to fluctuation effects in neural networks». *Phys. Rev. E* **75**, 051919 (2007).
- [7] BULLMORE, E. & SPORNS, O. «Complex brain networks: graph theoretical analysis of structural and functional systems». *Nat. Rev. Neurosci.* **10**, 186–198 (2009).
- [8] CAREY, N. *Junk DNA: A Journey Through the Dark Matter of the Genome* (Columbia University Press, New York, 2015).
- [9] CHIALVO, D. R. «Emergent complex neural dynamics». *Nat. Phys.* **6**, 744–750 (2010).
- [10] DESTEXHE, A. «Self-sustained asynchronous irregular states and Up Down states in thalamic, cortical and thalamocortical networks of nonlinear integrate-and-fire neurons». *J. Comput. Neurosci.* **27**, 493–506 (2009).
- [11] DROSSEL, B. «Random boolean networks». In SCHUSTER, H. G. (ed.) *Reviews of nonlinear dynamics and complexity*, vol. 1, chap. 3, 69–110 (Wiley VCH, Weinheim, 2008).
- [12] FORTUNA, M. A., BONACHELA, J. A. & LEVIN, S. A. «Evolution of a modular software network». *Proc. Natl. Acad. Sci. USA* **108**, 19985–19989 (2011).

-
- [13] FRIEDMAN, E. J. & LANDSBERG, A. S. «Hierarchical networks, power laws, and neuronal avalanches». *Chaos* **23**, 013135 (2013).
- [14] FUHRER, T., ZAMPIERI, M., SÉVIN, D. C., SAUER, U. & ZAMBONI, N. «Genomewide landscape of gene–metabolome associations in *escherichia coli*». *Mol. Sys. Biol.* **13**, 907 (2017).
- [15] GOUDARZI, A., TEUSCHER, C., GULBAHCE, N. & ROHLF, T. «Emergent criticality through adaptive information processing in boolean networks». *Phys. Rev. Lett.* **108**, 128702 (2012).
- [16] GREIL, F. & DROSSEL, B. «Dynamics of critical kauffman networks under asynchronous stochastic update». *Phys. Rev. Lett.* **95**, 048701 (2005).
- [17] GROS, C. *Random Boolean networks* (Springer, Berlin Heidelberg, 2011).
- [18] HAIMOVICI, A., TAGLIAZUCCHI, E., BALENZUELA, P. & CHIALVO, D. R. «Brain Organization into Resting State Networks Emerges at Criticality on a Model of the Human Connectome». *Phys. Rev. Lett.* **110**, 178101 (2013).
- [19] HENKEL, M., HINRICHSSEN, H. & LÜBECK, S. *Non-equilibrium Phase Transitions: Absorbing phase transitions*. Theoretical and mathematical physics (Springer, Berlin, 2008).
- [20] HESSE, J. & GROSS, T. «Self-organized criticality as a fundamental property of neural systems». *Front. Sys. Neurosci.* **8** (2014).
- [21] KAISER, M. & HILGETAG, C. C. «Optimal hierarchical modular topologies for producing limited sustained activation of neural networks». *Front. Neuroinform.* **4** (2010).
- [22] KAUFFMAN, S. «Metabolic stability and epigenesis in randomly constructed genetic nets». *J. Theor. Biol.* **22**, 437–467 (1969).
- [23] KAUFFMAN, S. A. *The origins of order: Self-organization and selection in evolution* (Oxford university press, New York, 1993).
- [24] KAUFFMAN, S., PETERSON, C., SAMUELSSON, B. & TROEIN, C. «Genetic networks with canalizing boolean rules are always stable». *Proc. Natl. Acad. Sci. USA* **101**, 17102–17107 (2004).
- [25] KAUFFMAN, S., PETERSON, C., SAMUELSSON, B. & TROEIN, C. «Random boolean network models and the yeast transcriptional network». *Proc. Natl. Acad. Sci. USA* **100**, 14796–14799 (2003).

- [26] KITANO, H. «Systems biology: a brief overview». *Science* **295**, 1662–1664 (2002).
- [27] KITANO, H. «Computational systems biology». *Nature* **420**, 206–210 (2002).
- [28] LINKENKAER-HANSEN, K., NIKOULINE, V. V., PALVA, J. M. & ILMONIEMI, R. J. «Long-range temporal correlations and scaling behavior in human brain oscillations». *J. Neurosci.* **21**, 1370–1377 (2001).
- [29] MARKRAM, H. *et al.* «Reconstruction and simulation of neocortical microcircuitry». *Cell* **163**, 456–492 (2015).
- [30] MARRO, J. & DICKMAN, R. *Nonequilibrium phase transitions in lattice models* (Cambridge University Press, Cambridge, 2005).
- [31] MERCER, T. R., DINGER, M. E. & MATTICK, J. S. «Long non-coding rnas: insights into functions». *Nat. Rev. Gen.* **10**, 155–159 (2009).
- [32] MEUNIER, D., LAMBIOTTE, R. & BULLMORE, E. «Modular and hierarchically modular organization of brain networks». *Front. Neurosci.* **4**, 200 (2010).
- [33] MORETTI, P. & MUÑOZ, M. A. «Griffiths phases and the stretching of criticality in brain networks». *Nat. Comm.* **4**, – (2013).
- [34] MUÑOZ, M. A. «Colloquium: Criticality and dynamical scaling in living systems». *arXiv preprint arXiv:1712.04499* (2017).
- [35] MUÑOZ, M. A. & PASTOR-SATORRAS, R. «Stochastic theory of synchronization transitions in extended systems». *Phys. Rev. Lett.* **90**, 204101 (2003).
- [36] MURPHY, B. K. & MILLER, K. D. «Balanced amplification: a new mechanism of selective amplification of neural activity patterns». *Neuron* **61**, 635–648 (2009).
- [37] OKUJENI, S., KANDLER, S. & EGERT, U. «Mesoscale architecture shapes initiation and richness of spontaneous network activity». *J. Neurosci.* **37**, 3972–3987 (2017).
- [38] RÄMÖ, P., KESSELI, J. & YLI-HARJA, O. «Perturbation avalanches and criticality in gene regulatory networks». *J. Theor. Biol.* **242**, 164–170 (2006).
- [39] ROSENBLUM, M. G., PIKOVSKY, A. & KURTHS, J. *Synchronization – A universal concept in nonlinear sciences* (Cambridge University Press, Cambridge, 2001).

-
- [40] RUBINOV, M., SPORNS, O., THIVIERGE, J.-P. & BREAKSPEAR, M. «Neurobiologically realistic determinants of self-organized criticality in networks of spiking neurons». *PLoS Comp. Biol.* **7**, e1002038 (2011).
- [41] SHEW, W. L., YANG, H., PETERMANN, T., ROY, R. & PLENZ, D. «Neuronal avalanches imply maximum dynamic range in cortical networks at criticality». *J. Neurosci.* **29**, 15595–15600 (2009).
- [42] SHMULEVICH, I., KAUFFMAN, S. A. & ALDANA, M. «Eukaryotic cells are dynamically ordered or critical but not chaotic». *Proc. Natl. Acad. Sci. USA* **102**, 13439–13444 (2005).
- [43] SPORNS, O. *Networks of the Brain* (MIT Press, Cambridge, 2010).
- [44] STERIADE, M., NUNEZ, A. & AMZICA, F. «A novel slow (< 1 Hz) oscillation of neocortical neurons in vivo: depolarizing and hyperpolarizing components». *J. Neurosci.* **13**, 3252–3265 (1993).
- [45] YAN, K.-K., FANG, G., BHARDWAJ, N., ALEXANDER, R. P. & GERSTEIN, M. «Comparing genomes to computer operating systems in terms of the topology and evolution of their regulatory control networks». *Proc. Natl. Acad. Sci. USA* **107**, 9186–9191 (2010).
- [46] ZHOU, C., ZEMANOVÁ, L., ZAMORA-LÓPEZ, G., HILGETAG, C. & KURTHS, J. «Hierarchical Organization Unveiled by Functional Connectivity in Complex Brain Networks». *Phys. Rev. Lett.* **97** (2006).

Annexes

Appendix

Introduction to critical phenomena

A.1 On the Itô-Stratonovich dilemma	243
References	244

A.1

On the Itô-Stratonovich dilemma

Let's consider a general Langevin equation of the form,

$$\dot{\phi} = a(\phi) + b(\phi) \xi(t)$$

The Itô-Stratonovich dilemma arises as a result of the “appropriate” integration of Langevin equations with delta-correlated noise, $\xi(\mathbf{x}, t)$, with $\langle \xi(t) \rangle = 0$ and $\langle \xi(t) \xi(t') \rangle = \frac{\sigma^2}{2} \delta(t - t')$. In a nutshell, instead of $\delta(t - t')$ it is possible to consider a function with a sharp peak (e.g. $\langle \xi(t) \xi(t') \rangle = \frac{1}{2\tau} e^{-\frac{|t-t'|}{\tau}}$, because it remained doubtful whether a delta-function have some physical sense), both causing a jump in $\phi(t)$. However, while the noise is affecting the system, the value of $b(\phi)$ is wholly indeterminate. A possible prescription is to consider the value before the jump, or the mean value during the jump [1–3].

The first one, the Itô convention, is equivalent to the next Fokker-Planck equation,

$$\dot{P}(\phi, t) = -\frac{\partial}{\partial \phi} a(\phi) P(\phi, t) + \frac{\sigma^2}{2} \frac{\partial^2}{\partial \phi^2} b^2(\phi) P(\phi, t)$$

while the second one, the Stratonovich convention, is equivalent to,

$$\dot{P}(\phi, t) = -\frac{\partial}{\partial \phi} a(\phi) P(\phi, t) + \frac{\sigma^2}{2} \frac{\partial}{\partial \phi} b(\phi) \frac{\partial}{\partial \phi} b(\phi) P(\phi, t)$$

In addition, the change of variables in the Langevin equation, under the Stratonovich choice, is exactly the same as in ordinary calculus but, in the other case, new transformation laws should be formulated. Pleasantly, both formalisms are equivalent, under the following transformations [1],

An Itô SDE	$\dot{\phi} = a(\phi) + b(\phi) \xi(t)$
is equivalent to the Stratonovich SDE	$\dot{\phi} = \left[a(\phi) - \frac{1}{2} b(\phi) \partial_{\phi} b(\phi) \right] + b(\phi) \xi(t)$

or conversely,

the Stratonovich SDE	$\dot{\phi} = \alpha(\phi) + \beta(\phi) \xi(t)$
is equivalent to the Itô SDE	$\dot{\phi} = \left[\alpha(\phi) + \frac{1}{2} \beta(\phi) \partial_{\phi} \beta(\phi) \right] + \beta(\phi) \xi(t)$

However, not all is rosy: the physical modeling of noisy phenomena, most of the time, draw from a Langevin equation with multiplicative noise, and not from a Fokker-Planck equation that distinguish between them. Thus, both formalisms lead to completely different results, and the proper prescription should be chosen a priori. Generally, there exists specific examples to argue that the Itô convention is the most suitable option for systems with internal noise, i.e. that cannot be switched off and thus, the isolated system is inconceivable (such as decay processes, chemical reactions or emissions of photons) while the Stratonovich convention is the appropriate in the case of external noise, where it can be switched off and $a(\phi)$ constitutes the deterministic dynamics of the isolated system (noise generators in electric circuits or growth of species under external perturbations like weather) [1, 3]. Finally, take present that, for the simple case in which $b(\phi)$ is a constant, both conventions are fully equivalent and the dilemma blurs completely.

References

- [1] GARDINER, C. W. *Handbook of stochastic methods: for physics, chemistry and the natural sciences; 3rd ed.* Springer Series in Synergetics (Springer, Berlin, 2004).
- [2] TORAL, R. & COLET, P. *Stochastic numerical methods: an introduction for students and scientists* (John Wiley & Sons, Weinheim, 2014).
- [3] VAN KAMPEN, N. G. *Stochastic processes in physics and chemistry*, vol. 1 (Elsevier, 1992).

Landau-Ginzburg theory of cortical dynamics

B.1	Robustness against dynamical and structural changes	247
B.1.1	Changes in the dynamics	247
B.2	Detrended fluctuation analysis	251
B.3	On the definition of avalanches	253
B.3.1	Oscillations coexisting with scale invariance	253
B.3.2	On avalanches measure	254
References	257

B.1

Robustness against dynamical and structural changes

B.1.1

Changes in the dynamics

In this appendix we confirm the robustness of the results and conclusions presented in the main part with respect to the modification of diverse ingredients and modeling details. In particular, we first discuss the full model including synaptic plasticity, but without truncating the equation for activity in a series expansion and, second, we consider inhibition as encapsulated in the well-known Wilson-Cowan equations as a chief regulatory mechanism (rather than synaptic plasticity).

B.1.1.1 Non-truncated excitatory-activity equation

The dynamics in a mesoscopic region of the cortex or “unit” is described by a Wilson-Cowan equation [14] for the excitatory activity –such that the activity grows with the incoming current through a sigmoid response function– together with the Tsodyks-Markram TM model for synaptic plasticity [9]:

$$\begin{cases} \dot{\rho} = -\alpha\rho + (1 - \rho) \tanh(a\rho R + p) + h \\ \dot{R} = \frac{1}{\tau_R} (\xi - R) - \frac{1}{\tau_D} \rho R. \end{cases} \quad (\text{B.1.1})$$

In Figure B.1.1, we illustrate that a linear-stability analysis reproduces a Hopf bifurcation scenario, as in the most relevant case (case A) discussed in the chapter. When noise and spatial coupling are added, and the system is studied on a two-dimensional lattice, a synchronous irregular regime of network spikes, as well as an asynchronous irregular regime of nested oscillations –fully analogous to their corresponding counterparts in the the main text– are found, as graphically illustrated by the lower panels of Figure B.1.1. This unveils the existence of a synchronization transition and confirms that the simplified truncated equation for the activity considered in the main text is a valid approximation of the full dynamics. Here we do not show a detailed analysis of the synchronization transition nor of the emergence of scale-free avalanches; but, let us remark that we have not found any substantial qualitative difference with respect to the case discussed in the paper in any of our exploratory checks.

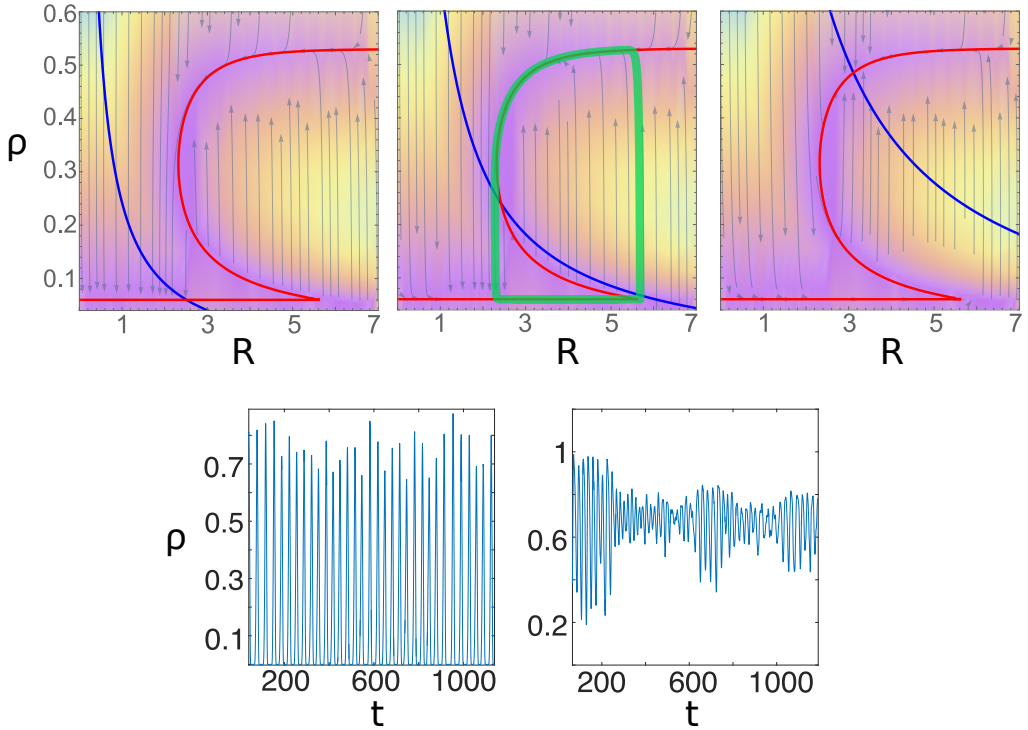


Figure B.1.1: Analysis of the model of Eq. B.1.1. Upper panels: deterministic phase portrait with $\xi = 5, 12, 28$ (from left to right), respectively, showing a down state, a limit cycle and up state regimes, as in the case A of the main text. Other parameters are $\alpha = a = 1$, $\tau_D^{-1} = 0.033$, $\tau_R = 500$, $p = -0.34$, $h = 0.06$. Varying parameter values, it is possible to find either a similar Hopf bifurcation (case A) or a saddle node bifurcation (case B), as in the model with the truncated expansion. Lower panels: Temporal evolution of the total activity $\rho(t)$ on a two-dimensional lattice with $N = 64^2$ (after having introduced noise and coupling); in the (left) synchronous (network spiking) and in the (right) asynchronous (nested oscillations) regimes, respectively, revealing the presence of a synchronization phase transition between the two regimes; parameter values: $\xi = 5$ and $\xi = 13$, respectively.

B.1.1.2 Beyond the TM model. The Wilson-Cowan approach

In this section we consider the Wilson-Cowan equations [14], including both excitatory and inhibitory neural populations for each mesoscopic region or unit. In this case, inhibition plays the role of chief homeostatic mechanism, regulating the level of the overall network activity. More specifically, we consider a version of the Wilson-Cowan dynamics, including also intrinsic noise as corresponds to large but finite (mesoscopic) regions. Such a model was derived in a very interesting work from an underlying microscopic model [2], and is described by the following set of stochastic equations for the densities of excitatory (E) and inhibitory (I) neurons:

$$\begin{cases} \dot{E}_i &= -\alpha E_i + (1 - E_i) \tanh[\omega_{EE} E_i - \omega_{IE} I_i + h] \\ &\quad + \sigma \sqrt{\alpha E_i + (1 - E_i) \tanh[\omega_{EE} E_i - \omega_{IE} I_i + h]} \\ \dot{I}_i &= -\alpha I_i + (1 - I_i) \tanh[\omega_{EI} E_i - \omega_{II} I_i + h] \\ &\quad + \sigma \sqrt{\alpha I_i + (1 - I_i) \tanh[\omega_{EI} E_i - \omega_{II} I_i + h]}, \end{cases} \quad (\text{B.1.2})$$

where α is the decay rate for the activity, h is an external driving field, σ is the noise amplitude, and ω_{ij} (with $i, j = E, I$) are the couplings between population i and j within a single unit; particularly important here is the auto-excitation coupling ω_{EE} , which we take as a control parameter. First of all, these equations are analyzed in the (noiseless) mean field limit. By increasing ω_{EE} , the system exhibits a transition from a “down” state to an “up” state (see Fig. B.1.2). Thus, a saddle-node bifurcation separates a state of high activity from a state of low activity, we found no track of a possible Hopf bifurcation. However, very interestingly, as soon as noise is switched on (i.e. $\sigma \neq 0$), a noise-induced phenomenon appears: trajectories nearby the up-state fixed point, can escape from its basin of attraction as a result of fluctuations, and are then almost deterministically driven towards the down state, where a similar mechanism makes them escape with some probability. This phenomenon has been recently scrutinized in a very interesting work, where the role of non-normal forms has been emphasized [2]. This mechanism, generates in an effective way a noise-induced limit cycle between up and down states, which plays the same role as the deterministic limit cycle (Hopf bifurcation) of case A. As a matter of fact, computer simulations of units described by Eq.(B.1.2), and coupled diffusively, give rise to the phenomenology illustrated in Fig.B.1.2: as the control parameter ω_{EE} is increased, the system undergoes a phase transition from a synchronous phase with very distinctive network spikes, to an asynchronous regime with nested oscillations, as it happens in the model with synaptic plasticity. Thus, also in this case, the phases are the same as in the main text and a synchronization transition appears between them.

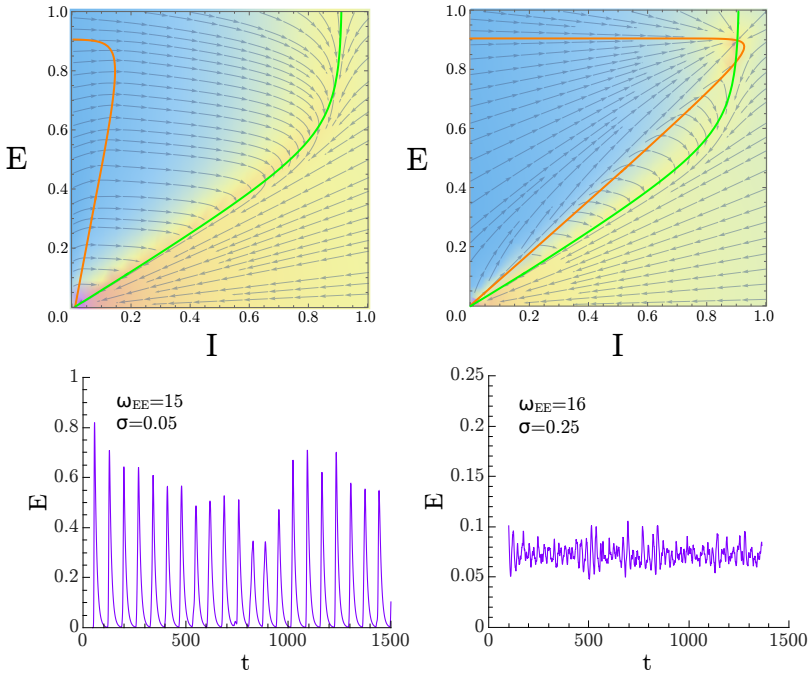


Figure B.1.2: Upper panels: mean-field analysis of the Wilson-Cowan set of Eqs. (B.1.2) describing both excitatory and inhibitory neural populations at each single unit, with parameters such that a noise-induced limit cycle (see [7]) in between a down and an up state can emerge once a non-vanishing noise is switched on. Observe that there is (left) a stable down-state fixed point ($\omega_{EE} = 4$) and a (right) stable up state ($\omega_{EE} = 16$); however the basin of attraction of the up state is small, and a relatively small fluctuation can induce the system state to go beyond the saddle-node line, where deterministic trajectories take the system toward the down state. In the lower panels we illustrate results of a computer simulation for a two-dimensional lattice of coupled noisy units, Eq.(B.1.2), corresponding to (left) synchronous/network-spiking and (right) asynchronous/nested-oscillation regimes. Parameter values: $D = 1$, $\omega_{EI} = 4.65$, $\omega_{IE} = 14.0$, $\omega_{II} = 2.8$, $h = 10^{-3}$ and $\alpha = 0.1$. Control parameter $\omega_{EE} = 15$ for SI regime and $\omega_{EE} = 16$ for the AI regime.

B.2

Detrended fluctuation analysis

In this section we present an additional criterion to discriminate whether the system lays at a critical point or in either the subcritical or the supercritical phases. The method is based on the fact that, at the critical point of a (second order) phase transition, the (time-dependent) order parameter, as measured in any finite system, shows long-range temporal correlations (long-memory effects), which can be quantified by measuring its Hurst exponent [8]. The Hurst exponent of a time series is a measure of the dispersion of a process on a scaling support. For example the Hurst exponent of an uncorrelated signal (white noise) is $\alpha = 1/2$, since the root mean square translation distance after n steps of a Wiener process, i.e. an unbiased random walk (the process obtained by integrating white noise), is proportional to \sqrt{n} . For correlated signals (colored noises) one expects bigger Hurst exponents (as a reference, $\alpha \simeq 1$ is found for pink noise). The Hurst exponent can be calculated by splitting the time series into adjacent windows, plotting the square-root displacement from the mean as a function of the window size and evaluating the exponent of the resulting power law (see below). More specifically, “detrended fluctuation analysis” (DFA) is a technique for measuring the Hurst exponent in a non-stationary time series: the “detrending” operation allows to remove fictitious memory effects related to non-stationarity, and it basically consists in subtracting the local “trend” (usually a linear fit) of the signal before performing the analysis on each window. DFA consists of two steps: the data series $\rho(t)$ is shifted by its mean $\bar{\rho}$ and integrated (cumulatively summed):

$$\mathcal{P}(\tau) = \sum_{t=1}^{\tau} (\rho(t) - \bar{\rho}); \quad (\text{B.2.1})$$

then segmented into k windows of various sizes n , and for each window size, a fluctuation function $F(n)$ is calculated, as

$$F(n) = \sqrt{\frac{1}{T} \sum_{h=1}^k \sum_{\tau=1}^n \left(\mathcal{P}^{(n)}(\tau + (h-1)n) - X_{\mathcal{P}}^{(n)} \right)^2} \quad (\text{B.2.2})$$

where $X_{\mathcal{P}}^{(n,h)}$ is the linear regression of $\mathcal{P}^{(n)}(\tau)$, with $\tau \in [(h-1)n, hn]$, the superscript indicates the dependence on the window size n and $T = kn$ is the total length of the time series. If $F(n) \sim n^{-\alpha}$, then α is the Hurst exponent [7, 12].

We performed a DFA on the global signal $\rho(t)$ coming out of our computer simulations for different values of the control parameter ξ (in the synchronous and asynchronous phases as well as at the critical point). Results are shown in Fig.B.2.1: (i) the fluctuations in the asynchronous phase grow approximately as the square root of the window length, as predicted for white noise behavior; (ii) in the synchronous phase, above a certain characteristic length, the dependence is very weak, remarking the existence of a certain degree of order, i.e. a characteristic time scale at which there is order, i.e. synchronization; (iii) just at the critical point the growth of the fluctuations is anomalously large, confirming the existence of long-range correlations, signature of criticality. Therefore from the global activity signal we are able –through a DFA analysis– to discriminate whether long-range correlations, characteristic of criticality, emerge or not.

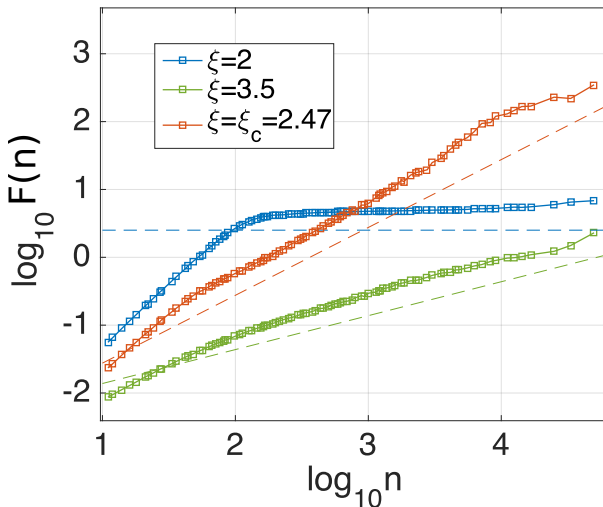


Figure B.2.1: Detrended fluctuation analysis of the macroscopic signal for control parameter $\xi = 2, 2.47, 3.5$ in the synchronous, critical, and asynchronous regimes, respectively. The considered system size is $N = 2^{14}$. Other parameter values are taken as in the main text. Close to the transition point the DFA shows an Hurst exponent close to 1, implying long-range autocorrelations, a fingerprint of criticality.

B.3

On the definition of avalanches

B.3.1

Oscillations coexisting with scale invariance

Usually, scale-free avalanches of activity can be measured at the critical point of an *absorbing-state phase transition*. When the concept of “avalanche” is employed to describe the critical point of a synchronization phase transition, the marginal oscillatory nature of the system unavoidably introduces a characteristic time scale –i.e. the period of the oscillation– which, in principle, is in contrast with the idea of scale-invariance. However, the two concepts can coexist –at least within certain limited scales– as illustrated in Fig. B.3.1. We show how the structure (e.g. the peaks) in the avalanche-time distribution (inset) corresponds to the period of oscillation of a macroscopic variable (the total number of spikes, in the main plot); for instance, an isolated network synchronization event has a typical duration of 2000 (in arbitrary units), a sequence of two, about 5000, etc. On the other hand, the whole distribution, once these peaks are ignored can be approximately described as a power law with the expected exponent values.

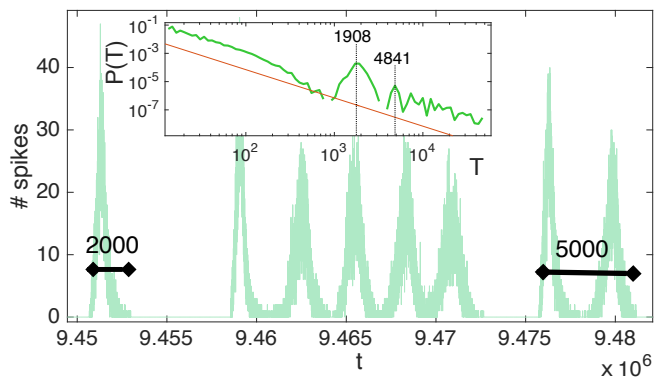


Figure B.3.1: Analysis of the structure underlying the avalanche-duration distributions. The main figure shows the total number of spikes at time t . Irregular oscillations of the global activity can be recognized, as the system is close to the edge of the synchronization phase transition. The characteristic period of an isolated oscillation corresponds to the peak in the avalanche duration distribution, while its multiples correspond to smaller peaks. System size $N = 128^2$.

B.3.2

On avalanches measure

As it has already been widely discussed in the literature, not all power laws are a signature of criticality [1, 10, 11]. In this section we highlight some possible sources of error while investigating the relation between self-similarity and criticality in the brain.

B.3.2.1 Non critical avalanches

In a simple continuous-time stochastic process describing the activity of a system, the duration of an avalanche could be defined as the extent of the time interval during which activity stays over a threshold (i.e. an avalanche begins/ends when the activity signal crosses beyond/below threshold). Let us suppose, for argument's sake that the original signal was a Wiener process (unbiased random walk), this would correspond to determining the statistics of first passage times through a barrier (i.e. the threshold); this is well known (both numerically and analytically) to be scale-invariant, as a consequence of the lack of any characteristic scale, but not critical in the sense of lying at the edge of a phase transition.

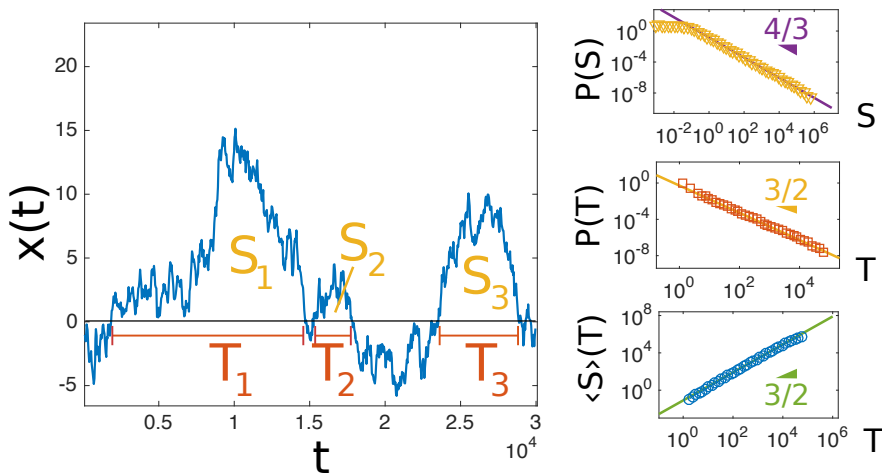


Figure B.3.2: Illustration of the first return time statistics of a Random Walk. Left panel: sketch of the process together with the illustration of the sizes and durations of three avalanches. Threshold is set to 0. Right panels (from up to down): size and duration distributions, and average size of a given duration, showing good agreement between numerical results (open symbols) and analytical ones (full lines).

Thus let us note that if the global activity of a neural system happens to fluctuate around a stable sustained state, when performing an analysis of avalanching behavior through a thresholding procedure, cascades of activity would result scale free distributed, just as an effect of fluctuations. In fact, this scenario, at a macroscopic scale, is equivalent to an Ornstein-Uhlenbeck process:

$$\dot{x}(t) = -ax(t) + h + \sigma\eta(t), \quad (\text{B.3.1})$$

where $\eta(t)$ is a delta-correlated, white noise with zero mean and unitary variance; the linear term (force) $-ax$ corresponds to the derivative of a parabolic potential bounding the walker close to h/a . Note that with $a = 0$ this is nothing but the usual free random walker or Wiener process [4]. The force introduces an upper cutoff in the first return times (i.e. avalanche duration) statistics, which, otherwise, follows the same exponents as the unbiased random walk. Thus, studying avalanches by analyzing fluctuations about a given threshold in a process with a well-defined steady-state value, one recovers power-laws, up to a scale controlled by $1/a$. These, however, are not critical in the sense of lying at the edge of a continuous phase transition.

B.3.2.2 On avalanche size

Also, particular attention is needed for the correct definition of the “size” of an avalanche: for example in a few recent publications [5, 13], the authors used a definition of *size* which leads to a misclassification of the power law exponent and thus, to a possible misinterpretation of the results. Indeed, the defined size of an avalanche is the integral of the activity during the avalanche (instead of the integral of the activity *over threshold* during the avalanche); this is illustrated in Fig.B.3.3. Proceeding in this way, the actual size is corrected with an additional term proportional to the avalanche duration (as also illustrated in the Figure). This additional term complicates the scaling analysis.

In particular, given that a standard random walk (or a Ornstein-Uhlenbeck process describing fluctuations around a mean value) has first-return times distributed as $P(T) \sim T^{-3/2}$ ($\alpha = 3/2$), the wrong measure have a correction to the true asymptotic behavior which scales with an exponent $\tau \approx 3/2$, which actually comes from including in the measure of the size an extra part proportional to the duration of the avalanche [5, 13]. Observe, therefore, that this $3/2$ has nothing to do with a critical branching process (beside the numerical coincidence): it is a spurious effect, coming from the first-passage time distribution of an effective Ornstein-Uhlenbeck process. In particular, both sizes and times turn out to be distributed with the same exponent with this definition of size, which is not the case in critical branching processes. One needs to go to huge system sizes, to see the actual scaling.

Finally, we should remark that another couple of recent papers underline the “perils” associated with thresholding, which can certainly be a source of confusion [3, 6].

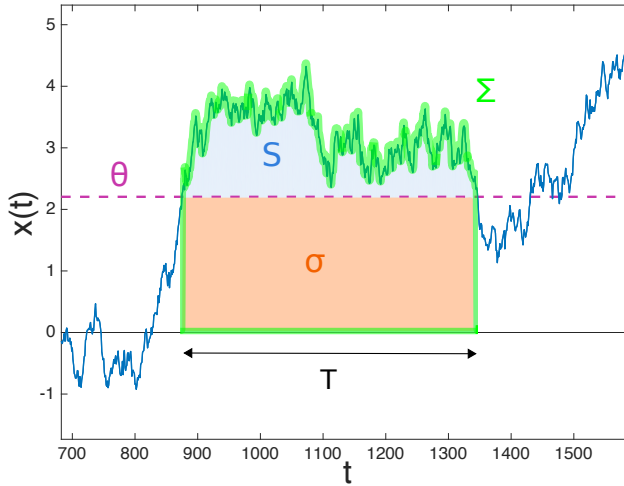


Figure B.3.3: Analysis of first-passage times in a stochastic process; θ (magenta dashed line) is the threshold value employed to define crossings. S is the proper avalanche size (area above threshold, colored in blue in figure), T is its duration, Σ (delimited by the green contour) is the misleading definition of the avalanche size, as used in [13]. One has $\Sigma = S + \sigma$, with σ colored in orange in figure (note that $\sigma \propto T$).

References

- [1] BEGGS, J. & TIMME, N. «Being Critical of Criticality in the Brain». *Front. Physiol.* **3**, 163 (2012).
- [2] BENAYOUN, M., COWAN, J. D., VAN DRONGELEN, W. & WALLACE, E. «Avalanches in a stochastic model of spiking neurons». *PLoS Comp. Biol.* **6**, e1000846 (2010).
- [3] FONT-CLOS, F., PRUESSNER, G., MOLONEY, N. R. & DELUCA, A. «The perils of thresholding». *New J. Phys.* **17**, 043066 (2015).
- [4] GARDINER, C. W. *Handbook of stochastic methods: for physics, chemistry and the natural sciences; 3rd ed.* Springer Series in Synergetics (Springer, Berlin, 2004).
- [5] LARREMORE, D. B., SHEW, W. L., OTT, E., SORRENTINO, F. & RESTREPO, J. G. «Inhibition causes ceaseless dynamics in networks of excitable nodes». *Phys. Rev. Lett.* **112**, 138103 (2014).
- [6] LAURSON, L., ILLA, X. & ALAVA, M. J. «The effect of thresholding on temporal avalanche statistics». *J. Stat. Mech. Theory Exp.* **2009**, P01019 (2009).
- [7] LINKENKAER-HANSEN, K., NIKOULINE, V. V., PALVA, J. M. & ILMONIEMI, R. J. «Long-Range Temporal Correlations and Scaling Behavior in Human Brain Oscillations». *J. Neurosci.* **21**, 1370–1377 (2001).
- [8] MANTEGNA, R. N. & STANLEY, H. E. *Introduction to econophysics: correlations and complexity in finance* (Cambridge University Press, Cambridge, 1999).
- [9] MARKRAM, H. & TSODYKS, M. «Redistribution of synaptic efficacy between pyramidal neurons». *Nature* **382**, 807–810 (1996).
- [10] MITZENMACHER, M. «A Brief History of Generative Models for Power Law and Lognormal Distributions». *Internet Math.* **1**, 226–251 (2002).
- [11] NEWMAN, M. E. J. «Power laws, Pareto distributions and Zipf's law». *Contemp. Phys.* **46**, 323–351 (2005).
- [12] PENG, C.-K., HAVLIN, S., STANLEY, H. E. & GOLDBERGER, A. L. «Quantification of scaling exponents and crossover phenomena in nonstationary heartbeat time series». *Chaos* **5**, 82–87 (1995).

- [13] POIL, S.-S., HARDSTONE, R., MANSVELDER, H. D. & LINKENKAER-HANSEN, K. «Critical-state dynamics of avalanches and oscillations jointly emerge from balanced excitation/inhibition in neuronal networks». *J. Neurosci.* **32**, 9817–9823 (2012).
- [14] WILSON, H. R. & COWAN, J. D. «Excitatory and inhibitory interactions in localized populations of model neurons». *Biophys. J.* **12**, 1–24 (1972).

Kuramoto model

C.1	Ott-Antonsen ansatz	261
C.1.1	Lorentz distribution of natural frequencies	264
C.2	Complex networks	265
C.2.1	Critical point in homogeneous graphs	265
C.2.2	Equally frequency distributed oscillators $\omega_i = 0$	268
	References	271

C.1

Ott-Antonsen ansatz

Remember the equation 3.2.13,

$$\frac{\partial f}{\partial t} + \frac{\partial}{\partial \theta} \{f [\omega + kR \sin(\psi - \theta)]\} = 0$$

and the assumption that $f(\theta, \omega, t)$ can be expanded in Fourier series as,

$$f(\theta, \omega, t) = \frac{g(\omega)}{2\pi} \left[1 + \sum_{n=1}^{\infty} \left(\hat{f}_n(\omega, t) e^{in\theta} + \hat{f}_n^*(\omega, t) e^{-in\theta} \right) \right] \quad (\text{C.1.1})$$

Thus, by inserting the Fourier series in our continuity equation, it can be shown that,

i) $\frac{\partial f}{\partial t}$

$$\frac{\partial f}{\partial t} = \frac{\partial}{\partial t} \left\{ \frac{g(\omega)}{2\pi} \left[1 + \sum_{n=1}^{\infty} \left(a^n(\omega, t) e^{in\theta} + \bar{a}^n(\omega, t) e^{-in\theta} \right) \right] \right\}$$

Multiplying by $\int_0^{2\pi} d\theta e^{-i\theta}$ in both sides,

$$\int_0^{2\pi} d\theta e^{-i\theta} \frac{\partial f}{\partial t} = \frac{\partial}{\partial t} \left\{ g(\omega) \sum_{n=1}^{\infty} \left[\left(a^n \int_0^{2\pi} \frac{d\theta}{2\pi} e^{i(n-1)\theta} + \bar{a}^n \int_0^{2\pi} \frac{d\theta}{2\pi} e^{i(-n-1)\theta} \right) \right] \right\}$$

and remembering that, $\int_0^{2\pi} \frac{d\theta}{2\pi} e^{in\theta} = \delta_{n,0}$ is the Kronecker delta function,

$$\int_0^{2\pi} d\theta e^{-i\theta} \frac{\partial f}{\partial t} = g(\omega) \frac{\partial}{\partial t} \sum_{n=1}^{\infty} \left(a^n \delta_{n-1,0} + \underbrace{\bar{a}^n \delta_{-n-1,0}}_0 \right) = g(\omega) \dot{a}(\omega, t)$$

ii) $\frac{\partial}{\partial \theta} (f \cdot \omega)$

$$\begin{aligned} & \int_0^{2\pi} d\theta e^{-i\theta} \frac{\partial}{\partial \theta} (f \cdot \omega) = \\ & \int_0^{2\pi} d\theta e^{-i\theta} \frac{\partial}{\partial \theta} \left\{ \omega \frac{g(\omega)}{2\pi} \left[1 + \sum_{n=1}^{\infty} \left(a^n(\omega, t) e^{in\theta} + \bar{a}^n(\omega, t) e^{-in\theta} \right) \right] \right\} = \\ & \omega g(\omega) \sum_{n=1}^{\infty} in \left(a^n \int_0^{2\pi} \frac{d\theta}{2\pi} e^{i(n-1)\theta} - \bar{a}^n \int_0^{2\pi} \frac{d\theta}{2\pi} e^{i(-n-1)\theta} \right) = \\ & i\omega g(\omega) \sum_{n=1}^{\infty} \left(a^n \delta_{n-1,0} - \underbrace{\bar{a}^n \delta_{-n-1,0}}_0 \right) = i\omega g(\omega) a(\omega, t) \end{aligned}$$

iii) $\frac{\partial}{\partial \theta} \left[f \cdot \frac{k}{2i} (Ze^{-i\theta} - \bar{Z}e^{i\theta}) \right]$

$$\begin{aligned} & \int_0^{2\pi} d\theta e^{-i\theta} \frac{\partial}{\partial \theta} \left[P \cdot \frac{k}{2i} (Ze^{-i\theta} - \bar{Z}e^{i\theta}) \right] = \\ & g(\omega) \frac{k}{2i} \int_0^{2\pi} \frac{d\theta}{2\pi} e^{-i\theta} \frac{\partial}{\partial \theta} \left\{ (Ze^{-i\theta} - \bar{Z}e^{i\theta}) + \sum_{n=1}^{\infty} \left[a^n (Ze^{i(n-1)\theta} - \bar{Z}e^{i(n+1)\theta}) \right. \right. \\ & \quad \left. \left. + \bar{a}^n (Ze^{i(-n-1)\theta} - \bar{Z}e^{i(-n+1)\theta}) \right] \right\} = \\ & g(\omega) \frac{k}{2i} \int_0^{2\pi} \frac{d\theta}{2\pi} e^{-i\theta} \left\{ (-iZe^{-i\theta} - i\bar{Z}e^{i\theta}) + i \sum_{n=1}^{\infty} \left[a^n \left((n-1)Ze^{i(n-1)\theta} - (n+1)\bar{Z}e^{i(n+1)\theta} \right) \right. \right. \\ & \quad \left. \left. + \bar{a}^n \left((-n-1)Ze^{i(-n-1)\theta} - (-n+1)\bar{Z}e^{i(-n+1)\theta} \right) \right] \right\} = \\ & g(\omega) \frac{k}{2i} \left\{ \left(-iZ \underbrace{\int_0^{2\pi} \frac{d\theta}{2\pi} e^{-2i\theta}}_0 - i\bar{Z} \int_0^{2\pi} \frac{d\theta}{2\pi} \right) \right. \\ & \quad + i \sum_{n=1}^{\infty} \left[a^n \left((n-1)Z \int_0^{2\pi} \frac{d\theta}{2\pi} e^{i(n-2)\theta} - (n+1)\bar{Z} \int_0^{2\pi} \frac{d\theta}{2\pi} e^{in\theta} \right) \right. \\ & \quad \left. \left. + \bar{a}^n \left((-n-1)Z \int_0^{2\pi} \frac{d\theta}{2\pi} e^{i(-n-2)\theta} - (-n+1)\bar{Z} \int_0^{2\pi} \frac{d\theta}{2\pi} e^{-in\theta} \right) \right] \right\} = \end{aligned}$$

$$\begin{aligned}
 g(\omega) \frac{k}{2i} \left\{ -i\bar{z} + i \sum_{n=1}^{\infty} \left[a^n \left((n-1) z \delta_{n-2,0} - (n+1) \underbrace{\bar{z} \delta_{n,0}}_0 \right) \right. \right. \\
 \left. \left. + \bar{a}^n \left((-n-1) \underbrace{Z \delta_{-n-2,0}}_0 - (-n+1) \underbrace{\bar{Z} \delta_{-n,0}}_0 \right) \right] \right\} = \\
 g(\omega) \frac{k}{2i} (-i\bar{Z} - ia^2 Z) = g(\omega) \frac{k}{2} (a^2 Z - \bar{Z})
 \end{aligned}$$

$$\boxed{\dot{a} + i\omega a + \frac{k}{2} (a^2 Z - \bar{Z}) = 0}$$

q.e.d.

For the second condition, introducing the Fourier series expansion in the definition of Z ,

$$\begin{aligned}
 Z &= \int_{-\infty}^{+\infty} d\omega \int_0^{2\pi} e^{i\theta} f(\theta, \omega, t) d\theta = \\
 &\int_{-\infty}^{+\infty} g(\omega) d\omega \int_0^{2\pi} \frac{d\theta}{2\pi} e^{i\theta} \left[1 + \sum_{n=1}^{\infty} (a^n e^{in\theta} + \bar{a}^n e^{-in\theta}) \right] d\theta = \\
 &\int_{-\infty}^{+\infty} g(\omega) d\omega \sum_{n=1}^{\infty} (a^n \delta_{n+1,0} + \bar{a}^n \delta_{-n+1,0}) = \int_{-\infty}^{+\infty} g(\omega) d\omega \bar{a}(\omega, t)
 \end{aligned}$$

C.1.1

Lorentz distribution of natural frequencies

Be a Cauchy-Lorentz distribution for $g(\omega)$,

$$g(\omega) = \frac{\gamma}{\pi [\gamma^2 + (\omega - \Omega_0)^2]} \Rightarrow Z = \int_{-\infty}^{+\infty} \frac{\gamma}{\pi [\gamma^2 + (\omega - \Omega_0)^2]} d\omega \bar{a}(\omega, t)$$

The integral can be done taking a contour in the ω lower half-plane. But taking $g(\omega) = (2\pi i)^{-1} [(\omega - \Omega_0 - i\gamma)^{-1} - (\omega - \Omega_0 + i\gamma)^{-1}]$, one can see that the integral corresponds to the residue in the pole $\omega = \Omega_0 - i\gamma$. Thus, $Z = \bar{a}(\Omega_0 - i\gamma, t)$.

Employing the above equation, evaluated in $\omega = \Omega_0 - i\gamma$, we have,

$$\dot{Z} + (\gamma - i\Omega_0) Z + \frac{k}{2} (\bar{Z} Z^2 - Z) = 0$$

with the additional condition,

$$\dot{Z} = \frac{d}{dt} (R e^{i\psi}) = (\dot{R} + i\dot{\psi} R) e^{i\psi}$$

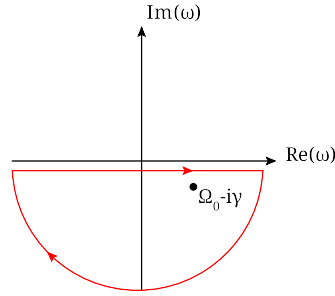


Figure C.1.1: Integration contour

Finally, the next set of differential equations can be derived,

$$(\dot{R} + i\dot{\psi} R) e^{i\psi} + (\gamma - i\Omega_0) R e^{i\psi} + \frac{k}{2} (R^3 - R) e^{i\psi} = 0$$

$$\frac{\dot{R}}{R} + i\dot{\psi} + \gamma - i\Omega_0 + \frac{k}{2} (R^2 - R) = 0$$

$$\begin{cases} \dot{R} = -\gamma R + \frac{k}{2} R (1 - R^2) \\ \dot{\psi} = \Omega_0 \end{cases}$$

C.2

Complex networks

C.2.1

Critical point in homogeneous graphs

We need two particular assumptions of a network with enough connections and formed only by a giant component, assuming a global order parameter, $Re^{i\Psi}$. Besides, we are going to take into account a “mean-field” hypothesis, replacing the local field of each vertex by a global field acting over all the nodes, as usually done in the “annealed” approximation, being the connectivity matrix [1, 3],

$$a_{ij} \approx \frac{k_i k_j}{\langle k \rangle N} \quad (\text{C.2.1})$$

Under this assumptions, the global field becomes,

$$Re^{i\Psi} \approx \frac{r_i e^{i\psi_i}}{k_j} \approx \frac{1}{N} \sum_i \frac{k_i}{\langle k \rangle} e^{i\theta_i} = \frac{1}{N} \sum_i \frac{k_i}{\langle k \rangle} (\cos \theta_i + i \sin \theta_i) \quad (\text{C.2.2})$$

Taking the stationary state condition ($\dot{\theta}_i = 0$) in this last equation, we have now,

$$\omega_i = k_i \sigma R \sin(\theta_i - \Psi) \Rightarrow \frac{\omega_i}{k_i \sigma R} = \sin(\theta_i - \Psi)$$

and in a well suited frame of reference (with $\Psi = 0$),

$$\theta_i = \arcsin\left(\frac{\omega_i}{k_i \sigma R}\right); \quad \frac{|\omega_i|}{k_i \sigma R} \leq 1 \Rightarrow |\omega_i| \leq k_i \sigma R$$

Using the fact that $\cos(\arcsin(x)) = \sqrt{1-x^2}$,

$$R = \frac{1}{N} \sum_{i=1}^N \frac{k_i}{\langle k \rangle} \sqrt{1 - \left(\frac{\omega_i}{k_i \sigma R}\right)^2} \Theta\left(1 - \frac{\omega_i}{k_i \sigma R}\right)$$

where $\Theta(x)$ is the Heavside step function.

If we take the continuum limit ($N \rightarrow \infty$), considering some frequency distribution¹,

$$R = \frac{1}{\langle k \rangle} \sum_k k P(k) \int_{-k\sigma R}^{k\sigma R} d\omega g(\omega) \sqrt{1 - \left(\frac{\omega}{k\sigma R}\right)^2} = \frac{1}{\langle k \rangle} \sum_k k P(k) U(k\sigma R) \tag{C.2.3}$$

From this equations we can see that the higher the connectivity, k , the higher the effective coupling strength, ($\sim k\sigma$), synchronizing for smaller values of σ . For simplicity without loss of generality, we are going to consider the particular case of a uniform distribution of natural frequencies,

$$g(\omega) = \frac{1}{2\gamma} \quad \omega \in (-\gamma, \gamma)$$

in which case, the function $U(k\sigma R)$, sets out the form,

$$U(k\sigma R) = \begin{cases} \frac{1}{2\gamma} \int_{-k\sigma R}^{k\sigma R} d\omega g(\omega) \sqrt{1 - \left(\frac{\omega}{k\sigma R}\right)^2} = \frac{\pi k\sigma R}{4\gamma} & k\sigma R \leq \gamma \\ \frac{1}{2\gamma} \int_{-\gamma}^{\gamma} d\omega g(\omega) \sqrt{1 - \left(\frac{\omega}{k\sigma R}\right)^2} = \frac{\gamma k\sigma R \sqrt{1 - \left(\frac{\gamma}{k\sigma R}\right)^2} + (k\sigma R)^2 \arcsin\left(\frac{\gamma}{k\sigma R}\right)}{2\gamma k\sigma R} & k\sigma R > \gamma \end{cases} \tag{C.2.4}$$

In the same way as the “all-to-all” coupling scheme, those oscillators with $|\omega_i| \leq \sigma r_i$ will synchronize, being the coupling condition now,

$$\gamma \leq k\sigma R \Rightarrow k \geq \frac{\gamma}{\sigma R}$$

where x is defined as $x \equiv k\sigma R$.

¹It is worth stressing that the complete graph ($a_{ij} = 1 \forall i \neq j$ y $P(k) = \delta_{k,N}$), being the coupling strength $\sigma \rightarrow \frac{\sigma}{N}$, enables us to recover the Eq. (3.2.10).

Again, there are two contributions for the coupled and uncoupled states, from Eq. (C.2.3),

$$\begin{aligned}
 R &= \frac{1}{\langle k \rangle} \left[\sum_{k \leq \frac{\gamma}{\sigma R}} k P(k) U(x) + \sum_{k > \frac{\gamma}{\sigma R}} k P(k) U(x) \right] \\
 &= \frac{1}{\langle k \rangle} \left[\sum_{k \leq \frac{\gamma}{\sigma R}} k P(k) \frac{k \sigma \pi R}{4\gamma} + \sum_{k > \frac{\gamma}{\sigma R}} k P(k) \frac{\gamma x \sqrt{1 - \left(\frac{\gamma}{x}\right)^2} + x^2 \arcsin\left(\frac{\gamma}{x}\right)}{2\gamma x} \right] \\
 &= \frac{1}{\langle k \rangle} \left[\frac{\sigma \pi R}{4\gamma} \left(\underbrace{\sum_{k \leq \frac{\gamma}{\sigma R}} k^2 P(k) + \sum_{k > \frac{\gamma}{\sigma R}} k^2 P(k)}_{\langle k^2 \rangle} - \sum_{k > \frac{\gamma}{\sigma R}} k^2 P(k) \right) \right. \\
 &\quad \left. + \sum_{k > \frac{\gamma}{\sigma R}} k P(k) \frac{\gamma x \sqrt{1 - \left(\frac{\gamma}{x}\right)^2} + x^2 \arcsin\left(\frac{\gamma}{x}\right)}{2\gamma x} \right] \\
 &= \frac{1}{\langle k \rangle} \left[\frac{\sigma \pi R}{4\gamma} \langle k^2 \rangle - \frac{\sigma \pi R}{4\gamma} \sum_{k > \frac{\gamma}{\sigma R}} k^2 P(k) + \sum_{k > \frac{\gamma}{\sigma R}} k P(k) \frac{\gamma k \sigma R \sqrt{1 - \left(\frac{\gamma}{x}\right)^2} + x k \sigma R \arcsin\left(\frac{\gamma}{x}\right)}{2\gamma x} \right] \\
 &= \frac{1}{\langle k \rangle} \left[\frac{\sigma \pi R}{4\gamma} \langle k^2 \rangle + \sum_{k > \frac{\gamma}{\sigma R}} k^2 P(k) \left(-\frac{\sigma \pi R}{4\gamma} + \frac{\gamma \sigma R \sqrt{1 - \left(\frac{\gamma}{x}\right)^2} + x \sigma R \arcsin\left(\frac{\gamma}{x}\right)}{2\gamma x} \right) \right] \\
 &= \frac{1}{\langle k \rangle} \left[\frac{\sigma \pi R}{4\gamma} \langle k^2 \rangle - \sum_{k > \frac{\gamma}{\sigma R}} k^2 P(k) \frac{\sigma \pi R}{4\gamma} \left(1 - \frac{2}{\pi} \frac{\gamma}{x} \sqrt{1 - \left(\frac{\gamma}{x}\right)^2} + \arcsin\left(\frac{\gamma}{x}\right) \right) \right] \\
 &= \frac{\sigma \pi R}{4\gamma \langle k \rangle} \left[\langle k^2 \rangle - \sum_{k > \frac{\gamma}{\sigma R}} k^2 P(k) F\left(\frac{\gamma}{k \sigma R}\right) \right]
 \end{aligned}$$

being $F(y) = 1 - \frac{2}{\pi} \left[\arcsin(y) + y \sqrt{1 - y^2} \right]$.

Thus, we have,

$$R = \frac{\pi \sigma R}{4\gamma \langle k \rangle} \left[\langle k^2 \rangle - \sum_{k > \frac{\gamma}{\sigma R}} k^2 P(k) F\left(\frac{\gamma}{k \sigma R}\right) \right] \quad (\text{C.2.5})$$

where $F(x) = 1 - \frac{2}{\pi} \left[\arcsin(x) + x \sqrt{1 - x^2} \right]$ is a positive function for $0 \leq x < 1$ verifying the limit $\lim_{x \rightarrow 1} F(x) = 0$. So, we have the solution $R = 0$ for $\sigma < \sigma_c$ and another solutions of partial synchronization for $\sigma > \sigma_c$.

Besides, taking the lower limit when $\sigma \rightarrow \sigma_c$, it is possible to obtain the critical coupling strength, σ_c ,

$$\sigma_c = \frac{4\gamma \langle k \rangle}{\pi \langle k^2 \rangle} \quad (\text{C.2.6})$$

and, remembering the case of an uniform distribution of frequencies in the “all-to-all” coupling scheme,

$$\sigma_c = K_c \frac{\langle k \rangle}{\langle k^2 \rangle} \quad (\text{C.2.7})$$

C.2.2

Equally frequency distributed oscillators $\omega_i = 0$

At first, remember the Kuramoto model embedded in a complex network structure, without any type -or equally distributed- of natural frequencies,

$$\dot{\theta}_i = \sigma \sum_j A_{ij} \sin(\theta_j - \theta_i)$$

which in the infinite size limit ($t \rightarrow \infty$), always shows a synchronization transition for all non-vanishing values of the coupling strength, k , i.e. $\forall k > 0$. Thus, the approximation it can be considered that the difference between phases is negligible ($\theta_i \approx \theta_j \forall i, j$), with the purpose of take the Taylor series expansion,

$$\begin{aligned} \dot{\theta}_i &= \sigma \sum_j A_{ij} \sin(\theta_j - \theta_i) = \sigma \left[\sum_j A_{ij} \theta_j - \theta_i \sum_j A_{ij} \right] \\ &= \sigma \left[\sum_j A_{ij} \theta_j - \sum_j \delta_{ij} \left(\sum_l A_{jl} \right) \theta_j \right] \end{aligned}$$

$$\dot{\theta}_i = -\sigma \sum_j L_{ij} \theta_j$$

where $L_{ij} = \left[\delta_{ij} \left(\sum_l A_{jl} \right) - A_{ij} \right]$, corresponds exactly with the Laplacian matrix of a network, real and symmetric by definition.

Consider now thee eigenvalues decomposition, $L = V\Lambda V^T$, where V is the matrix whose columns are eigenvectors of L , and which make up and orthonormal basis in \mathbb{R}^N ; being Λ the eigenvalues matrix,

$$V = \left((v^1) (v^2) \dots (v^N) \right) \quad \Lambda = \begin{pmatrix} \lambda_1 & 0 & \dots & 0 \\ 0 & \lambda_2 & & \vdots \\ \vdots & & \ddots & 0 \\ 0 & \dots & 0 & \lambda_N \end{pmatrix}$$

where $V^T V = \mathbb{I}$ y $\sum_i v_i^l v_i^{l'} = \delta^{ll'}$.

Working with vectors, the differential equation in $\dot{\theta}_i$ could be determined,

$$\dot{\vec{\theta}} = -\sigma L \vec{\theta} \Rightarrow \vec{\theta}(t) = e^{-\sigma L(t-t_0)} \vec{\theta}(t_0) = V e^{-\sigma \Lambda(t-t_0)} V^{-1} \vec{\theta}(t_0)$$

and finally,

$$\theta_i(t) = \sum_l \sum_j e^{-\sigma \lambda_l t} v_i^l v_j^l \theta_j(0)$$

This sum must be closely scrutinized, to see that,

$$\theta_i(t) = \sum_l \sum_j e^{-\sigma \lambda_l t} v_i^l v_j^l \theta_j(0) = \sum_j e^{-\sigma \lambda_1 t} \underbrace{v_i^1 v_j^1}_{1/\sqrt{N}1/\sqrt{N}} \theta_j(0) + \sum_j e^{-\sigma \lambda_2 t} v_i^2 v_j^2 \theta_j(0) + \dots$$

the first term looks like $\frac{1}{N} \sum_j \theta_j(0) = 0$, and it could be easily equal to zero by choosing a well suited frame of reference. Thus, we will have,

$$\theta_i(t) = \sum_{l=2}^N \sum_j e^{-\sigma \lambda_l t} v_i^l v_j^l \theta_j(0)$$

excluding in the l-sum the first eigenvalue $\lambda_1 = 0$. On the other hand, remember that our complex order parameter is, $\langle z \rangle = \left\langle \frac{1}{N} \sum_i e^{i\theta_i} \right\rangle$, where the average $\langle \dots \rangle$ is done over initial conditions, and in the knowledge that –imposing this conditions over $l = 1$ – the stationary state is $\theta_i = 0$. Considering the Taylor expansion of the complex exponential,

$$\langle z \rangle \approx \left\langle \frac{1}{N} \sum_i \left(1 + i\theta_i - \frac{1}{2}\theta_i^2 \right) \right\rangle$$

It is possible to replace the sum for $\theta_i(t)$ on this average noticing that the leading order, $\theta_j(0)$, is linear and thus, its average over initial conditions vanishes. Corrections will be of second order, namely,

$$\langle z \rangle \approx 1 - \frac{1}{2N} \left\langle \sum_i \theta_i^2 \right\rangle$$

that is always real. Besides, every non-vanishing term in Taylor expansion will be real, because the imaginary terms are odd functions of $\theta_j(0)$. Thus, being $\langle z \rangle$ a stationary real value real ($\dot{\theta}_i = 0$), $\langle z \rangle = r e^{i\psi}$, is a proper measure of r , and it could be analyzed computationally.

Replacing again the sum of $\theta_i(t)$ in the second-order corrections, we have,

$$\langle z \rangle = 1 - \frac{1}{2N} \left\{ \sum_i \sum_{l'} \sum_{j'} e^{-k(\lambda_l + \lambda_{l'})t} v_i^l v_i^{l'} v_j^l v_j^{l'} \underbrace{\langle \theta_j(0) \theta_{j'}(0) \rangle}_{\sigma^2 \delta_{jj'}} \right\}$$

complying (by being a scalar product of orthonormal vectors) $\sum_i v_i^l v_i^{l'} = \delta_{ll'}$ and $\sum_j v_j^l v_j^{l'} = \delta_{ll'}$,

$$\langle z \rangle = 1 - \frac{\sigma^2}{2N} \sum_{l=2}^N e^{-2k\lambda_l t}$$

Regarding the continuum limit, taking into account a spectral density of eigenvalues [2], $\rho(\lambda) = e^{-\frac{1}{\lambda^a}}$,

$$1 - \frac{\sigma^2}{2N} \sum_{l=2}^N e^{-2k\lambda_l t} \approx \int d\lambda e^{-\frac{1}{\lambda^a}} e^{-2k\lambda t} = \int d\lambda e^{-f(\lambda)}$$

where the function $f(\lambda)$,

$$f(\lambda) = \frac{1}{\lambda^a} + 2k\lambda t \quad f'(\lambda) = -a\lambda^{-a-1} + 2kt$$

$$f'(\lambda_0) = 0 \Leftrightarrow \lambda_0 = \left(\frac{2kt}{a} \right)^{-\frac{1}{1+a}}$$

$$f''(\lambda) = a(a+1)\lambda^{-a-2} \Rightarrow f''(\lambda_0) = a(a+1) \left(\frac{2kt}{a} \right)^{\frac{2+a}{1+a}} > 0$$

Employing the saddle-point approximation in the above integral,

$$\int d\lambda e^{-f(\lambda)} \approx e^{-f(\lambda_0)} = e^{-(1+a)\left(\frac{2kt}{a}\right)^{\frac{a}{1+a}}}$$

$$\langle z \rangle \approx 1 - \frac{\sigma^2}{2N} e^{-(1+a)\left(\frac{2kt}{a}\right)^{\frac{a}{1+a}}}$$

Finally, in a Hierarchic Modular Network (HMN), $a = 1$ [2], the next approximation should be fulfilled,

$$1 - \langle z \rangle \propto e^{-2\sqrt{2kt}}$$

References

- [1] ARENAS, A., DÍAZ-GUILERA, A., KURTHS, J., Y. MORENO, Y. & ZHOU, C. «Synchronization in complex networks». *Phys. Rep.* **469**, 93–153 (2008).
- [2] MORETTI, P. & MUÑOZ, M. A. «Griffiths phases and the stretching of criticality in brain networks». *Nat. Comm.* **4**, – (2013).
- [3] UM, J., HONG, H. & PARK, H. «Nature of synchronization transitions in random networks of coupled oscillators». *Phys. Rev. E* **89**, 012810 (2014).

Langevin equations in balanced logarithmic potentials

D.1 Irrelevance of non-linear terms	275
D.2 First-return time distributions	276
References	277

Irrelevance of non-linear terms

For the directed percolation class in the mean-field limit, where spatial heterogeneity is neglected, Eq.(4.2.1) reduces to

$$\dot{\rho}(t) = a\rho - b\rho^2 + \sqrt{\rho}\eta(t). \quad (\text{D.1.1})$$

At criticality, i.e. $a = 0$, there is still a non-linear (saturation) term $-b\rho^2$ which introduces a characteristic maximal activity scale, thus apparently precluding scale-invariance. The way out of this apparent conundrum is that when studying avalanches in discrete/particle models, activity is created at a single location, and in the continuous limit, this corresponds to vanishing density of activity, $\rho = 0$. Thus, one needs to consider a large but finite system size, say Ω (e.g. one could think of a fully connected network with Ω nodes), and perform a finite-size scaling analysis. Defining y by $\rho = y/\Omega$ then –up to leading order in Ω – Eq.(D.1.1) reduces to $\dot{y}(\tilde{t}) = \sqrt{y}\eta(\tilde{t})$ where $\tilde{t} = \Omega t$. In other words, employing the correct rescaled variables y and \tilde{t} the saturation term is never “seen” by the expanding avalanche, which is compatible with the density being equal to zero, as the avalanche invades an infinitely large system. Observe that in the main text we keep the notation with ρ and t , for the sake of simplicity.

Similarly, the voter-model (or compact directed percolation [5] or neutral theory) class –characterized by two symmetric absorbing states– is described, as said above, by the Langevin equation [1]

$$\dot{\rho}(t) = D\nabla^2\rho(\mathbf{r}, t) + \sqrt{\rho(1-\rho)}\eta(\mathbf{r}, t), \quad (\text{D.1.2})$$

which, again, ignoring spatial dependencies and rescaling the variables, readily becomes the DRW equation, Eq.(4.2.4). The very same reasoning applies also to the other universality classes discussed in the Introduction (i.e. dynamical percolation and the Manna class); also in these cases the corresponding non-linear terms, describing saturation effects vanish upon properly rescaling the system.

On the other hand, beyond the mean-field limit, the non-linearities are essential and control the “renormalized” values of the avalanche exponents (see e.g. [4]), which differ for the various universality classes [6, 8], and avalanches can develop non-symmetric shapes [7].

D.2

First-return time distributions

Following the general result of A. Bray [2] (see also F. Colaiori [3]), here we summarize the computation of avalanche exponents for a random walk in a logarithmic potential. The general Fokker-Plank equation reads

$$\frac{\partial P(x, t)}{\partial t} = \mu \frac{\partial}{\partial x} \left(\frac{\partial P(x, t)}{\partial x} + \frac{\beta}{x} P(x, t) \right). \quad (\text{D.2.1})$$

To calculate the probability distribution $F(T)$ of the return times at which a walker starting close to the origin ($P(x, 0) = \delta(x - \epsilon), \epsilon \rightarrow 0$) first hits back the origin, the absorbing boundary condition $P(0, t) = 0$ needs to be imposed. Note that $F(T)$ is minus the probability flux at 0, $F(T) = -j(0, t = T)$, with

$$j(0, t = T) = -\mu \left[\frac{\partial P(x, t)}{\partial x} + \frac{\beta}{x} P(x, t) \right]_{x=0}. \quad (\text{D.2.2})$$

One can try a solution of the Eq.(D.2.1) of the form $P(x, t) = r(x) \exp(-\mu k^2 t)$ and note that the resulting equation can be converted into a Bessel Equation with the change of variable $r(x) = x^{\frac{1-\beta}{2}} R(x)$,

$$x^2 R''(x) + x R'(x) + (k^2 x^2 - \nu^2) R(x) = 0, \quad (\text{D.2.3})$$

where $\nu = (1 + \beta)/2$. The general solution of this last equation is a linear combination of Bessel functions of the first kind of order $\pm\nu$. Putting the pieces back together, employing the orthogonality property of the Bessel functions, and imposing the initial condition, leads to

$$\begin{aligned} P(x, t | \epsilon, 0) &= \left(\frac{x}{\epsilon} \right)^{1-\nu} \epsilon \int_0^\infty dk k [A J_\nu(k\epsilon) J_\nu(kx) \\ &+ B J_{-\nu}(k\epsilon) J_{-\nu}(kx)] e^{-\mu k^2 t}, \end{aligned} \quad (\text{D.2.4})$$

where A and B are numerical constants. The integral in Eq.(D.2.4) gives the modified Bessel function of the first kind $I_{\pm\nu}$ and, it is easy to compute the flux at the origin in the small ϵ limit [2, 3], leading to Eq.(4.2.8).

References

- [1] AL HAMMAL, O., CHATÉ, H., DORNIC, I. & MUÑOZ, M. A. «Langevin description of critical phenomena with two symmetric absorbing states». *Phys. Rev. Lett.* **94**, 230601 (2005).
- [2] BRAY, A. «Random walks in logarithmic and power-law potentials, nonuniversal persistence, and vortex dynamics in the two-dimensional XY model». *Phys. Rev. E* **62**, 103 (2000).
- [3] COLAIORI, F. «Exactly solvable model of avalanches dynamics for Barkhausen crackling noise». *Adv. Phys.* **57**, 287–359 (2008).
- [4] DOBRINEVSKI, A., LE DOUSSAL, P. & WIESE, K. J. «Avalanche shape and exponents beyond mean-field theory». *Europhys. Lett.* **108**, 66002 (2015).
- [5] ESSAM, J. «Directed compact percolation: cluster size and hyperscaling». *J. Phys. A* **22**, 4927 (1989).
- [6] LÜBECK, S. «Universal scaling behavior of non-equilibrium phase transitions». *Int. J. Mod. Phys. B* **18**, 3977–4118 (2004).
- [7] LAURSON, L. *et al.* «Evolution of the average avalanche shape with the universality class». *Nat. Comm.* **4** (2013).
- [8] MUÑOZ, M. A., DICKMAN, R., VESPIGNANI, A. & ZAPPERI, S. «Avalanche and spreading exponents in systems with absorbing states». *Phys. Rev. E* **59**, 6175 (1999).

Resumen en castellano

E.1	Introducción	281
E.1.1	"Criticalidad" más allá de la física	285
E.2	Conclusiones	294

E.1

Introducción

“La crisis consiste precisamente en el hecho de que lo viejo muere y lo nuevo no puede nacer: en este interregno se verifican los fenómenos desproporcionados más variados”

A. Gramsci

Imaginemos¹ por un momento que todas las leyes fundamentales de la Naturaleza pudieran ser entendidas, siendo reducidas a sus mecanismos microscópicos más básicos (por ejemplo, las partículas elementales o las interacciones fundamentales). ¿Sería posible resolver cualquier problema físico a partir de este conocimiento? Podemos predecir, de manera efectiva, el movimiento de una partícula clásica confinada en un potencial, así como el movimiento de dos partículas en interacción, pero el problema de los tres cuerpos –que no es integrable– presenta serios problemas. Para empeorar las cosas, los problemas usuales tratados por la física estadística comprenden un gran número de interacciones (del orden de 10^{24} , el número de Avogadro), haciendo imposible resolver analíticamente las ecuaciones de movimiento del sistema. En lugar de ello, bebiendo de las fuentes de la física estadística, podemos abordar dichos problemas físicos de muchos componentes desde un punto de vista macroscópico, con observables como la densidad media de partículas, la magnetización o su varianza, junto con su respuesta a estímulos externos.

A través de un análisis probabilístico de estos sistemas con un gran número de elementos en interacción (átomos, electrones...) en equilibrio termodinámico², la física estadística explica las leyes fenomenológicas y las propiedades macroscópicas (emergentes) de la materia, descritas en *fases* (sólidas o gaseosas, por ejemplo). Tales fases apenas guardan relación con la naturaleza de sus componentes microscópicos, pero muestran propiedades emergentes colectivas [3]. Dichas fases indican el nivel de orden (o desorden) del sistema, determinado por la presencia (o ausencia) de ciertas simetrías o correlaciones. Por ejemplo,

¹Todas las referencias citadas en esta sección corresponden a las mostradas en el capítulo 1.

²Sin flujos macroscópicos de materia o energía, que no es más que una burda simplificación de la realidad. La mayoría de los sistemas naturales están fuera del equilibrio, es decir, son sistemas de no equilibrio que permanentemente intercambian materia y energía, y cuyo estudio requiere de conceptos más generales.

tanto los diamantes como el grafito, compuestos por átomos de carbono, representan distintas fases debido a la estructura microscópica particular –es decir, la simetría inherente– del cristal. Igualmente, los copos de nieve y las gotas de agua representan distintas fases, que en este caso provienen del nivel de orden del sistema. En este sentido, la física estadística también explica los cambios entre estados de la materia y las *transiciones de fase*, en donde las simetrías pueden romperse espontáneamente –generando fases ordenadas– en una escala macroscópica, pero no en la escala de los componentes microscópicos.

Las transiciones de fase son ubicuas en la Naturaleza. En la vida diaria, el agua constituye el ejemplo más claro de cambios entre estados de la materia (por ejemplo, la fusión de cubitos de hielo o el agua hirviendo) y el ciclo del agua (que implica el intercambio de energía entre los tres estados del agua) es crucial para hacer posible la vida en la Tierra. El uso inteligente de una transición de fase –mediante la máquina de vapor– desencadenó la revolución industrial que marca el inicio de nuestra sociedad moderna.

Todas las transiciones de fase habituales (evaporación, fusión, sublimación o la evaporación) son transiciones de *primer orden* o discontinuas que tienen lugar en un régimen de coexistencia de fases, es decir, durante la transición existen algunas partes del sistema en cada fase macroscópica (el hielo no se convierte instantáneamente en agua líquida). Adicionalmente, existe cierta reminiscencia en el estado del sistema que depende de su historia, la denominada *histéresis*. Un caso ilustrativo que tiene lugar en el entorno de estas transiciones de fase es el agua superenfriada, donde el agua líquida, instantáneamente, se convierte en hielo al aplicarle un estímulo externo.

No obstante, existen también transiciones continuas o de *segundo orden* que no muestran ningún signo de histéresis (el ejemplo paradigmático es la transición paramagnética/ferromagnética del hierro en la temperatura de Curie o la transición del helio líquido al helio superfluido, que se muestra en la Fig. E.1.1). Éstas se caracterizan por tener correlaciones de largo alcance (y calor específico divergente) mostrando un comportamiento distintivo que se caracteriza por leyes de potencias de los distintos observables en torno al punto crítico. Por ejemplo, el fenómeno de la opalescencia crítica, que se produce justo en el punto crítico, provoca que el líquido, que normalmente es transparente, se vuelva turbio –debido a las grandes fluctuaciones en la densidad– cuando la temperatura se acerca a su valor crítico.

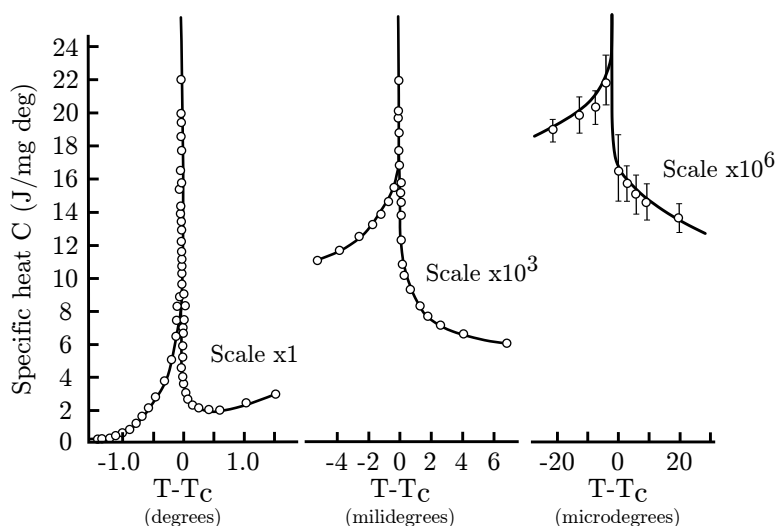


Figura E.1.1: Fluctuaciones de energía del Helio líquido frente a la distancia a la temperatura crítica ($2,17\text{ K}$, el denominado punto Lambda). A esta temperatura el helio líquido se convierte en helio superfluido. Debe destacarse, al margen de la divergencia, la ausencia de diferencias entre las distintas escalas de temperatura, es decir, la invariancia de escala alrededor del punto crítico. Datos de [17].

✳ **Universalidad** En una transición de fase continua, las propiedades (macroscópicas o colectivas) que emergen en el sistema dependen de muy pocos parámetros (la dimensión espacial y las simetrías inherentes). Si consideramos que las fluctuaciones pueden despreciarse (lo que es concebible, por ejemplo, en escenarios con una dimensión muy alta), solo las simetrías (y sus posibles cambios) juegan un papel importante en las propiedades macroscópicas del sistema en el punto crítico [11], surgiendo el siguiente corolario,

debido a la naturaleza finita del número de parámetros relevantes, el comportamiento de la mayoría de los sistemas reales en un punto crítico puede captarse a través de aproximaciones simples (la teoría de Landau para sistemas en equilibrio) y, por tanto, tales sistemas deben compartir la misma *clase de universalidad*.

Un bonito ejemplo real de este comportamiento se muestra en la Figura E.1.2, donde las curvas de coexistencia líquido-gas de muchos fluidos diferentes –desde el Ne al CH_4 – colapsan en una sola curva.

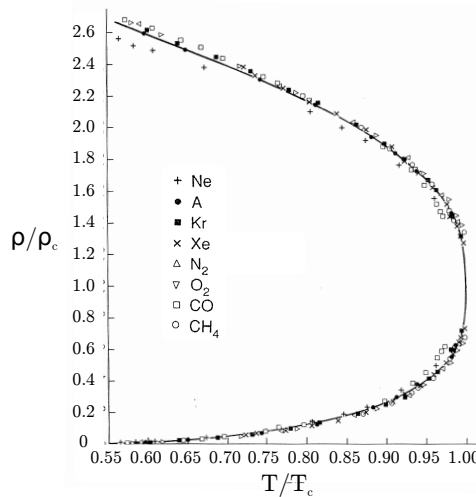


Figura E.1.2: Curva de coexistencia líquido-gas para muchos fluidos. Las magnitudes relevantes, es decir el parámetro de orden (la densidad) y el parámetro de control (la temperatura), han sido re-escaladas por sus valores críticos, colapsando todos los datos en una única curva universal. Se observa que el sistema atraviesa una transición de fase para cierta temperatura crítica (T_c) que claramente depende del compuesto específico. Adaptada de [11].

Esto sugiere la existencia de leyes para sistemas colectivos más allá de los detalles microscópicos particulares. En este sentido, la idea de clase de universalidad, es decir el hecho de que muchos modelos compartan el mismo comportamiento crítico (y por tanto, propiedades emergentes) independientemente de sus detalles microscópicos, emerge naturalmente.

Lo más interesante de todo es que, debido a su naturaleza estadística, el estudio y las aplicaciones de los fenómenos asociados a transiciones de fase (o "criticalidad") que procede de la física "pura" ha permeado muchos campos lejanos a ella: sociología, ecología, neurociencia o las ciencias de la Tierra. En particular, los fenómenos críticos constituyen un punto de partida para explicar o arrojar luz en muchos fenómenos poco entendidos –hasta ahora– como la emergencia de la ley de Gutenberg–Richter en los terremotos, la actividad neuronal del córtex, las erupciones solares o los incendios, entre otros [4–6, 12].

E.1.1

"Criticalidad" más allá de la física

Históricamente, como se ha discutido en el caso de la física, la mayoría de campos de las ciencias naturales (tales como la biología, la química o las ciencias de la Tierra) han centrado sus esfuerzos en un punto de vista reduccionista, es decir, el intento de explicar sistemas completos a través de un profundo entendimiento de sus componentes individuales e interacciones. Este punto de vista lleva a la asunción de que un sistema no es más que la suma de sus partes, por lo que el objetivo final de la Ciencia queda reducido –a partir de un conocimiento exhaustivo de escalas espaciales y unidades funcionales cada vez más pequeñas– a proporcionar un marco ordenado que arroje luz en los fenómenos naturales.

No obstante, el enfoque reduccionista presenta serios y evidentes problemas para explicar y prever el comportamiento de sistemas con un alto nivel de complejidad, como las células, las redes neuronales, los procesos ecológicos, los copos de nieve o el objetivo de converger con campos vírgenes como las ciencias sociales (la sociología o la economía, por ejemplo). Por tanto, el importante problema de cómo el orden puede emerger del desorden en los fenómenos naturales, o en los seres vivos, ha permanecido como un misterio durante mucho tiempo (como planteó Schrödinger en “¿Qué es la vida? El aspecto físico de la célula viva” [58]).

En un trabajo seminal publicado en 1972 y titulado “Más es Diferente” el premio Nobel Philip Anderson confronta este punto de vista notando que los sistemas complejos son irreducibles en sus partes constituyentes [3].

La habilidad de reducir todo a simples leyes fundamentales no implica la habilidad de empezar a partir de aquellas leyes y reconstruir el universo. La hipótesis construccionista fracasa cuando afronta la doble dificultad de "escala" y "complejidad".

Esta perspectiva conduce a mirar los problemas desde una perspectiva global, dejando de lado un comportamiento detallado y exhaustivo de los componentes individuales. Pero, la pregunta clave en este caso es, ¿cómo hacer esto? En particular, en este trabajo, Anderson señala que las rupturas de simetría son un claro ejemplo de fenómenos emergentes. Por tanto, es previsible que la física estadística –que une escalas físicas microscópicas y macroscópicas– y la teoría de transiciones de fase, tengan algo que decir en todo esto.

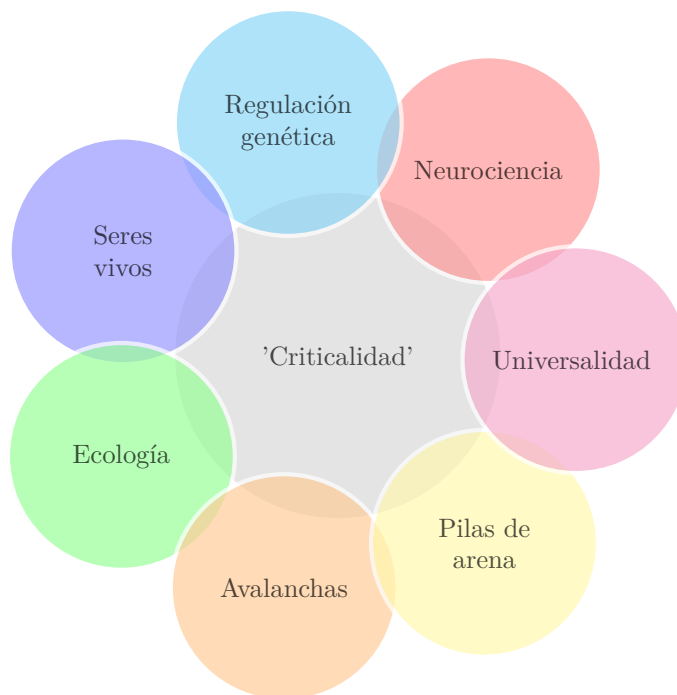
Los ejemplos de fenómenos colectivos (es decir, la emergencia de comportamientos coordinados en sistemas con un gran número de individuos que interactúan entre sí) es ubicua en la Naturaleza: los movimientos "en manada" aparecen en una gran variedad de especies (bandadas de pájaros, bancos de peces, langostas, colonias de hormigas, fitoplancton, krill o las myxobacterias). En el mismo sentido, diversas macroestructuras emergen para otras especies (por

ejemplo, colonias de hormigas, termiteros, colmenas o telarañas; ver la Figura E.1.3) y enormes patrones emergen espontáneamente en la superficie terrestre (por ejemplo, patrones en las dunas de arena, la Calzada del Gigante, o los –recientemente explicados– círculos de hadas de Namibia) así como los fractales son también ubicuos en la Naturaleza en todas sus escalas (desde las conchas marinas a los copos de nieve, las líneas costeras o los fiordos).



Figura E.1.3: De izquierda a derecha: fronda de un helecho, fósil de Ammonite (*Cleoniceras cleon*), ciclón extra-tropical cerca de Islandia en 2003 y la Galaxia Remolino. A pesar del sinfín de escalas que separan estos sistemas (desde *mm* a cientos de años luz) y las diferentes interacciones físicas que involucran, un gran patrón (una espiral logarítmica) emerge en todos ellos.

La Vida es evidentemente una fuente importante de *complejidad*, es decir, de fenómenos emergentes, una característica común que se expande a lo largo de la biología, las ciencias de la Tierra o las ciencias sociales; por tanto, cabe esperar que la mayoría de sistemas exhiban comportamientos (macroscópicos) colectivos con diversos niveles de orden (fases) que surgen de sus componentes (microscópicos). Pero, debe enfatizarse una pequeña pero importante apreciación, algunos de ellos pueden mostrar niveles organizativos intermedios: menos estructurados que un cristal, pero mucho más ordenados que un gas, los sistemas naturales (y los seres vivos) parecen estar –bajo ciertas circunstancias– entre el orden y el desorden [4, 6, 31, 48], es decir alrededor de un punto crítico. Por ejemplo, los sistemas biológicos deben ser resilientes frente a perturbaciones externas (una propiedad de una fase ordenada), pero también deben tener suficiente capacidad de respuesta frente a estímulos externos (siendo desordenados, careciendo de la robustez y la precisión que una maquinaria biológica requiere). La hipótesis de la "criticalidad" indica que la situación marginal entre estas dos tendencias inviables constituye una solución y un compromiso óptimo, fomentando beneficios adicionales, por ejemplo, de las interacciones de largo alcance.



En este sentido, se ha hipotetizado que este delicado balance entre el orden y el desorden confiere a los sistemas críticos un gran número de ventajas funcionales, tales como un gran repertorio de respuestas dinámicas, una mayor susceptibilidad a cambios ambientales, una óptima transmisión y almacenamiento de información así como un excelente solución intermedia entre estabilidad y flexibilidad. Esta perspectiva de que los sistemas biológicos puede extraer importantes beneficios de operar cerca de un punto crítico, es decir en el borde de una transición de fase de segundo orden (o continua), ha atraído un gran interés reciente [1, 4, 46], así como cierto escepticismo [10, 69].

No obstante, bajo esta hipótesis se han encontrado evidencias de "criticalidad" en muchos sistemas naturales tales como erupciones solares [12], pilas de arena [6], terremotos [5], mediciones de lluvia [32], incendios [40], vórtices en superconductores [23] o la formación de gotas [33], entre otros. Más recientemente, con el advenimiento de tecnologías de alto rendimiento, han aparecido evidencias empíricas en seres vivos, tales como comunidades de bacterias [72], el corazón humano [73], redes de neuronas [74], colonias de hormigas [76], el sistema auditivo [77] o la expresión genética [52], entre otros muchos [48].

Parece como si la "criticalidad" impregnase la Naturaleza, extendiendo su sombra sobre los fenómenos naturales y la materia viva. Por tanto, nuestro principal objetivo aquí es profundizar en la hipótesis de la "criticalidad", extendiendo sus horizontes teóricos a través del análisis de las (posibles) fases y transiciones de fase en la materia viva. Pero, no sólo a través de modelos abstractos, sino también replicando y contrastando las –muchas veces insuficientes– evidencias experimentales con el objetivo de tratar de entender características cuantitativas más específicas de la materia viva.

A pesar de todo, es importante tener en cuenta que los sistemas biológicos están intercambiando continuamente materia y energía y, por tanto, es difícil visualizar una descripción apropiada que se base sólo en postulados de equilibrio (recordemos que los conceptos explorados en la física estadística parten de la condición de equilibrio termodinámico). Por consiguiente, los postulados de equilibrio deben extenderse a descripciones de no equilibrio [30, 43] que se describen brevemente en el capítulo 1.

No obstante, a pesar de ser provocativa y cautivadora a la vez, esta hipótesis parece ser quimérica. Entre todas las posibilidades, ¿cómo pueden la materia viva (y los sistemas naturales) permanecer ajustados finamente a un valor específico y concreto? En este contexto, la teoría de criticalidad-autoorganizada (SOC, por sus siglas en inglés) proporciona un marco conceptual que explica, sin ninguna necesidad de un ajuste fino, la prevalencia en un punto crítico. Además, desde su origen, SOC ha estado estrechamente relacionada con el estudio de los fenómenos naturales (*"el objetivo de la ciencia de la criticalidad autoorganizada es profundizar en la comprensión de la cuestión fundamental de por qué la naturaleza es compleja, no simple, tal y como implican las leyes de la física"*, *Cómo funciona la Naturaleza*, Per Bak [4]), sugiriendo explicaciones razonables a muchos de los anteriores ejemplos. Mencionamos a las referencias [48, 70] para una perspectiva extendida y reciente sobre más ejemplos concretos y un completo resumen del tema.

En este punto, nos preguntamos si la hipótesis de la "criticalidad" puede operar en sistemas reales con actividad incesante. Asimismo, aunque SOC proporciona una convincente explicación a la innecesariedad de un ajuste fino, nos preguntamos si la "criticalidad" puede operar en la materia viva más allá de un solo punto, de alguna manera. Por otro lado, ¿existen mecanismos alternativos que expliquen ciertos hechos experimentales que se atribuyen a la "criticalidad"? ¿Es la "criticalidad" la solución evolutiva óptima, incluso en la presencia de perturbaciones externas?

Sin pérdida de generalidad, intentaremos arrojar luz en estas cuestiones a través del estudio de sistemas genéticos y neuronales, haciendo uso de diversos estudios experimentales, aproximaciones teóricas provenientes de la mecánica estadística, los sistemas complejos y los procesos estocásticos, así como análisis computacionales extensivos.

E.1.1.1 Dinámica neuronal

El cerebro de los mamíferos está compuesto por un gran número de neuronas con muchas conexiones entre ellas. En particular, un cerebro adulto contiene $8,6 \cdot 10^{10}$ neuronas entrelazadas por hasta 10^{15} sinapsis, pero de la misma forma, otras especies animales como los elefantes ($\sim 2,57 \cdot 10^{11}$), las ardillas grises ($\sim 4,5 \cdot 10^8$) o la rata topo ($\sim 2,7 \cdot 10^7$), cuentan con un formidable número de neuronas. Incluso el córtex cerebral humano, que juega un papel fundamental en funciones cognitivas superiores como la memoria, el razonamiento, la abstracción, el lenguaje o la consciencia, presenta un sorprendente número de neuronas corticales ($\sim 1,6 \cdot 10^{10}$, de manera interesante, la especie de delfín *Globicephala melas* –que ronda las $\sim 3,7 \cdot 10^{10}$ – excede el caso del córtex humano).

No obstante, las células neuronales (cuya estructura detallada es entendida en profundidad desde los trabajos pioneros de Ramón y Cajal y Golgi, entre otros) son capaces de generar señales eléctricas, disparando potenciales de acción, que estimulan las conexiones sinápticas salientes, y propagan la actividad a las neuronas vecinas. Así, es posible imaginar dos fases neuronales distintas: una quiescente, en la que el estado colectivo de las neuronas esté casi siempre apagado, es decir, la actividad no se propaga y otra activa, en la que el estado colectivo de las neuronas está siempre encendido, es decir, la actividad se propaga rápidamente. Por tanto, parece razonable apostar porque el estado colectivo de las neuronas no puede estar de forma continua en la fase activa o quiescente, dando lugar a algún tipo de fenómeno crítico. De hecho, se ha observado experimentalmente que tanto poblaciones neuronales *in vitro* como *in vivo* muestran disparos irregulares (al unísono) intercalados con períodos de inactividad, y que las desviaciones de esta actividad –ya sea por exceso o por defecto– son un síntoma de enfermedades como la epilepsia, el Parkinson, la esquizofrenia o el autismo [80].

En este sentido, es crucial el descubrimiento de Beggs y Plenz de avalanchas neuronales en el cerebro humano (ver la Figura E.1.4), en donde, los potenciales de campo (LFP, por sus siglas en inglés) disparan y, en conexión con un gran número de neuronas, producen picos de actividad a nivel colectivo separados por períodos de inactividad [9]. Esta observación es robusta (y universal) entre especies [54, 61], escalas y técnicas experimentales [9, 44, 67]. De hecho, se ha observado que la duración y el tamaño de estas avalanchas (es decir, el número total de neuronas que disparan) sigue una ley de potencias³ –sugiriendo algún tipo de invariancia de escala– que muestra escalado del sistema por tamaño finito, es decir, el tamaño máximo de avalancha se incrementa con el tamaño del sistema. Por supuesto, el paradigma de la "criticalidad" autoorganizada –incluyendo variantes conservadas y no conservadas– ha supuesto una constante

³Con los exponentes de un "branching process" de campo medio, $\alpha \approx 2$ y $\tau \approx \frac{3}{2}$ para la duración y el tamaño, respectivamente.

fuente de interpretación de estos fenómenos en neurociencia, dando lugar a modelos interesantes inspirados en SOC [15, 38, 45] que explican las avalanchas neuronales de actividad observadas experimentalmente.

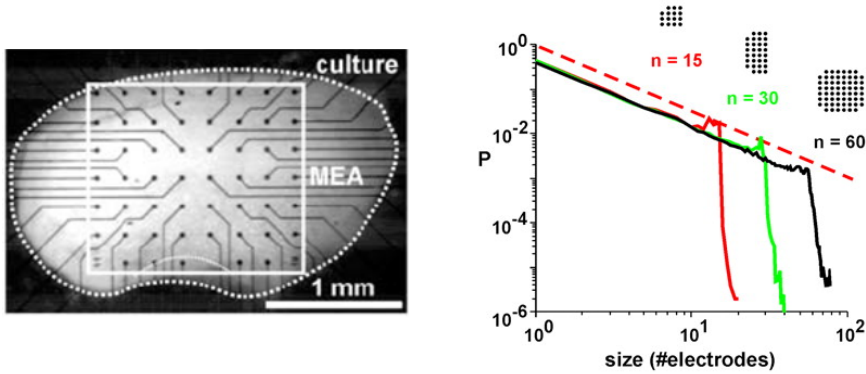


Figura E.1.4: (Izquierda) Población neuronal *in vitro* de la corteza somatosensorial de una rata, donde su actividad se monitoriza empleando una micromatriz. Los puntos negros representan electrodos. (Derecha) Distribución del número total de disparos (tamaño) separados por períodos de inactividad. Aparecen claramente leyes de potencias y su valor máximo solo depende del número de electrodos, es decir, del tamaño del sistema, sugiriendo invariancia de escala. Adaptada de [9, 53].

A partir de las series temporales del cerebro, también se ha descubierto que la actividad cortical muestra leyes de potencia en el espectro de potencia que siguen la forma $1/f$ [39]. Este decaimiento particular es una evidencia de correlaciones de largo alcance, y puede considerarse un sello distintivo de cierto comportamiento crítico. Por otro lado, se ha observado que el rango dinámico (relacionado con la susceptibilidad, es decir, la habilidad del sistema para responder ante estímulos externos) es máximo tanto en poblaciones neuronales *in vitro* como *in vivo* (que también presentan avalanchas neuronales) [28, 63].

Es importante subrayar que no hay aún ninguna explicación teórica completamente satisfactoria de por qué estos hechos experimentales son compatibles con los exponentes particulares de un "branching-process". En particular, no está claro si estos exponentes aparecen como una consecuencia genérica de como se definen las avalanchas temporales para ser medidas (estableciendo umbrales, discretizaciones temporales para poder discriminar su inicio y final o por un efecto de sub-muestreo debido a limitaciones tecnológicas y experimentales). De esta manera, se han propuesto también explicaciones alternativas. [69].

En general, usualmente se asume que una transición de fase inactiva/activa justifica la presencia de los exponentes de "branching-process" [30, 43]. No obstante, algunos resultados recientes han subrayado la evidencia de que las

avalanchas neuronales emergen junto con ritmos colectivos y oscilaciones neuronales [18], de una manera que sugiere que el punto de transición pueda ser de sincronización [29, 79]. Por otro lado, existen otras explicaciones que relacionan la dinámica cortical a un punto crítico de percolación ([67]) o que lo relacionan con el modelo de Ising ([25]). Resumiendo, a pesar de que existe un gran número de evidencias empíricas y teóricas que justifican la hipótesis de un cerebro crítico, aún no hay una explicación teórica completamente convincente, suponiendo un campo de investigación abierto en el que es necesario más trabajo.

E.1.1.2 Redes de regulación genética

El último antepasado común universal (LUCA, por sus siglas en inglés) es el hipotético ser vivo de la tierra del que todos descienden. Dicho (venerable) ancestro común, una bacteria unicelular, por supuesto, que vivió hace unos 3.5-3.8 mil millones de años, se estima compuesto por unos 355 genes [75]. Actualmente, el genoma bacteriano (artificial) mínimo (es decir, el conjunto de genes que lo componen), es una bacteria autorreplicante que contiene 437 genes, una cantidad mucho más pequeña que otras bacterias, mamíferos o plantas de la Naturaleza como, por ejemplo, la *E. Coli* ($\sim 5 \cdot 10^3$ genes), los humanos ($\sim 2,1 \cdot 10^4$ genes) o el arroz ($\sim 4 - 5 \cdot 10^4$ genes).

Este tablero de juego (el genotipo) puede dar lugar a diversos estados celulares (fenotipos, que resultan de la expresión de un genotipo fijo). Por tanto, la bacteria más simple puede mostrar una compleja e intrincada danza que implica la coordinación de miles de genes que se silencian y expresan.

En este sentido, Kauffman planteó una visión pionera al considerar que los estados celulares podían identificarse como atractores de la dinámica de las redes genéticas [36]. En este enfoque particular, modelando los genes como nodos de una red que se conectan (de una manera dirigida) a través de sus interacciones, se supone que, justo en el punto crítico (también denominado el "límite del caos") se obtiene la mejor manera de describir las redes biológicas reales. En este caso, la fase ordenada implica una dinámica convergente, es decir la respuesta a estímulos externos se borra al converger a una única base de atracción (o fenotipo) mientras que la fase desordenada conduce a grandes divergencias y a estados celulares completamente distintos. De nuevo, la "criticalidad" confiere un balance óptimo entre presentar una dinámica demasiado ordenada o estable y demasiado desordenada o ruidosa [36, 52, 64].

Los experimentos al respecto, no obstante, son muy limitados en este caso. Los estudios basados en micromatrices de ADN (que miden y comparan distintos niveles de expresión en células similares [22]), así como los experimentos de inactivación genética (donde se silencian genes individuales y se sigue la cascada de diferencias que se produce entre dos réplicas) han proporcionado algunas evidencias al respecto. Por ejemplo, el tamaño de avalancha en estos experimentos

de inactivación genética [56], así como el número de metabolitos afectados, parece decaer como una ley de potencias con exponente $\tau = 3/2$, siendo compatible con una transición de fase activa/inactiva. Por otro lado, a partir de numerosos experimentos con micromatrices se han inferido diversas estructuras que dan lugar a redes complejas y, que en general, presentan una distribución exponencial de reguladores y una distribución de ley potencial (o libre de escala) en el número de genes regulados ([2]). A través de diversas aplicaciones de modelos Booleanos sobre dichas redes, en diversas especies de bacterias, se ha observado que quizás puedan operar cerca de un punto crítico [8].

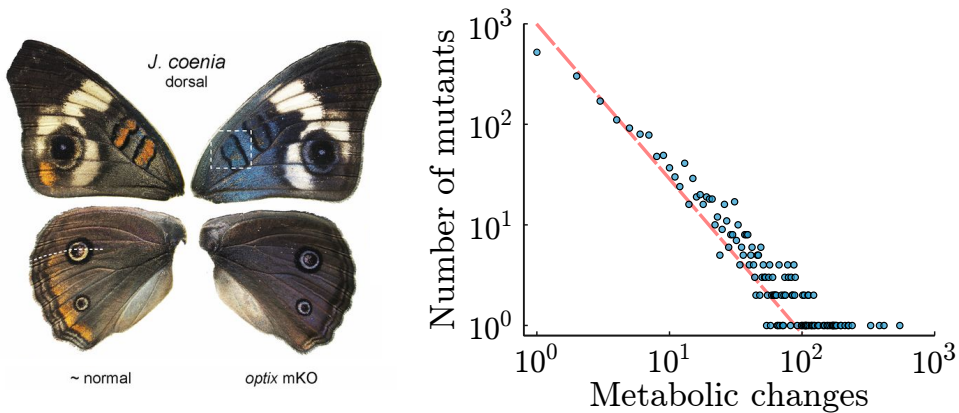


Figura E.1.5: (Izquierda) El gen *optix* coordina (y por tanto su inactivación provoca un cambio drástico) la pigmentación del color de la mariposa *J. coenia*. Figura de [82]. (Derecha) Número total de cambios metabólicos para diferentes réplicas mutantes (es decir, suprimiendo genes de forma individual) de *E. Coli*. Parece seguir una ley de potencias con exponente $\tau \approx 3/2$ (las líneas punteadas son guías visuales). Datos de [26].

A pesar de ser uno de los ejemplos clásicos de "criticalidad" en la materia viva, como ya indicaba Kauffman, debe tenerse especial cautela con los efectos (y peligros) de establecer umbrales en los experimentos de inactivación genética [48]. Son necesarias más y mejores medidas experimentales, tanto en avalanchas de daño como para generar redes genéticas más grandes, así como experimentos similares a los que analizan el rango dinámico en la redes neuronales, para poder discernir si, finalmente, las redes de regulación genética operan cerca de un punto crítico.

En particular, en esta tesis, trataremos de arrojar luz sobre ciertos problemas aún abiertos que conciernen a la hipótesis de la "criticalidad" en ambos campos. En particular, el desarrollo de un modelo mínimo (a la Landau) de la dinámica cortical que sea capaz de combinar tanto las avalanchas como las oscilaciones neuronales en un marco común, así como clarificar diversos métodos

que sean susceptibles de generar dinámicas con leyes de potencias lejos de un punto crítico. Trataremos también de entender los efectos de las redes –modulares y complejas– corticales reales (el conectoma humano) en la perspectiva común analizada (el paradigma de sincronización). Finalmente, abordaremos el problema de la "criticalidad" en modelos Booleanos de redes de regulación genética, con el objetivo de entender un poco mejor el proceso evolutivo que da lugar a su estructura particular y cómo las perturbaciones externas pueden afectar a dicha estructura.

E.2

Conclusiones

“Las cosas suceden a través de revoluciones, no gradualmente, precisamente porque los sistemas dinámicos se sitúan en un punto crítico.”

Per Bak

La hipótesis⁴ de la "criticalidad" plantea una idea fascinante, los seres vivos pueden operar en el entorno de un punto crítico, es decir, en el límite entre el orden y el desorden, arrojando luz en la comprensión de muchos fenómenos colectivos en la Naturaleza y, recientemente, en ciertas características específicas de los sistemas biológicos. Asimismo, ha mostrado su relación con muchos beneficios funcionales cruciales para la supervivencia, la proliferación y el refinamiento de la materia viva que evoluciona por selección natural.

Sobre esta base, a lo largo de esta tesis hemos profundizado en la idea de posibles pistas de "criticalidad" en la materia viva, así como en sus fases y fenómenos colectivos emergentes. En particular, hemos considerado ciertos sistemas biológicos particulares -neuronales y genéticos- susceptibles de ser analizados junto con características cuantitativas específicas, es decir, experimentos, e intentando dilucidar cómo de lejos se encuentra y cómo de precisa es la hipótesis de la "criticalidad".

✖ **La dinámica neuronal opera en el límite de una transición de fase de sincronización** En el contexto de los sistemas neuronales, la hipótesis de la "criticalidad" conjetura que la dinámica subyacente de las redes corticales es tal que se sitúa al borde de una transición de fase continua, separando fases (o regímenes) cualitativamente diferentes, con diferentes grados de orden [2, 9, 20, 41]. Sin embargo, cuáles son estas fases y cuál es la naturaleza del punto crítico, son preguntas que aún deben resolverse por completo.

En este sentido, nuestro modelo *a la Landau* de la dinámica cortical -enfocado en una dinámica reguladora controlada bien por la plasticidad sináptica o la inhibición- nos permite clasificar las posibles fases emergentes de las redes corticales en condiciones muy generales, simplemente considerando cierta estocasticidad intrínseca y cierta dependencia espacial. Aunque Buice y Cowan han

⁴Todas las referencias citadas en esta sección corresponden a las mostradas en el capítulo 7.

desarrollado un enfoque muy similar basado en transiciones de fase continuas, de una fase inactiva a una fase activa [6], creemos que este escenario no capta adecuadamente la esencia de la dinámica cortical, ya que, en las redes neuronales reales, existen mecanismos de integración y disparo, es decir, se requiere cierto umbral de actividad para poder disparar. De hecho, como captura el modelo de Wilson-Cowan, el umbral de la función de respuesta sigmoide impide la existencia de una transición de fase continua activa/inactiva. Además, en base a la naturaleza de impulsos de la dinámica de la actividad neuronal, nuestra teoría subraya el papel fundamental de las oscilaciones y la sincronización parcial –sugiriendo ese tipo de transición de fase– en la dinámica neuronal.

Desde un punto de vista experimental, nuestro modelo constituye –en un caso específico– una buena descripción del córtex durante etapas de sueño profundo o bajo el efecto de anestesia, donde se observan transiciones "up and down" [10, 44]. Pero, mejor aún, justo en el punto crítico de sincronización, nuestro modelo es óptimo para reproducir las observaciones experimentales de redes en estado de reposo [43], la existencia de correlaciones temporales de largo alcance en las oscilaciones alfa [28], así como el tamaño y la duración de las avalanchas –distribuidas como leyes de potencias– que reflejan la misma estadística que en los resultados experimentales, es decir, los exponentes críticos son compatibles con los de un "branching process" [2]. Además, nuestros resultados son compatibles con el modelo extremadamente detallado que ha desarrollado el proyecto "Human Brain Project" [29], en donde se sabe que la concentración de calcio modula el nivel de recursos sinápticos disponibles que regulan el estado del sistema. Adicionalmente, nuestro modelo es capaz de reproducir perfectamente los resultados empíricos *in vitro* para poblaciones neuronales con diversos niveles de heterogeneidad estructural a nivel mesoscópico [37].

✳ **La arquitectura de las redes corticales induce una región crítica amplia de sincronización** En el espíritu de los modelos de campos neuronales, y para preservar la esencia de un diseño minimalista, mostramos que ciertos modelos simples de sincronización (el modelo de Kuramoto), operando sobre las redes empíricas del cerebro humano, exhiben una fenomenología inesperadamente rica.

Dicha fenomenología es una amplia región crítica (que recuerda a una fase de Griffiths [33]) en la que emerge un comportamiento oscilatorio del parámetro de orden, que se deriva de la existencia de comunidades o módulos estructurales relativamente aislados. Aún más destacable es que también existen oscilaciones en el nivel de coherencia interna de los módulos de la red, lo que sugiere la existencia de una jerarquía completa de niveles anidados, como también se desprende de diversos estudios recientes [7, 32, 43, 46].

Al respecto, en ausencia de dispersión en la frecuencia de los osciladores, se consigue una coherencia perfecta en las redes jerárquicas siguiendo una dinámica de ordenamiento de "muñeca matryoshka" (es decir, ascendente), que

se ve frustrada en presencia de cierta dispersión intrínseca de frecuencias. Esto permite que el sistema quede atrapado en estados metaestables, y similares a "quimeras", con cierta coherencia local en los diversos niveles jerárquicos, lo que hace accesible, de una manera robusta y flexible, una gran variedad de atractores funcionales y repertorios dinámicos sin un ajuste ad-hoc a un punto crítico. Además, la estocasticidad permite que el sistema pueda recorrer un paisaje de sincronización complejo con múltiples barreras de potencial entre módulos mutuamente incoherentes, así como generar efectos de desincronización, lo que lleva a una dinámica enormemente enriquecida.

Curiosamente, esta fase intermedia reproduce la dinámica real que se encuentra en las oscilaciones alfa y en el estado de reposo del cerebro humano [4, 28], caracterizada por fluctuaciones muy lentas, de frecuencia típica $< 0,1Hz$. Además, los posibles saltos entre atractores, que se ha sugerido como mecanismo (en la dinámica neuronal real) que permite acceder a configuraciones funcionales muy variadas [9, 18, 41] se facilita en gran medida en el amplio régimen intermedio, sin necesidad de afinar a un punto crítico para garantizar las ventajas funcionales asociadas a la "criticalidad". Asimismo, justifica las regiones críticas observadas en diferentes modelos recientes de dinámica neuronal [13, 21, 40].

✖ Mecanismos no críticos de leyes de potencias en la dinámica neuronal

Desde un punto de vista teórico, los exponentes críticos de un "branching process", son compatibles con las avalanchas empíricas descubiertas por Beggs y Plenz [2]. Dado que todos los sistemas con estados absorbentes pueden exhibir avalanchas, que presentan invariancia de escala en un punto crítico, y las transiciones de fase activa/inactiva muestran los exponentes de "branching process" [19, 30], se han propuesto como explicación de las avalanchas neuronales. En este sentido, esperamos que el breve resumen expuesto ayude a evitar confusiones frecuentes en la literatura neurocientífica, así como subrayar la superuniversalidad de la clase de universalidad de percolación dirigida, que, de hecho, también está relacionada con las transiciones de fase de sincronización [35, 39].

Por otro lado, como mínimo, intentamos resaltar la necesidad –puesto que las leyes de potencias son una condición necesaria, pero no suficiente para la existencia de "criticalidad"– de mostrar diversos exponentes en los hallazgos empíricos/teóricos, así como de evitar una medida inadecuada de avalanchas sobre series temporales.

Por el contrario, hemos demostrado la emergencia de leyes de potencias genéricas (no críticas) en un modelo teórico con un pequeño estímulo externo [5]. Además, de una manera más realista, hemos entendido profundamente los mecanismos de "balanced amplification" propuestos por Benayoun et al. [3, 36] en el caso de poblaciones de neuronas excitadoras e inhibitoras, así como su extensión al caso de plasticidad sináptica como mecanismo regulador. Dicho mecanismo requiere la existencia de un punto fijo estable enriquecido con una

dinámica reactiva que permita grandes fluctuaciones inducidas por el ruido, que llevan al sistema a permanecer atrapado en un potencial logarítmico. Así, proporciona un candidato (no crítico) para modelar las transiciones entre estados "up and down" como los que aparecen en el cerebro durante el sueño o bajo los efectos de anestesia [10, 44]

Sin embargo, a pesar de que el mecanismo de "balanced amplification" puede mostrar avalanchas libres de escala, sus exponentes son compatibles con la conocida clase de universalidad del "random walk". Por lo tanto, aunque la dinámica reactiva puede ser clave en diversos mecanismos neuronales (tales como estados "up and down") y fomentar grandes fluctuaciones, no parece un candidato plausible para dar cuenta del gran número de hallazgos empíricos explicados por otros enfoques teóricos.

✖ La dinámica de las redes genéticas es ordenada o crítica, pero no caótica

Las redes de regulación genética constituyen otro caso que podría funcionar cerca de la "criticalidad", explotando sus múltiples beneficios.

Así, hemos demostrado que los modelos de redes booleanas aleatorias –con una dinámica de actualización estocástica inherente[16], que mimetiza las redes genéticas reales [15, 17, 22, 23]– entrenadas para realizar una tarea computacional determinada, pueden aprender mucho más rápido si tienen una conectividad K tal que estén cerca de la "criticalidad". En este sentido, desde un punto de vista evolutivo, aunque el proceso de aprendizaje es compatible con ser subcrítico, crítico o supercrítico, sin duda la "criticalidad" se fomenta en un sistema cuya evolución esté guiada por selección natural.

Los sistemas biológicos deben tener homeostasis, es decir, la capacidad de mantener sus condiciones internas incluso en presencia de fluctuaciones y ruido. Por tanto, en el mismo experimento computacional, hemos añadido formas extremas de ruido dinámico o estructural, imitando perturbaciones dinámicas o daños físicos en la red de transcripción. Bajo estos efectos, encontramos que la conectividad óptima para lograr el aprendizaje más rápido posible se encuentra profundamente dentro de la región subcrítica, lejos de la "criticalidad", y la distancia al punto crítico aumenta al aumentar la intensidad del ruido y no disminuye al aumentar el tamaño del sistema. Es decir, las redes biológicas reales que sobreviven en un mundo ruidoso deberían operar en regímenes subcríticos más que en un punto crítico.

Además, hemos recopilado muchas redes empíricas (genéticas y metabólicas) que muestran una conectividad bastante baja, lo que lleva a una dinámica subcrítica, bajo la consideración de que la dinámica subyacente a estas redes viene dada por funciones booleanas aleatorias [11, 24]. Nuestros resultados parecen compatibles con lo observado en una red de Kauffman para células eucariotas [42], así como para la red de transcripción de la levadura [25].

Por lo tanto, pese a que la hipótesis de la "criticalidad" sigue siendo una

posibilidad válida y fascinante, debe evaluarse críticamente en cada conjunto de circunstancias específicas, evitando hacer afirmaciones excesivamente generales. Además, junto con la necesidad de enfoques experimentales más precisos y extensos, solo se puede concluir que se necesitan modelos dinámicos mejores y más precisos para modelar las redes de regulación génica, así como para inferir el impacto de las características topológicas importantes (tales como las estructuras jerárquicas y modulares) de las redes empíricas.

✱ Arrojando luz sobre los circuitos regulatorios de los organismos celulares

La comprensión de la estructura (y la evolución) de las redes genéticas reales es clave para las propiedades colectivas emergentes de la función celular [26, 27]. Para este propósito, las redes de paquetes de Debian, como redes de flujo de información, ofrecen una oportunidad única para estudiar la evolución y las propiedades emergentes de las redes genéticas [12, 45].

Hemos encontrado que dichas redes de software sintéticas son capaces de recrear muchas de las propiedades emergentes que se observan en redes reales de regulación genética [1]. Por ejemplo, la estructura particular de la distribución de grados (entrante y saliente), un alto nivel de modularidad que ha surgido a lo largo de su evolución, así como valores similares de la -pequeña- longitud de camino medio que indica efectos de mundo pequeño. A su vez, ambos sistemas muestran una estructura altamente jerarquizada (mucho más pronunciada en el caso de las redes genéticas) que se ha hipotetizado que confiere una forma efectiva y robusta de transferir información y coordinar procesos.

Además, son capaces de reproducir las leyes de potencias encontradas en experimentos de inactivación genética [14, 38], permitiendo una explicación convincente (sin ningún signo de "criticalidad") y atendiendo solo a efectos estructurales. Del mismo modo, las redes sintéticas de Debian pueden respaldar la conjetura de que, al menos, uno de los roles del ADN no codificante en células eucariotas [8, 31] puede ser la monitorización y la minimización de errores durante el proceso de transcripción. En esencia, desempeñando un papel similar a los archivos de control en los paquetes de Debian.

✱ **Sobre cómo funciona la materia viva** Ciertamente, la hipótesis de la "criticalidad" es una solución tentadora y poderosa al misterio de cómo las propiedades colectivas (que emergen por doquier en la Naturaleza) surgen de forma conjunta con la gran cantidad de beneficios funcionales requeridos por los sistemas vivos.

En este sentido, no pretendemos dilucidar por completo la exactitud y la certeza de esta hipótesis, pero es de esperar que hayamos contribuido a arrojar luz sobre la transición de fase (de sincronización) en la que el córtex cerebral podría operar, y que, en lo que a nosotros respecta, es capaz de reproducir todos los principales hallazgos empíricos para las avalanchas neuronales. También

constituye un ejemplo de una transición de fase muy alejada de la usual activa/inactiva, algo muy interesante para sistemas con actividad o dinámica incesante. Pero, aún mejor, dicho punto crítico de sincronización puede extenderse si existen estructuras heterogéneas o modulares subyacentes, lo que sugiere una amplia región de dinámica donde operar -relevante para otros sistemas jerárquicamente organizados- en lugar de la línea estrecha que propone SOC.

Del mismo modo, hemos considerado esencial la evidencia empírica para proporcionar un enfoque teórico que vaya más allá de una hipótesis abstracta, es decir, más allá de una simple visión cualitativa. La hipótesis de la "criticalidad" debe proporcionar un gran número de medidas y predicciones cuantitativas (junto con las ya descubiertas, que, en nuestra opinión, no son lo suficientemente convincentes). Para ello, se necesitan sistemas más grandes, experimentos más precisos e integrales, desde una perspectiva interdisciplinar. En particular, la búsqueda de una prueba irrefutable, que podría ser la función cerebral, es un objetivo prioritario para justificar debidamente la hipótesis de la "criticalidad". Especialmente, esperamos que nuestro modelo Landau-Ginzburg haga su parte en la búsqueda de tal "santo grial" de la "criticalidad".

Por lo tanto, la hipótesis de la "criticalidad" no debe ser aún magnificada. Es un hecho innegable que los seres vivos no pueden ser ni demasiado quiescentes ni demasiado variables, por lo que para ser considerada como una explicación convincente, múltiples características cuantitativas específicas deberían surgir de esta hipótesis. De lo contrario, no deja de ser una tautología, es decir solo sugiere que tenemos modelos limitados -cuyo punto de máxima complejidad es el punto crítico- que dan lugar a una analogía compleja con los sistemas más complejos que conocemos, la materia viva en la Tierra. No obstante, creemos que en muchos casos esta hipótesis es acertada (ver [34] para ejemplos más específicos), pero la biología es lo suficientemente rica para fomentar que la materia viva opere en diferentes fases (más allá de la "criticalidad", no debemos olvidar que tales fases emergen de un comportamiento colectivo de una enorme cantidad de agentes interactuantes, que ya de por sí es un tema fascinante y cautivador). Por ejemplo, tenemos serias dudas, a la luz del enfoque Booleano, sobre la dinámica crítica en las redes de regulación genética, que están expuestas a numerosos factores de estrés externo. Del mismo modo, los experimentos de inactivación genética todavía están lejos de ser una evidencia de que exista dicha dinámica crítica, pues son susceptibles de interpretaciones alternativas (y convincentes). Esto solo refuerza la idea de que se necesitan experimentos más precisos e integrales para aclarar cómo de acertada es la hipótesis de criticidad.

Por lo tanto, en nuestra opinión, esta tesis plantea futuras vías de trabajo sobre cómo los mecanismos adaptativos, homeostáticos o autorreguladores pueden explicar que el cerebro opere al borde de una transición de fase de sincronización, así como el rol de estructuras topológicas más realistas y dinámicas neuronales más complejas (con retardos temporales, por ejemplo). De la misma manera,

la posibilidad de una transición de sincronización relacionada con la dinámica neuronal debe ser aclarada y analizada cuidadosamente tanto desde un punto de vista teórico como desde un punto de vista experimental, e idealmente aclarar desde un punto de vista formal a qué clase de universalidad pertenece. Por otro lado, debe explorarse el desarrollo de modelos dinámicos que puedan replicar las dinámicas de regulación genética (tal vez) cerca de un punto crítico. Del mismo modo, debería analizarse y aclararse la idea de una región crítica amplia que permita repertorios dinámicos ricos, y derivada de la estructura modular, en otros sistemas biológicos, tales como redes genéticas. De hecho, solo el diseño, la replicación y la explicación de más hallazgos y evidencias experimentales -que apoyen o refuten la hipótesis de la "criticalidad" en la materia viva- es, en sí mismo, un gran desafío y una gran fuente de trabajo.

Finalmente, creemos que la hipótesis de la "criticalidad" debe ser capaz de dilucidar por qué la Naturaleza y la materia viva son complejas, así como explicar sus características cuantitativas, resolviendo un misterio clave con enormes implicaciones. Después de todo, de acuerdo con Russell y Dirac, si una teoría posee algo de belleza (y, ciertamente, la "criticalidad" la tiene) también debería poseer algo de verdad. Aunque, también puede ser que -el también complejo-Dios, bajo la suposición (altamente improbable) de que exista, sea un físico estadístico.